A Coordinated Control of PMSG based Wind Turbine Generator to Improve Fault-ride-through Performance and Transient Stability

A Thesis Submitted in Fulfillment of the Requirements for

the Degree of Doctor of Philosophy

PAPAN DEY

Master of Engineering Science, University of Malaya, Malaysia

School of Engineering

College of Science, Engineering and Health

RMIT University

November 2018

DECLARATION

I certify that except where due acknowledgement has been made, the work is that of the author alone; the work has not been submitted previously, in whole or in part, to qualify for any other academic award; the content of the thesis is the result of work which has been carried out since the official commencement date of the approved research program; any editorial work, paid or unpaid, carried out by a third party is acknowledged; and, ethics procedures and guidelines have been followed. I acknowledge the support I have received for my research through the provision of an Australian Government Research Training Program Scholarship.

Name: Papan Dey
Date: 28.11.2018

ABSTRACT

With the high penetration of wind power into the medium and low voltage power grid, ensuring power quality and transient stability following the utility grid codes become challenging nowadays. Wind power fluctuates with the variation of wind speed which leads to the voltage regulation and frequency control problems in the power grid.

Among the issues wind power systems are facing, grid fault is a major one. According to the utility grid codes, wind turbine generators (WTGs) need to have enough fault ride through (FRT) capability. Different configurations of power converters and control techniques have been developed to address this issue. However, a coordinated controller which is capable of the grid voltage regulation, frequency control, and DC link overvoltage minimisation altogether at the time of grid faults is yet to be reported in any literature. This PhD research is focused on developing such a coordinated control method for a permanent magnet synchronous generator (PMSG) based WTG. This coordinated control combines a pitch angle control, a flux weakening control and a reactive power control to enhance the low voltage ride through (LVRT) capability of the PMSG based variable speed wind energy conversion system (WECS). The design process of the controller parameters and the stability of proposed control strategy have been analysed. Here, the pitch angle controller is modified to adjust the pitch for wind power smoothing as well as LVRT enhancement during variable wind speeds and grid fault respectively. The flux weakening controller is used to reduce the flux linkages of PMSG by supplying negative field regulating current to reduce the DC link overvoltage during grid voltage dips. Additionally, static compensator (STATCOM) or grid side converter (GSC) is used to provide reactive power support during the grid faults. Extensive simulations of the proposed method have been carried out under different cases. The proposed control method is compared with the braking chopper (BC) and the battery energy storage system

(BESS) based conventional controls via simulations results and are verified to perform better in providing FRT.

Frequency stability of the grid connected WECS after the fault recovery is also an important issue which needs to be solved. If the frequency fluctuation goes beyond the safe limit, the power system will collapse creating a cascaded failure that was seen in the South Australian Power System in 2016. Therefore, it is essential to provide primary frequency control support for a stable operation of the power system. Two control methods are considered in this PhD research to provide the grid frequency stability.

A simultaneous controller is developed based on the inertia support from the wind turbine and the DC-link capacitor energy to provide the primary frequency control from a PMSG based variable speed WECS. Another approach is developed based on the PMSG flux linkage controller with a Superconducting Magnetic Energy Storage (SMES). The SMES is considered here due to its higher efficiency over other energy storage devices. In this approach, the PMSG flux increases or decreases according to the frequency variation. Similarly, SMES also absorbs or injects some amount of real power when the system frequency is increased or decreased.

Both strategies are verified with the WTGS connected to the single and multi-machine power systems under different wind speeds, load demand variations, and grid faults. Time series simulation results illustrate that a significant enhancement of frequency regulation is achieved with both proposed controllers.

ACKNOWLEDGEMENT

First, thanks to God for his willingness to provide me the opportunity to do this research work.

I would like to express my sincere gratitude to my research supervisor Dr. Manoj Datta. During my research he provided me good support and proper guidance. His patience, experience and vision always encouraged me to follow the right track. I am extremely grateful to share his thoughts and advices during my PhD study.

I would also like to thank my research co-supervisor Dr. Nuwantha Fernando for his guidance and support.

Thanks are due to the RMIT University for providing me the RMIT PhD International Scholarship (RPIS) for this research study.

I would like to thank my lab-mates for their support to carry out this research work.

I would also like to thank my wife and parents for their unwavering support and encouragement throughout the course of my studies.

TABLE OF CONTENTS

LISTS OF FIGURES

LISTS OF TABLES

LISTS OF ABBREVIATION

PMSG	Permanent Magnet Synchronous Generator
LVRT	Low Voltage Ride Through
DC	Direct Current
VSC	Voltage Source Converter
MSC	Machine Side Converter
GSC	Grid Source Converter
PCC	Point of Common Coupling
FRT	Fault Ride Through
WT	Wind Turbine
BC	Braking Chopper
ESS	Energy Storage System
BESS	Battery Energy Storage System
FBESS	Flow Battery Energy Storage System
FESS	Flywheel Energy Storage System
SMES	Superconducting Magnetic Energy Storage
EDLC	Electrical Double-Layer Capacitor
MPPT	Maximum Power Point Tracker
CSC	Current Source Converter
OLTC	Online Load Tap Changer

WECS	Wind Energy Conversion System
APF	Active Power Filter
WTG	Wind Turbine Generator
ANN	Artificial Neural Network
GA	Genetic Algorithm
PSO	Particle Swarm Optimization
PR	Proportional Resonant
PI	Proportional Integral
MTDC	Multi Terminal DC
LFC	Load Frequency Control
TCSC	Thyristor Controlled Series Capacitor
SSSC	Static Synchronous Series Compensator
STATCOM	Static Compensator
SVC	Static Var Compensator
DVR	Dynamic Voltage Restorer
MERS	Magnetic Energy Recovery Switch
BPA	Blade Pitch Angle
SDBR	Series Dynamic Braking Resistor
UPFC	Unified Power Flow Controller
GCR	Grid connection requirements

HVDC	High Voltage DC
MPC	Model Predictive Control
EMF	Electromotive Force
SG	Synchronous Generator
FL	Fuzzy Logic

NOMENCLATURE

R_s	Stator resistance
V_{as}, $V_{\beta s}$, I_{as}, $I_{\beta s}$	a-β components of the stator voltage and current
L_{as}, $L_{\beta s}$	a and β-axis stator inductances
V_{ds}, V_{qs}, I_{ds}, I_{qs}	d-q components of the stator voltage and current
L_{ds}, L_{qs}	d and q-axis stator inductances
ω_e	the electrical angular speed of generator
Φ, P	Flux and pole number
V_{dc}	DC-link voltage
C_{dc}	DC-link capacitance
ω_f	Angular frequency
L_f, R_f	R-L filter inductance and resistance
V_{df}, V_{qf}	d and q-axis components of the point of common coupling (PCC) voltage
e_{df}, e_{qf}	AC voltage of the grid side converter (GSC)
I_{df}, I_{qf}	d and q-axis currents of the GSC
I_{fn}	Filter current at the tuning frequency
I_{Lh}	Load harmonic current
K_p	Proportional constant
K_i	Integral constant

T_d	Time constant
β	Pitch angle
T_m	Driving torque of turbine
J_t	Total equivalent inertia
F	Friction coefficient
$I_r(t)$	Reference current
$I_f(t)$	Injected inverter current
I_q*	q axis reference saturation current
I_{qref}	q axis reference current
I_{dref}	d axis reference current
T_{ref}	Reference torque
K_H	Weighting constant
I_{abc}	Measured three phase currents
I_{abc*}	Reference three phase currents
D	Duty cycle

LIST OF PUBLICATIONS

Most of the research works have been published or submitted for review.

Journals:

1. **P.Dey,** M.Datta, N.Fernando, "Control Strategies of Grid Connected Permanent Magnet Synchronous Generator based Wind Turbines: An Overview'', in *IEEE Transaction on Sustainable Energy* (Will be submitted)*
2. **P.Dey**, M.Datta,N.Fernando, "Design of a Coordinated Controller for Low Voltage Ride Through Enhancement of a PMSG based Wind Turbine'', *IEEE Transaction on Power System* (Will be submitted)*
3. **P.Dey**, M.Datta,N.Fernando, "Transient Stability Enhancement of Wind Farm Connected to Power System under Single and Repetitive Grid Disturbances'', *IEEE Transaction on Sustainable Energy* (Will be submitted)*

Conferences:

1. **P.Dey**, M.Datta, N.Fernando, "PI and PR Current Controllers based Flux weakening to Limit DC link Capacitor Overvoltage in WECS under Grid Faults", *ISGT-Asia*, Australia, 2016
2. **P.Dey**, M.Datta, N.Fernando, T. Senjyu, "A Method to Reduce DC link Overvoltage of PMSG based WECS during LVRT'', *TENCON*, Singapore, 2016
3. **P.Dey**, M.Datta, N.Fernando, T. Senjyu, "Comparison of Synchronous and Stationary Frame PI based Flux weakening Control for DC link overvoltage Minimization'', *TENCON*, Singapore,2016
4. **P.Dey**, M.Datta, N.Fernando, "A Coordinated Control of Grid connected PMSG based Wind Energy Conversion System Under Symmetrical and Asymmetrical Grid Fault'', *ECCE-Asia*, Taiwan, 2017

*These papers are used to prepare thesis chapter two, three, four and five.

5. **P.Dey**, M.Datta, N.Fernando, T. Senjyu, "Fault-ride-through Performance Improvement of a PMSG based Wind Energy Systems via coordinated control of STATCOM'', *ICIT*, France,2018
6. **P.Dey**, M.Datta, N.Fernando, T. Senjyu, "Coordinated Control Design and Analysis of a PMSG based Wind Energy Systems during Repetitive Grid Faults'', *ICIT*, France, 2018
7. **P.Dey**, M.Datta, N.Fernando, T. Senjyu, "Fuzzy-based Coordinated Control to Reduce DC-link Overvoltage of a PMSG based Wind Energy Systems during Grid Faults'', *EPECS*, Japan, 2018
8. **P.Dey**, M.Datta, "Primary Frequency Control by PMSG based Wind Energy Conversion System:A Coordinated Approach", *ECCE-Asia*, Korea, 2019(Submitted)

CHAPTER ONE

INTRODUCTION

1.1. Research Background

Increased air pollutions and impacts of global warming, depletion of fossil fuels, and associated costs of fossil fuel-based power generation have made renewable energy sources like solar and wind as feasible and sustainable energy solutions for the future power grid. With the high penetration of wind power into the medium and low voltage power grids, assurance of power quality and transient stability following the utility grid codes becomes challenging. Wind power fluctuates with the variation of wind speed which impact the grid voltage regulation and frequency control consequently creating frequency and voltage instabilities. These voltage and frequency transients can then lead to cascaded failure of power grid, specially at the time of grid faults.

Different types of generators are used in wind turbine such as squirrel cage induction generator, wound rotor induction generator, doubly fed induction generator and permanent magnet synchronous generator. They are normally known as Type 1, Type 2, Type 3 and Type 4 respectively. Type 1 generator is directly grid coupled. It is robust, simple and cheap. But it has limited variable speed and it is not controllable. Type 2 generator is robust, but it has also narrow speed range. For Type 3 generator wide speed range is possible and power decoupling is also maintained. But its control system is complex and somewhat expensive. Type 4 generator has also the same characteristics of Type 3, however; its control system is less complex although somewhat expensive [1], [2].

According to the major utility grid codes, wind turbine generators (WTGs) need to have adequate fault ride through (FRT) capability for the low voltage ride through (LVRT) and the high voltage ride through (HVRT). In Australia, on 28th September 2016,

a complete power system blackout occurred in the entire state of South Australia (SA). Major investigations found that this is happened as the "voltage ride through" settings on the wind farms were set lower than it should be. As most of the faults create low voltage in the power system, having proper and adequate LVRT is very important for the wind power systems.

In the context of research background just described before, this chapter focuses on the causes and effects of grid faults which are followed by the FRT based solutions. Then, the research objectives, research questions and the overall thesis structure are outlined in this chapter.

1.1.1. Grid Fault

Power system grid fault is an abnormal condition that causes flow of extremely high currents which usually damage power system devices and apparatus [3], [4]. Depending on the number of power lines and involvement of the ground or not different types of fault can be categorised which usually occur in the power grid. Short circuit faults may include with line to line, single line to ground, three lines or three lines to ground, and two lines to ground faults. Along with many transient instabilities, these faults create voltage sag and voltage swell in the grid voltage [5], [6].

1.1.1.1. Symmetrical Fault

Symmetrical fault is also known as balanced fault. Three lines fault (L-L-L) and three lines to ground fault (L-L-L-G) are two types of symmetrical faults. These faults are the most dangerous and severe for the power system, however, they do not occur frequently. Symmetrical faults are only 2-5% of the total power system faults.

1.1.1.2. Asymmetrical Fault

Asymmetrical faults occur frequently in the power system however, they are not as severe as the symmetrical faults. Three types of faults namely the line to ground (L-G), line to

line (L-L) and double lines to ground (LL-G) fault are considered as the asymmetrical faults. Among them, L-G fault is the most common.

Asymmetrical fault is known as the unbalanced fault as it causes unbalanced currents in the power system.

1.1.1.3 Fault Current Calculations

Although symmetrical faults don't occur frequently, it is easy to calculate fault currents considering the symmetrical fault scenario for a power system and that's the industry practice. To take the advantage of using the AC circuit theory and to calculate symmetrical rms fault current, three types of networks are used to represent the power system for the duration of faults. First one is referred as the momentary network which is used to calculate first cycle rms fault current. In this scenario, rotating machine sources and loads are presented by their sub-transient reactance's. Second one is called the interrupting network or the contact parting. It is used to calculate the fault rms current for the circuit breaker minimum contacting times of 1.5 to 4 cycles after the short circuit fault is occurred. For this, the rotating machine sources and loads are represented by different values of constant reactance. Finally, the steady state network or 30 cycles network is used to calculate the minimum short circuit current for relay actuation. For this, rotating machine sources and loads are represented with transient reactance of a larger value which is related to the amplitude of the fault current. Therefore, it is evident that to avoid the recurring grid faults, relay and fuse settings and their time intervals are very important [7].

1.1.2. Reasons of Grid Fault

The system failure and the equipment failure are considered as the two common cases of grid power outages. These are normally happened due to weather, spikes, vehicles, bushfires and animals.

1.1.3. Problems Associated With the Grid Faults and Their Effects on the WTG

Due to the grid faults and the associated transient instability, wind turbine shaft experiences increased mechanical speed, vibration and stress which can damage the shaft. WTG's sudden speed acceleration also leads to over current in the stator windings of the generator and overvoltage in the DC-link bus of the electrical energy conversion system [6]. Normally two back-to-back VSCs are employed in a grid connected PMSG wind energy system to attain full control of the injected active and reactive powers into the grid. When a grid fault occurs, the GSC is usually prevented from supplying all the generator's active power to the power grid as it is used for the reactive power support to provide FRT. So, the voltage of DC link rises rapidly, and the power system frequency also fluctuates. The imbalance between the mechanical input power of the generator and its electrical output power accelerates the generator [8]. The generator as well as the power converters are damaged by this over-current if the condition prevails. Subsequently, a total of the wind farm cut-out happens. The stability of network might be at risk for loss of large MW power for weak grid connection to wind farm.

Generators of different sizes have different LVRT capacities. Large generators have high inertia so after the recovery of grid fault, they cannot go to stable condition immediately. However, small capacity generators can go into stable operating condition very quickly after the grid fault recovery due to their low inertia and quick active power matching to the load demand. During the grid faults, the speed variation is low for the large generators compared to the small-scale wind turbine generators as the large ones have higher inertia.

1.1.4. Solutions to the Problems Associated With the Grid Faults

To maintain the DC link voltage below its acceptable upper limit, dissipation of the excess active power or the reduction of generated power should be necessary at the time of grid faults to provide enough reactive power support from the GSC [9]. Recovery of the WTG

based wind farms from the grid fault conditions is commonly known as the LVRT. The design of LVRT capability enhancement are based on the grid variables such as the DC bus voltage, grid frequency, the voltage during the faults, voltage overshoots at recovery and response times, and the WTG variables such as the rotor current and the rotor speed [10]. As the sudden loss of wind power from the grid due to the grid faults can create severe transient instabilities, hence, actions should be taken to prevent wind farms disconnection from the grid [11].

The control methods to minimise DC-link over-voltage and to realise the LVRT of PMSG-based wind turbine, mainly include Passive methods: e.g., installing an unloading circuit at the DC-link bus of the converter to consume the surplus power; installing an energy storage device at the DC link bus, a super capacitor to quickly exchange active power; installing an auxiliary converter in parallel to the DC link bus to provide a bypass for the overflowing power [12]. These arrangements require installing additional devices, therefore, increase the size of converter and system cost as well as the controller becomes somehow complicated [13]. So, many researches focused on the active methods which don't require additional cost or additional Active methods rely on the advanced controller design and nowadays many research are carried on this area.

1.1.5. WTG related Grid Codes

The grid code is a technical document which establishes the rules of governing the operation, maintenance and development of the utility grid WTGs must meet the grid code when connecting to the grid. The specifications of the grid code for the WTGs are given as dynamic and static requirements. The static requirements discuss the power flow to the transmission grid and the steady state behaviour [14]. On the other hand, the desired WTG behaviour during disturbance periods and faults are discussed in the dynamic requirements. Usually, these requirements cover power factor regulation, voltage

operating range, DC voltage control, frequency operating range, voltage ride through requirements and grid support capability. Voltage ride through capability, frequency control, and DC link voltage control are considered as the biggest challenges in WTG design and manufacturing technology [15].

Operators of different transmission systems must adapt the respective grid codes enabling the WTG connection to the power system without restrictions as well as ensuring the security of the power supply [16]. Wind turbine manufactures, wind farm developers, utilities and existing system users are the main groups comprised of this process [17]. On one side manufactures and developers of wind farm, have to meet the new requirements that increase wind farms cost, however; they are interested in a clear set of requirements that will allow standard production, and on the other hand, the utilities and existing users are concerned about the safety of power system with a large number of WTGs.

Denmark and Germany are the first countries that adapted the grid codes for wind power integration in high voltage networks as the penetration level of wind power is high in both countries. Specific grid codes for voltage networks under 100 kV have been developed by the Danish system operators, Eltra and Elkraf in 2004 [18]. This is the first grid code which specified the requirements for the FRT and was implemented in wind farms in Denmark though in many literature listed the the first grid code was developed by the E.On power system operator in Germany [19].

A new grid code was published in 2004 by the FERC in USA regulates the grid connected generators, but it was not exactly adjusted for the WTGs [20]. Based on the Danish and German grid codes, different grid operators of USA and Canada had set their own standards as shown in Fig. 1.1.

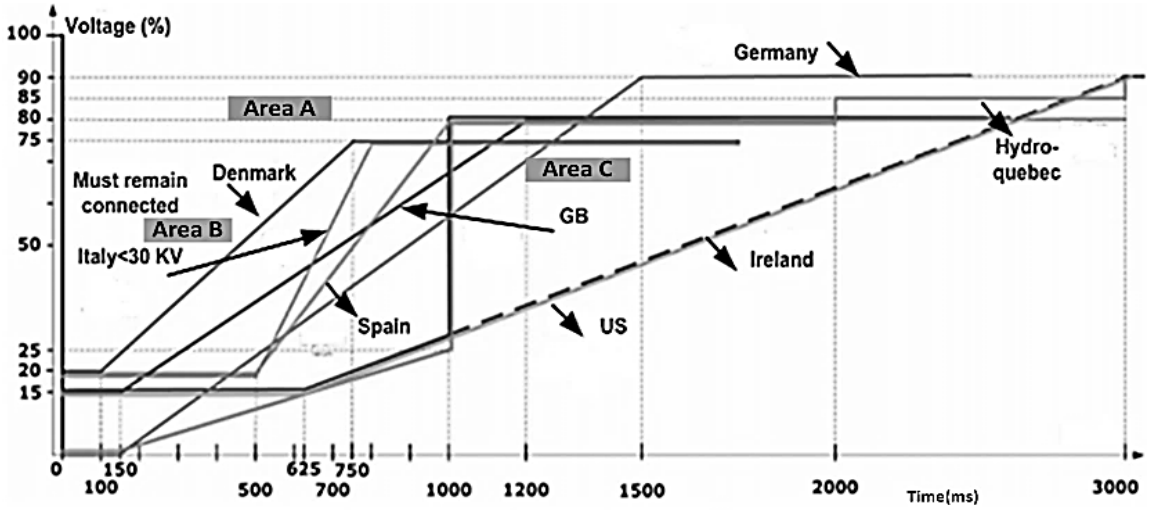

Fig. 1. 1. LVRT requirements for different countries [21]

A new grid code was proposed in Spain in March 2005. Currently, Ireland, UK, Netherlands and Sweden are in the process of redefining their grid codes [22].

Still many other countries require WTGs disconnection when the grid faults occur [23], however, based on the Danish grid codes as shown in Fig. 1, most grid operators are adjusting their grid codes.

The most important requirements from the WTGs include active and reactive power regulation, frequency control as well as capabilities of voltage regulation at the time of grid fault.

According to the Danish grid codes shown in Fig. 1, the following requirements must be met for the symmetrical and asymmetrical grid faults [24], [25]:

- **Area A**: The WTG must remain connected to the grid and maintain regular power production.

- **Area B**: The WTG must remain connected to the grid for 150 ms when the grid voltage dropped to 20% of its nominal value. By supplying reactive power, the WTG must provide maximum voltage support to ride through the fault. WTG should also generate active power immediately after the fault clearance to support the grid frequency.

- **Area C**: The WTG can be disconnected from the grid.

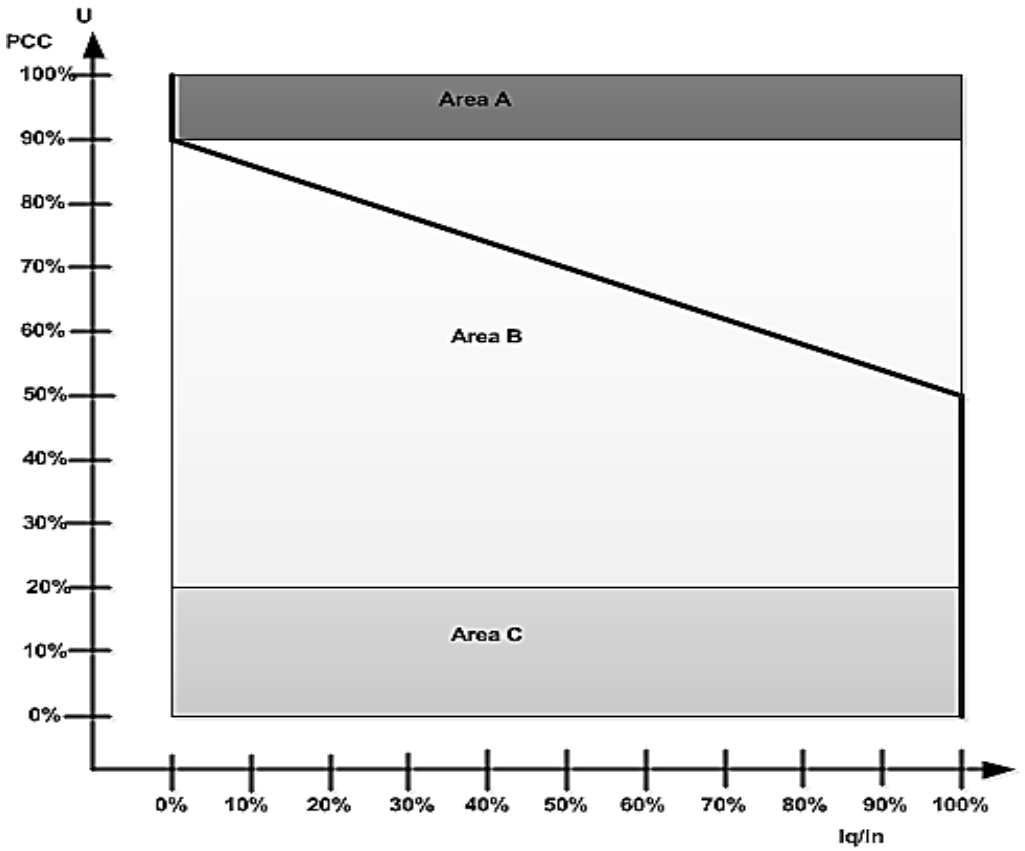

(a)

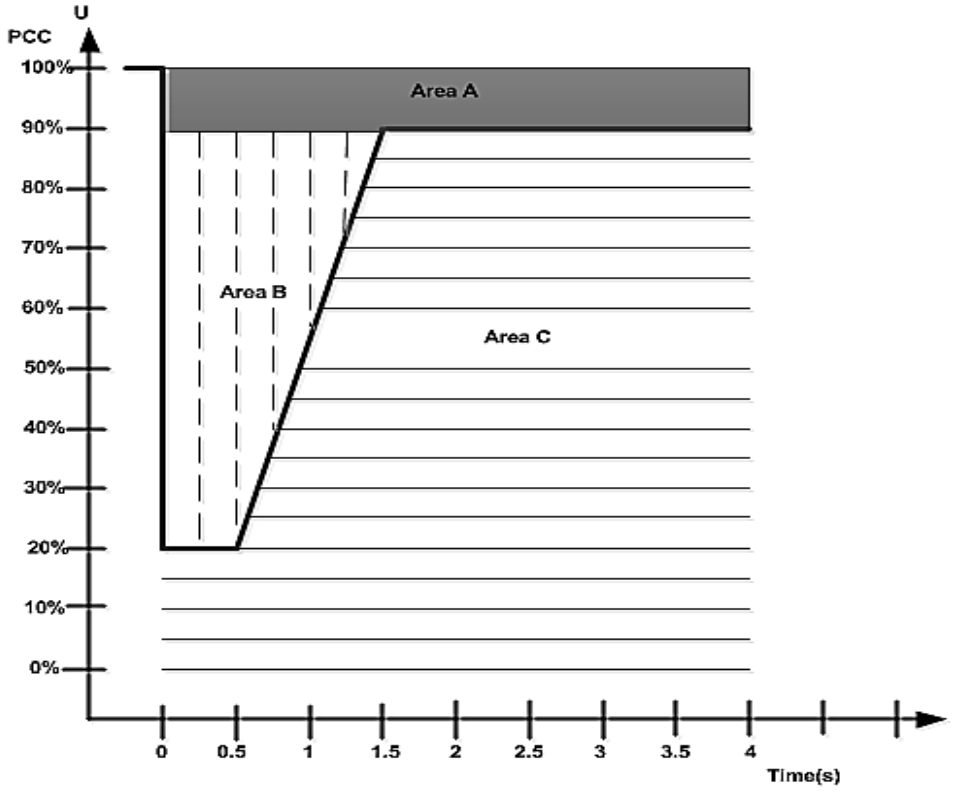

(b)

Fig. 1. 2. Danish grid code (a) Requirement of LVRT (b) Requirement of reactive power support [24]

1.2. Research Problem Statements

It is essential to analyse the impacts of grid faults on the WTG. When asymmetrical or an asymmetrical grid fault occurs in the power grid, active power imbalance occurs between generator side and the grid side of the WECS as the GSC is used to supply maximum reactive power. So, the PMSG speed goes up and mechanical vibration increases. AS the GSC is not able to transfer the incoming power from the MSC side to grid the DC link voltage increases beyond its maximum limit and the system frequency fluctuates due to immediate unbalance between the load demand and the power supply. The power converters may be failed due to over current and if this condition persists for more than 150 ms, according to the grid code WECS should be disconnected. The stability of network will be at risk due to big loss of wind generated active power.

Therefore, the LVRT actions should be taken based on grid code requirement to prevent WTG's sudden disconnection from the grid during the faults.

1.3. Research Motivation and Scope

WTGs should be properly controlled to ride through the grid faults which should minimise the severe voltage drops and frequency deviations. The voltages of one or more phases at the PCC may abruptly drop to near to zero in the time of grid fault. This results in large stator current transients, leading to high currents flowing through the converters. These make the whole system unstable and can damage the sophisticated power converters. Therefore, a control method needs to be developed which can collectively address all the issues related to grid faults and wind power variations.

The scope of this PhD research is to deploy an effective control technique which would be able to enhance fault ride through according to the grid codes. Performance of the controller is a key factor to improve the efficiency of the WECS under the grid faults. Qualitative and quantitative assessments during the transients can also provide deeper

insights into the power system network with a quick decision to maintain dynamic stability and power system security.

1.4. Research Aim and Objectives

The main aim of this PhD research is to develop a controller for the PMSG and back to back converters based WECS to enhance fault ride through, frequency control, and injection of the reactive power for grid voltage support. This aim can be achieved by accumulating the following objectives.

- To develop a novel controller for the MSC to minimise the DC link over voltage at the time of grid faults.
- To develop an improved pitch angle controller for the variable wind speeds.
- To develop a coordinated control between the MSC controller, the pitch angle controller and the GSC controller for reactive power support
- To develop a frequency controller to minimise frequency deviations after the grid fault recovery.

1.5. Research Questions

To fulfil the objectives given in Section 1.4, following research questions have been formulated and answered. These research questions have been described along with their significance and related contribution-based publications.

1.5.1 Research Question 1 (RQ1)

How the different parameters of wind energy conversion system behave in the various grid fault scenarios and how a control technique can be applied to enhance the voltage ride through performance of the PMSG based WTG minimising the DC link over voltage and without using any extra circuits or energy storage system?

Significance

Grid integration of PMSG based WTG has become an important part of the current electrical power generation mix. Penetration of large scale wind power into the grid can cause severe voltage recovery problems following the grid faults on the power network. So, it is important to analyse the behaviour of the system during grid faults based on (i) how the faults impact the wind turbines and (ii) how the response of the wind turbines influences the post-fault behaviour of the power system. During a symmetrical (balanced) and an asymmetrical (unbalanced) grid faults, high voltage is induced in the PMSG. This induced voltage is higher enough compared to the usual EMF of the PMSG. It also exceeds the maximum allowable voltage of the MSC. To overcome this situation, the induced EMF should be constrained to be less than the applied voltage by reducing the air gap flux linkages.

Solution

The flux weakening control can be used as a novel approach to reduce the airgap flux linkages. Although, flux weakening control is an established technique in the field of motor drives, it has not been used in any reported research to support the voltage ride through of the PMSG based WTG, specially to minimise the DC link over voltage.

Contribution

At the time of symmetrical and asymmetrical grid faults, high voltage is induced in the rotor of the PMSG due to the flux linkages between the stator and the rotor. During this period, this mutual flux linkage must be decreased to maintain constant stator voltage and to keep the DC link voltage within its acceptable limit. To apply flux weakening control, in the flux weakening region, it is required to limit the current and voltage of the converter and the generator. The voltage limit is selected based on the generator's rated voltage or the DC link voltage. So, a constant DC link voltage can be achieved with a flux weakening control. The proposed flux weakening method weakens the flux by supplying a negative

field regulating current considering the maximum voltage limit of the MSC. It is developed based on the synchronous and stationary reference frames for different control parameters and fault duration.

Publications

1. **P.Dey**, M.Datta, N.Fernando, "PI and PR Current Controllers based Flux weakening to Limit DC link Capacitor Overvoltage in WECS under Grid Faults", *ISGT-Asia*, Australia, 2016

2. **P.Dey**, M.Datta, N.Fernando, T. Senjyu "A Method to Reduce DC link Overvoltage of PMSG based WECS during LVRT'',*TENCON*, Singapore, 2016

3. **P.Dey**, M.Datta, N.Fernando, T. Senjyu "Comparison of Synchronous and Stationary Frame PI based Flux weakening Control for DC link overvoltage Minimization'',*TENCON*, Singapore, 2016

1.5.2 Research Question 2 (RQ2)

How a variable speed pitch angle controller can be used in coordinated manner with the flux weakening control to enhance the fault ride through performance of the WTG?

Significance

Wind speed varies with the weather which produces fluctuating output power from the PMSG based WTG. This can cause instability in the power system especially when there are loads which are sensitive to the variations of grid voltage and the frequency. Therefore, a pitch angle control system is required to smooth the WTG output power fluctuations. During small voltage fluctuations, a properly-tuned pitch angle controller can perform sufficiently. However, it cannot perform well during large voltage fluctuations. Therefore, a coordinated control could be a possible solution to satisfy the grid code requirements and to minimise these voltage and frequency fluctuations.

Solution

A coordinated control method is developed based on the flux weakening control of research question 1 and a pitch angle control. The pitch angle control has a slow response however; the flux weakening control has a fast response. Coordinating them is an interesting challenge. Responses of these controllers are analysed based on their system transfer functions. When the pitch control is triggered, producing negative α-axis current in the MSC controller by the flux weakening control can help to reduce the DC-link overvoltage. This also helps to achieve a better LVRT performance during the symmetrical and asymmetrical faults. Hence the necessity of including the both controllers and their coordination have been justified.

Contribution

Mode of the pitch angle control is changed according to the requirement of smoothing the output power fluctuations or the DC link overvoltage minimisation. The proposed flux weakening controller is used to reduce the DC link overvoltage. Moreover, a reactive power supporting arrangement is used to improve the grid voltage profile. Reactive power support from the GSC or STATCOM with super capacitor is used here to achieve the continuous operation during the grid faults.

Publications

1. **P.Dey**, M.Datta, N.Fernando, " A Coordinated Control of Grid connected PMSG based Wind Energy Conversion System Under Symmetrical and Asymmetrical Grid Fault'', *ECCE-Asia*,Taiwan,2017

2. **P.Dey**, M.Datta, N.Fernando, "Coordinated Control Design and Analysis of a PMSG based Wind Energy Systems during Repetitive Grid Faults'', *ICIT*, France, 2018

3. **P.Dey**, M.Datta, N.Fernando, "Fault-ride-through Performance Improvement of a PMSG based Wind Energy Systems via Coordinated Control of STATCOM'', *ICIT*, France, 2018

4. **P.Dey**, M.Datta, N.Fernando, T. Senjyu, "Fuzzy Logic based Coordination Controller for PMSG Wind Energy Conversion to Enhance Low Voltage Ride Through'', *EPECS*, Japan, 2018

1.5.3 Research Question 3 (RQ3)

After the improved FRT achieved by using the methods developed in RQ1 and RQ2, how to devise and deploy a quick frequency control strategy to ensure frequency stability and overall transient stability of the post-fault power system?

Significance

To maintain the grid frequency within the acceptable limits, it is necessary that the total power generated be equal to the power consumed by the system loads and electrical losses in the grid. Immediately after the FRT, a power imbalance occurs in the grid as sudden active power outputs from the WTGs are injected to the grid creating an oversupply of the generated power. Grid frequency increases due to this generation and demand imbalance which can in turn make the power system unstable. Therefore, it is important to address this issue and develop a fast controller to control the gird frequency immediately after the power system recovery from the grid faults as well as to tackle the usual frequency deviations.

Solution

To address the grid-frequency deviations, particularly the under frequency, the stored kinetic energy in the rotating mass of the WTGs or the stored energy from an energy storage device can be used to deliver additional power to the system. On the other hand, to address the over frequency, a combination of pitch angle control, generator speed control, and charging an energy storage device can be used to retain the active power and load balance.

Contribution

Two approaches are designed to enhance the primary frequency control from the PMSG based variable speed WTG. For the first approach, a simultaneous controller is developed based on the physical inertial support from the wind turbine and the virtual inertial support from the DC-link capacitor's stored energy. The second approach is developed based on the PMSG flux control and the Superconducting Magnetic Energy Storage System (SMES). The developed control strategies are verified under single and multi-machine power systems for different wind speeds and grid faults.

Publications

1. **P.Dey**, M.Datta, "Primary Frequency Control by PMSG based Wind Energy Conversion System: A Coordinated Approach", *ECCE-Asia*, Korea, 2019(Submitted)

1.6. Rationale for Research

Some FRT methods used in the PMSG based WTG systems are more expensive than the others due to the use of additional power electronic switches, coupling transformer, magnetic inductance, high power resistance, super capacitors etc. On the other hand, modification of the controllers is more economic for the voltage ride through methods as they do not use any additional devices. Thus, modified controllers have recently received much attention in the wind power research community. Most of the existing works are based on single controller either in the grid side or in the machine side. Few researches have used controllers on the both machine and grid sides simultaneously in a coordinated manner.

That's why, this PhD research investigated developing a hybrid and coordinated control method based on the pitch angle control and the flux weakening control which is applied on the both machine and grid sides during different grid fault scenarios. Moreover, the reactive power support based on either the GSC or STATCOM during the fault period is

also considered. The impact of PMSG wind turbine's LVRT control on the power system transient stability during both the asymmetrical and symmetrical grid faults are not well reported in the previous literatures.

Additionally, frequency regulation after the grid fault recovery or for any frequency deviation events for different wind speeds are not addressed properly in the literatures. Therefore, being different from the previously reported research works, this PhD research is aimed to focus on simultaneous control approaches to overcome both the voltage and frequency fluctuation issues.

1.7. Thesis Structure

The research work presented in this thesis is divided into six chapters. Overall idea, background, problem statement, motivation and scope, objectives of the PhD project with three research questions have been discussed in the Chapter one.

Extensive literature review on the different FRT techniques is presented in the Chapter two which includes the existing LVRT strategies to improve the capability of the WTGs to operate without disconnecting from the grid at the time of grid faults. Moreover, various frequency control methods are reviewed thoroughly in the Chapter 2. This chapter helps to identify the research gaps in the existing literatures and the new research directions.

The basic construction of a grid connected PMSG based WECS with back to back converter topology is presented in the Chapter three. The key components of WECS are described thoroughly. In this Chapter, the proposed flux weakening control strategy is presented to minimise the DC-link overvoltage which is the novel contribution of this PhD research This Chapter also includes the design of different current controllers which can be used to implement the proposed flux weakening control. The proposed flux weakening controller is compared with the conventional Braking Chopper to minimise

the DC-link overvoltage and then the simulation results for the symmetrical and asymmetrical grid faults are analysed and presented in this Chapter.

The Chapter four gives the description of a coordinated controller which is developed based on the proposed flux weakening controller and a modified pitch angle controller. Effectiveness of the proposed coordinated controller is tested under different types of grid fault with different wind speed profile. This Chapter also gives an illustration of transient stability enhancement of the grid connected WECS under single and repetitive grid faults. A comparison of the proposed controller with the conventional energy storage-based system is also presented in this Chapter.

The coordinated controller which is developed in the Chapter four is modified and a reactive power controller is added with this coordinated controller. This is presented in the Chapter five. This Chapter includes two different types of coordinated controller. The simulation results are then presented to validate the effectiveness of the proposed controllers to enhance the transient stability of grid connected WECS under the symmetrical and asymmetrical grid faults. Then this chapter presents the comparative analysis of the proposed controller performance with the conventional Braking chopper system for the verification purpose.

Two frequency control strategies based on the inertia control, the flux linkage control and SMES systems are developed in the Chapter six. Simulation results are obtained for the usual frequency deviation as well as for the frequency fluctuations after a grid fault recovery. The simulation was carried for the WTG connected to the single machine and the multi machine systems using constant, step and real wind speed profiles.

The conclusions of the PhD research, contributions the research and suggestions for future work are finally presented in the Chapter seven with appendixes to follow.

REFERENCES

[1] Gevorgian, V., Muljadi, E., "Wind power plant short circuit current contribution for different fault and wind turbine topologies", *Ninth Annual Int. Workshop on Large-Scale Integration of Wind Power into Power Systems as well as on Transmission Networks for Offshore Wind Power Plants*, Québec, Canada, 18–19 October 2010, pp. 1–8.

[2] N. Goudarzi, W. D. Zhu, "A review on the development of wind turbine generators across the world", *International Journal of Dynamics and Control*, vol. 1, no. 2, pp. 192-202, 2013.

[3] N. M. Freire, J. O. Estima, and A. J. Marques Cardoso, "Open-circuit fault diagnosis in PMSG drives for wind turbine applications," *IEEE Transactions on Industrial Electronics,* vol. 60, pp. 3957-3967, 2013.

[4] J. Yang, "Fault analysis and protection for wind power generation systems," University of Glasgow, 2011.

[5] M. Chowdhury, W. Shen, N. Hosseinzadeh, and H. Pota, "A review on transient stability of DFIG integrated power system," *International Journal of Sustainable Engineering,* pp. 1-12, 2015.

[6] H. M. Abdel-Mageed, "Simulation of the Different Transmission Line Faults for a Grid Connected Wind Farm with Different Types of Generators," *International Journal of Electrical and Computer Engineering (IJECE),* vol. 2, pp. 35-45, 2011.

[7] Mercede, Frank J., "How to perform short circuit calculations," *www.ecmweb.com*, 1st June,1999. [Online]. Available: https://www.ecmweb.com/content/how-perform-short-circuit-calculations. [Accessed Nov. 12, 2018].

[8] R. Mittal, K. Sandhu, and D. Jain, "Low voltage ride-through (LVRT) of grid interfaced wind driven PMSG," *ARPN Journal of Engineering and Applied Sciences,* vol. 4, pp. 73-83, 2009.

[9] L. Yan, C. Yongning, W. Zhen, W. Linjun, and L. Chao, "Study on LVRT capability of D-PMSG based wind turbine," in *Power Engineering and Automation Conference (PEAM), IEEE*, 2011, pp. 154-157.

[10] J. Li, S. Hu, D. Kong, and H. XU, "Studies on the Low Voltage Ride Through Capability of Fully Converted Wind Turbine with PMSG [J]," *Automation of Electric Power Systems,* vol. 19, pp. 92-95, 2008.

[11] M. Molinas, J. A. Suul, and T. Undeland, "Low voltage ride through of wind farms with cage generators: STATCOM versus SVC," *IEEE Transactions on Power Electronics,* vol. 23, pp. 1104-1117, 2008

[12] K. Vinothkumar and M. Selvan, "Novel scheme for enhancement of fault ride-through capability of doubly fed induction generator-based wind farms," *Energy Conversion and Management,* vol. 52, pp. 2651-2658, 2011.

[13] Y. Li, Y.-n. Chi, and Z. Wang, "Study of LVRT capability of D-PMSG based Wind turbine," in *Power Engineering and Automation Conference (PEAC). Wuhan, China: IEEE*, 2011, pp. 154-157

[14] F. Iov, R. Teodorescu, F. Blaabjerg, B. Andersen, J. Birk, and J. Miranda, "Grid code compliance of grid-side converter in wind turbine systems," in *37th IEEE Power Electronics Specialists Conference, PESC'06,2006.* pp. 1-7.

[15] C. P. Butterfield, W. Musial, J. Jonkman, P. Sclavounos, and L. Wayman, *Engineering challenges for floating offshore wind turbines*: National Renewable Energy Laboratory Golden, CO, USA, 2007.

[16] M. Tsili and S. Papathanassiou, "A review of grid code technical requirements for wind farms," *IET Renewable Power Generation,* vol. 3, pp. 308-332, 2009.

[17] A. Johnson and N. Tleis, "The development of grid code requirements for new and renewable forms of generation in Great Britain," *Wind Engineering,* vol. 29, pp. 201-216, 2005.

[18] M. Altin, Ö. Göksu, R. Teodorescu, P. Rodriguez, B.-B. Jensen, and L. Helle, "Overview of recent grid codes for wind power integration," in *2010 12th International Conference on Optimization of Electrical and Electronic Equipment (OPTIM),* pp. 1152-1160.

[19] M. Tsili, C. Patsiouras, and S. Papathanassiou, "Grid code requirements for large wind farms: a review of technical regulations and available wind turbine technologies," in *Proceedings of EWEC*, 2008.

[20] D. Blakeway and C. B. White, "Tapping the Power of Wind: FERC Initiatives to Facilitate Transmission of Wind Power," *Energy LJ,* vol. 26, p. 393, 2005.

[21] B. Singh and S. Singh, "Wind power interconnection into the power system: a review of grid code requirements," *The Electricity Journal,* vol. 22, pp. 54-63, 2009.

[22] B. Singh and S. Singh, "Wind power interconnection into the power system: a review of grid code requirements," *The Electricity Journal,* vol. 22, pp. 54-63, 2009.

[23] D. Energinet, "Technical regulation 3.2. 5 for wind power plants with a power output greater than 11 kW," Technical report2010.

[24] J. J. Justo, F. Mwasilu, and J.-W. Jung, "Doubly-fed induction generator-based wind turbines: A comprehensive review of fault ride-through strategies," *Renewable and Sustainable Energy Reviews,* vol. 45, pp. 447-467, 2015.

[25] Meegahapola Lasantha, Datta Manoj, Nutkani Inam, Conroy James. Role of fault ride-through strategies for power grids with 100% power electronic-interfaced distributed renewable energy resources. *WIREs Energy Environ.* vol.7, 2018.

CHAPTER TWO

LITERATURE REVIEW

2.1. Introduction

This chapter describes the design and operating principles of different low voltage ride through (LVRT) and frequency regulation techniques reported in the literature. Moreover, brief reviews of different types of control techniques are provided based on their behaviours and the LVRT enhancement capability. These methods are compared with each other considering their advantages and disadvantages. Although different control methods are available, it is of paramount importance to identify the most effective control method based on its application and performance.

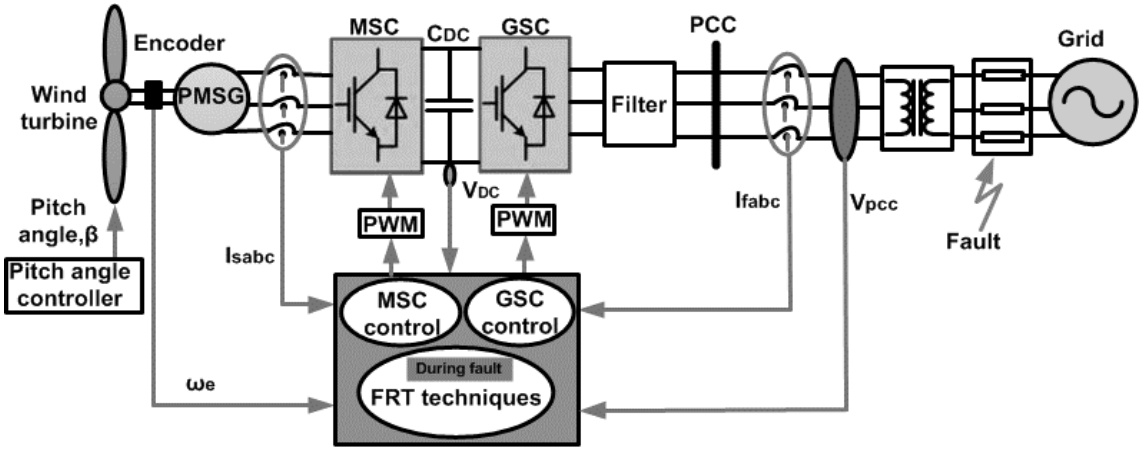

Fig.2. 1. A PMSG based wind energy conversion system (WECS) with control block

A PMSG based WECS is shown in Fig.2.1. It is divided into wind turbine part which is controlled by pitch angle controller, PMSG part which is controlled by machine side converter (MSC) and the grid part that is controlled by grid side converter (GSC). GSC is connected to the grid via filter, transformer and transmission lines. During the grid fault condition different fault ride through techniques are applied.

2.2. Fault Ride Through Techniques

Quite a many technique has been reported and discussed in the literature to enhance the fault ride through performance of a grid connected WECS. These methods can be categorized as passive and active methods as shown in Fig.2.1 and can be described as [1]:

a) Protection circuit-based configurations and controls (passive methods),

b) Installation of reactive power injection -devices (passive methods) and

c) Modified (specific) or improved control structures for the machine side and grid side converters (active methods).

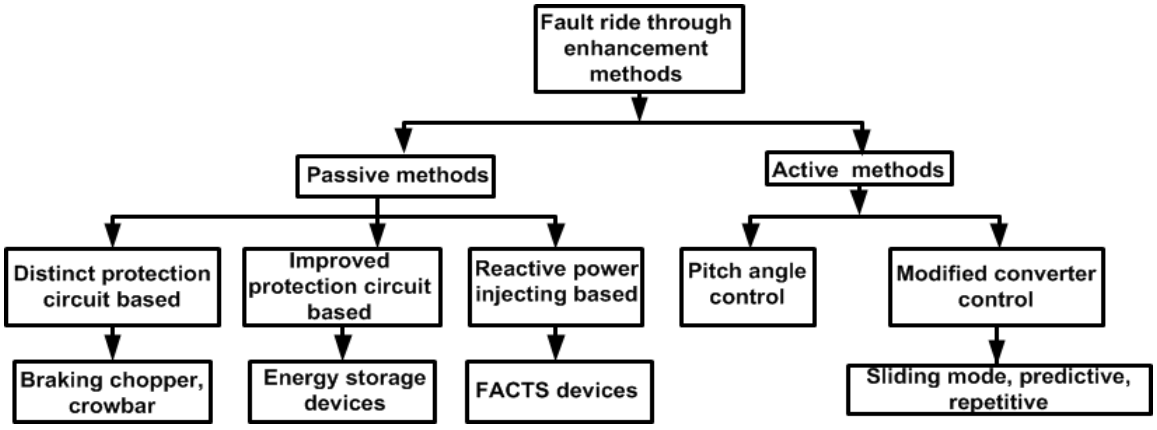

Fig.2. 2. Different FRT methods used for a PMSG based WTG

2.2.1. Passive Methods

2.2.1.1. Energy Storage Systems based Method

Nowadays energy storage systems (ESSs) are used in different applications. Wind power plants are one of the renewable power generators where the ESSs have important roles in connecting the WTGs to the grid or for a stand-alone operation. Generally, ESSs can be attached to the DC link capacitor of the back-back converter structure via a bi-directional DC-DC converter [2]. When grid fault occurs, ESSs can absorb the additional energy available at the DC-link, preventing its overvoltage. After the fault clearance, the saved energy can be injected to the grid. In addition to LVRT enhancement capability, ESSs can implement the frequency fluctuation reduction or power smoothing, peak load

shaving, time shifting and so on [3]. Based on the characteristics of different ESSs and their usage [4], quick responding energy storages like the EDLC, FESS and SMES are well suited for the LVRT capability enhancement applications. The main disadvantage of the ESS based method it it requited a large capacity of ESS when severe voltage sag occurs.

2.2.1.2. Braking Chopper based Method

In some literature, a Braking Chopper (BC) or active crowbar system is proposed to be placed with the DC-link to dissipate the excess active power during the grid faults [5], [6]. Braking chopper consists of a high-power resistor with a series switch. The advantage of this structure is low cost and simple control. The duty ratio for the BC switch is formulated based on the the DC-link voltage error after passing through a simple PI controller. BC can only dissipate active power and cannot help to inject any reactive power to the grid as it needs to dissipate all the generated active power to increase the gird side converter's reactive power injection capacity. Additionally, BC or crowbar resistance needs to be designed carefully to provide minimal consumption of energy and sufficient damping.

2.2.1.3. The DC-link Capacitor Sizing

The DC-link capacitor sizing method resembles to the crowbar configuration to some extent except that this method protects the IGBTs from overvoltage. Also, it can dissipate the excess energy without affecting the rotor currents [7].

2.2.1.4. FACTs Devices

For reactive power injection and voltage recovery at the PCC, uses of FACTs based compensation have been proposed in [8]. FACTS devices can be classified into three groups according to their connection methods: shunt connection, series connection, and hybrid connection.

2.2.1.4.1. Shunt Type Compensation

A Static Var Compensator (SVC) comprises of a mechanically switched capacitors and thyristor-controlled reactors is considered as a shunt type compensator. The reactors are variably switched into the circuit according to thyristor phase angle modulation control, providing injection (or absorption) of variable MVAR to the system. SVCs can enhance the LVRT strategy with a low cost [9].

Another shunt compensator, the STATCOM is a self-commutating VSC that converts DC voltage into three-phase AC output voltages. It is smaller, faster and has higher controllable bandwidth than the SVC. For LVRT, it injects a controllable reactive current which is independent of the grid voltage. Thus, STATCOM increases the stability margin in transient condition. In voltage sag condition, it provides more reactive power output compared to the SVC [10].

Due to the rapid improvements in power semiconductor device technology, shunt compensator like the active power filters (APF) have been considered as an effective solution to improve the power quality. The APFs use power electronic converters that insert harmonic components into the electrical network that cancel out nonlinear load harmonics [11]. With the harmonic compensating ability, APFs are also capable of reactive power control and LVRT. It works like a STATCOM to support the grid in weak voltage condition. In the development of APFs two types of converter are used. They are: current fed APF and voltage fed APF. It behaves as a non-sinusoidal current source to meet the non-linear load harmonic current requirement in current fed type load structure. Higher losses and higher values of parallel AC power capacitors make them unsuitable though they are considered sufficiently reliable. Moreover, in multistep or multilevel modes they cannot be used to enhance the performance in higher ratings. Voltage-fed PWM inverter is the other converter used in an APF. It has a self-supporting DC bus voltage with a large DC link capacitor. As it is cheaper, lighter, and expandable to

multilevel and multistep versions to increase the performance with lower switching frequencies, this structure is more dominant in the development of an AFP.

2.2.1.4.2. Series Type Compensation

As a series type compensator, TCSC works based on an effective impedance which can be increased almost immediately during a grid fault by the firing angle control of the TCSC thyristors which in turn increases the capability of power transfer. The TCSC compensates the low voltage and limits the short circuit current. Although it has a good over-current compensation capability, its operating range is limited for a wide range of use [12].

Another series compensator, SSSC, is comprised of a VSC connected in series to the PCC via a coupling transformer. An equal and opposite voltage to the DC link-voltage rise is provided by the SSSC during the low voltage dips. To provide and maintain the DC link voltage, an energy storage is required to recompensate the losses of SSSC. SSSC has a wider operating range compared to the TCSC. But its structure is complex and additional protection arrangements are needed to handle the over-currents [13].

DVR is a series type compensator which consists of a three-phase converter connected to a transformer and has a load element (or source) connected in the DC-link. The DVR produces a synchronized voltage which is the difference between the voltage prior to a fault occurrence and the fault voltage during a grid fault. The injected synchronized voltage can vary in phase and amplitude with allowed exchanges of reactive and active powers between the grid and the DVR. As the grid voltage drop is not sensed by the GSC, the DVR is not suitable for a large voltage sag because of it lacks large voltage support capability [14].

Lastly, the MERS configuration is a series compensator which is simpler as well as low cost to provide overcurrent protections with same capacitive operating range like the

SSSC to provide the LVRT. Recently, their usage is attractive as the initial ON state losses are lower with the new low-voltage on-state IGBTs [15]. For operation in single phase, it is similar to a single-phase full bridge which uses four switches. However, the capacitor size is several times smaller and the control technique is different [16].

2.2.1.4.3. Hybrid Compensation

A hybrid compensator, like the UPFC is a back-back combination of a shunt converter and a series converter that are coupled by a common DC-link. Bi-directional active power can be exchanged between the shunt terminals and series terminals of the converters. The series converter injects a voltage which has two orthogonal components. The *q*-axis component contributes in phase angle and the *d*-axis component contributes in magnitude variation. The function of shunt converter is to compensate reactive power requirements by providing the inductive or capacitive VAR or simply regulating the voltage. Therefore, UPFC can be used for the LVRT enhancement [17]. Among all the FACTS devices, hybrid compensators are good choice to provide LVRT . However, these devices incur higher cost than other methods.

2.2.1.5. Other Methods

Along with the passive methods, some other methods are used for the LVRT from a PMSG-based WECS. Most of them didn't gain much attention. Some examples are as the SDBR, an electronic OLTC and so on. The SDBR is a series connected resistor between the WECS and the PCC. In normal condition, it is short circuited but in the grid fault condition, it is brought in the main power circuit [18]. The main shortcoming of SDBR is that it is lacking the injection of reactive current to the grid same as the BC method.

An electronic OLTC based method is introduced in [19]. The tap changing transformer is same as those presently used in the grid connected WECS, however; to increase the

supply current to the desired extent, an extended tap range is set at the grid side. In the tap changing, the required speed is provided by using an electronic tap changing mechanism. which can increase the generator side voltage which helps to provide the LVRT capability.

2.2.2. Active Methods

All the passive methods mentioned in the previous sections need additional equipment which adds to the total cost of the system. Considering this drawback, many active methods for the LVRT have been proposed in the literature, specially to manage the system properly under variable wind speeds and grid fault conditions.

2.2.2.1. Control of Blade Pitch Angle (BPA)

One of the active methods is the control of the blade pitch angle. During grid faults, under voltage relay identifies the voltage sag and the pitch angle (PAC) controller is activated. As the captured wind power is directly proportional to the performance coefficient [20], the maximum performance coefficient is achieved at BPA=0 when rotational speed is optimum. For avoiding malfunction and keeping the generator speed within a safe limit, the BPA is controlled to decrease the captured wind power under cut-out or furling wind speeds. The actuators of blade pitch are powerful enough to fully pitch the blades in a short time however; during a grid fault condition, the high rate of restoring power creates a large amount of dynamic forces and stress [21]. The BPA is a relatively cheap method as it doesn't need any additional devices [22]. However, in a weak power grid, e.g., an islanded microgrid, it has some limitations as its response rate is slow, therefore, creating possible frequency deviations. As fault ride through support should be provided within 150 ms, the BPA is not a suitable solution for the stability of the weak power system. However, if it is designed properly by a suitable controller and if it is equipped with

another faster ride through strategy, then the hybrid method can satisfy the grid code requirements.

2.2.2.2. Modified Back-to-back Converter Controllers

Interfacing of power electronic converters between the grid and machine sides can be employed for LVRT capability enhancement. Each of the power converters has control loops to control some system variables like the grid voltage and grid current. In conventional methods, the grid-side-converter (GSC) controls DC-link voltage and the maximum power point tracking (MPPT) under variable wind speeds is achieved and is implemented in the machine-side-converter (MSC).

In [23], a generator de-loading approach is introduced for the LVRT. Hence, the DC-link voltage is kept within the safe limit. However, in the case of grid faults, the GSC can go out of control for the de-loading purpose.

In [24], a new control structure is introduced to provide the LVRT. In this structure, the MSC controls the DC-link voltage and the MPPT is achieved by the GSC. In this method, when voltage dips occur in the grid and DC-link voltage rises from the nominal value, wind power generation is reduced in PMSG, resulting in reduced input power to the DC-link.

In [25], LVRT capability of the structure reported in [24] is investigated by using a proportional-integral (PI) controller. Furthermore, the GSC acted as a STATCOM in the grid fault condition and is compared with the BC method with a conventional back-to-back controller. The comparison showed better performances of the proposed method.

In [26], a LVRT scheme for a PMSG based wind turbine is proposed based on the feedback linearization theory. The DC link voltage is controlled by the MSC instead of the GSC. Due to nonlinear relationship between the DC-link voltage and the reference

power, the feedback linearization was applied to enhance the LVRT capability. By applying this method, DC-link voltage overshoot is reduced. The main advantages of this new controller are the simple implementation, low cost, grid codes compliance and no use of additional devices. However, it requires further study to investigate its performances under variable wind speeds and to ensure stable operation of the WTG.

Many literatures proposed a combination of hardware modifications and control strategies. A combined control scheme for the GSC is proposed in [27] which consists of a DC circuit braking resistor, the turbine blade pitch angle and the back-back converter controls. It has been found that the controller can protect the power electronic components and mechanical part of the wind turbine during the occurrence of prolonged voltage dips. However, its feasibility is not justified experimentally.

Another solution is proposed in [28] where the MSC is configured to be a three-phase diode rectifier-based boost circuit and the VSC is used as the GSC. The boost converter is used to make the DC link voltage stable and the GSC is used to track the wind maximum power. During the voltage dips, the proposed control scheme helped the WTG to remain connected to the grid. However, it has some limitations which are related to the wind turbine speed-power characteristics and its full range of operation needs further examination. The traditional control scheme presented in [28] suffers from the usual DC-link overvoltage at the time of grid faults which can damage the MSC and the GSC.

In [29], a nonlinear controller is proposed based on the feedback linearization theory. This controller improves the conventional linear current controller's behaviour by keeping the levels of current within their acceptable limits. It is also applicable for the larger voltage dips. However, too many sensing variables and complex mathematical algorithm make its implementation difficult.

The work presented in [30] suggests a nonlinear controller to maintain the currents within the design limits. Like [29], this controller is based on the feedback linearization theory and through a sliding mode approach it is applied to the system. It is robust against the system uncertainties and perturbations. The suggested approach overcomes the usual feedback linearization controller's shortcomings however still needs complex implementations. A new control scheme based on the CSC is developed in [31] for the LVRT. It does not need any external braking resistors or energy storage devices. A unified DC-link current controller is developed to maintain the DC-link current in the within the acceptable range; thus, it can support to recovery of the grid voltage.

However, at MW level this technique presents several technical and operational issues such as the unsymmetrical performance characteristics due to the predominant nonlinear nature of the power converters and a sluggish transient response due to the low bandwidth in the modulation stage [32].

Recently, finite-control-set based model predictive control (FCS-MPC) strategy [33] is used as a simple and promising alternative to control the power electronic converters. This method eliminates the need for linear regulators and modulators. The FCS-MPC is a nonlinear control method and provides an approach which is better suited to control the power converters while mitigating the the disadvantages associated with the classical linear regulators [34]. The FCS-MPC approach for the LVRT enhancement for the grid-connected WECS were studied in [34] and [35] through simulation results. However, the generator-side converter control and complete WECS response during the grid voltage dips were not analysed.

For many grid codes, LVRT requirements under asymmetrical grid faults are still under discussion and consideration. In the draft grid code "SDLWindV" of Germany, WECSs are required to inject positive-sequence reactive current during asymmetrical grid faults,

which represents the future trends of the LVRT requirements under the asymmetrical faults. In [36], a control method to feed the positive-sequence reactive current without minimizing the oscillation of DC link voltage is proposed. The proposed scheme is expected to help PMSG-based WECSs to meet the new LVRT requirements for the asymmetrical faults.

Table 2.1 summarizes a comparison between the mentioned methods based on technical parameters. From Table 2.1 it is found that some LVRT methods are more expensive than other due to their power electronic switches, coupling transformer, magnetic inductance, high power resistance, super capacitors etc. In conclusion, the modified controllers are more economic LVRT methods as they do not use any additional devices.

Table 2.1: Comparison of LVRT methods

Methods	Cost	Complexity	DC link overvoltage	Reactive current injection	Additional devices
PAC	Low	Low	Yes	Medium	No
ESS(EDLC)	High	Medium	No	Medium	Yes
BC	Medium	Medium	No	Medium	Yes
FACTS(DVR)	High	High	No	Good	Yes
SDBR	Medium	Medium	No	Low	Yes
De-loading loop	Low	Low	No	Medium	No
New controller	Low	medium	No	Good	No

It is also evident from the literature review that in most cases single controller is not able to provide enough LVRT support. So, the researchers are now more focused on developing hybrid controllers to improve the LVRT performance of grid connected WECS.

Different coordinated controllers such as the use of pitch angle control combined with an unloading circuit have been proposed in [37]. Hybrid controllers based on the PI and fuzzy logic control for the FRT has been developed in [38]. However, the operation cost and maintenance difficulty are higher for these controllers. Coordinated control of pitch angle and braking chopper is presented in [39]. This type of arrangements requires additional devices that can decrease the system reliability as well as increase the system cost. Power coordinated control of WTGs is studied in [40]. Although the extra circuits are not necessary in this structure, it is not capable to inject enough reactive power to support the grid voltage under a grid fault. Moreover, its feasibility under the asymmetrical faults is not verified. Therefore, it is necessary to develop and implement a complete coordinated control which can support the FRT for both the symmetrical and asymmetrical grid fault scenarios.

Flux weakening control [41] is an established technique for motor drives. However; its application to provide LVRT for a PMSG based WECS is not reported exclusively in any literature so far. For the flux weakening region, it is required to impose design limits on the currents and voltages of the converter and the generator. The voltage limit is usually selected based on the generator's rated voltage or the DC link capacitor's rated voltage. So, the flux weakening control of the PMSG based WECS can be used to limit the DC link overvoltage during the symmetrical and asymmetrical grid voltage dips. Taking this concept for implementation, a flux weakening control method is adopted in this PhD work to minimize the DC link overvoltage.

The operating mode of a pitch angle controller can be modified and adjusted to smooth the wind output power fluctuations as well as it can be used for the DC link voltage control. Overall, an accurate control of the DC-link voltage and a quick injection of reactive power, and a fast responding pitch angle controller are necessary and should be coordinated to enhance the LVRT performance.

Therefore, this PhD research is focused on developing a new coordinated control method to improve the FRT capability as well as the transient stability of the PMSG based variable speed WTG. The proposed coordinated control consists of a pitch angle control, a flux weakening control and a reactive power control which will be described in detail in the coming chapters.

2.3. Frequency Control Strategies

The load frequency control (LFC) is very important to maintain stable power system dynamics and operations during the load variations and grid faults. Various LFC methods are reported in the literature.

With the conventional MPPT control, grid-frequency deviations above the maximum is allowed by the grid codes in some countries while WECS is connected to the grid. In countries like China about 27% of yearly wind energy is curtailed as many of the wind farms operated with the MPPT control without a frequency regulation [42], [43]. In the past, wind farms are disconnected during severe frequency deviations. However, modern control methods which are developed based on the inertia emulation and droop control are suitable to withstand [44] the high impact of frequency deviations during critical state of transients.

Grid connection requirements have introduced regulations to support grid frequency from the WTG. For example, if the grid frequency goes above 50.2 Hz, the active power of wind farms must be reduced with a gradient of 40% of the power available per Hz [45]. At that point, a 10% ramp rate of grid capacity per minute is accepted [46].

In case of grid frequency deviations, most of the recommended approaches [47], [48], [49] use the stored kinetic energy in the rotating mass of the WTG to deliver additional power to the system. Over frequency occurs due to a surplus in generated power compared to the load demand and the under frequency occurs due to a shortage in the power

generation. Therefore, a frequency maintaining power reserve is necessary within the WECS to operate the power systems without large frequency deviations in a power system with high wind power penetration. A combination of the pitch angle control and speed control has been used to retain this power reserve subject to the operating points. The range of operations can be distributed into low, medium, and high-wind-speed regions [50].

Due to the intermittent nature and fluctuation of wind speeds and powers, the LFC problem becomes complex with the grid connected WECS. In such cases, the LFC needs to be addressed with a complementary technology. The dynamics of WECS are related to the LFC and are discussed [51]. In [52], a modification in economic dispatch, unit commitment, frequency controls and regulation at the significant level of capacity of the wind generation has been presented. A study to analyse the effects of small wind turbines output on the LFC is presented in [53]. It is observed from [53] that the uncontrollable load variations cannot be compensated if these occur at a rate faster than the system's response rate.

In [54], a self-excited induction generator-based WTG with an isolated resistive load is considered for constant voltage, variable speed and constant frequency power supply. A simplified model has been developed based on a control strategy to maintain the constant frequency and the terminal voltage of generator in under variable wind speeds or load variations. However, it considered only the resistive load. LFC or active power sharing in the HVDC connected wind farms during generation or load changes of the system is illustrated in [55]. It introduces a coordinated control but its application in real system is not verified.

In [56], with a load estimation and a BESS based frequency control method is discussed. The deviation of frequency in low and high frequency domains are reduced by the WTGs

using a pitch angle and the charge/discharge control of the BESS. However, the use of BESS makes the controller complex and also increases the system cost.

Frequency regulation via the speed control of WTG is presented in [57]-[59]. The proposed methods are effective however; the controllers can be modified to achieve better damping for the oscillations.

In [60], H_∞ control based on the droop characteristics is used for the frequency control along with the parallel operation of batteries. Though droop control is improved however, this method is based on heuristic assumptions.

In [61], a robust fuzzy logic based PID controller with PSO optimization is proposed in isolated diesel-wind hybrid power system. For this hybrid system, frequency controller design of the SMES with a loop shaping and GA based tuning of controller parameters is discussed in [62]. Though the optimization techniques provide good response, however the control system becomes complicated.

In [63], the variations of load power demand are successfully met by the WTG's output power with the energy stored or released from the ESS. Also, the frequency deviations are suitably controlled within a small range.

In [64], the wind power generation and integration effects on the control of power system frequency is discussed. Coordination control of the WTG and the electric double layer capacitor (EDLC) for LFC in an autonomous hybrid renewable energy system is presented in [65]. The use of EDLC increases the system cost significantly.

In [66], the frequency control based on the MPC with an ESS is investigated with real measurements from the power grid. Two frequency control strategies have been discussed in [67] for variable speed and variable pitch WTGs. The first one is built on the de-loading for wind speed control to avoid the converter over loading and second one uses a pitch-

controlled de-loading for fast LFC action. Coordinated control of the TCPS and SMES for LFC is proposed in [68] for doubly fed induction generators.

Fuzzy logic controller is proposed in [69] to control system frequency for a three-area interconnected power system. A mathematical modelling is built in [70] with regards to numerous types of wind generators dependency for variations of system frequency. These models are then executed in a Newton Raphson-based power flow algorithm with frequency control devices. It can estimate the steady state operating point after frequency regulation. However, the considered index can measure frequency disturbances only at one node and is not enough to reflect the frequency deviations for different nodes.

With several controllable loads, a supplementary LFC method is suggested in [71]. In [72], discussions about the controllable loads and a cogeneration unit for LFC is carried. With the autonomous distributed vehicle for grid frequency control creating a distributed spinning reserve is proposed in [73].

Another accumulated electric vehicle-based battery storage demonstrating vehicle to grid system is proposed in [74] for frequency control. However, the implementation of these strategies [72]- [74] might increase computational complexity and more attention should be given to maintain the frequency control signals for different power nodes.

In [75], a separate frequency control unit to control the voltage and frequency of a variable speed WECS is suggested. The unit consists of a dump load, phase locked loop (PLL) and a proportional derivative controller. Though the control provides a good frequency response, however; it is not validated for a real system.

In [76], primary LFC (PLFC) is embedded in the PMSG control system. The PLFC is developed based on the control of the kinetic energy stored in rotational mass of the wind turbine. It can be achieved by a power output reference control of the PMSG, hence the fluctuations of frequency can be decreased.

In [77] a PID type fuzzy controller is considered for frequency control to avoid slow oscillating responses and complex equations associated with the conventional PID controllers. The controller is robust, and the response is adequate. However, this is not verified by experimental results.

The physical inertia of the wind power system plays a vital role as it relates to the sensitivity to the frequency under unbalancing of power; when variations of load or generation appear in the power system if the system inertia is low, the rate of frequency change is high. An electrical decoupling is created between the grid and the machine by the intermediate DC link bus [78]. Such decoupling leads to a lower participation of the kinetic energy stored in the wind power system for grid frequency control. With a properly implemented machine side control, it can be compensated.

In [79], energy storage based primary frequency controls are presented. It is observed that by controlling generator torque, the power reserve can be obtained for frequency control. This method also permits some contribution to this power reserve by using a portion of the kinetic energy available in the wind turbine blade inertia. In [80], frequency control is managed by using controllable loads. The controllable load is used to maintain the load demand-power supply balance by suppressing the frequency deviations. The frequency control is achieved by controlling the active power of the inverters connected to the controllable loads.

[81] presented a frequency regulation method by a coordination control of the WTG and a battery. It estimated the load by using a disturbance observer in a small power system. The load variation is reduced in the low frequency domain by a pitch angle control and by the battery charge/discharge actions in high frequency domain. The battery output command is determined according to the estimated load, percentage of the state of charge (SoC) of the battery and the high frequency component of the frequency deviations. As the system cost is high, a cost-effective control strategy should be preferred. Different

frequency control methods are summarized in Table 2.2 and their characteristics, advantages and disadvantages are compared.

Table 2.2: Comparison of different frequency control methods

Control methods		Advantages	Disadvantages	Primary control	Secondary control
Inertial [44]	1.Hidden inertia	Simple,	Slow	Yes	-
	2.Fast power reserve	Compensate power loss	Need accurate model	Yes	-
Droop [44]		Flexibility, economic	Slow, poor harmonic sharing	Yes	-
De loading [67]	1.Pitch control	Simple, provide high reserve	Slow response	Yes	-
	2.Speed control	Fast, Provide high reserve	Rotor speed increase	Yes	-
Wind farm level	1.Local control	High response	Need energy storage	Yes	-
	2.Central control	Dynamic response high	Complex	-	Yes
Power system level [65], [77], [79], [81]	1.Wind-Thermal Coordination Control	Better frequency behaviour	Complex structure	-	Yes
	2.Wind Power Penetration Impact on Frequency Stability	Can be used in large scale	Response time slow	-	Yes

From the frequency control literature reviews, it is evident that the inertia emulation and energy storage devices could be better choices for frequency control PMSG based WECS. Though the traditional battery is popular, its efficiency is still somehow low, and its cost is high, especially for larger capacity. Therefore, as a cost-effective solution a

SMES is adopted in this PhD research to provide the better efficiency. Moreover, the system frequency is regulated by controlling the PMSG flux linkage. Based on these ideas, two frequency regulation approaches are developed in this research to regulate the usual frequency deviations as well as frequency deviations after the grid fault recovery.

2.4. Summary

The literature review presented in this chapter clearly shows that so many control methods are developed to mitigate the grid fault related issues. Different configurations of FRT techniques are discussed from where the active method is considered for its effectiveness to improve the FRT performance. The hybrid configuration of the control methods can be an attractive choice among the active methods.

Considering the state-of-the-art research on the FRT and frequency control, a coordination of the flux weakening controller, a reactive power control and a pitch angle controller is proposed as an effective solution in this PhD research for improving LVRT performance during the symmetrical and asymmetrical grid faults. Moreover, by providing an inertia support, a PMSG flux linkage control and by using the SMES, frequency stability of the power system with the grid connected WECS are improved.

REFERENCES

[1] T. H. Nguyen and D.-C. Lee, "Ride-through technique for pmsg wind turbines using energy storage systems," *Journal of Power Electronics,* vol. 10, pp. 733-738, 2010.

[2] F. Díaz-González, A. Sumper, O. Gomis-Bellmunt, and R. Villafáfila-Robles, "A review of energy storage technologies for wind power applications," *Renewable and Sustainable Energy Reviews,* vol. 16, pp. 2154-2171, 2012.

[3] S. Tohidi and M.-i. Behnam, "A comprehensive review of low voltage ride through of doubly fed induction wind generators," *Renewable and Sustainable Energy Reviews,* vol. 57, pp. 412-419, 2016.

[4] Y. Li, Y.-n. Chi, and Z. Wang, "Study of LVRT capability of D-PMSG based Wind turbine," in *Power Engineering and Automation Conference (PEAC). Wuhan, China: IEEE*, 2011, pp. 154-157.

[5] Z. Qiu, K. Zhou, and Y. Li, "Modeling and control of diode rectifier fed PMSG based wind turbine," in *Electric Utility Deregulation and Restructuring and Power Technologies (DRPT), 2011 4th International Conference on*, 2011, pp. 1384-1388.

[6] S. Muyeen, R. Takahashi, T. Murata, J. Tamura, M. Ali, Y. Matsumura*, et al.*, "Low voltage ride through capability enhancement of wind turbine generator system during network disturbance," *IET Renewable Power Generation,* vol. 3, pp. 65-74, 2009.

[7] M. Singh, V. Khadkikar, and A. Chandra, "Grid synchronisation with harmonics and reactive power compensation capability of a permanent magnet synchronous generator-based variable speed wind energy conversion system," *IET Power Electronics,* vol. 4, pp. 122-130, 2011.

[8] H.-p. Li and J.-m. Yang, "The performance research of large scale wind farm connected to external power grid," in *Power Electronics Systems and Applications, 2009. PESA 2009. 3rd International Conference on*, 2009, pp. 1-5.

[9] M. M. Chowdhury, M. E. Haque, A. Gargoom, and M. Negnevitsky, "A direct drive grid connected wind energy system with STATCOM and super-capacitor energy storage," in *2012 IEEE International Conference on Power System Technology (POWERCON),* pp. 1-6.

[10] N. Hasegawa and T. Kumano, "Low voltage ride-through capability improvement of wind power generation using dynamic voltage restorer," in *Proceedings of the 5th IASME/WSEAS International Conference on Energy: Environment*, 2010, pp. 166-171.

[11] E. Larsen, K. Clark, S. Miske, and J. Urbanek, "Characteristics and rating considerations of thyristor-controlled series compensation," *IEEE Transactions on Power Delivery,* vol. 9, pp. 992-1000, 1994.

[12] S. Zhang, K.-J. Tseng, S. S. Choi, and T. D. Nguyen, "Advanced control of series voltage compensation to enhance wind turbine ride through,"*IEEE Transactions on Power Electronics,* vol. 27, pp. 763-772, 2012.

[13] M. N. Eskander and S. I. Amer, "Mitigation of voltage dips and swells in grid-connected wind energy conversion systems," *IETE Journal of Research,* vol. 57, pp. 515-524, 2011.

[14] G. Wenming, W. Yun, H. Shuju, and X. Honghua, "A survey on recent low voltage ride-through solutions of large scale wind farm," in *2011 Asia-Pacific*, *Power and Energy Engineering Conference (APPEEC),* 2011, pp. 1-5.

[15] S. Raphael and A. Massoud, "Unified power flow controller for low voltage ride through capability of wind-based renewable energy grid-connected systems," in

*2011 8th International Multi-Conference on Systems, Signals and Devices (SSD),*2011, pp. 1-6.

[16] A. Causebrook, D. J. Atkinson, and A. G. Jack, "Fault ride-through of large wind farms using series dynamic braking resistors (March 2007)," *IEEE Transactions on Power Systems,* vol. 22, pp. 966-975, 2007.

[17] D. Ramirez, S. Martinez, C. Carrero, and C. A. Platero, "Improvements in the grid connection of renewable generators with full power converters," *Renewable Energy,* vol. 43, pp. 90-100, 2012.

[18] A. K. Thet and H. Saitoh, "Pitch control for improving the low-voltage ride-through of wind farm," in *Transmission & Distribution Conference & Exposition: Asia and Pacific, 2009*, 2009, pp. 1-4.

[19] Y. Xiao-ping, D. Xian-feng, F. Fan, and T. Lu-lin, "Low voltage ride-through of directly driven wind turbine with permanent magnet synchronous generator," in *Asia-Pacific Power and Energy Engineering Conference, 2009*, pp. 1-5.

[20] M. Nasiri, J. Milimonfared, and S. Fathi, "A review of low-voltage ride-through enhancement methods for permanent magnet synchronous generator-based wind turbines," *Renewable and Sustainable Energy Reviews,* vol. 47, pp. 399-415, 2015.

[21] O. A. Lara, N. Jenkins, J. Ekanayake, P. Cartwright, and M. Hughes, "Wind energy generation modeling and control," *A John Wiley and Sons, Ltd,* 2009.

[22] G. Michalke, A. D. Hansen, and T. Hartkopf, "Control strategy of a variable speed wind turbine with multipole permanent magnet synchronous generator," in *2007 European Wind Energy Conference and Exhibition*, 2007.

[23] H. Geng, G. Yang, D. Xu, and B. Wu, "Unified power control for PMSG-based WECS operating under different grid conditions," *IEEE Transactions on Energy Conversion,* vol. 26, pp. 822-830, 2011.

[24] K.-H. Kim, Y.-C. Jeung, D.-C. Lee, and H.-G. Kim, "LVRT scheme of PMSG wind power systems based on feedback linearization," *IEEE Transactions on Power Electronics,* vol. 27, pp. 2376-2384, 2012.

[25] J. Conroy and R. Watson, "Low-voltage ride-through of a full converter wind turbine with permanent magnet generator," *IET Renewable Power Generation,* vol. 1, pp. 182-189, 2007.

[26] F. Deng and Z. Chen, "Low-voltage ride-through of variable speed wind turbines with permanent magnet synchronous generator," in *Industrial Electronics, 2009. IECON'09. 35th Annual Conference of IEEE*, 2009, pp. 621-626.

[27] A. Mullane, G. Lightbody, and R. Yacamini, "Wind-turbine fault ride-through enhancement,"*, IEEE Transactions on Power Systems,* vol. 20, pp. 1929-1937, 2005.

[28] J. Matas, M. Castilla, J. M. Guerrero, L. Garcia De Vicuna, and J. Miret, "Feedback linearization of direct-drive synchronous wind-turbines via a sliding mode approach," *Power Electronics,* vol. 23, pp. 1093-1103, 2008.

[29] J. Dai, D. Xu, B. Wu, and N. R. Zargari, "Unified DC-link current control for low-voltage ride-through in current-source-converter-based wind energy conversion systems," *IEEE Transactions on Power Electronics,* vol. 26, pp. 288-297, 2011.

[30] V. Yaramasu, B. Wu, S. Alepuz, and S. Kouro, "Predictive Control for Low Voltage Ride-Through Enhancement of Three-Level Boost and NPC Converter based PMSG Wind Turbine," *IEEE Transactions on Industrial Electronics*, vol.61, no. 12, December 2014.

[31] S. Kouro, P. Cortés, R. Vargas, U. Ammann, and J. Rodríguez, "Model predictive control—A simple and powerful method to control power converters," *IEEE Transactions on Industrial Electronics,* vol. 56, pp. 1826-1838, 2009.

[32] M. Rivera, V. Yaramasu, A. Llor, J. Rodriguez, B. Wu, and M. Fadel, "Digital predictive current control of a three-phase four-leg inverter," *IEEE Transactions on Industrial Electronics,* vol. 60, pp. 4903-4912, 2013.

[33] V. Yaramasu, B. Wu, M. Rivera, and J. Rodriguez, "Enhanced model predictive voltage control of four-leg inverters with switching frequency reduction for standalone power systems," in *2012 15th International Power Electronics and Motion Control Conference (EPE/PEMC),*2012, pp. DS2c. 6-1-DS2c. 6-5.

[34] S. Alepuz, S. Busquets-Monge, J. Bordonau, P. Cortes, J. Rodriguez, and R. Vargas, "Predictive current control of grid-connected neutral-point-clamped converters to meet low voltage ride-through requirements," in *Power Electronics Specialists Conference, PESC 2008*, pp. 2423-2428.

[35] S. Alepuz, S. Busquets-Monge, J. Bordonau, P. Cortés, and S. Kouro, "Control methods for low voltage ride-through compliance in grid-connected NPC converter-based wind power systems using predictive control," in *Energy Conversion Congress and Exposition, ECCE* 2009, pp. 363-369.

[36] Y. Guo, H. Geng, and G. Yang, "LVRT capability and improved control scheme of PMSG-based WECS during asymmetrical grid faults," in *IECON,39th Annual Conference of the IEEE*, 2013, pp. 5294-5299.

[37] J.Conroy and R. Watson, "Low-voltage ride-through of a full converter wind turbine with permanentmagnet generator," *IET Renewable Power Generation*, vol. 1, pp. 182-189, 2007.

[38] M.Q.Duong, F. Grimaccia, S. Leva, M. Mussetta, and K. H. Le, "Hybrid controller for transient stability in wind generators," in *Power Systems Conference (PSC)*, Clemson University, 2015, pp. 1-7.

[39] A. Uehara, A. Pratap, T. Goya, T. Senjyu, A. Yona, N. Urasaki, et al., "A coordinated control method to smooth wind power fluctuations of a PMSG-based WECS," *IEEE Transactions on Energy Conversion*, vol. 26, pp. 550-558, 2011.

[40] Z. Liu, C. Liu, and G. Li, "Power coordinated control of wind turbines with permanent magnet synchronous generator for low voltage ride through," in *IEEE PES General Meeting| Conference & Exposition*, 2014, pp. 1-5.

[41] M. Li, "*Flux-Weakening Control for Permanent-Magnet Synchronous Motors Based on Z-Source Inverters"*, December 2014.

[42] Z.-S. Zhang, Y.-Z. Sun, J. Lin, and G.-J. Li, "Coordinated frequency regulation by doubly fed induction generator-based wind power plants," *IET Renewable Power Generation,* vol. 6, pp. 38-47, 2012.

[43] X. Zhang, H. Li, and Y. Wang, "Control of DFIG-based Wind Farms for Power Network Frequency Support," *International Conference on Power System Technology (POWERCON)*, 2010.

[44] J. Morren, S. W. De Haan, W. L. Kling, and J. Ferreira, "Wind turbines emulating inertia and supporting primary frequency control," *IEEE Transactions on Power Systems,* vol. 21, pp. 433-434, 2006.

[45] Grid Code: High and Extra High Voltage, E. ON Netz GmbH, Bayreuth, Germany, 2006.

[46] R. Cardenas, R. Pena, S. Alepuz, G. Asher, "Overview of control systems for the operation of DFIGs in wind energy applications", *IEEE Transaction on Industrial Electronics*, vol. 60, no. 7, pp. 2776-2798, Jul. 2013.

[47] X. Zhu, Y. Wang, L. Xu, X. Zhang, and H. Li, "Virtual inertia control of DFIG-based wind turbines for dynamic grid frequency support," in *IET Conference on Renewable Power Generation (RPG 2011),*2011, pp. 1-6.

[48] D. Gautam, L. Goel, R. Ayyanar, V. Vittal, and T. Harbour, "Control strategy to mitigate the impact of reduced inertia due to doubly fed induction generators on large power systems," *IEEE Transactions on Power Systems,* vol. 26, pp. 214-224, 2011.

[49] I. D. Margaris, S. A. Papathanassiou, N. D. Hatziargyriou, A. D. Hansen, and P. Sorensen, "Frequency control in autonomous power systems with high wind power penetration," *IEEE Transactions on Sustainable Energy,* vol. 3, pp. 189-199, 2012.

[50] C. Evangelista, P. Puleston, F. Valenciaga, and L. M. Fridman, "Lyapunov-designed super-twisting sliding mode control for wind energy conversion optimization," *IEEE Transactions on Industrial Electronics,* vol. 60, pp. 538-545, 2013.

[51] S. Javid, R. Hauth, T. Younkins, T. Reddoch, and P. Barnes, "A method for determining how to operate and control wind turbine arrays in utility systems," *IEEE Transactions on Power Apparatus and Systems,* pp. 1335-1341, 1985.

[52] R. Schlueter, G. Park, M. Lotfalian, H. Shayanfar, and J. Dorsey, "Modification of power system operation for significant wind generation penetration," *IEEE Transactions on Power Apparatus and Systems,* pp. 153-161, 1983.

[53] D. H. Curtice and T. Reddoch, "An assessment of load frequency control impacts caused by small wind turbines," *IEEE Transactions on Power Apparatus and Systems,* pp. 162-170, 1983.

[54] Y. Üçtuğ and M. Demirekler, "Modelling, analysis and control of a wind-turbine driven self-excited induction generator," in *IEE Proceedings on Generation, Transmission and Distribution*, 1988, pp. 268-275.

[55] L. Fan, Z. Miao, and D. Osborn, "Wind farms with HVDC delivery in load frequency control," *IEEE Transactions on Power Systems,* vol. 24, pp. 1894-1895, 2009.

[56] A. Uehara, T. Senjyu, A. Yona, and T. Funabashi, "A frequency control method by wind farm & battery using load estimation in isolated power system," *International Journal of Emerging Electric Power Systems,* vol. 11, 2010.

[57] B. Singh and G. K. Kasal, "Voltage and frequency controller for a three-phase four-wire autonomous wind energy conversion system," *IEEE Transactions on Energy Conversion,* vol. 23, pp. 509-518, 2008.

[58] T. Senjyu, M. Tokudome, A. Uehara, T. Kaneko, A. Yona, H. Sekine*, et al.*, "A new control methodology of wind farm using short-term ahead wind speed prediction for load frequency control of power system," in *Power and Energy Conference, PECon, 2008,* pp. 425-430.

[59] J. M. Mauricio, A. Marano, A. Gómez-Expósito, and J. L. Martinez Ramos, "Frequency regulation contribution through variable-speed wind energy conversion systems," *IEEE Transactions on Power Systems,* vol. 24, pp. 173-180, 2009.

[60] T. Goya, E. Omine, Y. Kinjyo, T. Senjyu, A. Yona, N. Urasaki*, et al.*, "Frequency control in isolated island by using parallel operated battery systems applying H∞ control theory based on droop characteristics," *IET Renewable Power Generation,* vol. 5, pp. 160-166, 2011.

[61] C. Chokpanyasuwan, S. Pothiya, S. Anantasate, W. Pattaraprakorn, and P. Bhasaputra, "Robust Fuzzy logic-PID controller for wind-diesel power system using particle swarm optimization," *In Proceedings of GMSARN International*

Conference on Sustainable Development, Kunming, China, 12–14 November 2008, pp. 1–4.

[62] I. Ngamroo, "Robust frequency control of wind-diesel hybrid power system using superconducting magnetic energy storage," *International Journal of Emerging Electric Power Systems,* vol. 10, 2009.

[63] D.-J. Lee and L. Wang, "Small-signal stability analysis of an autonomous hybrid renewable energy power generation/energy storage system part I: time-domain simulations," *IEEE Transactions on Energy Conversion,* vol. 23, pp. 311-320, 2008.

[64] R. Doherty, A. Mullane, G. Nolan, D. J. Burke, A. Bryson, and M. O'Malley, "An assessment of the impact of wind generation on system frequency control," *IEEE Transactions on Power Systems,* vol. 25, pp. 452-460, 2010.

[65] M. Nayeripour, M. Hoseintabar, and T. Niknam, "Frequency deviation control by coordination control of FC and double-layer capacitor in an autonomous hybrid renewable energy power generation system," *Renewable Energy,* vol. 36, pp. 1741-1746, 2011.

[66] M. Khalid and A. Savkin, "An optimal operation of wind energy storage system for frequency control based on model predictive control," *Renewable Energy,* vol. 48, pp. 127-132, 2012.

[67] P. Moutis, S. A. Papathanassiou, and N. D. Hatziargyriou, "Improved load-frequency control contribution of variable speed variable pitch wind generators," *Renewable Energy,* vol. 48, pp. 514-523, 2012.

[68] P. Bhatt, S. Ghoshal, and R. Roy, "Coordinated control of TCPS and SMES for frequency regulation of interconnected restructured power systems with dynamic

participation from DFIG based wind farm," *Renewable Energy,* vol. 40, pp. 40-50, 2012.

[69] H. Bevrani and P. R. Daneshmand, "Fuzzy logic-based load-frequency control concerning high penetration of wind turbines," *IEEE Systems Journal,* vol. 6, pp. 173-180, 2012.

[70] L. M. Castro, C. R. Fuerte-Esquivel, and J. H. Tovar-Hernández, "Solution of power flow with automatic load-frequency control devices including wind farms," *IEEE Transactions on Power Systems,* vol. 27, pp. 2186-2195, 2012.

[71] T. Masuta and A. Yokoyama, "Supplementary load frequency control by use of a number of both electric vehicles and heat pump water heaters," *IEEE Transactions on Smart Grid,* vol. 3, pp. 1253-1262, 2012.

[72] M. D. Galus, S. Koch, and G. Andersson, "Provision of load frequency control by PHEVs, controllable loads, and a cogeneration unit," *IEEE Transactions on Industrial Electronics,* vol. 58, pp. 4568-4582, 2011.

[73] Y. Ota, H. Taniguchi, T. Nakajima, K. M. Liyanage, J. Baba, and A. Yokoyama, "Autonomous distributed V2G (vehicle-to-grid) satisfying scheduled charging," *IEEE Transactions on Smart Grid,* vol. 3, pp. 559-564, 2012.

[74] J. R. Pillai and B. Bak-Jensen, "Integration of vehicle-to-grid in the western Danish power system," *IEEE Transactions on Sustainable Energy,* vol. 2, pp. 12-19, 2011.

[75] Y. Oğuz, İ. Güney, and H. Çalık, "Power quality control and design of power converter for variable-speed wind energy conversion system with permanent-magnet synchronous generator," *The Scientific World Journal,* vol. 2013, 2013.

[76] M. Rosyadi, A. Umemura, R. Takahashi, and J. Tamura, "Damping Load Frequency in Multi-area Power System using Wind Farm Cooperated Primary Load Frequency Control," 3rd *Renewable Power Generation Conference* (RPG 2014), pp.1-6.

[77] F. Ronilaya and H. Miyauchi, "Frequency and voltage control for an autonomous distributed variable-speed wind turbine based on a PID-type fuzzy controller with battery support," *International Review on Modelling and Simulations (IREMOS),* vol. 7, pp. 271-278, 2014.

[78] B. Bousseau, R. Belhomme, E. Monnot, N. Laverdure, D. Boëda, D. Roye*, et al.*, "Contribution of windfarms to ancillary services," in *CIGRE 2006*, 2006.

[79] M. El Mokadem, V. Courtecuisse, C. Saudemont, B. Robyns, and J. Deuse, "Experimental study of variable speed wind generator contribution to primary frequency control," *Renewable Energy,* vol. 34, pp. 833-844, 2009.

[80] A. Pratap, N. Urasaki, and T. Senjyu, "Instantaneous frequency and voltage control of PMSG-based WECS using controllable load," in *IEEE 10th International Conference on Power Electronics and Drive Systems (PEDS),*2013, pp. 468-473.

[81] A. Uehara, T. Senjyu, A. Yona, and T. Funabashi, "Frequency control by coordination control of WTG and battery using load estimation," in *International Conference on Power Electronics and Drive Systems, 2009.*, pp. 216-221.

CHAPTER THREE

DC LINK OVERVOLTAGE MINIMISATION UNDER GRID FAULTS

3.1. Introduction

This chapter presents the grid connected WECS with back to back converter topology considering different aspects of power circuit parameters selection. Here, for the DC link overvoltage minimization, as a novel control application, the flux weakening controller is proposed. The proposed method is developed based on the synchronous and stationary reference frame current controllers. A comparative analysis of these current controllers has been presented with time series simulation results. Then on the basis of these results, the effective flux weakening controller is selected. Furthermore, the selected controller is compared with the conventional Braking Chopper (BC) method for DC link overvoltage minimization.

3.2. PMSG based WECS Modelling and Controller Design

3.2.1. Back to Back Converter Modelling and Design

A VSC based PMSG wind turbine comprises mostly of three parts: a wind turbine, a PMSG, and VSCs. VSC configuration is based on back to back converter topology as shown in Fig.3.1. In the turbine drive train, the wind turbine rotor blades catch wind energy which is then transferred to the generator. The generator is a standard permanent magnet synchronous machine, converts mechanical energy into electrical energy. Through a frequency converter its stator windings are attached with the grid. Two current-regulated voltage-source PWM converters build the frequency converter: a MSC and a GSC, with a DC voltage link in between these two.

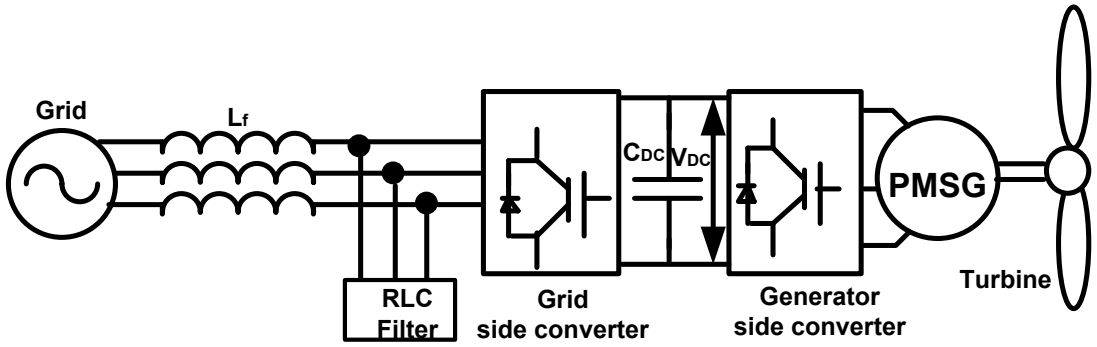

Fig.3. 1. Grid connected PMSG wind energy system with back to back converter

The grid side voltage is *d*-axis oriented; hence voltage of *q*-axis is zero.

The power circuit is designed based on the following main parameters:

a) Filter inductor selection, L_f

b) DC side capacitor selection, C_{DC}

c) DC side capacitor voltage selection, V_{DC}

These components are designed by consider:

a) Source voltage should be sinusoidal

b) The distortion of source line current is assumed around 5% to select inductor, L_f

c) The switching frequency is chosen such a way that it can compensate the highest order of harmonics

d) To ensure good filtering inverter output current and voltage should maintain a certain level of voltage and current ripples

3.2.2.1. Selection of L_f

For selection of the proper inductor value, the main criterion is to choose the peak ripple current [1], [2]. To calculate the ripple current, resistance of inductor is not considered [3]. The required inductance is given by

$$L_F = \frac{V_S}{2\sqrt{6} f_s \Delta I_{f(p-p)\max}} \tag{3.1}$$

Where $\Delta I_{f(p-p)\max}$ = 15% of peak current for compensation. The high frequency

harmonics as well as low frequency harmonics can be can be compensated with the output filter inductor.

3.2.1.2. Selection of DC Side Capacitor, C_{DC}

The instantaneous power flow principle is used for the DC side capacitor design [4]. Value of C_{DC} can be selected by decreasing the ripple of voltage. C_{DC} can be found from equation:

$$C_{DC} = \frac{\Pi \times I_{f,rated}}{\sqrt{3} \times \omega \times V_{DC,(p-p)\max}} \tag{3.2}$$

Where, $V_{DC(p-p)\max}$ is the peak to peak ripple voltage and $I_{f,\ rated}$ is the rated injecting current.

3.2.1.3. Capacitor Voltage Estimation, V_{DC}

Two main purposes are served by the DC side capacitor which is to maintain DC voltage with fewer distortions and to maintain real power balance between generation and demand during steady and transient period [5].

During normal condition, the real power demand and supply between source and load is equal. The balance of real power between source and demand will be disturbed if the condition of demand is changed. The DC capacitor voltage is changed for this and it is away from reference.

The DC link voltage value confirms that the converter supply current time derivatives are required to compensate the selected harmonics. Based on this, the voltage of DC link capacitor equation is as:

$$V_{DC} = \frac{2\sqrt{2}V_s}{1.155} \tag{3.3}$$

The voltage value is preferred for a nonlinear load and it is based on the rated load power and the compensated maximum distortion [5]. According to the system capacity, it is chosen as

$$V_S < V_{DC} \leq 2V_S$$

3.2.2. Design of Shunt Passive Filter

Shunt passive filter plays a role to eliminate harmonics current from the source [6]. A single tuned passive filter has been chosen in this system. It is designed to trap the harmonics by adding reactor X_L=X_C at the tuned frequency. The data required for this design and the procedural steps are presented in Table 3.1.

The shunt *L*-*C* passive filter, tuned at 5th order harmonic frequency is connected to the three-phase power line. A low impedance path is provided for the harmonics. The filter size is an important parameter here and the effectiveness of the filter depends on:

$$\varepsilon\% = I_{fn} / I_{Lh} \qquad (3.4)$$

Where I_{fn}, the filter current at the tuning frequency and I_{Lh} is the load harmonic current. The *R, L, C* values of the passive filter is calculated based on Table 3.1.

Table 3.1: Passive filter parameter calculation

Required data	Calculation procedure
1.Reactive power consumed, Q_c & Supply voltage, V	$Q_c = V^2 / X_c = \frac{n^2}{n^2 - 1}$
2.Supplyfrequency, f	$X_L = 2\pi fL$, $X_c = 1/2\pi fC$
3.Natural frequency, f_r	$f_r = \frac{1}{2\pi\sqrt{LC}}$
4.Harmonic order, n	$n = f_n / f_1 = \sqrt{X_c / X_L}$
5. Quality factor, *Q.F.*	$Q.F. = X_L * f_n / R$

3.2.3. Modelling of the PMSG, Grid and DC link with Vector Control

A grid connected PMSG based WECS with converter control is presented in Fig.3.2. It has three main modules: wind turbine, PMSG with the MSC and the GSC connected to the grid. The MSC and the GSC are coupled via a DC-link capacitor. The system is

connected to grid via transformer and transmission lines. The PMSG equations are stated in the synchronous *d-q* coordinates as

$$V_{ds} = R_s I_{ds} + L_{ds} \frac{dI_{ds}}{dt} - \omega_e L_{qs} I_{qs} \qquad (3.5)$$

$$V_{qs} = R_s I_{qs} + L_{qs} \frac{dI_{qs}}{dt} + \omega_e L_{ds} I_{ds} + \omega_e \varphi \qquad (3.6)$$

Where R_s is the stator winding resistance, V_{ds}, V_{qs}, I_{ds}, I_{qs} are the stator voltage and current *d-q* components respectively, L_{ds} and L_{qs} are the *d* and *q*-axis stator inductances that are equal in the surface–mounted PMSG, and the electrical angular speed of generator is ω_e. The electromagnetic torque is stated as:

$$T_e = \frac{3}{2}\frac{P}{2}\varphi I_{qs} \qquad (3.7)$$

Where φ and P are the magnetic flux and the pole number respectively.

The DC-link capacitor voltage is given by:

$$CV_{DC} \frac{dV_{DC}}{dt} = P_{Gen} - P_{Grid} \qquad (3.8)$$

Where V_{DC}, C, P_{Gen}, and P_{Grid} are the DC voltage, DC capacitance, DC-link incoming power, and the outgoing power respectively. The points of common coupling (PCC) dynamics in the *d-q* frame are stated as:

$$e_{df} = R_f I_{df} + L_f \frac{dI_{df}}{dt} - \omega_f L_f I_{qf} + V_{df} \qquad (3.9)$$

$$e_{qf} = R_f I_{qf} + L_f \frac{dI_{qf}}{dt} + \omega_f L_f I_{df} + V_{qf} \qquad (3.10)$$

Where ω_f, L_f, R_f , V_{df}, V_{qf}, e_{df}, e_{qf}, I_{df}, and I_{qf} are the grid voltage angular frequency, filter inductance, filter resistance, the *d* and *q*-axis components of the PCC voltage, the *d* and *q*-axis components of the AC voltage and current respectively. Using the PMSG and grid equations in the *a-β* and *d-q* coordinates the controllers are developed [7].

3.2.3.1. Control of MSC

MSC is controlled by applying zero *d*-axis component of stator current. Furthermore, an optimal torque control with the maximum power tracking is implemented in that side. Two independent PI control loops develop the controller as shown in Fig.3.2. They control the *d*-axis and *q*- axis current such as current of *d* axis to be zero and current of *q* axis can utilize the torque of generator.

3.2.3.2. Control of GSC

GSC is controlled by two PI controllers as shown in Fig. 3.2. The *d*-axis PI loop is used to control the DC link voltage and real power and the *q*-axis PI loop is used to control the reactive power or to regulate the grid voltage [7].

3.3. Flux Weakening Control Method

There are two constraints should be considered during flux control algorithm namely as the maximum current and the maximum voltage. For a motor-drive system, the current is limited by the motor's thermal dissipation and cooling means. And the drive side determines maximum voltage that is limited by DC bus voltage.

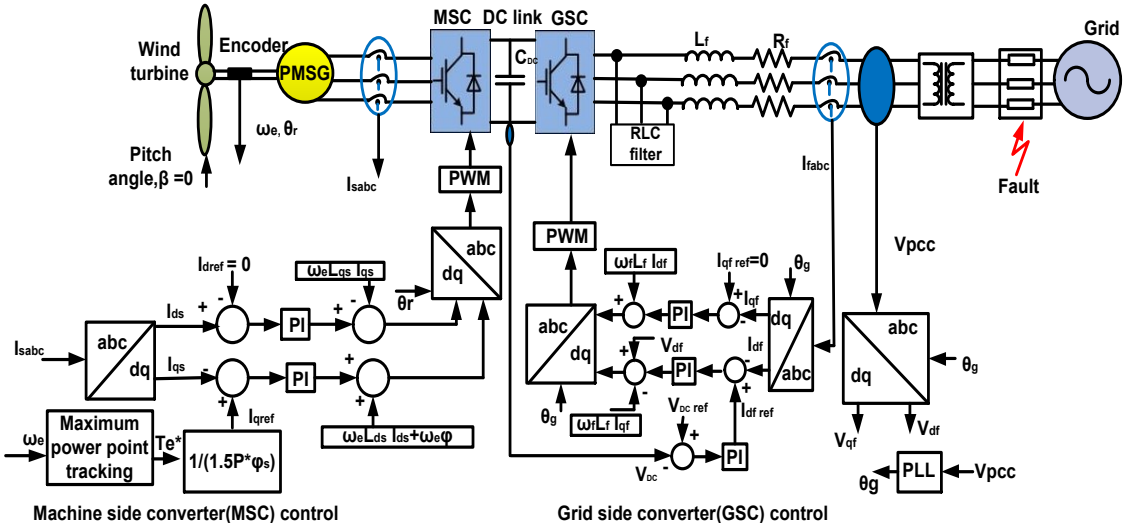

Fig.3. 2. Grid connected PMSG with back to back converter

During the grid faults, negative and positive sequence rotor fluxes are induced in the rotor of the PMSG based WECS. This flux induced voltage is greater than the usual stator

voltage and exceeds the limit of the MSC voltage resulting in high EMF. This higher EMF produces overcurrent in the rotor circuit and creates overvoltage in the DC-link capacitor and can damage the converter as well as the capacitor.

Being PMSG, the magnetic field of the rotor is constant, so the induced EMF increases according to the rotor speed. As the rotor speed increases during the grid fault, the magnetic field of the rotor should be adjusted to maintain the rotor speed within the rated speed which can, in turn, keep the DC-link capacitor voltage constant.

The three phase currents of PMSG can be defined in rotating *d*-*q* frames where I_d and I_q are considered as the flux component and torque component respectively. So, the *d*-axis current is related to the flux linkage variation of the rotor.

The voltage and current limits of a converter are given as

$$V_d^2 + V_q^2 \le V_{\max}^2 \qquad (3.11)$$

$$I_d^2 + I_q^2 \le I_{\max}^2 \qquad (3.12)$$

$$V_{\max} = 1/\sqrt{3} V_{DC} \qquad (3.13)$$

Where $V_{\max}$ is the maximum MSC voltage and it is determined based on the MSC modulation and the rated DC-link capacitor voltage, V_{DC} as expressed in equation (3.13). $I_{\max}$ is the maximum MSC current and it is defined by the generator and MSC power ratings.

Using equation (3.11) and (3.12), voltage and current limitation circles are drawn as shown in Fig. 3.3 (a) ($\omega_1 > \omega_2 > \omega_3 > \omega_4 > \omega_5$). They are denoted by a dotted-line circle and solid-line circle respectively. It will shrink as the operating speed is increased [8]. Beyond the PMSG rated speed, the operating points should always be within the circle of voltage limit.

As shown in Fig. 3.3 (a), at above the base speed of the generator, the limitation circle of voltage diminishes to the left side of the *q*-axis. For normal operation, $I_{d\,ref}$ is set to zero

to maximise the torque per ampere ratio. However, during grid faults $I_{d\,ref}$ changes and it becomes negative to weaken the total flux induced in PMSG windings. The proposed controller operation logic is shown in Fig.3.3(b).

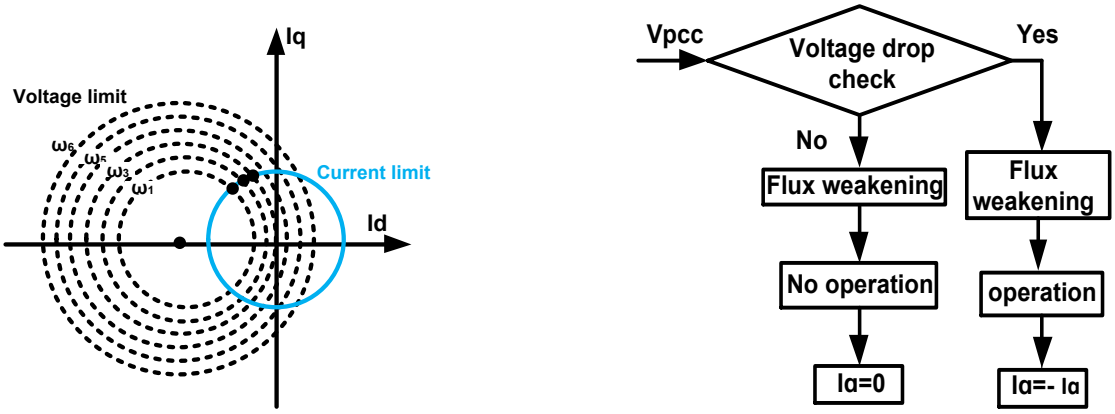

(a) (b)

Fig. 3. 3. Flux weakening control for MSC (a) Voltage and current limitation circles (b) Flow chart

3.3.1. Flux Weakening Using Synchronous PI Current Controller

Fig. 3.4 illustrates the flux weakening control for machine side to minimize the DC link overvoltage during fault scenarios. The current controller output (voltage reference) and the converter output voltage difference is used to calculate the $I_{d\,ref}$. The output voltage of converter is limited by the DC-link voltage and this control scheme helps to maximise the DC-link voltage utilisation as well as current control capability. The current reference of q-axis is saturated, and it is calculated as

$$I_q^* = \sqrt{I_{qref}^{\,2} - I_{dref}^{\,2}} \qquad (3.14)$$

Where the q-axis reference saturation is I_q*, the flux-weakening controller output is I_{dref}. Difference between the voltage limitation and the dq voltage references magnitude V_d* and V_q* is passed through PI current controller and I_{dref} is obtained. The PI controller output is limited between - I_{dqmax} and 0. The required torque gives I_{qref} current and it is limited by equation (3.14) [9].

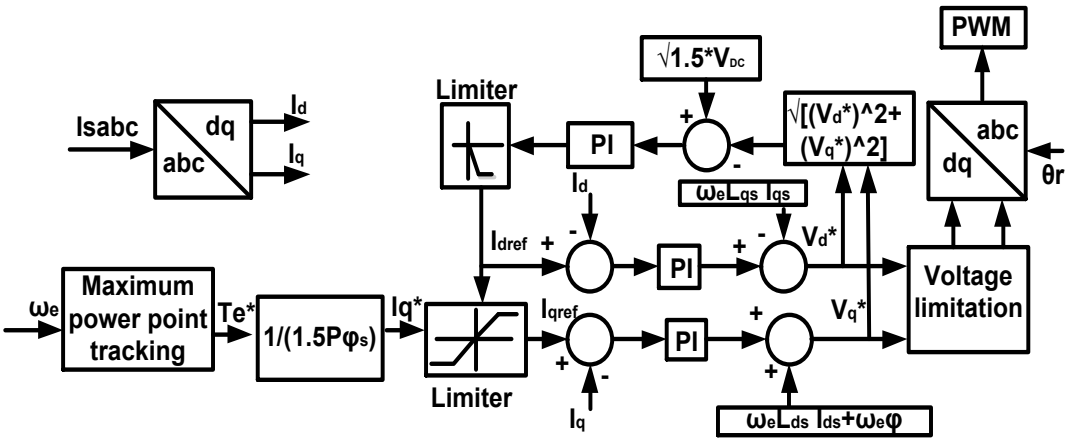

Fig.3. 4. Flux weakening control with synchronous PI

3.3.2. Flux Weakening Using Stationary PI Current Controller

The *abc* three phase current errors are directly passed over a simple PI controller in stationary frame as shown in Fig.3.5. A balanced three-phase voltage must always need for the PWM voltage references. In the stationary frame, only conversions of two phases are required as the third reference voltage can be calculated by $V_c = -V_a - V_b$.

It is widely accepted that in an AC current controlled scheme, a simple PI regulator in stationary frame is inadequate; subsequently the gains of controller cannot be fixed enough high for steady-state error elimination [10]. But gain of this controller is limited due to the sampling and transport delays rather than the plant characteristics [11]. The accepted value of controller performance can be achieved by setting the values of PI gains to maximum. The advantage of this technique is that only one synchronous reference frame transformation is required for the reference currents. Furthermore, computational complexity and the possible transform-induced measurement error are also reduced.

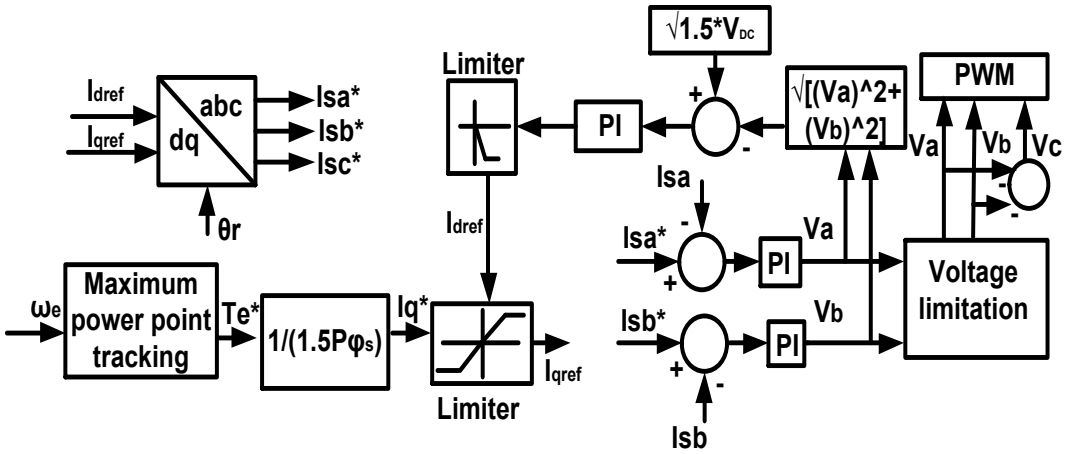

Fig.3. 5. Flux weakening control with stationary PI

3.3.3. Flux Weakening Using Stationary frame PR Current Controller

Generally, synchronous frame PI current controller is used in the traditional flux weakening control. However, it needs a higher number of axis transformations. Moreover, it is unable to track the sinusoidal reference current and cannot produce zero steady state error.

The synchronous PI controller uses feed forward terms and cross coupling terms in the *d-q* reference frames for better dynamic performance. These terms are not constant rather depend on the circuit parameters as well as on the temperature. These affect the robustness of the control system. To overcome the issues regarding the synchronous frame PI controller, a PR current controller-based flux weakening control is designed and is shown in Fig. 3.6. The integrator is normally used to eliminate the steady-state error. The performance of this integrator is enhanced via equation (3.15). It is transformed into a resonator for tracking the sinusoidal reference current.

$$G_{AC}(S) = G_{DC}(S - j\omega_0) + G_{DC}(S + j\omega_0) \qquad (3.15)$$

Now the equivalent transfer function $G_{AC}(S)$ is

$$G_{AC}(S) = K_i(S) * \frac{2S}{S^2 + \omega_0{}^2} \qquad (3.16)$$

So, the PR controller transfer function is

$$G_{PR}(S) = K_P + K_i(S) * \frac{2S}{S^2 + \omega_0{}^2} \qquad (3.17)$$

Where, K_i, K_p and ω_0 are the integral constant, proportional constant, and the resonant frequency respectively.

The three phase stator currents are measured and converted into orthogonal α-β currents using the Clarke transformation. The difference between the real machine voltage and the controller output voltages (V_α^*, V_β^*) passes through a PI controller. The output of PI controller is limited by 0 to -I_{dmax}. It generates the I_d reference current. Based on the I_d reference current, the I_q reference current is defined. The difference between maximum converter current, $I_{\max}$ and I_d reference current generates the I_q reference current.

The generated I_d and I_q reference currents are transformed to α-β coordinate quantities to obtain the required I_α reference current. The voltage references are also saturated as:

$$V_{\alpha\beta}{}^* \leq \sqrt{1.5} V_{DC} \qquad (3.18)$$

with $V_{\alpha\beta}$ * is the saturated voltage references where the phase is kept constant.

It is observed that, there is no coupling terms $\omega_e L_{ds} I_{ds}$, $\omega_e L_{ds} I_{qs}$ and feed forward compensation term $\omega_e \varphi$, in the PR based flux weakening controller whereas they are presented in the conventional PI based flux weakening controller. So, PR based flux weakening controller eliminates the effect of parameter variations on the control loop and the system robustness is improved.

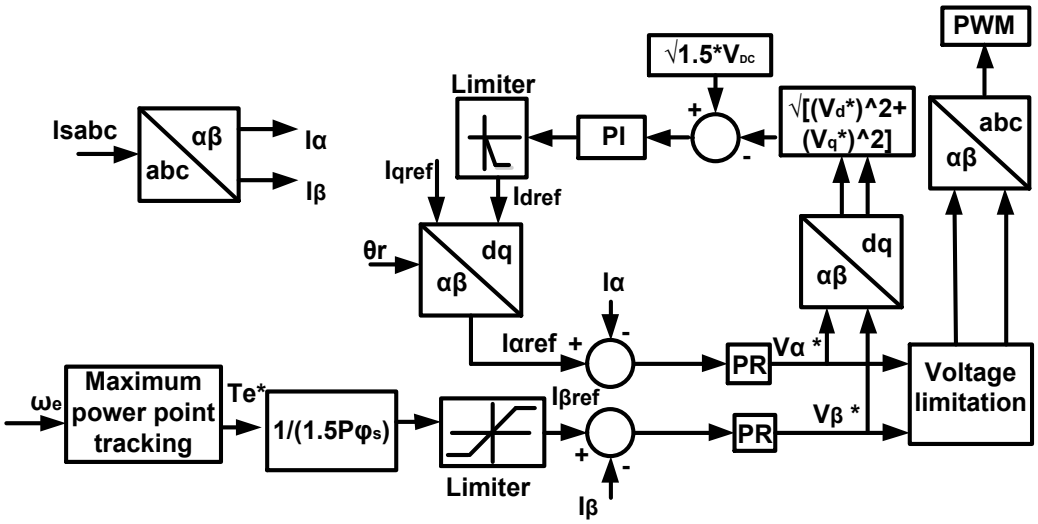

Fig. 3. 6. PR based Flux weakening control for MSC

3.4. Conventional Control with the Braking Chopper (BC)

The BC [12] is used in the DC link for the active power dissipation during the grid faults. It comprises of a high-power resistor with a series switch which is shown in Fig.3.7 (a). Control of BC is based on voltage limit. The real voltage frequently tracks the reference voltage in a hysteresis- band. Pre-set higher and lower tolerance limits are matched to the extracted signal as shown in Fig.3.7 (b). If the signal is within the tolerance band, no switching action is taken. Switching occurs whenever the voltage signal crosses the threshold voltage limit.

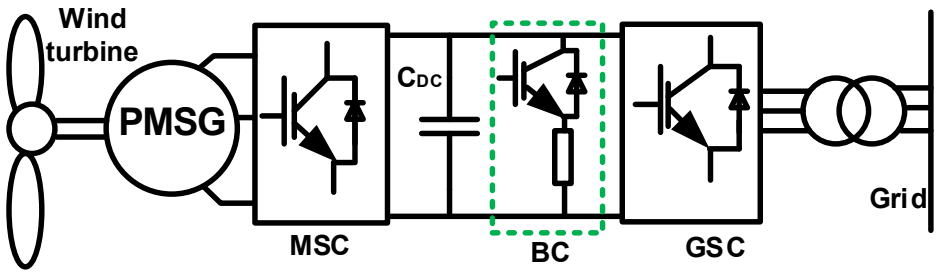

(a)

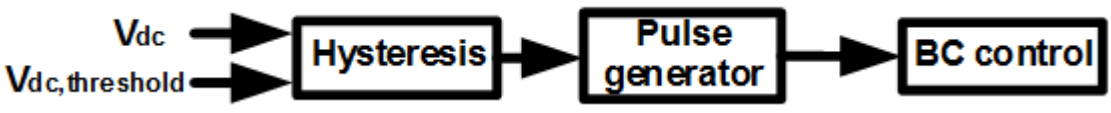

(b)

Fig. 3. 7.(a) Wind turbine with BC protection (b) BC controller block diagram

3.5. Simulation Results and Analysis

Numerical simulation results are obtained under constant wind speed in MATLAB/SIMULINK for synchronous and stationary frame-based PI controller, stationary frame PR controller and conventional BC during grid faults. The simulation time is for 2 second. Simulation parameters are listed in Appendix A.

3.5.1. Performance under a Symmetrical Fault with the Synchronous frame PI Current Controller

A three line to ground fault is occurred at the middle of transmission line at t= 1second.The system fault is cleared at 1.2 second. As shown in Fig.3.8 (a) the grid voltage is reduced from 100% of its nominal value to 10% at the time of system fault. The active power injected to the grid is zero but PMSG injects rated power into the DC link. As a consequence, the net DC bus voltage is increased to approximately three times its rated value for synchronous PI based controller as shown in Fig. 3.8(c) without any LVRT control. This exposes the power converters to unstable operation. When the LVRT control acts, the large DC voltage is reduced significantly. From Fig. 3.8(c) it is found that DC link voltage is regulated well in synchronous PI control (K_p = 1, K_I = 80).

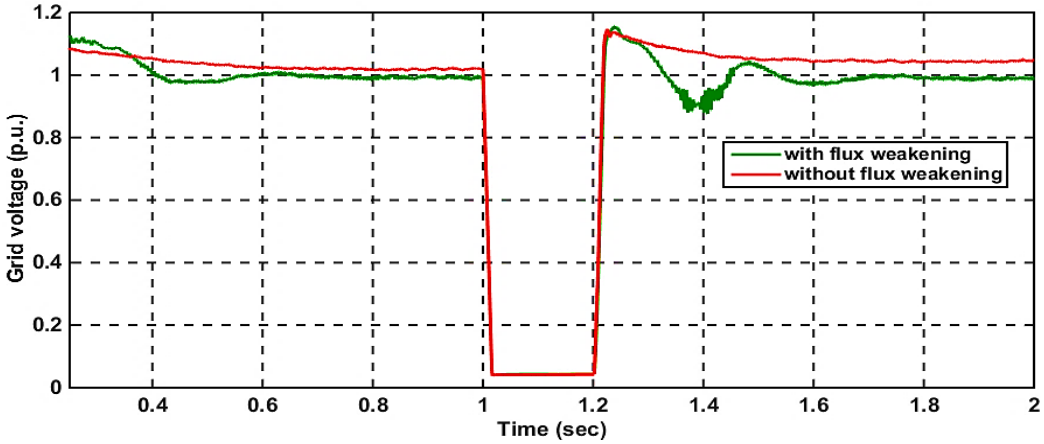

(a)

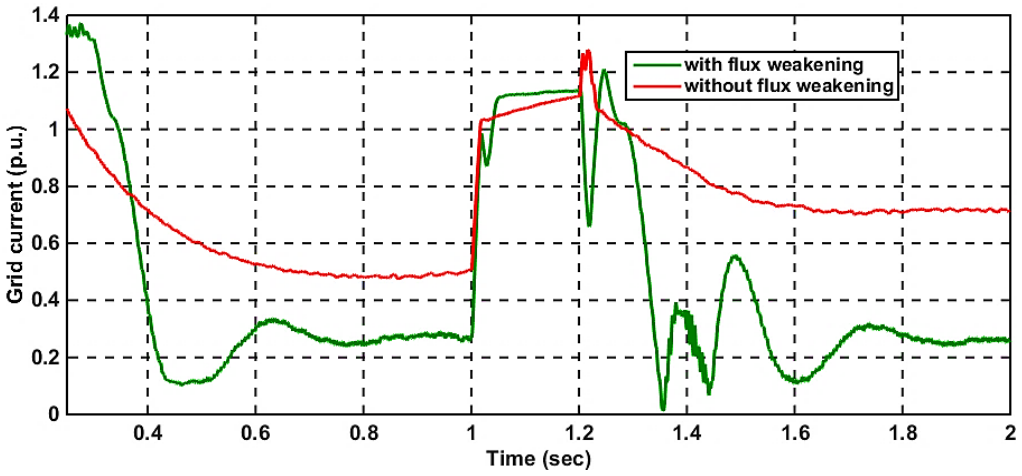
with flux weakening
without flux weakening
Grid current (p.u.)
Time (sec)

(b)

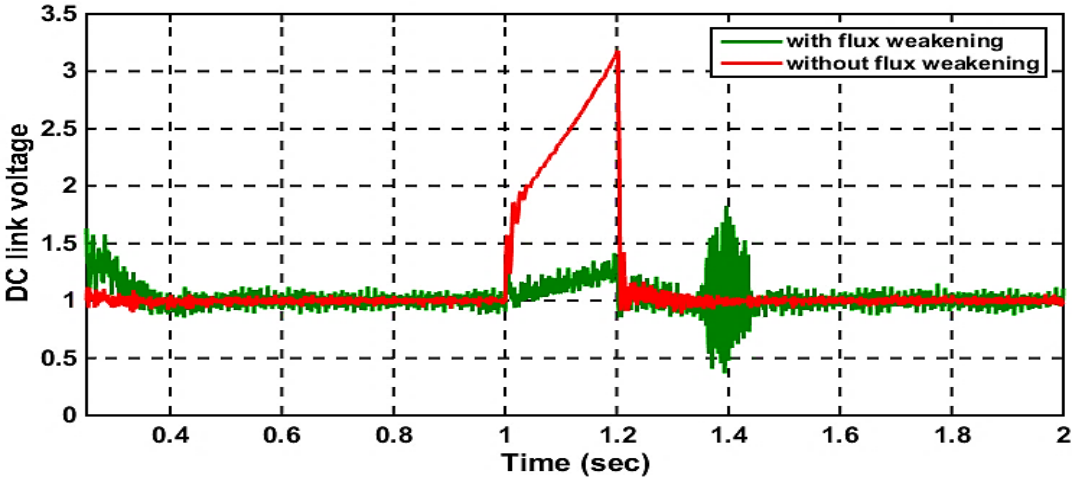
with flux weakening
without flux weakening
DC link voltage
Time (sec)

(c)

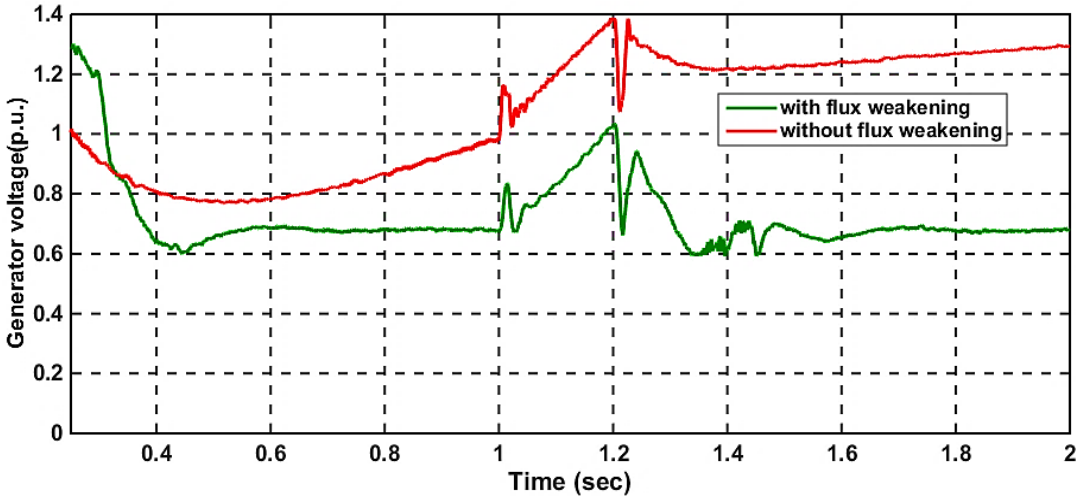
with flux weakening
without flux weakening
Generator voltage(p.u.)
Time (sec)

(d)

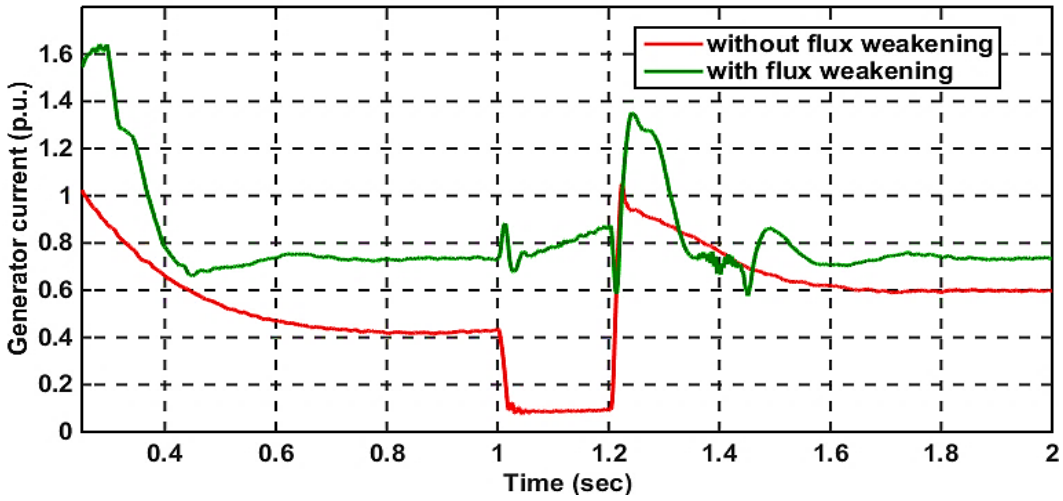

(e)

Fig.3. 8. Simulation results for synchronous PI controller a) Grid voltage b) Grid current c) DC link voltage d) Generator voltage e) Generator current

It is observed from Fig. 3.8(a) and Fig. 3.8(b) that after using flux weakening controller, some small fluctuations occurred in the grid voltage as well as in the grid current. These are due to the voltage limiter setting and the tuning of controller parameters. Similarly, at 1.3s there are some voltage fluctuations in DC link voltage due to the PI controller gain settings as shown in Fig.3.8(c). Most of these fluctuations and transients are within the acceptable limits and these could be worse if not selected properly creating large overshoot.

3.5.2. Performance under an Asymmetrical Fault with the Synchronous frame PI Current Controller

A double line to ground fault is considered as the most common type of grid fault is applied at 1second lasting for 0.2 second. As shown in Fig. 3.9(a) a large grid voltage dip is occurred and the grid voltage is reduced from 100% of its nominal value to 40%. High frequency oscillation happens due to transmission line inductance and the parasitic capacitance. Consequently, the net DC bus voltage is increased to approximately 1.7 times its rated value for synchronous PI based controller as shown in Fig. 3.9(c) without

any LVRT control. The LVRT control takes action and the fault is cleared at 1.2s. From Fig. 3.9(c) it is seen that the DC link voltage is controlled well within the acceptable limit in synchronous PI based flux weakening control.

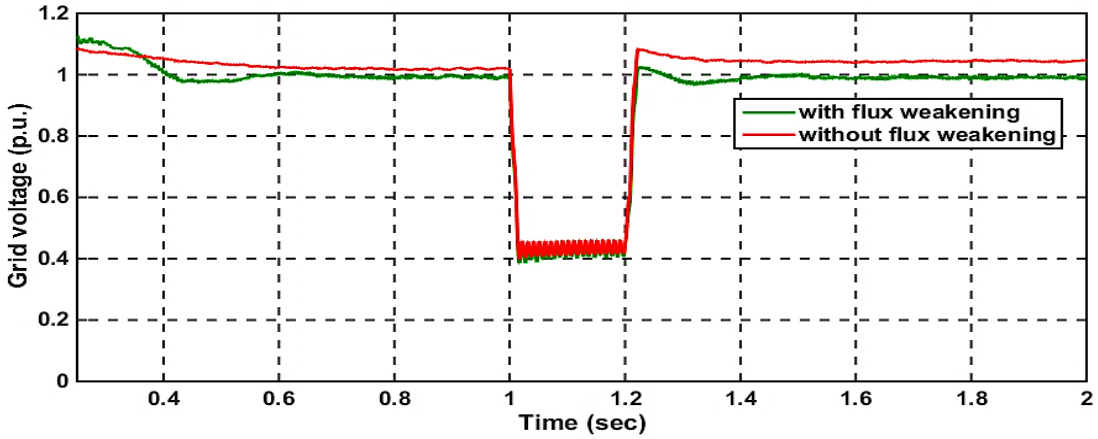

(a)

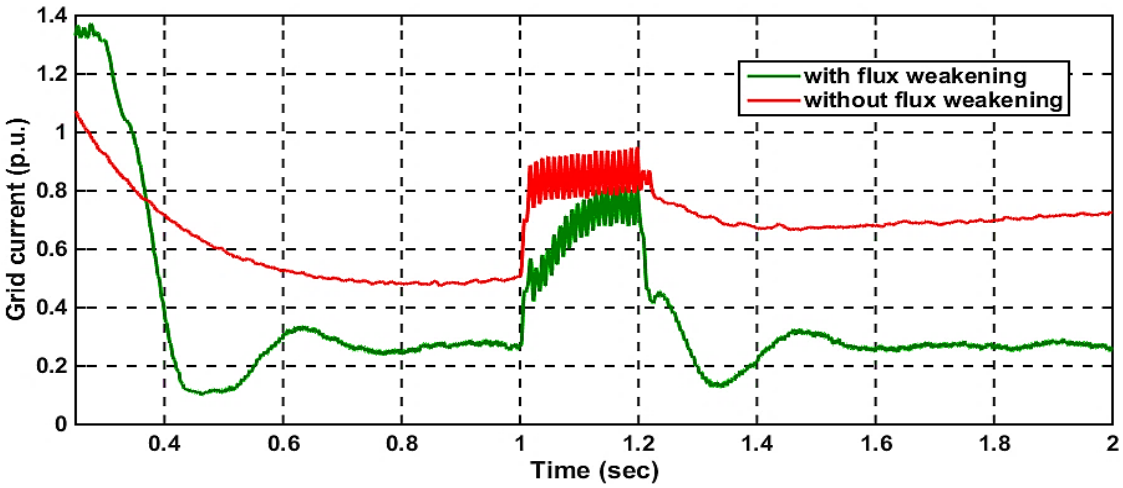

(b)

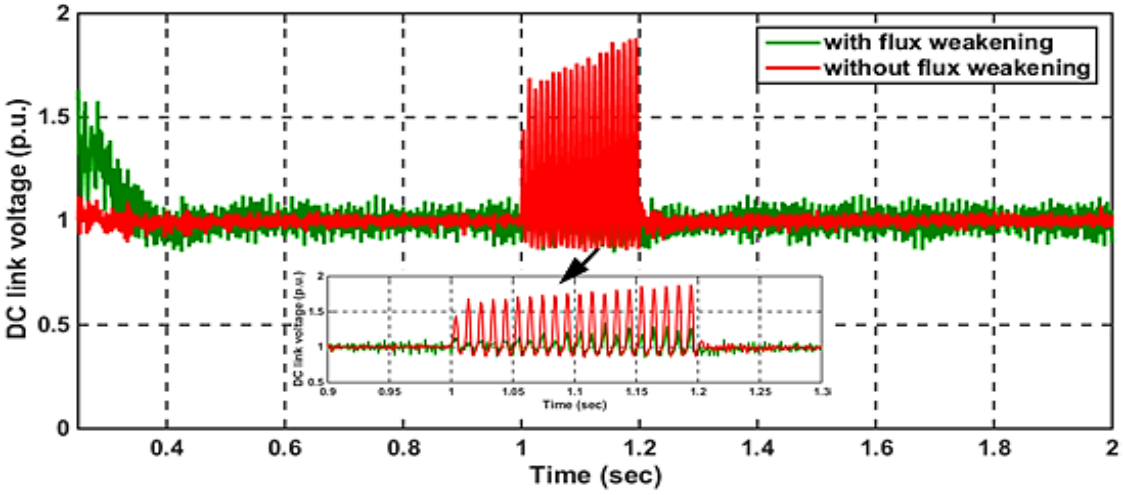

(c)

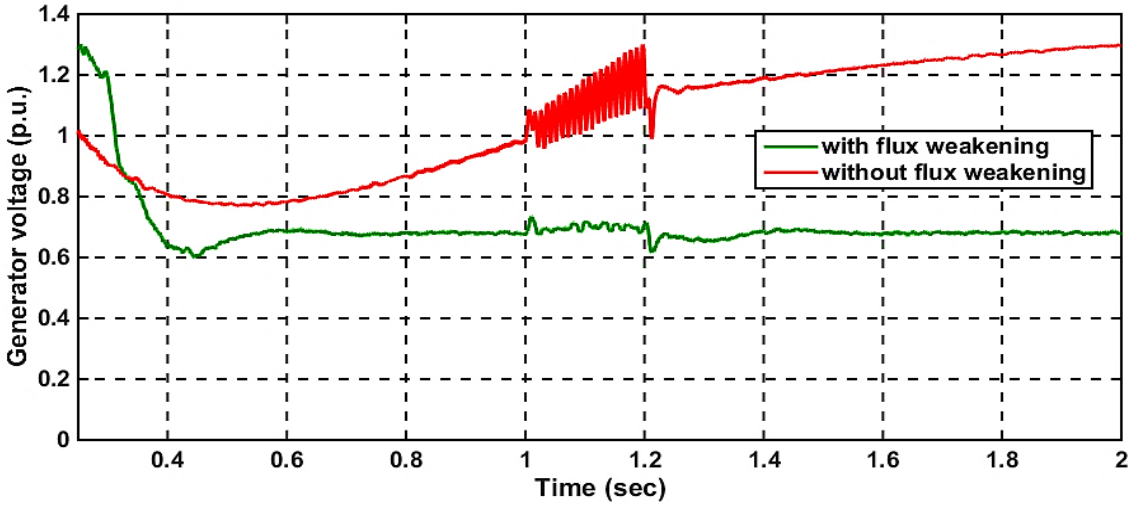

(d)

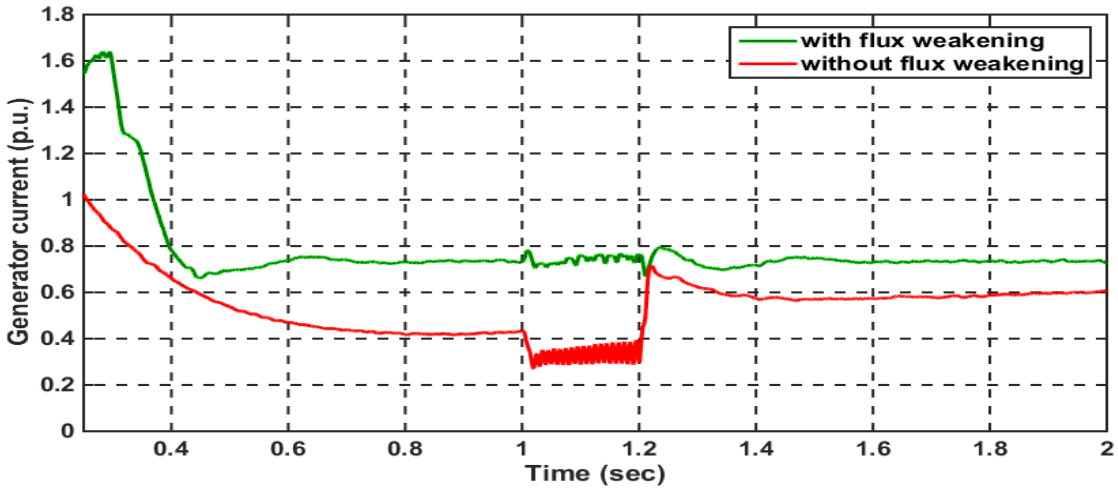

(e)

Fig.3. 9. Simulation results for synchronous PI controller a) Grid voltage b) Grid current c) DC link voltage d) Generator voltage e) Generator current

3.5.3. DC link overvoltage minimisation with different PI Controller parameters

PI controller gains play a vital role on the performance of the flux weakening controller. During the grid fault, the flux weakening controller should operate and the controller parameters should be adjusted accordingly to achieve better performance. From Fig.3.8(c) and Fig.3.9(c) it is observed that though DC link voltage is limited well but some fluctuations occurs. To overcome this issue new parameters of PI controller (K_P = 0.1, K_I = 10) are chosen. The performance of flux weakening controller depends on how

the controller values are properly tuned and selected. Well-tuned controller gains will produce less overshoots and the smoother waveform of DC link voltage can be obtained. Fig.3.10 shows the simulation results for the DC link voltage during same grid fault scenario with different machine side PI controller parameters. The symmetrical and asymmetrical grid fault occurs at 1s lasts for 0.2 s. The DC link voltage goes beyond its limit for both types of fault without any controller as shown in Fig.3.10(a) and Fig.3.10(b). Now the flux weakening controller is applied at 0.8s to 1.2s instead of 1s to 1.2s to avoid the controller interactions. The DC link voltage is regulated well by using the proposed flux weakening controller.

It is observed from Fig.3.10 that there are some ripples in DC link voltage at 0.8s. However, it is too slight to influence the performance of the proposed flux weakening controller.

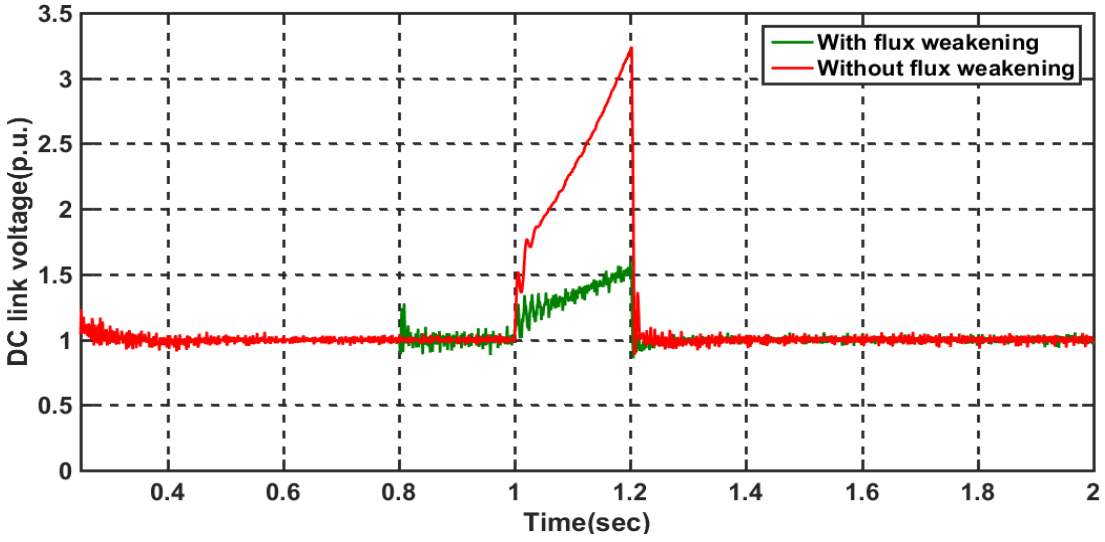

(a)

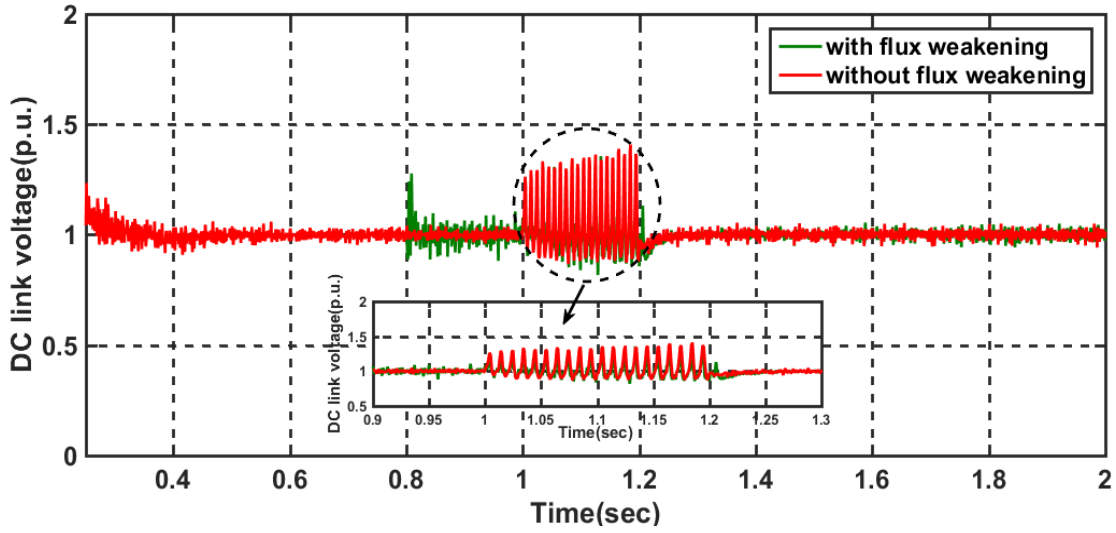

(b)

Fig.3. 10. Simulation results for DC link voltage with different control parameters a) Symmetrical fault b) Asymmetrical fault

3.5.4. Performance Under a Symmetrical Fault with the Stationary frame PI current Controller

A three line to ground fault is occurred at the middle of transmission line at t= 1second.The system fault is cleared at 1.2 second. As shown in Fig. 3.11(a), the grid voltage is reduced from 100% of its nominal value to 10% at the time of system fault. The active power injected to the grid is zero but PMSG injects rated power into the DC link. As a consequence, the net DC bus voltage is increased to approximately six times for stationary PI based controller as shown in Fig. 3.11(c) respectively without any LVRT control. This exposes the power converters to unstable operation. When the LVRT control takes action the large DC voltage is reduced significantly. From Fig. 3.11(c) it is found that DC link voltage is regulated well in stationary PI control.

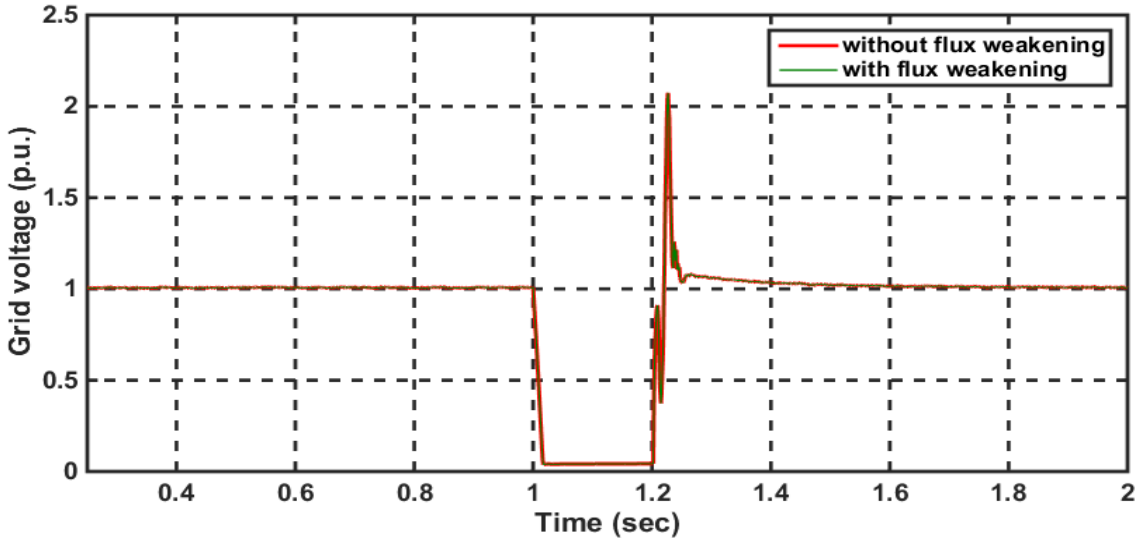
without flux weakening
with flux weakening
Grid voltage (p.u.)
Time (sec)
2.5
2
1.5
1
0.5
0
0.4
0.6
0.8
1
1.2
1.4
1.6
1.8
2

(a)

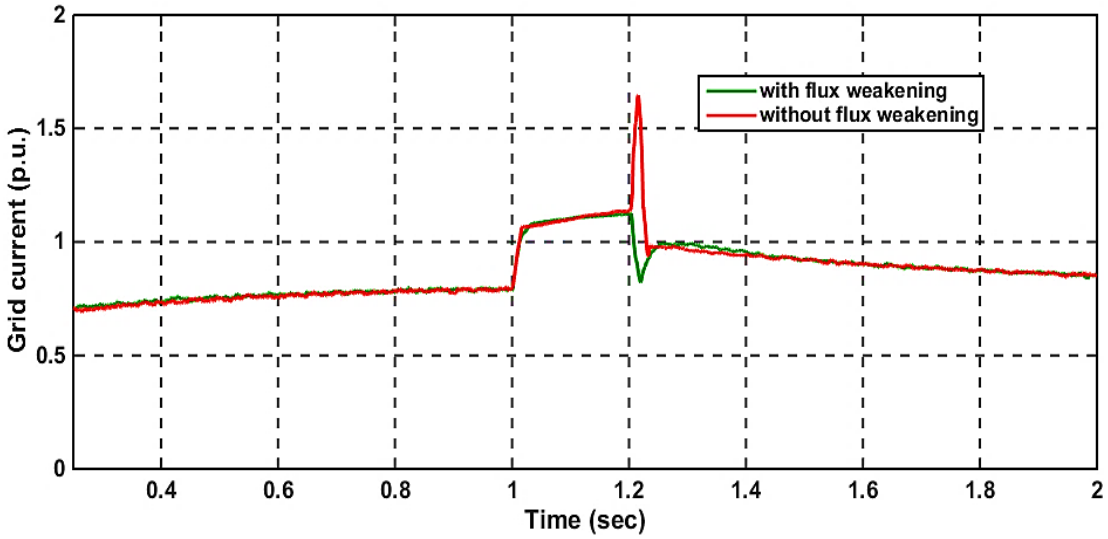
with flux weakening
without flux weakening
Grid current (p.u.)
Time (sec)
2
1.5
1
0.5
0
0.4
0.6
0.8
1
1.2
1.4
1.6
1.8
2

(b)

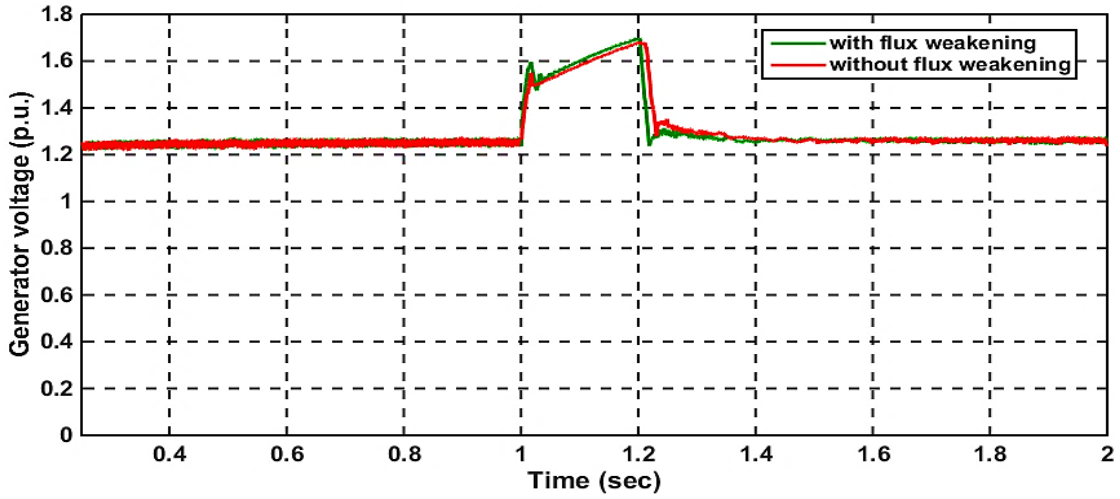
with flux weakening
without flux weakening
Generator voltage (p.u.)
Time (sec)
1.8
1.6
1.4
1.2
1
0.8
0.6
0.4
0.2
0
0.4
0.6
0.8
1
1.2
1.4
1.6
1.8
2

(c)

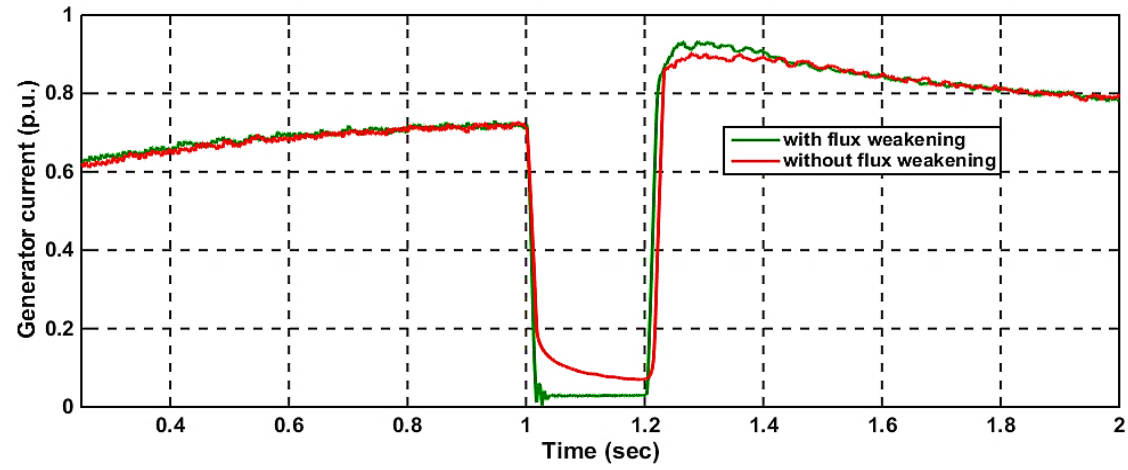

(d)

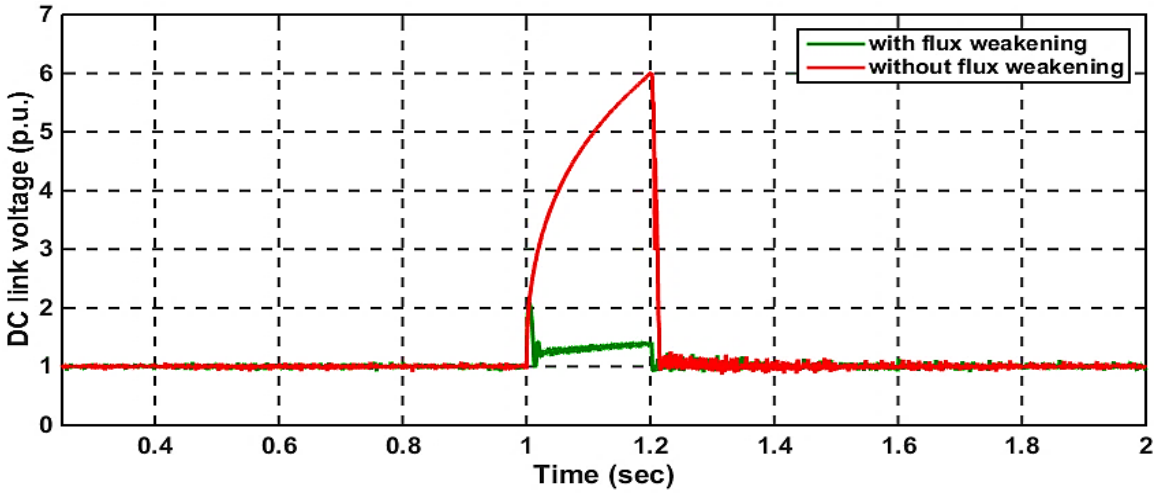

(e)

Fig.3. 11. Simulation results for stationary PI controller a) Grid voltage b) Grid current c) DC link voltage d) Generator voltage e) Generator current

3.5.5. Performance Under an Asymmetrical Fault with the Stationary frame PI Current Controller

A double line to ground fault is considered as the most common type of grid fault is applied at 1second lasting for 0.2 second. As shown in Fig. 3.12(a), a large grid voltage dip is occurred, and the grid voltage is reduced from 100% of its nominal value to 40%. As a consequence, the net DC bus voltage is increased to approximately 1.7 times its rated value for stationary PI based controller as shown in Fig. 3.12(c) without any LVRT

control. The LVRT control takes action and the fault is cleared at 1.2s. From Fig. 3.12(c) it is seen that the DC link voltage is controlled well within the acceptable limit in stationary PI based flux weakening control.

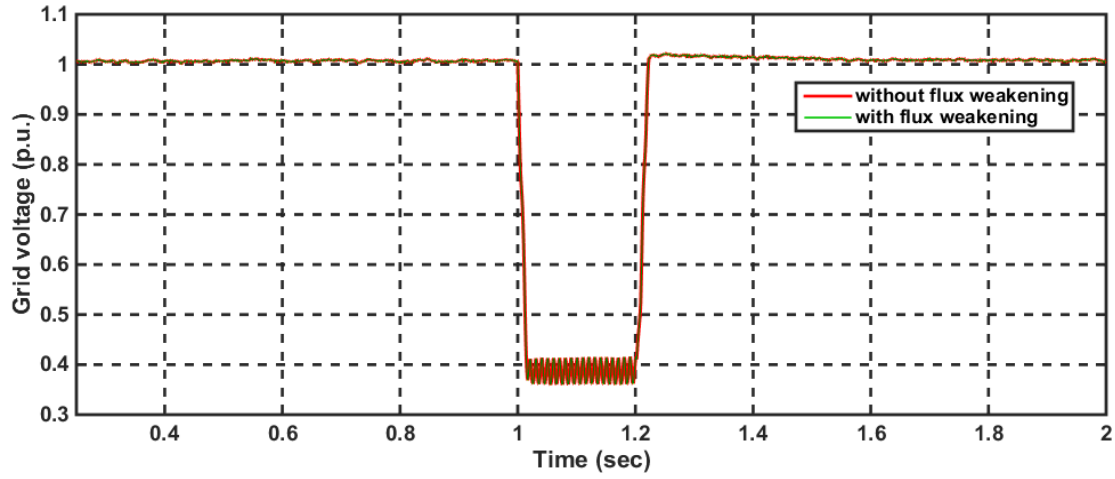

(a)

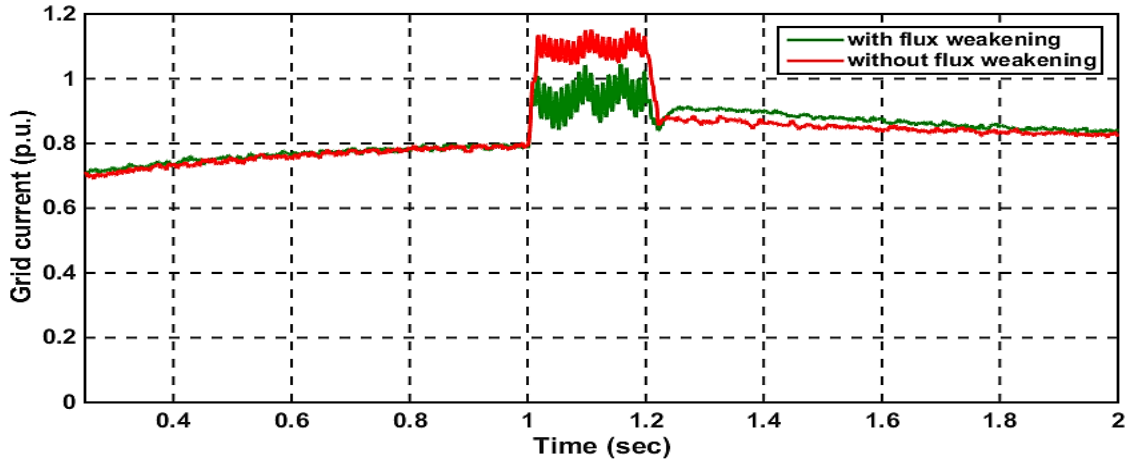

(b)

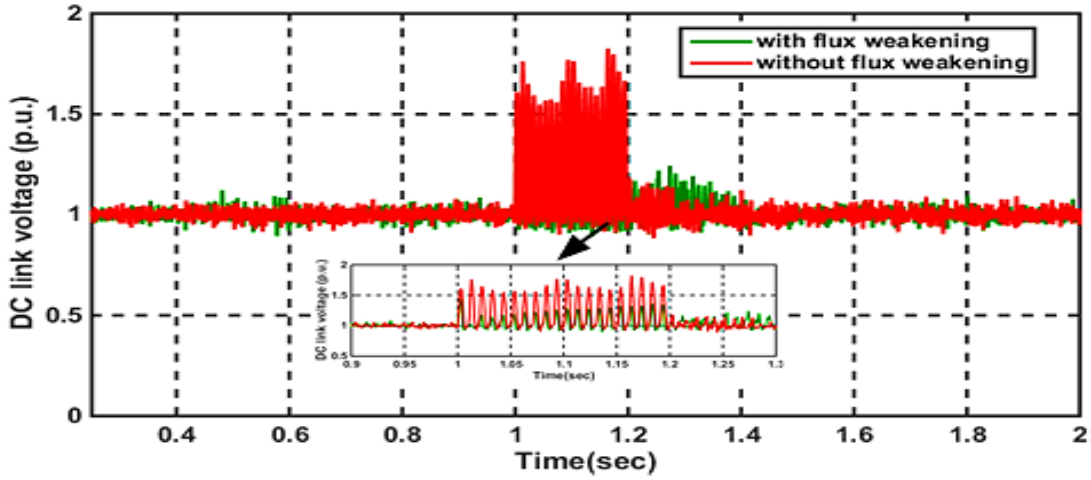

(c)

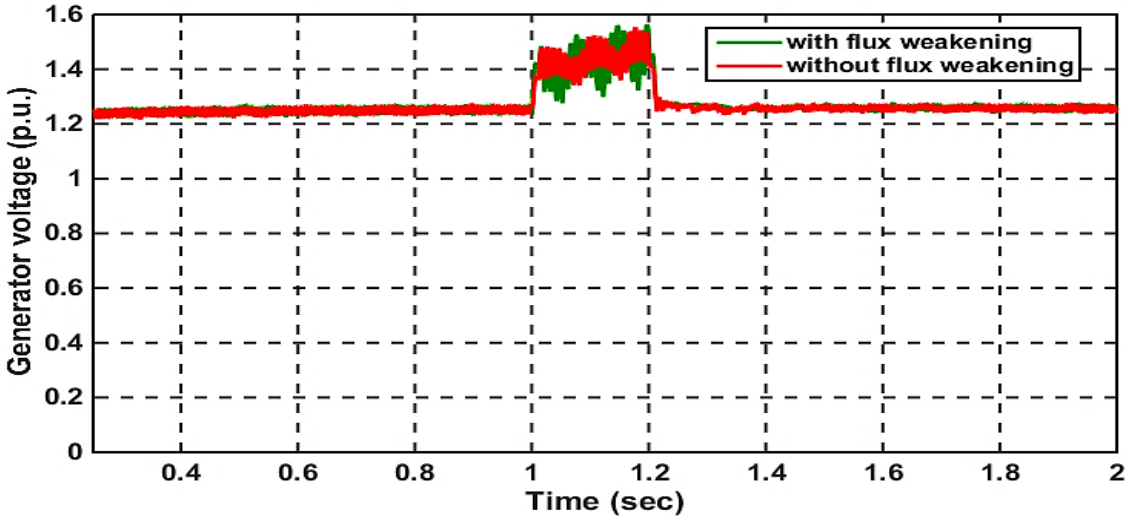

(d)

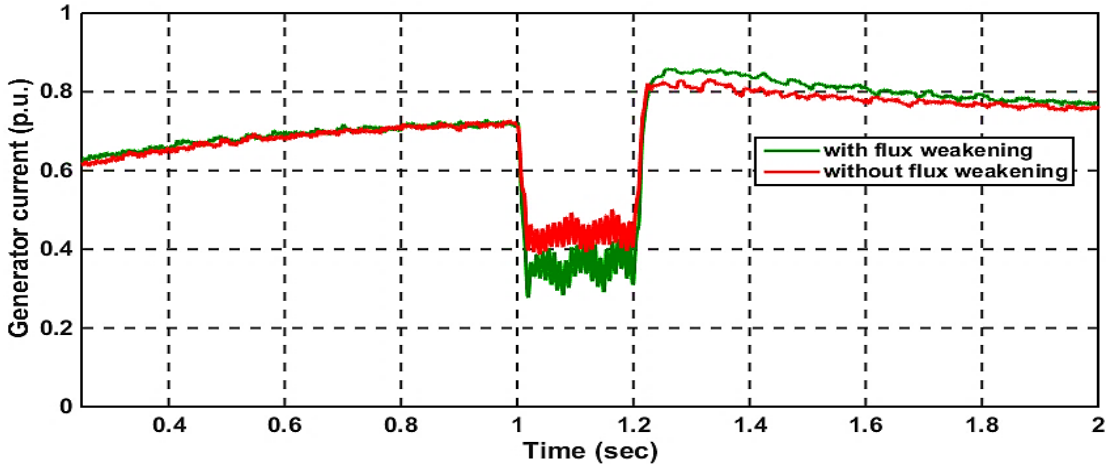

(e)

Fig.3. 12. Simulation results for stationary PI controller a) Grid voltage b) Grid current c) DC link voltage d) Generator voltage e) Generator current

From Fig. 3.8(c), Fig.3.9(c), Fig.3.11(c) and Fig.3.12(c) it is observed that the DC link voltage is reduced by about 80% with fewer transients in stationary PI based flux weakening control where in synchronous PI based flux weakening control it is reduced by about 60% with more transient value during symmetrical fault. And for asymmetrical fault overall fluctuations and transients are less in stationary PI based flux weakening control than that of the synchronous PI based flux weakening control.

3.5.6. Performance under a Symmetrical Fault with the Stationary frame PR Current Controller

A three line to ground fault is considered as the most severe type of grid fault and is applied on the 25-kV line at 1s which is lasting for 0.2s. As shown in Fig. 3.13(a), a large dip in the grid voltage is occurred and the grid voltage is reduced from 100% of its nominal value to 10%. The active power injected to the grid is zero but PMSG inserts rated power to the DC link. As a result, the net voltage of DC bus is enlarged to almost four times for the PR based controller as exposed in Fig. 3.13(e) respectively without any FRT control. The converters experience some harmonics in DC voltage for unbalance AC grid. The FRT control takes action and the fault is cleared at 1.2s. Grid current, generator voltage, and generator current during this condition are shown in Figs. 3.13(b) to (d) for the PR controller respectively. From Fig. 3.13(e) it is found that the DC link voltage is better regulated within the acceptable limit by the PR based flux weakening control. A behavior of generator speed is displayed in Fig.3.13 (f).

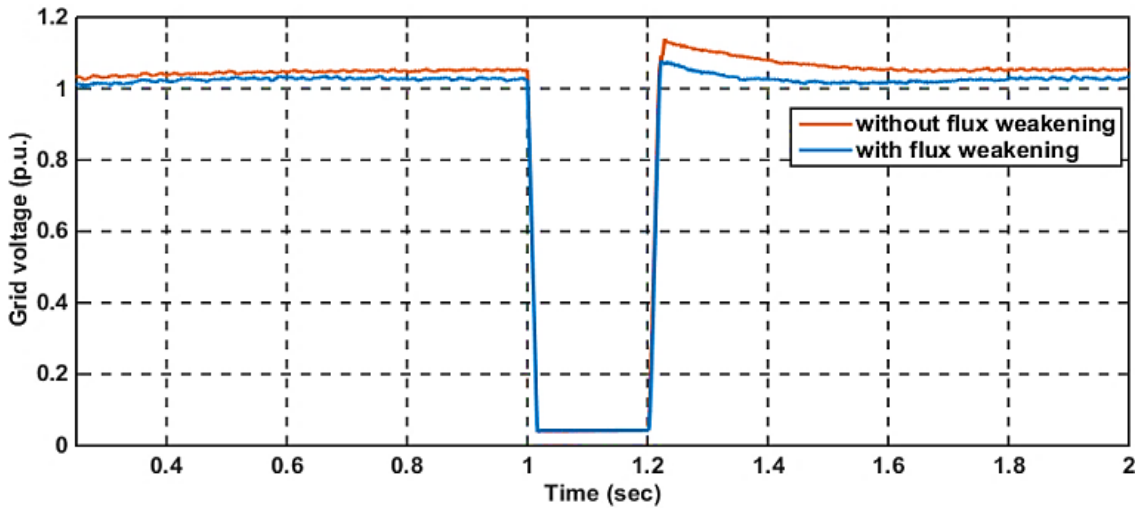

(a)

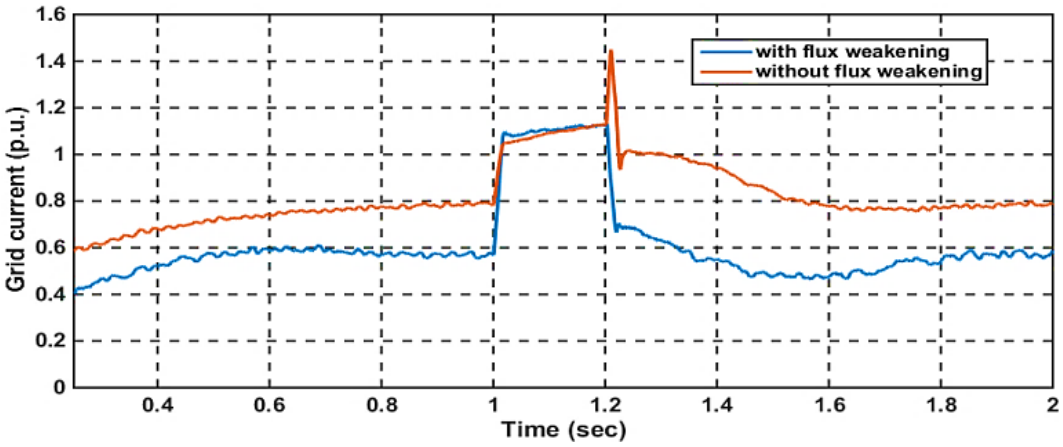
with flux weakening
without flux weakening
Grid current (p.u.)
Time (sec)

(b)

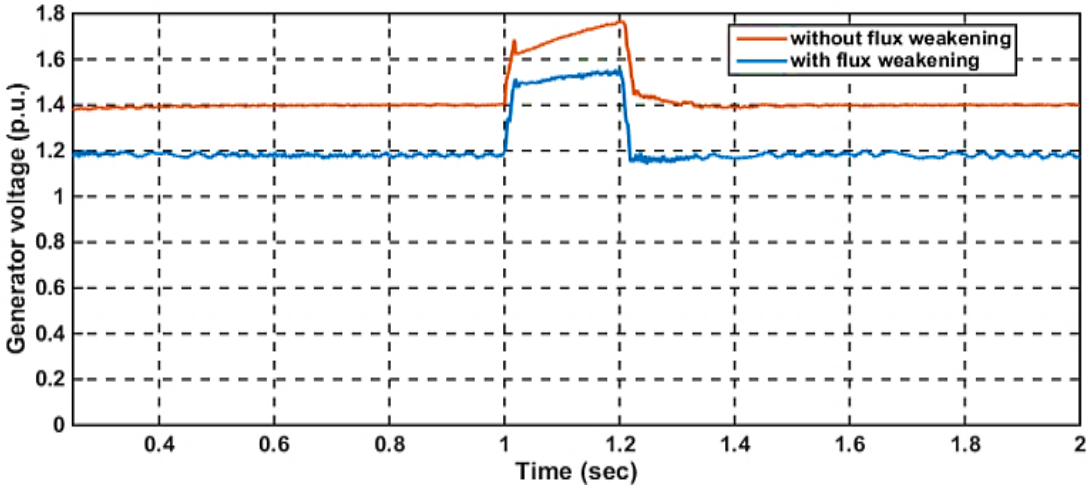
without flux weakening
with flux weakening
Generator voltage (p.u.)
Time (sec)

(c)

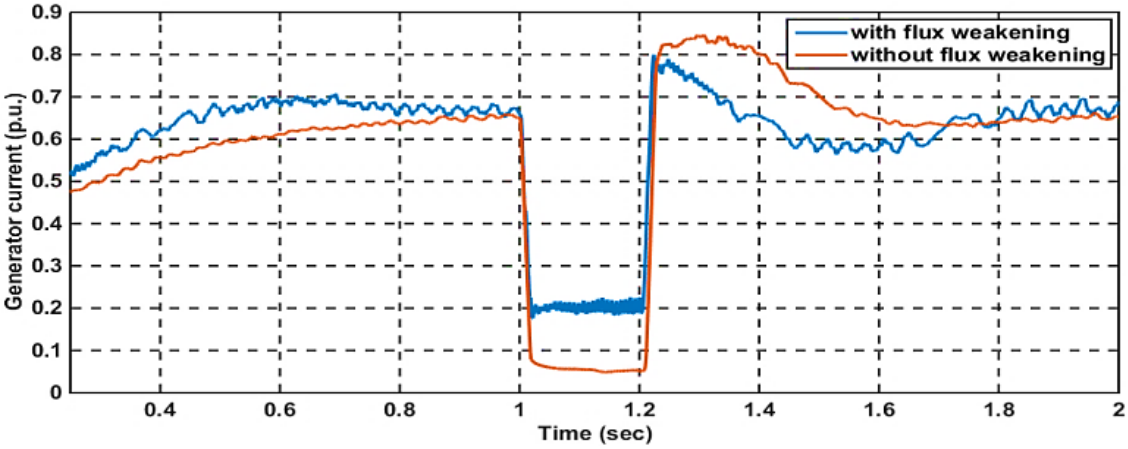
with flux weakening
without flux weakening
Generator current (p.u.)
Time (sec)

(d)

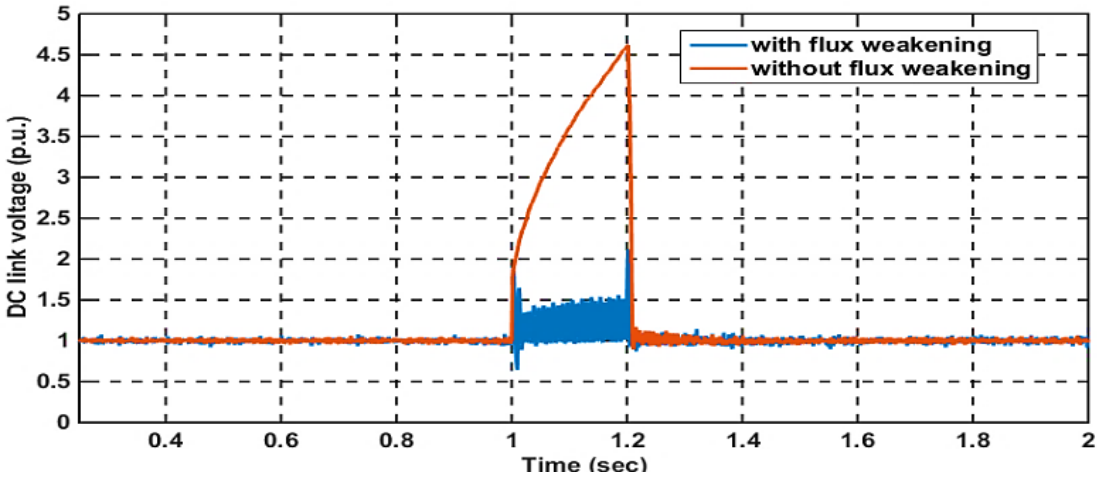

(e)

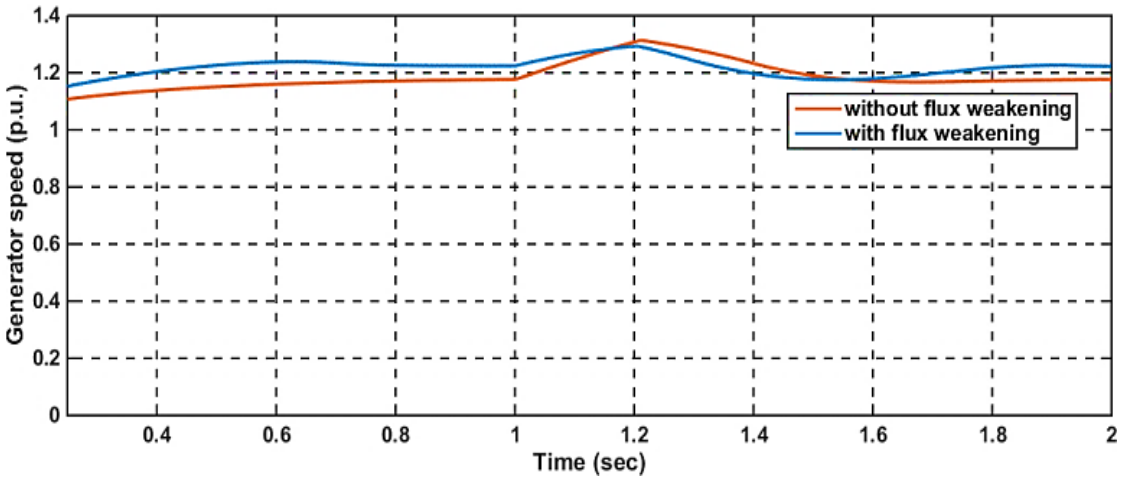

(f)

Fig.3. 13. Simulation results during symmetrical fault for PR controller a) Grid voltage b) Grid current c) Generator voltage d) Generator current e) DC link voltage f) Generator speed

3.5.7. Performance under an Asymmetrical Fault with the Stationary frame PR Current Controller

A double line to ground fault is considered as the most common type of grid fault and is applied on the 25 kV line at 1s which is lasting for 0.2s. As shown in Fig. 3.14(a), a large dip in the grid voltage is occurred and the grid voltage is reduced from 100% of its nominal value to 40%. As a result, the net voltage of DC link is enlarged to almost 1.7 times its rated value for the PR based controller as shown in Fig. 3.14(e), without any

FRT control. The converters experience some harmonics in DC voltage for unbalance AC grid. The FRT control takes action and the fault is cleared at 1.2s. Grid current, generator voltage, and generator current during this condition are presented in in Figs. 3.14(b) to (d) for the PR controller. From Fig. 3.14(e) it is found that the DC link voltage is well maintained within the acceptable limit by the PR based flux weakening control. Behaviors of generator speed for both controllers are displayed in Fig.3.14 (f).

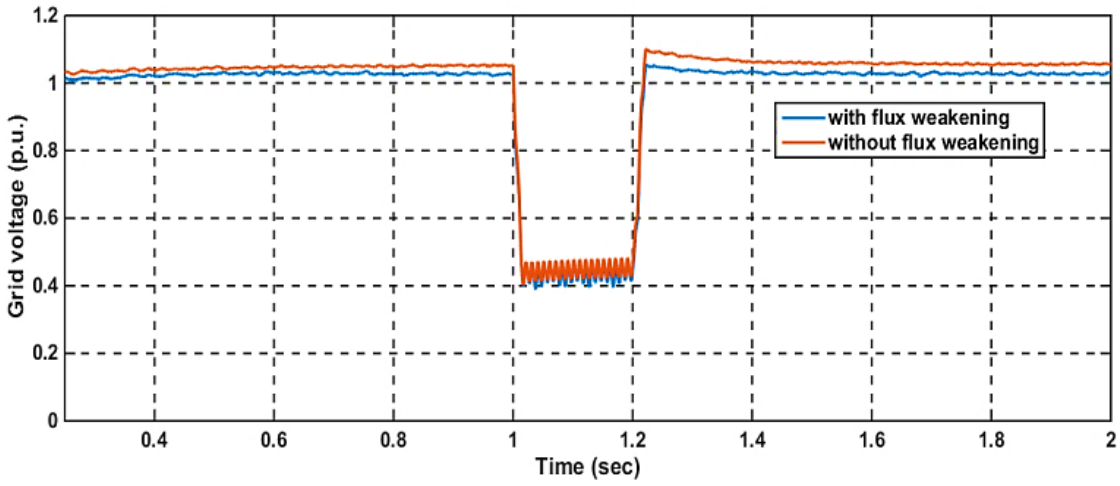

(a)

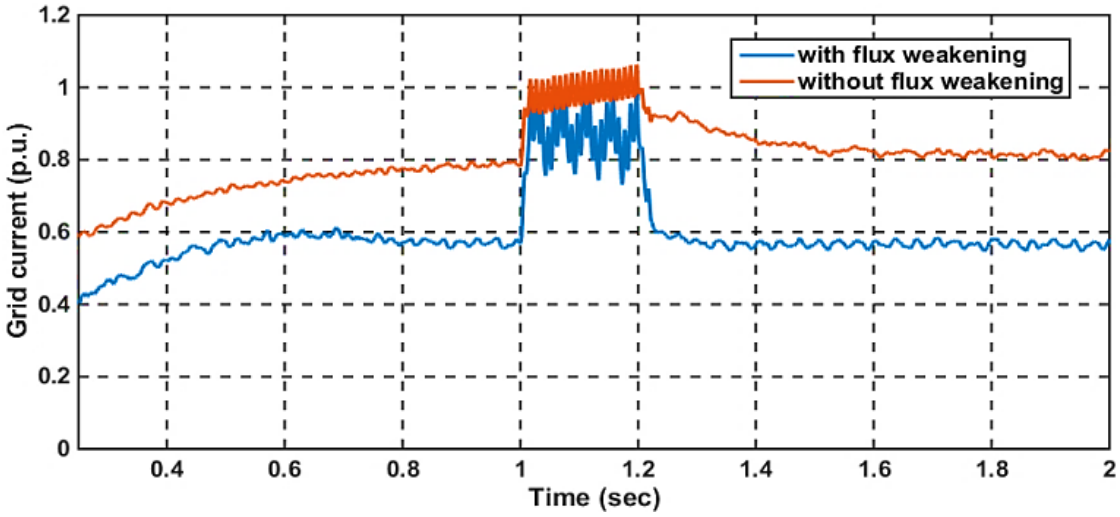

(b)

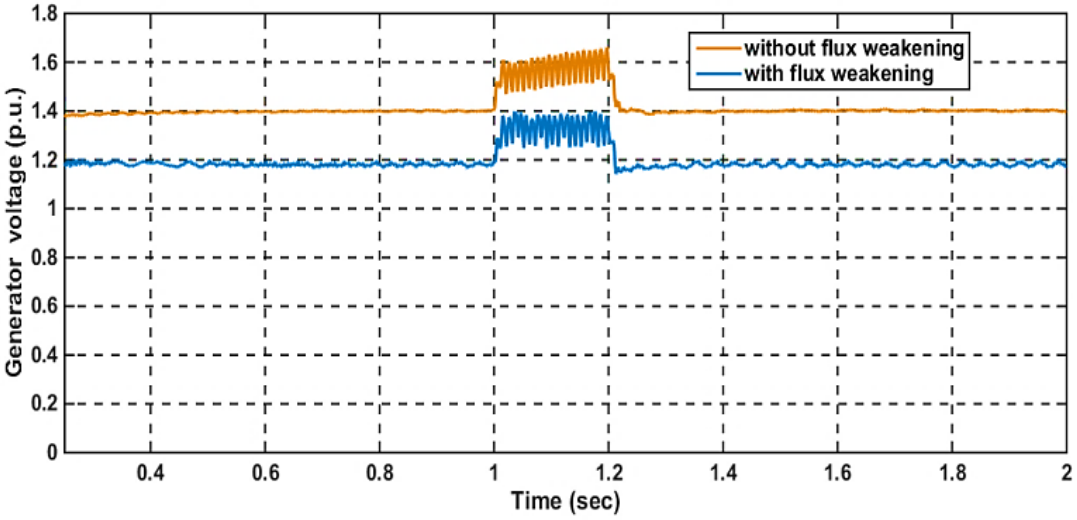
without flux weakening
with flux weakening
Generator voltage (p.u.)
Time (sec)

(c)

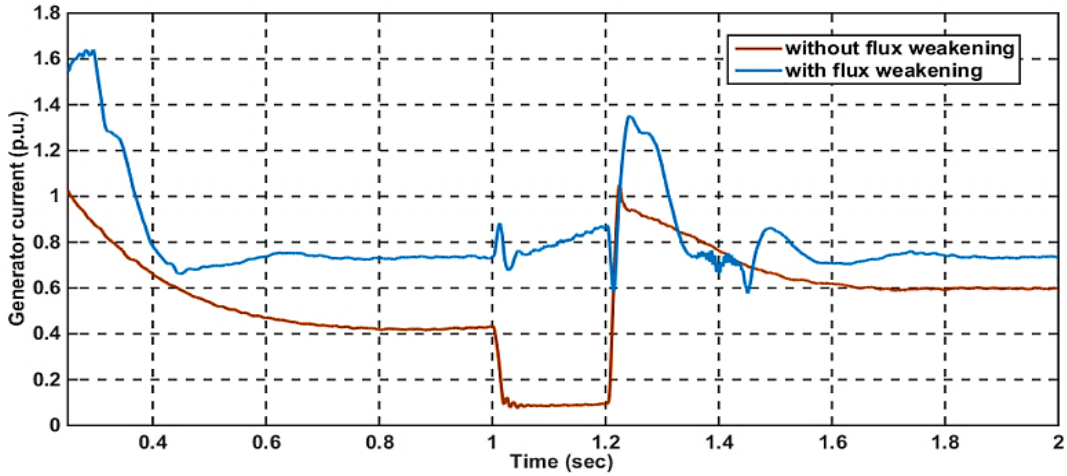
without flux weakening
with flux weakening
Generator current (p.u.)
Time (sec)

(d)

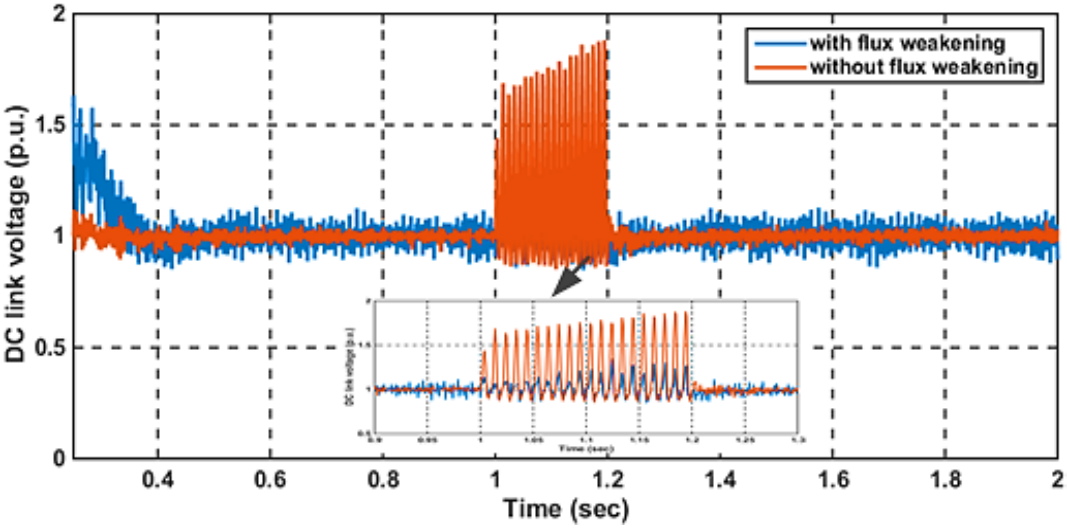
with flux weakening
without flux weakening
DC link voltage (p.u.)
Time (sec)

(e)

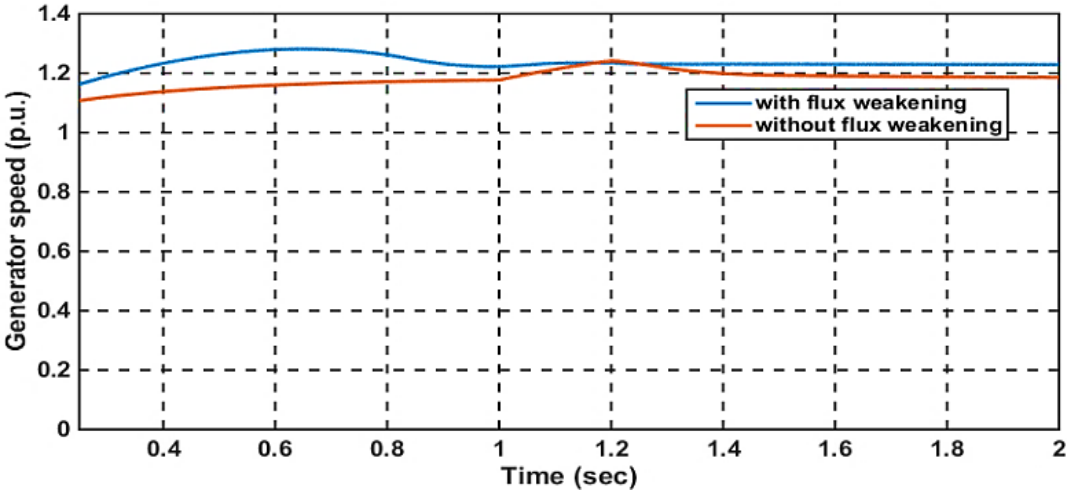

(f)

Fig.3. 14. Simulation results during asymmetrical fault for PR controller a) Grid voltage b) Grid current c) Generator voltage d) Generator current e) DC link voltage f) Generator speed

Based on the previous results and analysis, it can be concluded that the stationary frame-based controller provides better response than the synchronous frame-based controllers [13], [14]. So, the general stationary frame PR based flux weakening controller is considered in this research to minimise the DC link overvoltage for its robustness.

Now another time series simulation is done in different voltage dip and different fault duration to verify the effectiveness of PR based flux weakening controller [15]. Then the results are compared with conventional BC.

3.5.8. Comparison under a Symmetrical Fault with the Stationary PR and the Conventional BC

A three line to ground fault is considered as the most severe type of grid fault and is applied on the 25 kV line at 1s which is lasting for 0.5s. As shown in Fig.3.15 (a) and Fig. 3.16(a), a large dip in the grid voltage is occurred and the grid voltage is reduced from 100% of its nominal value to 30%. As a consequence, the dc-link voltage is increased to approximately 1.5 times its rated value as shown in Fig. 3.15(e) and Fig. 3.16(e)

respectively without any LVRT control. The LVRT control takes action and the fault is cleared at 1.5s. Grid current, generator voltage, generator current during this condition are shown in Figs. 3.15(b) to(d) and Figs. 3.16(b) to(d) for the conventional control and the proposed control respectively. From Fig. 3.15(e) and Fig. 3.16(e), it is observed that the DC link voltage is well regulated within the acceptable limit with the proposed control and overall fluctuations and transients are less than that of the conventional control.

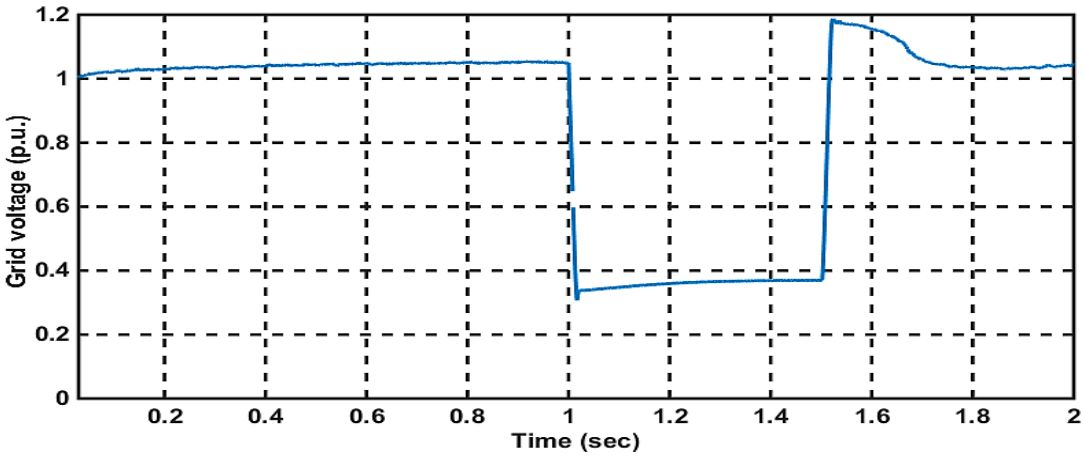

(a)

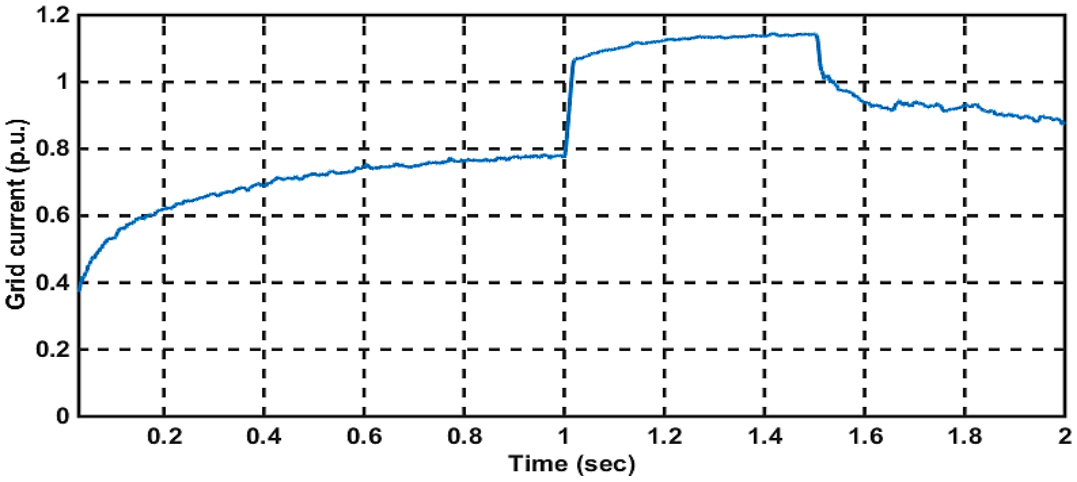

(b)

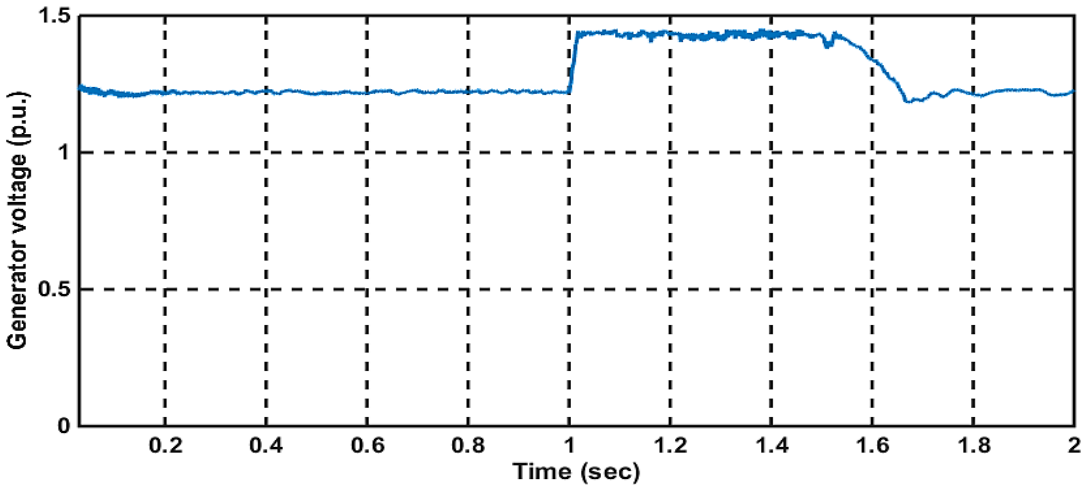

(c)

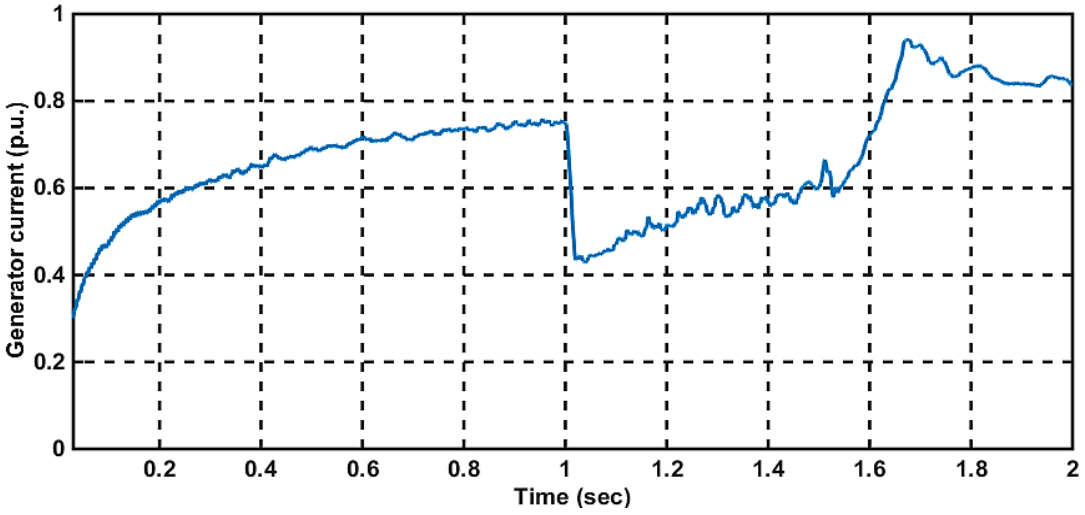

(d)

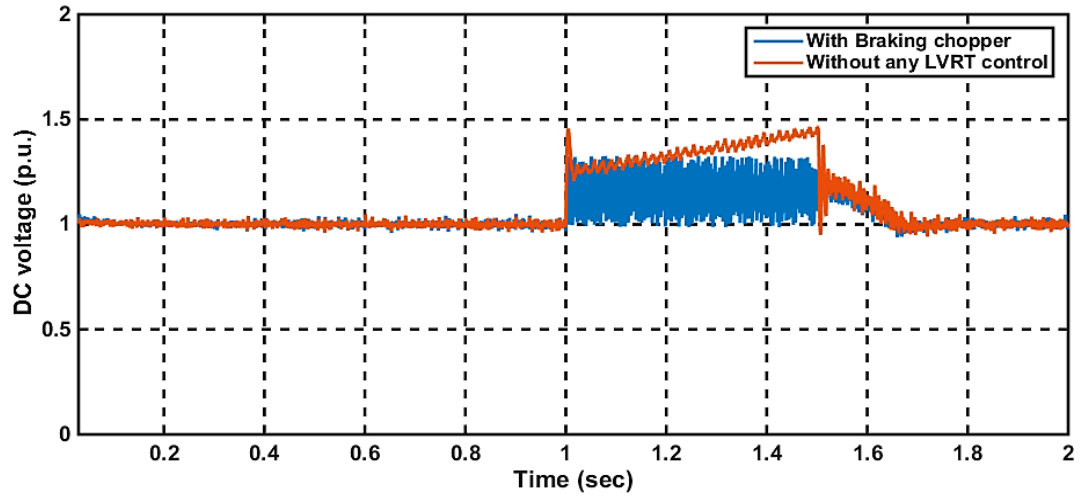

(e)

Fig.3. 15. Simulation results for BC a) Grid voltage b) Grid current c) Generator voltage d) Generator current e) DC voltage

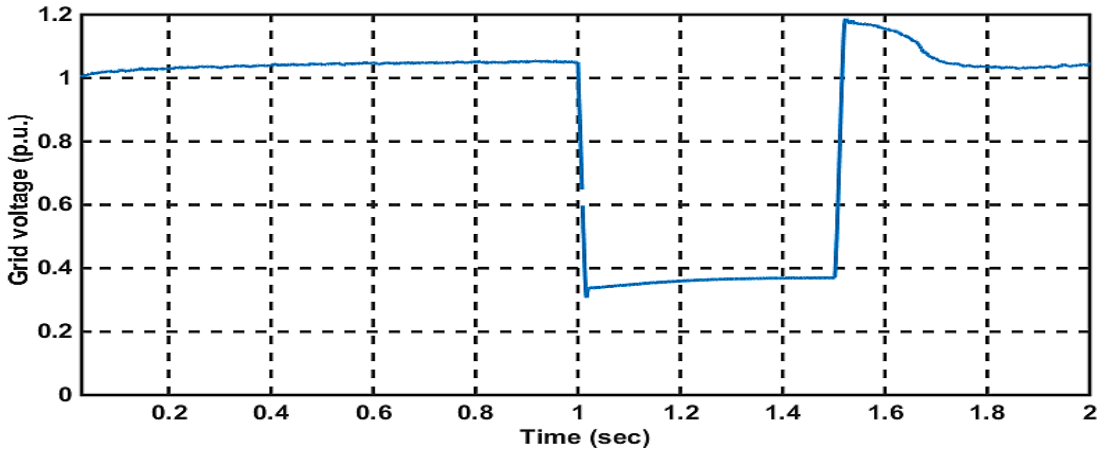
Grid voltage (p.u.)
Time (sec)
1.2
1
0.8
0.6
0.4
0.2
0
0.2
0.4
0.6
0.8
1
1.2
1.4
1.6
1.8
2

(a)

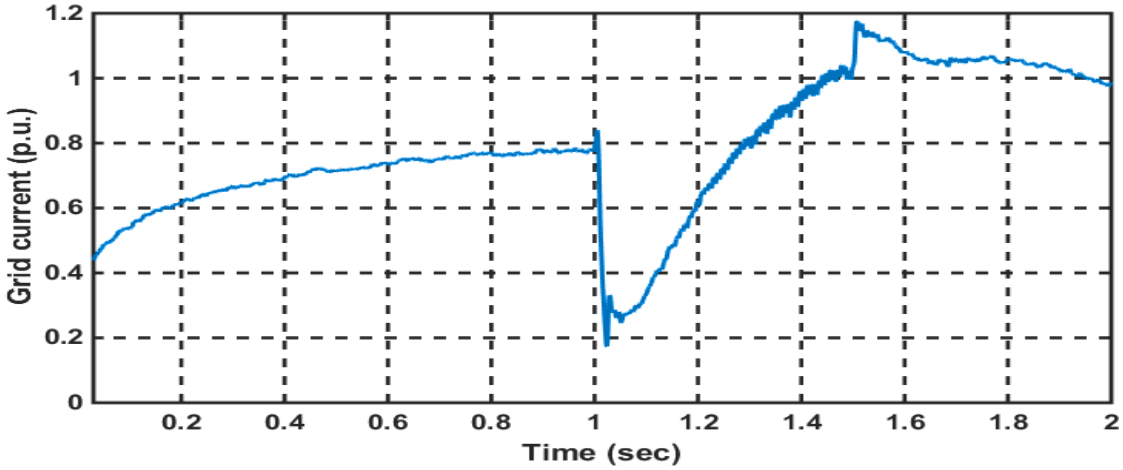
Grid current (p.u.)
Time (sec)
1.2
1
0.8
0.6
0.4
0.2
0
0.2
0.4
0.6
0.8
1
1.2
1.4
1.6
1.8
2

(b)

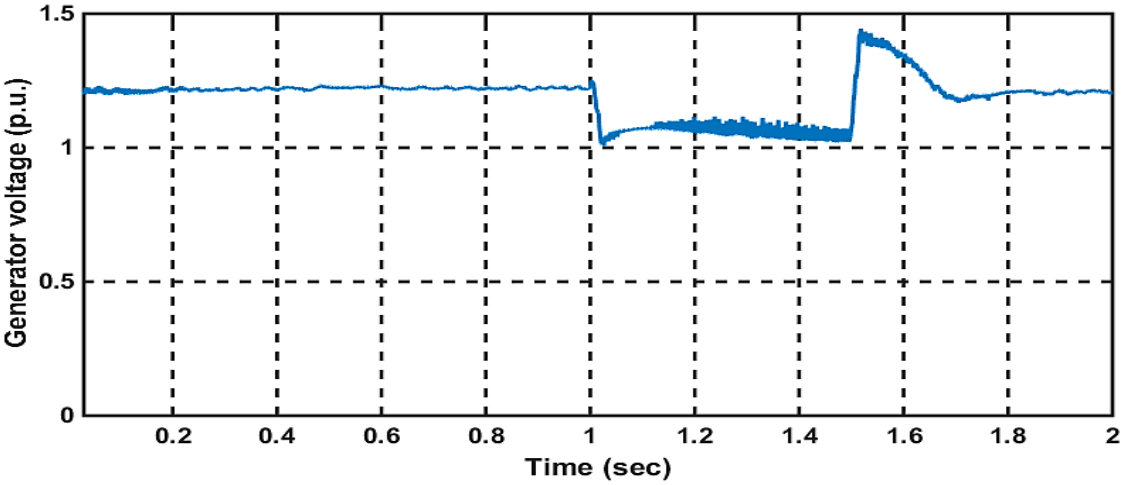
Generator voltage (p.u.)
Time (sec)
1.5
1
0.5
0
0.2
0.4
0.6
0.8
1
1.2
1.4
1.6
1.8
2

(c)

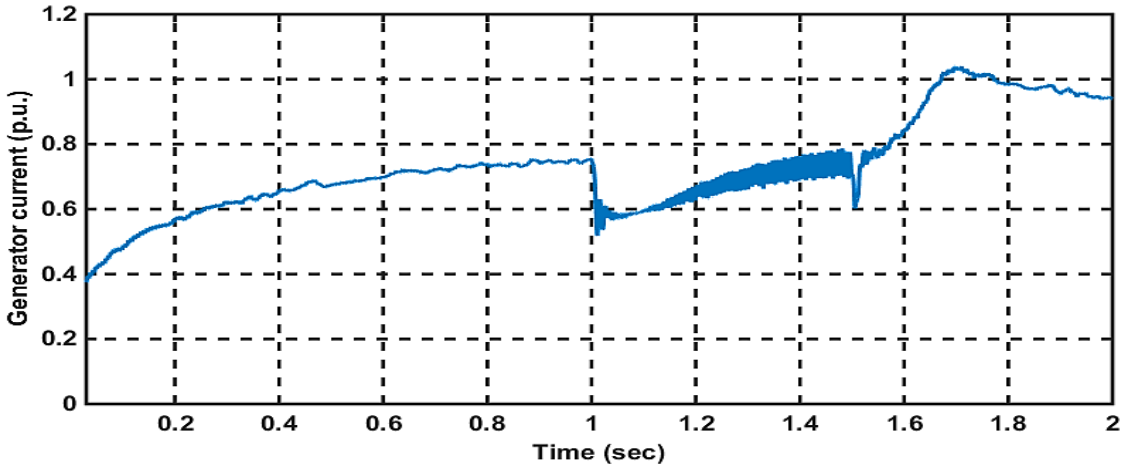

(d)

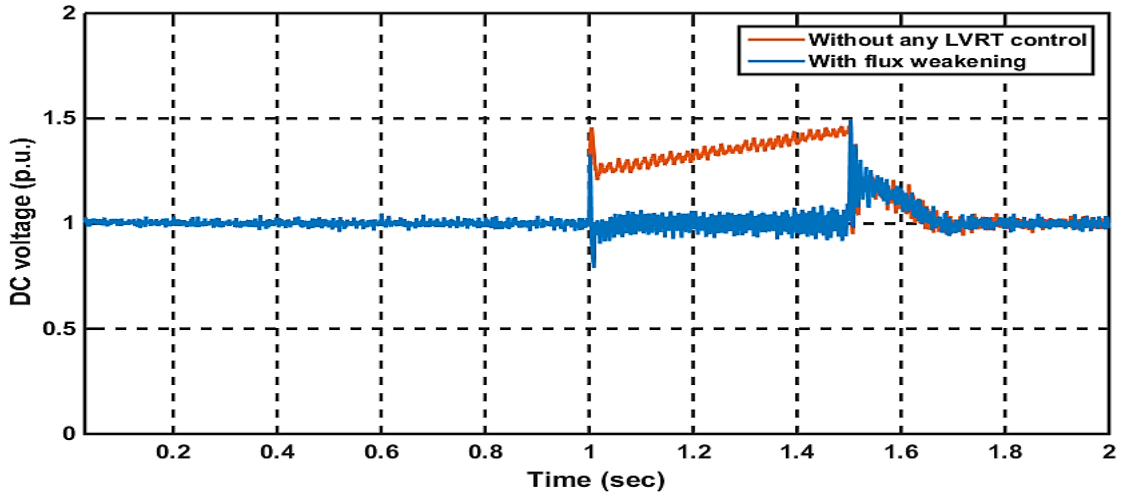

(e)

Fig.3.16. Simulation results for flux weakening controller a) Grid voltage b) Grid current c) Generator voltage d) Generator current e) DC voltage

3.5.9. Comparison under an Asymmetrical Fault with the Stationary PR and the Conventional BC Controller

For second simulation scenario, a double line to ground fault is considered as the most common type of grid fault and is applied on the 25 kV line at 1s which lasting for 0.5s. As shown in Fig.3.17(a) and Fig. 3.18(a), a medium dip in the grid voltage is applied and the grid voltage is reduced from 100% of its nominal value to 60%. As a consequence, the DC link voltage is increased to approximately 1.4 times its rated value as shown in

Fig. 3.17(e) and Fig. 3.18(e) respectively without any LVRT control. The LVRT control takes action and the fault is cleared at 1.5s. Grid current, generator voltage, generator current during this condition are shown in Figs. 3.17(b) to(d) and Figs. 3.18(b) to(d) for the conventional control and the proposed control respectively. From Fig. 3.17(e) and Fig. 3.18(e), it is observed that the DC link voltage is well regulated within the acceptable limit with the proposed control and overall fluctuations and transients are less than that of the conventional control.

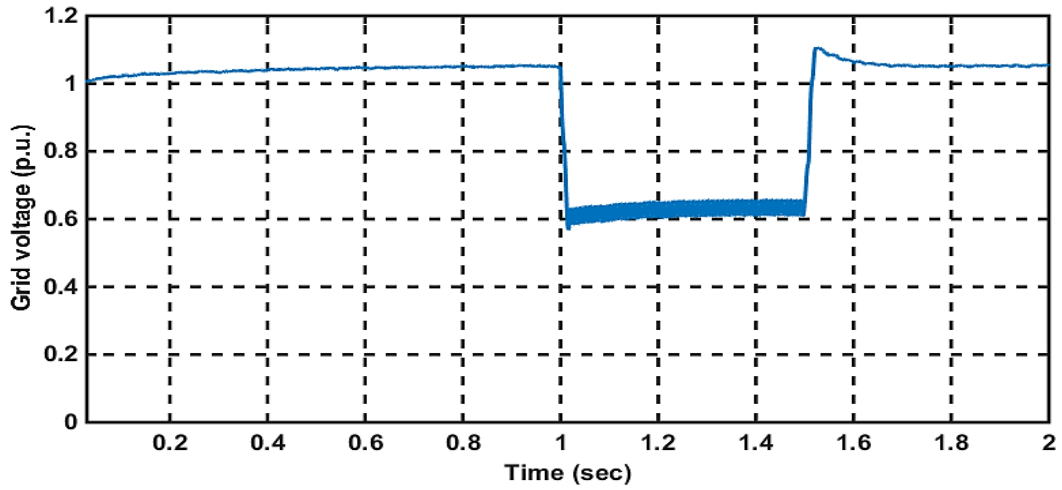

(a)

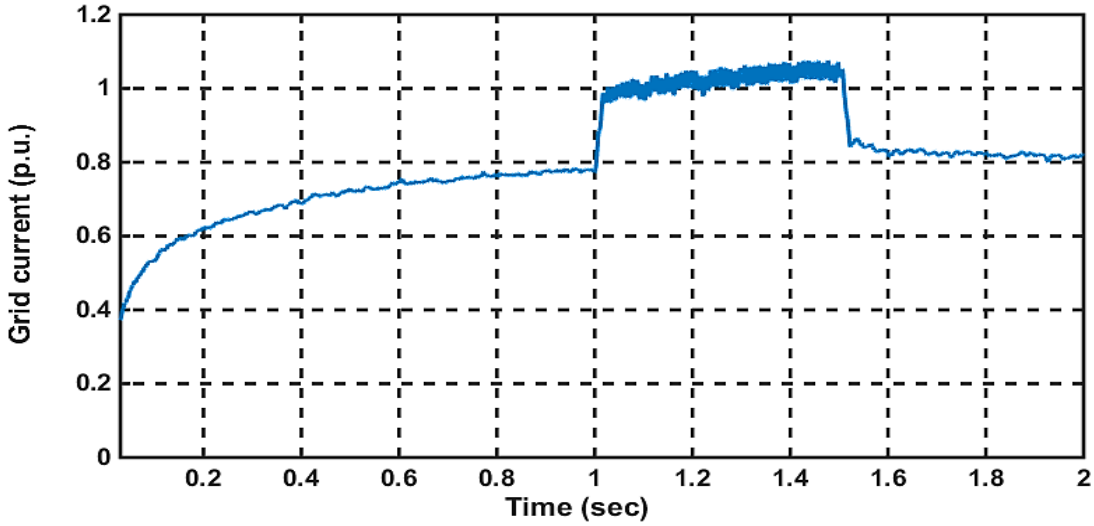

(b)

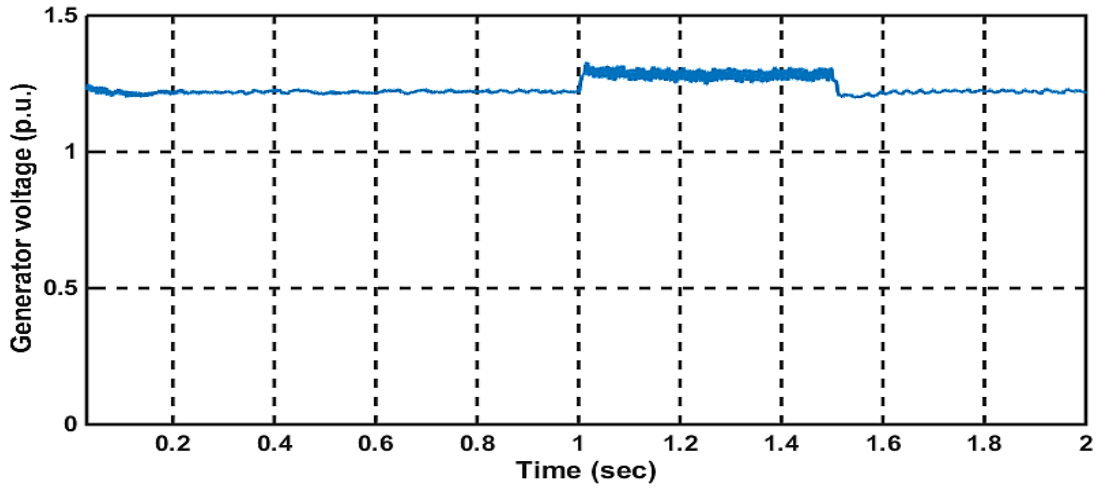

(c)

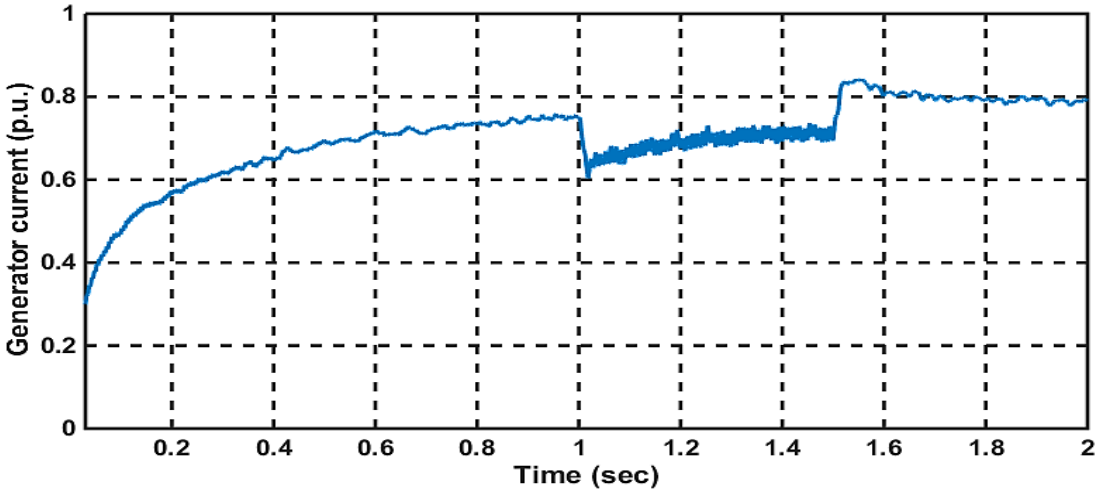

(d)

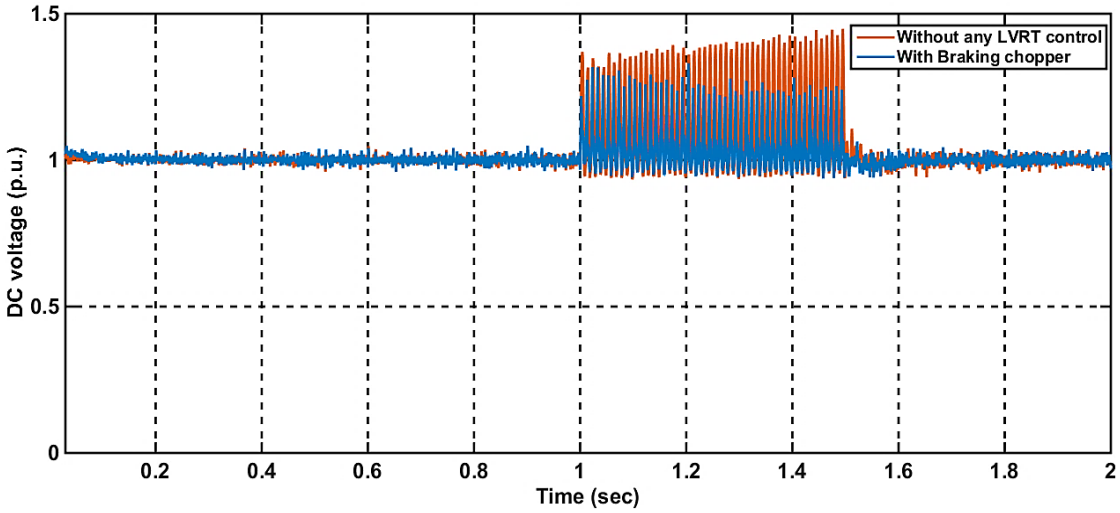

(e)

Fig.3. 17. Simulation results for BC a) Grid voltage b) Grid current c) Generator voltage d) Generator current e) DC voltage

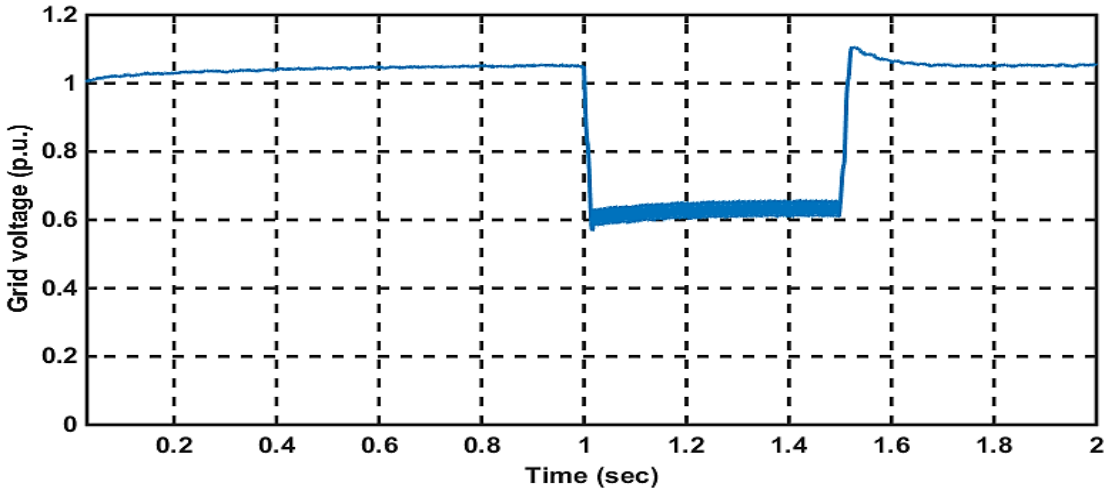
Grid voltage (p.u.)
Time (sec)
1.2
1
0.8
0.6
0.4
0.2
0
0.2
0.4
0.6
0.8
1
1.2
1.4
1.6
1.8
2

(a)

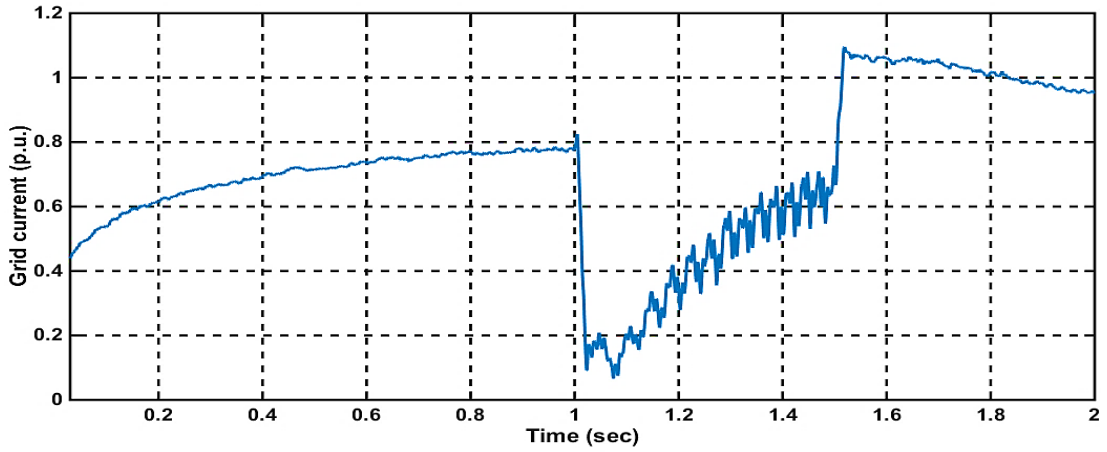
Grid current (p.u.)
Time (sec)
1.2
1
0.8
0.6
0.4
0.2
0
0.2
0.4
0.6
0.8
1
1.2
1.4
1.6
1.8
2

(b)

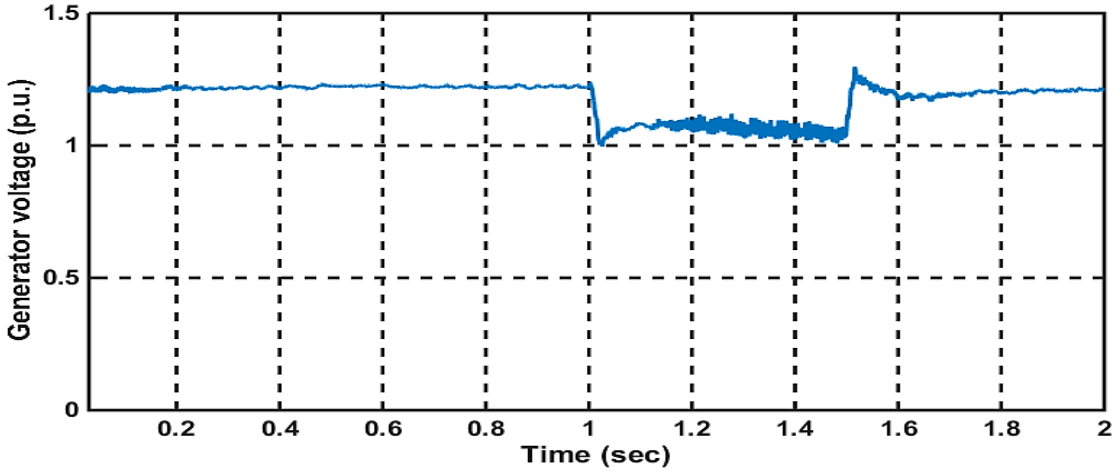
Generator voltage (p.u.)
Time (sec)
1.5
1
0.5
0
0.2
0.4
0.6
0.8
1
1.2
1.4
1.6
1.8
2

(c)

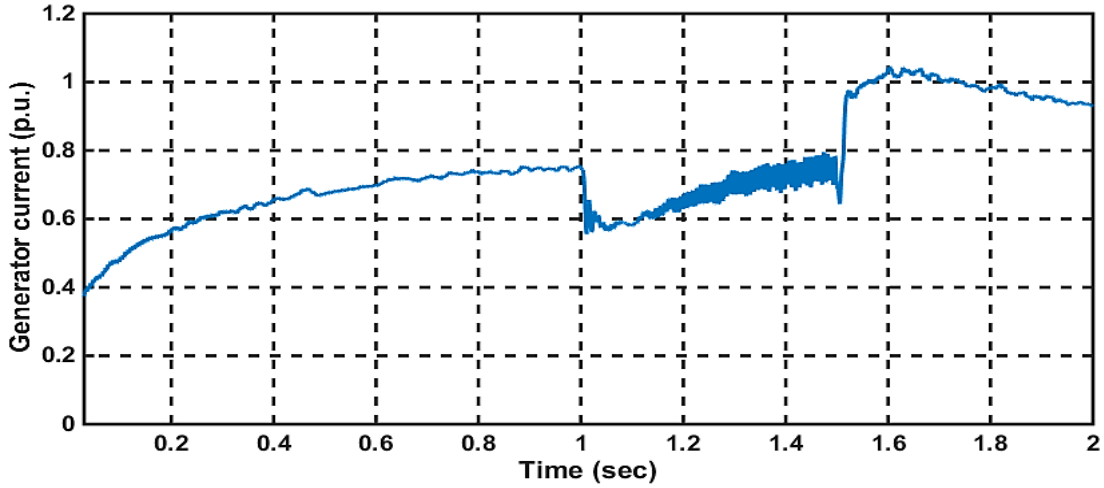

(d)

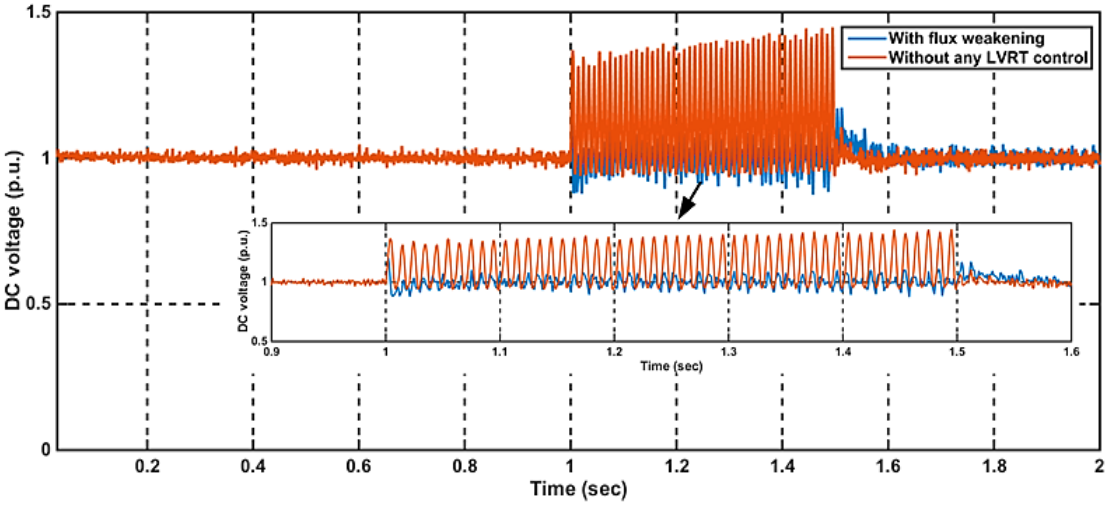

(e)

Fig.3.18. Simulation results for flux weakening controller a) Grid voltage b) Grid current c) Generator voltage d) Generator current e) DC voltage

3.6. Summary

Back to back converter topology is usual structure for the grid connected PMSG based WECS. Selection of parameters of the power converters is presented. In addition, the design of shunt passive filter to eliminate fifth order harmonics is also described. To limit the DC-link capacitor overvoltage under a grid fault and to provide a better LVRT, a control technique based on the flux weakening from the motor drives is proposed. From the numerical simulation results, it is observed that the PR based flux weakening

controller is more capable of limiting the DC-link overvoltage under symmetrical and asymmetrical grid faults. Due to the simplicity and effectiveness of the proposed controller, it can be a superior choice compared to the conventional BC based method. The proposed flux weakening control can be used to develop a coordinated control to provide a better FRT solution during and after the grid fault transient period which is presented in the next chapter.

REFERENCES

[1] S. K. Chauhan, M. C. Shah, R. R. Tiwari, and P. Tekwani, "Analysis, design and digital implementation of a shunt active power filter with different schemes of reference current generation," *IET Power Electronics*, vol. 7, pp. 627-639, 2014.

[2] F. Krim, "Parameters estimation of shunt active filter for power quality improvement," in *5th International Power Engineering and Optimization Conference (PEOCO),* 2011, pp. 306-311.

[3] E. C. Sekaran, P. N. Anbalagan, and C. Palanisamy, "Analysis and simulation of a new shunt active power filter using cascaded multilevel inverter," *Journal of Electrical Engineering-Bratislava-*, vol. 58, p. 241, 2007.

[4] S. Jain, P. Agrawal, and H. Gupta, "Fuzzy logic-controlled shunt active power filter for power quality improvement", *IEEE Proceedings-Electric Power Applications*, vol. 149, pp. 317-328, 2002.

[5] K. Jalili and S. Bernet, "Design of filters of active-front-end two-level voltage-source converters," *IEEE Transactions on Industrial Electronics*, vol. 56, pp.1674-1689, 2009.

[6] M. Tavakoli Bina and E. Pashajavid, "An efficient procedure to design passive LCL filters for active power filters," *Electric Power Systems Research*, vol. 79, pp. 606-614, 2009.

[7] L. Wang, S. Chai, D. Yoo, L. Gan and K. Ng, "PID and Predictive Control of Electrical Drives and Power Converters Using MATLAB/Simulink", Singapore:*Wiley*, 2014

[8] Z. Zhou, F. Scuiller, J. F. Charpentier, M. El Hachemi Benbouzid and T. Tang,"Power smoothing control in a grid-connected marine current turbine system for compensating swell effect", *IEEE Transaction on Sustainable Energy*, vol. 4, pp. 816-826, 2013.

[9] P. Sandulescu, F. Meinguet, X. Kestelyn, E. Semail, and A. Bruyere, "Control Strategies for Open-End Winding Drives Operating in the Flux-Weakening Region," *IEEE Transaction on Power Electronics*, vol. 29, pp. 4829-4842, 2014.

[10] Y. Jiang, Q. Pu, S. Huang, Z. Xu, K. Huang, and L. Xiao, "Improved method on flux-weakening control of permanent magnet synchronous motor in electric vehicles," in *International Conference on Electrical Machines and Systems (ICEMS)*, 2011, pp. 1-4.

[11] D. G. Holmes, T. A. Lipo, B. P. McGrath, and W. Y. Kong, "Optimised design of stationary frame three phase ac current regulators," *IEEE Transaction on Power Electronics,* vol. 24, no. 11, pp. 2417–2426, Nov. 2009.

[12] Y. Li, Y.-n. Chi, and Z. Wang, "Study of LVRT capability of D-PMSG based Wind turbine," in *IEEE Power Engineering and Automation Conference (PEAC), Wuhan, China:* 2011, pp. 154-157.

[13] P. Dey, M. Datta and N. Fernando, "Comparisons of PI and PR current controllers-based flux weakening to limit DC-link capacitor overvoltage in PMSG based wind energy system," in *IEEE Innovative Smart Grid Technologies-Asia (ISGT-Asia),* 2016, pp. 29-34.

[14] P. Dey, M. Datta, N. Fernando, and T. Senjyu, "Comparison of synchronous and stationary frame pi-based flux weakening controls for DC-link overvoltage minimisation of WECS under grid fault," in *IEEE Region 10 Conference (TENCON),* 2016, pp. 655-660.

[15] P. Dey, M. Datta, N. Fernando, and T. Senjyu, "A method to reduce DC-link overvoltage of PMSG based WECS during LVRT," in *IEEE Region 10 Conference (TENCON),* 2016, pp. 1894-1899.

CHAPTER FOUR

COORDINATED CONTROLLER DESIGN FOR THE FRT

4.1. Introduction

This chapter presents a coordinated control which combines the pitch angle control of a WTG and the proposed flux weakening control of PMSG presented in the Chapter 3. This coordination control is used to enhance the LVRT capability of PMSG based variable speed WECS. In this strategy, the pitch angle controller adjusts the pitch for the wind power smoothing as well as the DC link overvoltage minimization control during variable wind speeds and the grid faults respectively. The flux weakening controller is used to reduce the flux linkages of the PMSG by supplying a negative field regulating current to reduce the DC link overvoltage during grid voltage dips. The design process of controller parameters and the stability of the proposed control strategy have been analyzed. Extensive simulations for the proposed method have been carried out under different cases in MATLAB/SIMULINK. The effectiveness of the proposed controller is then verified and compared with the ESS based conventional controller.

4.2. Coordinated Control Scheme: Combining Pitch Angle Control and Flux Weakening Control

The proposed control strategy can be demonstrated by combining the pitch angle control and the flux weakening control presented in the Chapter 3. The total control block diagram is shown in Fig. 4.1. This new control method is developed to smooth the WTG's power output and to limit the DC link over voltage.

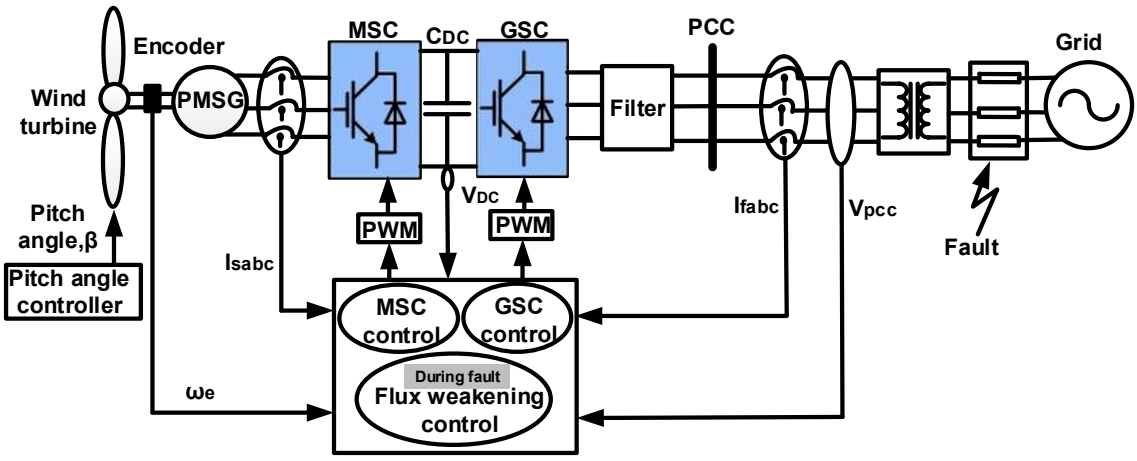

Fig.4.1. The coordinated control block diagram of the PMSG based WECs for LVRT.

4.2.1. Pitch Angle Control Design

The operational diagram of the pitch angle control is shown in Fig. 4.2(a). The switching logic of the normal operation and FRT operation mode are shown in Fig. 4.2(b). During normal operations, the pitch angle control is activated when the wind speed is higher than the rated wind speed [1]. During the grid fault, the pitch angle control is modified based on the DC-link capacitor voltage. The controller is developed in four parts namely PI controller, servo delay, pitch angle saturation and rate limiter [2], [3]. The difference between the rated DC-link capacitor voltage and the measured one or the difference between the rated rotor speed and the measured one is passed through the PI controller. The pitch angle controller consists of a servomotor and it is modelled by using a first order delay system with a time constant (T_d). Pitch rate of change decides the response of reducing the mechanical power to prevent the over-speeding of the generator during both higher wind speed and grid fault.

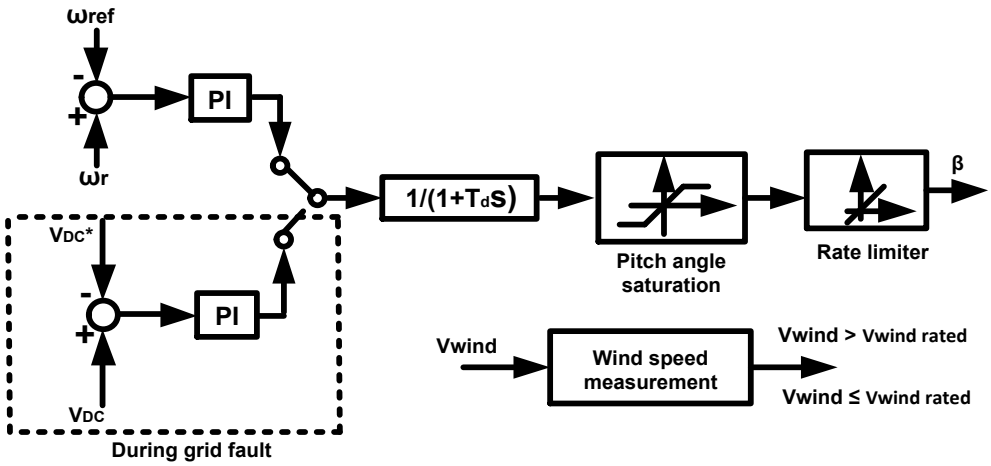

(a)

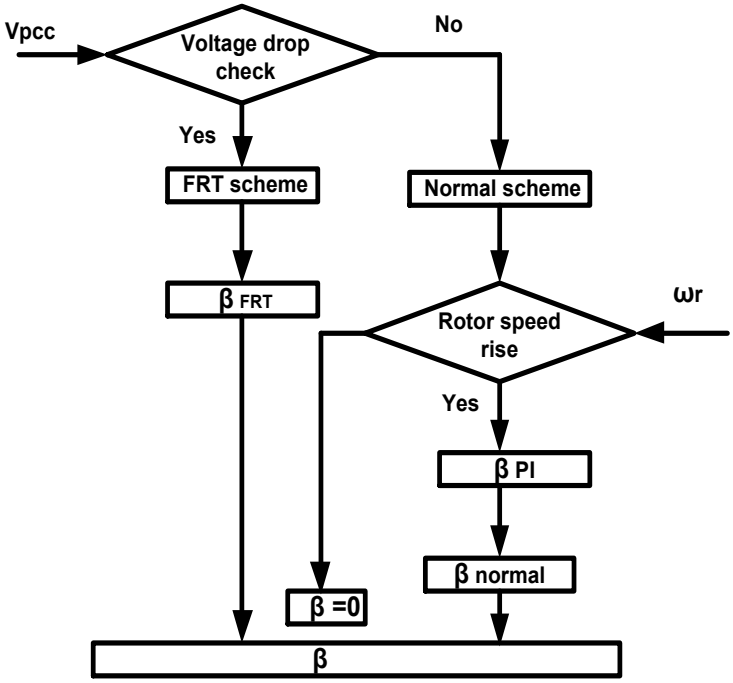

(b)

Fig.4. 2. Pitch angle control system a) Block diagram b) Flow chart

4.2.2. Flux Weakening Control Design

The PR based flux weakening control diagram is shown in Fig. 4.3(a). Using Clarke transformation three phase AC currents can be converted into orthogonal α-β currents. The difference between PR current controllers output voltages (V_α^*, V_β^*) and the

converter DC link voltage is passed through a PI controller and a limiter to generate the I_d reference current for flux weakening control. I_q reference current is the difference between maximum converter current and I_d reference current. Then the I_d and I_q reference currents are transformed to generate I_α reference current. It can be noticed that, there is no coupling terms $\omega_e L_s I_{ds}$, $\omega_e L_s I_{qs}$ and feed forward compensation term $\omega_e \varphi_s$, eliminating the impact of the circuit parameters on the control system, which improves system robustness [4]. The proposed controller operation logic is shown in Fig.4.3 (b).

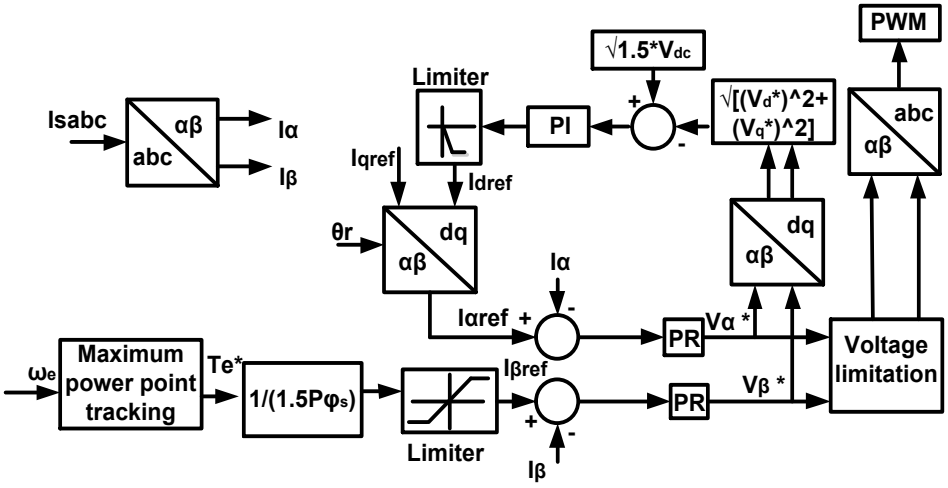

(a)

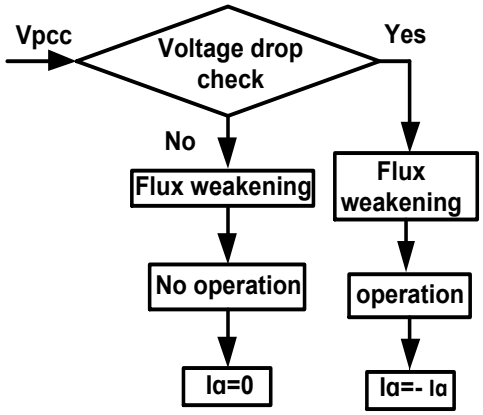

(b)

Fig.4. 3. PR based Flux weakening control for MSC a) Block diagram b) Flow chart

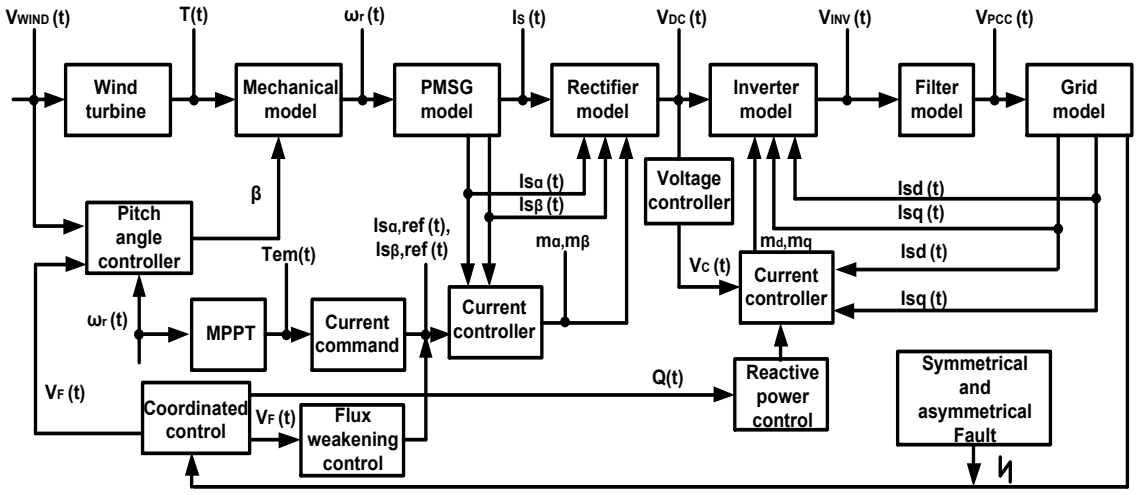

Fig.4. 4. PMSG based WECS with controllers

4.3. Coordinated System Controller Design and Stability Analysis

The developed WTG block diagram with control method is shown in Fig.4.4 which is the basis for transfer function synthesis. This mainly deals with system stability by calculating the total transfer function which consists of different sub transfer functions. So, the total transfer function is developed from a mathematical model, control scheme and multiplying the sub transfer function of each part [5].

The grid connected PMSG based WECS consists of a wind turbine, PMSG, rectifier, DC capacitor, inverter, filter, transformer, transmission line and Grid. It is inconvenient to determine the transfer function of the total system using a single function. So, it is better to derive transfer function of each element. Then it can connect each other with the signal flow path [5], [6]. This section represents the overall transfer function of the system with required number of interconnected blocks.

4.3.1. Modelling of the WTG System

It comprises a wind turbine, a PMSG and a rectifier with DC link capacitor.

4.3.1.1. Wind Turbine Dynamics

Using generator convention, the generator speed and torque of wind turbine follows from

$$T_m(t) = T_e(t) + J_t \frac{d\omega_r(t)}{dt} + F\omega_r(t) \qquad (4.1)$$

Where T_m is the driving torque of turbine, J_t is the total equivalent inertia and the friction coefficient is F. The transfer function of a mechanical model G_T (ratio of rotor speed to the change of torque) is expressed in the Laplace domain as

$$G_T(S) = \frac{\omega_r(S)}{T(S)} = \frac{1}{J_t S + F} \qquad (4.2)$$

4.3.1.2. PMSG Modelling

Using PMSG equations in Laplace domain

$$I_S(S) = \frac{1}{R_S + L_S S}[-V_S(S) + \varphi * P * \omega_r(S)] \qquad (4.3)$$

Where $I_s(s)$ is a phase current, $V_s(s)$ is a phase voltage and $\omega_r(s)$ is a rotor speed. From equation 4.3 phase impedance is obtained from the ratio of phase voltage and phase current which is not included here for calculation. So, the PMSG transfer function is (the phase current to a rotor speed ratio) given as

$$G_G(S) = \frac{1}{R_S + L_S S}[\varphi * P] \qquad (4.4)$$

4.3.1.3. Rectifier Dynamics

The three- phase inverter in machine side works as a rectifier and it's three phase voltage is expressed as

$$V_{abc} = \frac{\sqrt{3}}{2} V_{DC} \sum_{n=1}^{\infty} A_n \sin n(\omega t + \theta) \qquad (4.5)$$

So, the transfer function of rectifier becomes

$$G_R(S) = \frac{V_{DC}(S)}{V_{abc}(S)} = \frac{2}{\sqrt{3}} * \frac{1}{\sum_{n=1}^{\infty} A_n \frac{S\sin\theta + n\omega\cos\theta}{S^2 + (n\omega)^2}} \qquad (4.6)$$

So, the open loop transfer function of PMSG based wind turbine generator (WTG) without controller becomes

$$G_{WTG}(S) = G_T(S) * G_G(S) * G_R(S) \tag{4.7}$$

The switching function can be ignored to calculate the transfer function. So, the open loop transfer function is as

$$G_{WTG}(S) = \frac{V_{DC}(S)}{T(S)} = \frac{1}{J_t L_s S^2 + (F * L_S + J_t * R_s)S + F * R_s}[\varphi * P] \tag{4.8}$$

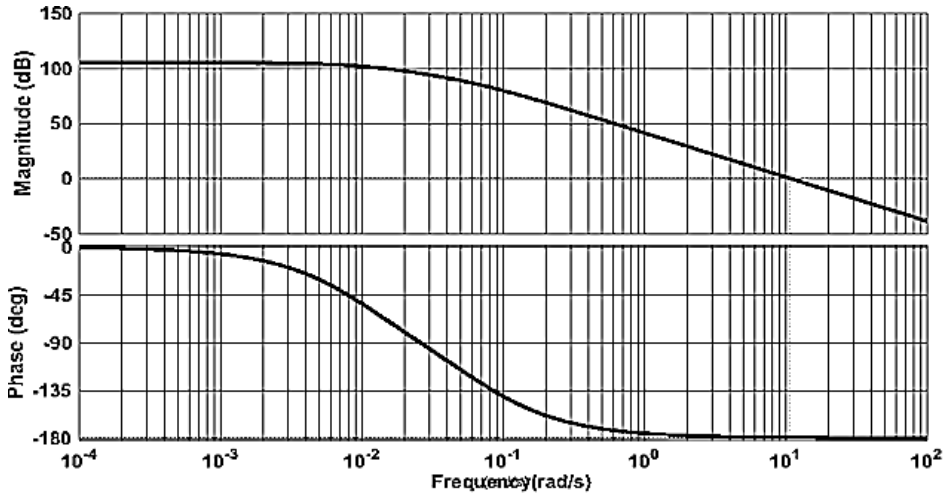

(a)

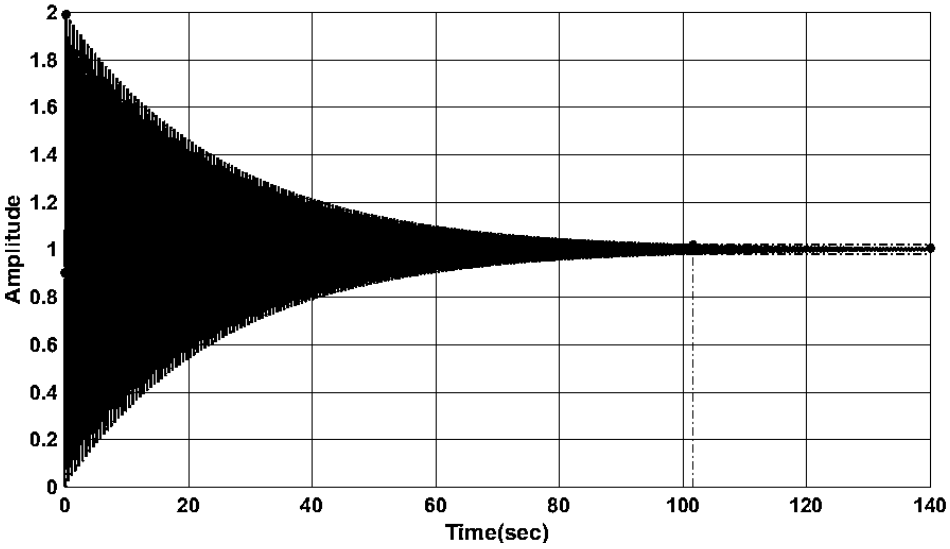

(b)

Fig.4. 5. (a) Bode plot for open loop (b) Step response for close loop

Now the open loop and close loop transfer function are obtained by putting the values of parameters. The bode plot and step response of the system are obtained as shown in Fig. 4.5(a) and Fig.4.5(b) correspondingly.

From this figure, it is observed that the close loop system is stable, but the step response is not satisfactory as its overshoot is high and the settling time is large. So, it is required to include the controller to make the system robust with desired response.

4.3.1.4. Design of the MSC Current Controller

The current controller block diagram is shown in Fig.4.6. It consists of a PR controller, a PWM converter and PMSG. The transfer function of each component is as

1. For PR controller, the transfer function

$$G_{PR}(S) = K_P + K_i(S) * \frac{2S}{S^2 + \omega_0{}^2} \quad (4.9)$$

2. PWM inverter introduces delay into a whole system and it is modelled by first order transfer function where time constant is defined as $T_{PWM} = 1/f_{PWM}$ where f_{PWM} is a switching frequency.

And the transfer function becomes

$$G_{PWM}(S) = \frac{1}{1 + T_{PWM} S} \quad (4.10)$$

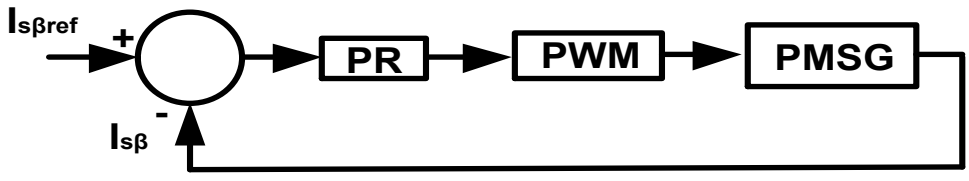

Fig.4. 6. PMSG with current controller

3. And PMSG transfer function becomes

$$G_G(S) = \frac{1}{R_S + L_S S} [\varphi * P] \quad (4.11)$$

The PR current controller gains are obtained via the modulus optimum tuning criteria by using those equations [7], [8].

Now the current controller transfer function is

$$G_{IS}(S) = G_{PR}(S) * G_G(S) * G_{PWM}(S) \qquad (4.12)$$

4.3.1.5. WTG with the Pitch Angle Control

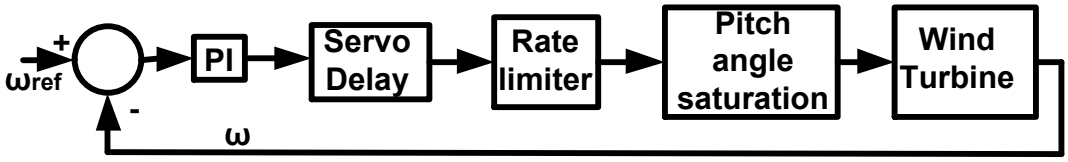

Fig.4. 7. Wind turbine with pitch angle control

The simplified pitch angle control loop is shown in Fig.4.7. The transfer function of each block is as

1. For PI transfer function becomes

$$G_{PI}(S) = K_P(1 + T_i S)/T_i S \qquad (4.13)$$

Where $T_i = K_p/K_i$

2. For servo delay transfer function becomes

$$G_D(S) = 1/(1 + T_\beta S) \qquad (4.14)$$

Normally delay time, T_β is considered as 0.2s. As rate limiter and pitch angle saturation block create some delay so the equivalent delay is considered as 0.5s.

3. The wind turbine transfer function becomes

$$G_T(S) = \frac{1}{J_t S + F} \qquad (4.15)$$

Now the total transfer function of pitch angle controller becomes

$$G_P(S) = G_{PI}(S) * G_D(S) * G_T(S) \qquad (4.16)$$

4.3.2. Grid Side Converter Modelling

The grid side part comprises a voltage source, filter, and an inverter. The grid side equations are transformed in Laplace domain and the transfer function of each component in block diagram is follows as

1. The transfer function of DC link capacitor

$$G_C(S) = \frac{V_{dc}(S)}{I_d(S)} = \frac{1}{CS} \qquad (4.17)$$

2. The grid transfer function

$$G_{GD}(S) = \frac{I(S)}{V_{INV}(S)} = \frac{1}{L_f S + R} \qquad (4.18)$$

So, the grid side open loop transfer function becomes

$$G_K(S) = G_C(S) * G_{GD}(S) \qquad (4.19)$$

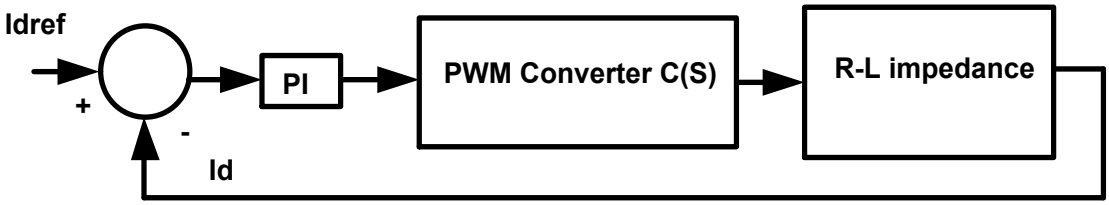

Fig.4. 8. Inner loop current controller block diagram

4.3.2.1. Design of Current Controller for the GSC

Fig.11 represents the general block diagram of current controller. The transfer function of each component in block diagram is expressed as

1. For PI controller transfer function becomes

$$G_{PI}(S) = K_P(1 + T_i S)/T_i S \qquad (4.20)$$

Where $T_i = K_p/K_i$

2. PWM inverter introduces delay into a whole system and it is modelled by first order transfer function where time constant is defined as $T_{PWM} = 1/f_{PWM}$ where f_{PWM} is a switching frequency. And the transfer function becomes

$$G_{PWM}(S) = \frac{1}{1 + T_{PWM} S} \qquad (4.21)$$

3. The grid transfer function

$$G_{GD}(S) = \frac{1}{L_f S + R} \qquad (4.22)$$

So, the open loop transfer function becomes

$$G_X(S) = G_{PI}(S) * G_{PWM}(S) * G_{GD}(S) \qquad (4.23)$$

4.3.2.2. Design of the Voltage Controller for the GSC

Generally, in a cascade control system, the inner loop is tuned according to "modulus optimum" condition but the outer loop is tuned according to "symmetrical optimum" condition [7]-[9]. So, the PI controller gains are obtained via using the symmetrical optimum method. The voltage controller block diagram is shown in Fig.4.9.

Thus, the DC link voltage control loop transfer function can be obtained via

1. For PI transfer function becomes

$$G_{PI}(S) = K_P(1 + T_i S)/T_i S \qquad (4.24)$$

Where $T_i = K_p/K_i$

2. For current controller close loop transfer function becomes

$$G_{CI}(S) = 1/(1 + T_{eq} S) \qquad (4.25)$$

Where $T_{eq} = 2 * T_{PWM}$

3. For plant

$$G_C(S) = \frac{1}{C_{DC} S} \qquad (4.26)$$

So, the open loop transfer function becomes

$$G_Y(S) = G_{PI}(S) * G_{CI}(S) * G_C(S) \qquad (4.27)$$

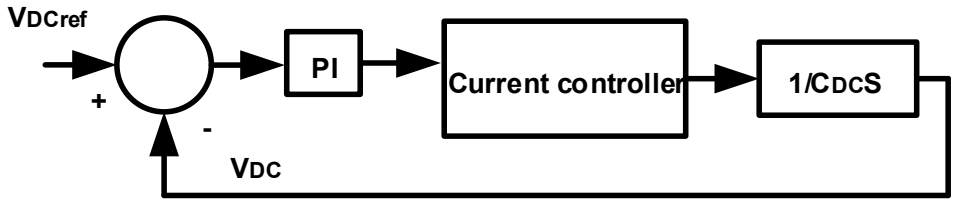

Fig.4. 9. Outer loop voltage controller block diagram

4.3.3. Overall Transfer Function of the Grid Connected WECS with the Controllers During Normal Condition

The complete transfer function of a grid connected WECS with a controller is obtained by multiplying the sub transfer function of the mechanical model, PMSG model, converter and grid as follows:

$$G_T(S)=\frac{V_{PCC}(S)}{T(S)} = \frac{K_1S^3+K_2S^2+K_3S+K_4}{(D_1S^{11}+D_2S^{10}+D_3S^9+D_4S^8+D_5S^7+D_6S^6+D_7S^5+D_8S^4+D_9S^3+D_{10}S^2+D_{11}S+D_{12})} \quad (4.28)$$

Where K_1, K_2, K_3, K_4, D_1, D_2, D_3, D_4, D_5, D_6, D_7, D_8, D_9, D_{10}, $D_{11}$and D_{12} are derived from equations (4.4), (4.12), (4.16), (4.23) and (4.27).

From equation (4.28) it is found that the system is high order. A high order system often contains less significant poles which create little impact on the system response. So, a low-order approximating system can be derived from the original high-order system [10]. In this system design, the dominant poles of transfer function are considered, and insignificant poles are neglected with regard to the transient response. So, the system order is reduced, and it is expressed as

$$G_{RT}(S)=\frac{-XS^2-YS+Z}{AS^2+BS+C} \quad (4.29)$$

Where *A, B, C, X, Y* and *Z* are constant and the parameters are presented in Appendix B. The step response and the Nyquist plot obtained from the reduced order model are presented in Fig. 4.10 (a) and Fig. 4.10 (b). From those figures it is observed that the

system is stable, and the response is fast with very small overshoot. The Hankel Singular Values (HSV) [10], [11] for reduced order model system is shown in Fig.4.11. The larger HSV for a state means the state contains higher energy. So, from this figure it is found that the state 1 has high energy than other state.

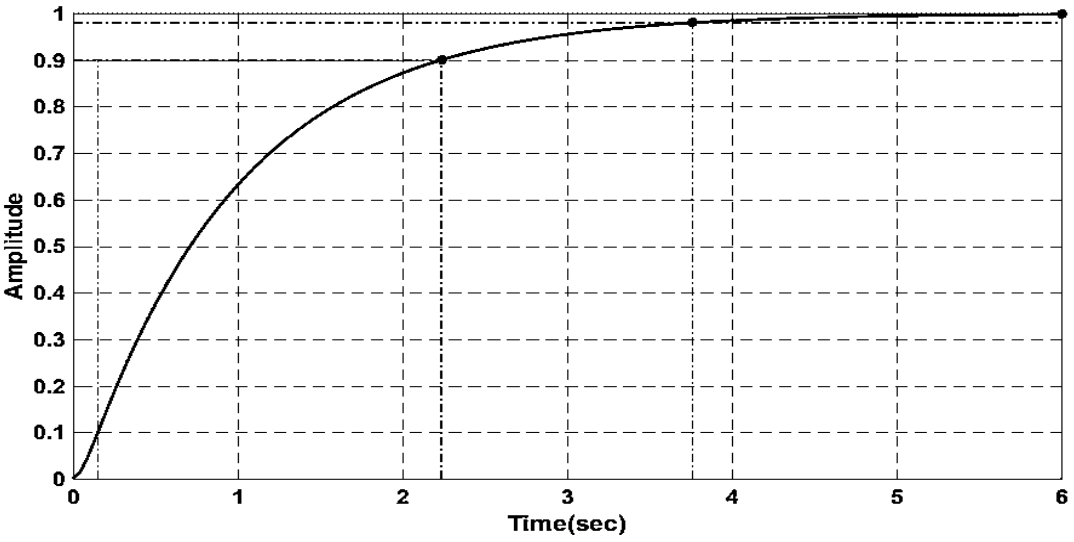

(a)

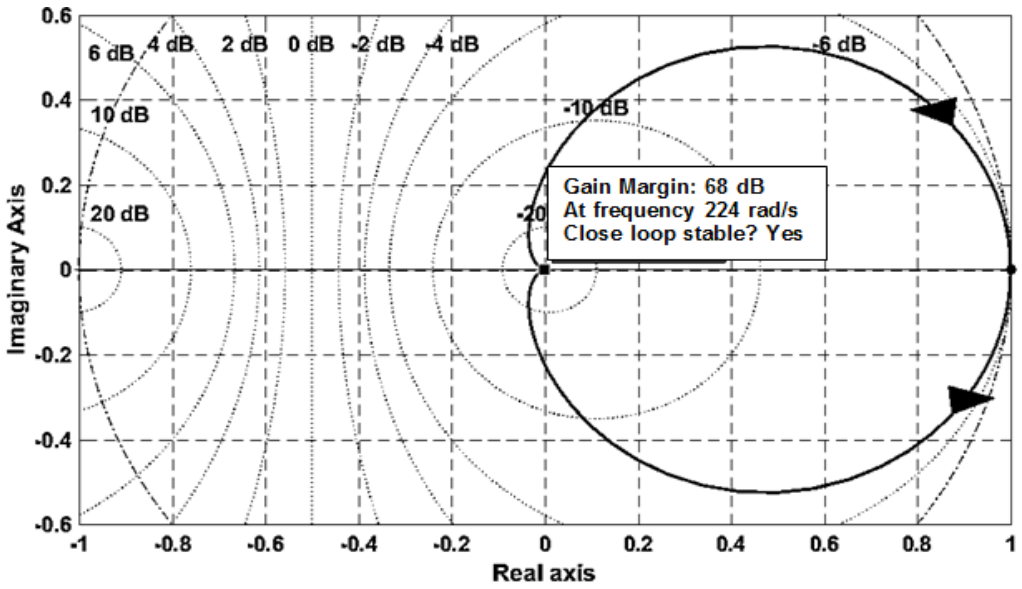

(b)

Fig.4. 10. (a) Step response for reduced order model (b) Nyquist plot for reduced order model

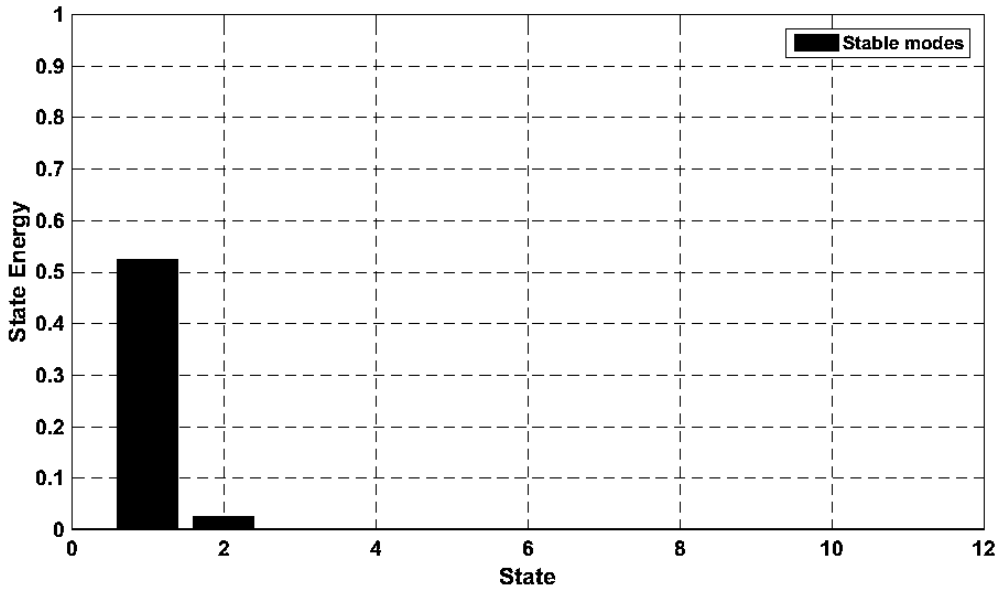

Fig.4. 11. Response for reduced order model

4.3.4. During Grid Faults

4.3.4.1. Flux Weakening Controller Design

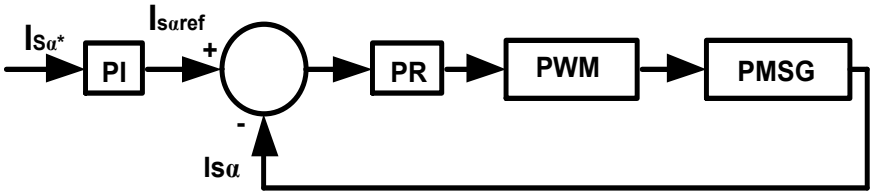

Fig.4. 12. PMSG with flux weakening controller

With flux weakening the block diagram of the current controller become changed and a PI current controller is added to the controller. So, the current controller transfer function is derived by multiplying the equations (4.12) and (4.27).

So, the open loop transfer function becomes

$$G_F(S) = G_{PI}(S) * G_{IS}(S) \qquad (4.30)$$

4.3.4.2. Pitch Angle Controller Design

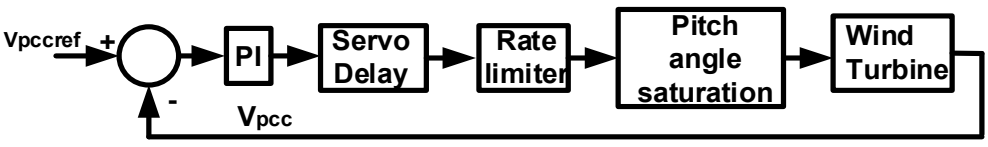

Fig.4. 13. Wind turbine with pitch angle control

Fig.4.13 represents the block diagram of pitch angle controller. The transfer function of each component in block diagram follows as

1. For PI transfer function becomes

$$G_{PI}(S) = K_P(1 + T_i S)/T_i S \tag{4.31}$$

Where $T_i = K_p/K_i$

2. For servo delay transfer function becomes

$$G_D(S) = 1/(1 + T_\beta S) \tag{4.32}$$

Normally T_β is chosen as 0.2s. As rate limiter and pitch angle saturation block create some delay. So, the equivalent delay is considered as T_β =0.5s.

3. The wind turbine transfer function becomes

$$G_T(S) = \frac{1}{J_t S + F} \tag{4.33}$$

So, the total transfer function becomes

$$G_P(S) = G_{PI}(S) * G_D(S) * G_T(S) \tag{4.34}$$

4.3.4.3. Complete Transfer Function of Grid Connected WECS During Fault Condition

The complete transfer function of a grid connected WECS with controller during fault is obtained by multiplying the sub transfer function of mechanical model, PMSG model, converter and grid as follows:

$$G_F(S) = \frac{V_{PCC}(S)}{T(S)} = \frac{L_1 S^4 + L_2 S^3 + L_3 S^2 + L_4 S + L_5}{(M_1 S^{11} + M_2 S^{10} + M_3 S^9 + M_4 S^8 + M_5 S^7 + M_6 S^6 + M_7 S^5 + M_8 S^4 + M_9 S^3 + M_{10} S^2 + M_{11} S + M_{12})} \tag{4.35}$$

Where L_1, L_2, L_3, L_4, L_5, M_1, M_2, M_3, M_4, M_5, M_6, M_7, M_8, M_9, M_{10}, M_{11} and M_{12} are derived from equations (4.4), (4.12), (4.16), (4.23), (4.30), (4.30) and (4.34). The values are presented in Appendix B.

The system order is reduced by balanced truncation method and it is expressed as

$$G_{FT}(S) = \frac{-MS^2 - NS + O}{PS^2 + QS + R} \qquad (4.36)$$

Where *P, Q, R, M, N* and *O* are constant, and the parameters are shown in the Appendix. From Fig. 4.14(a) it is observed that it has fast step response with very little overshoot. The Nyquist plot in Fig. 4.14(b) shows the stability of the system. The HSV for reduced order model system is also shown in Fig.4.15.

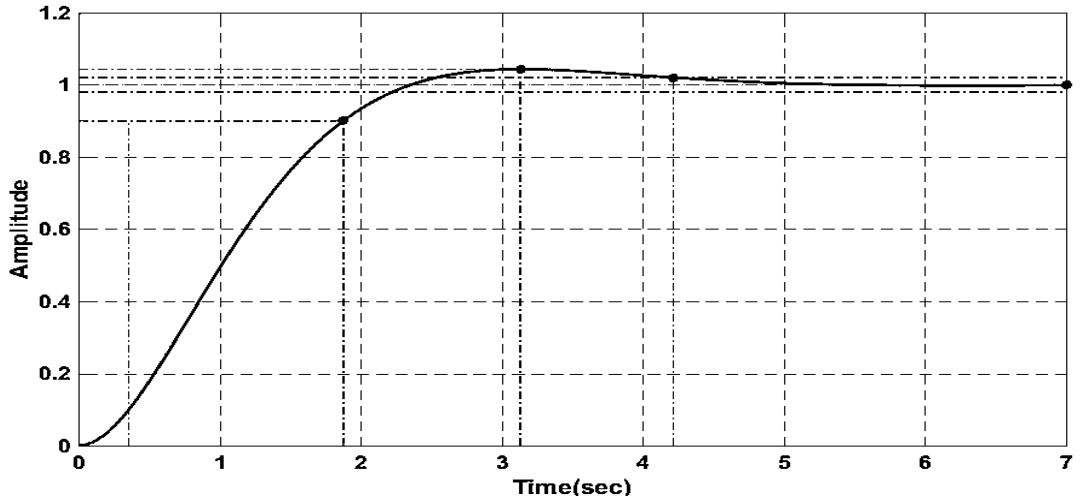

(a)

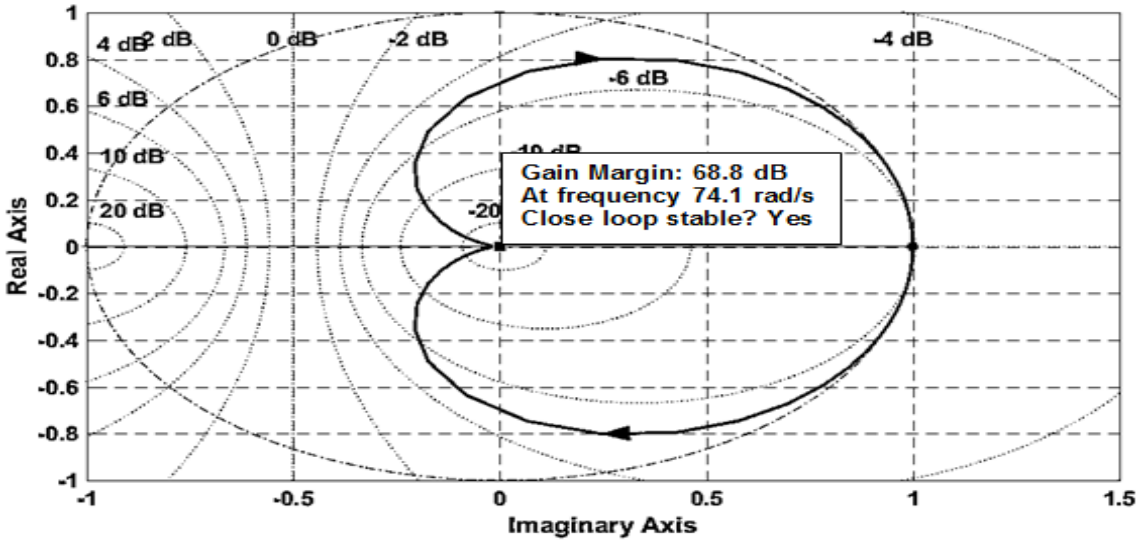

(b)

Fig.4. 14. (a) Step response for reduced order model (b) Nyquist plot for reduced order model

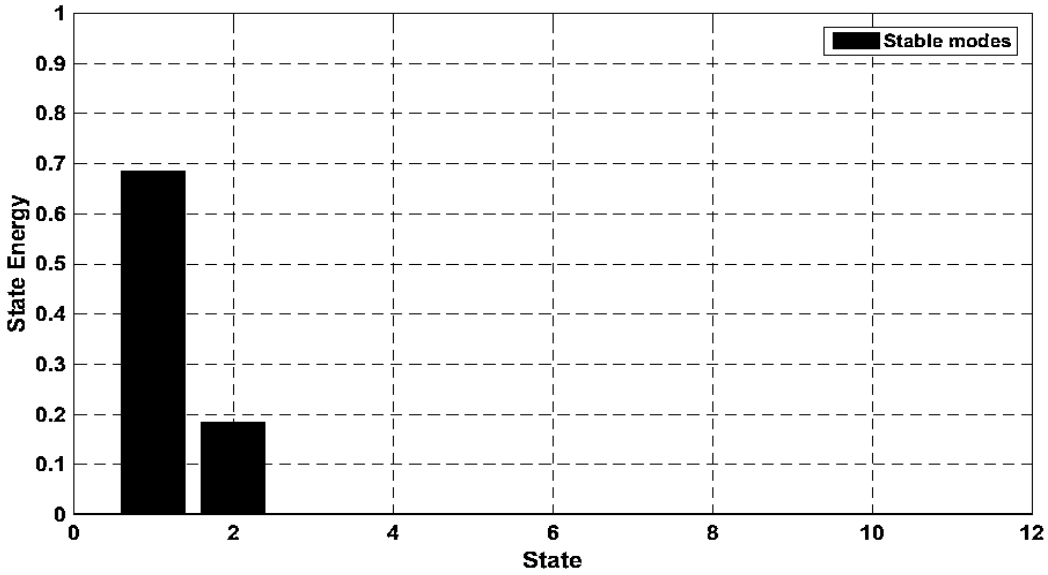

Fig.4. 15. Response for reduced order model

4.4. Conventional Control With the ESS

Energy Storage System (ESS) is used to dissipate the excess DC link active power at the time of grid faults [12], [13]. ESSs are linked with the DC link by DC-DC converter as shown in Fig.4.16 (a). During the fault, it absorbs the excess energy which can limit the DC link overvoltage. This energy can be injected into the grid following the fault clearance. A PWM comparator is used to generate the switching pulses for ESS. The comparator is developed based on pre-set higher and lower voltage tolerance limits as shown in Fig.4.16 (b). The DC link voltage is compared with this band. If the DC voltage is in the tolerance band, ESS will not operate. Whenever DC voltage crosses the threshold voltage limit ESS will absorb the extra power and reduce the overvoltage in DC link. Parameters of ESS are shown in Appendix B.

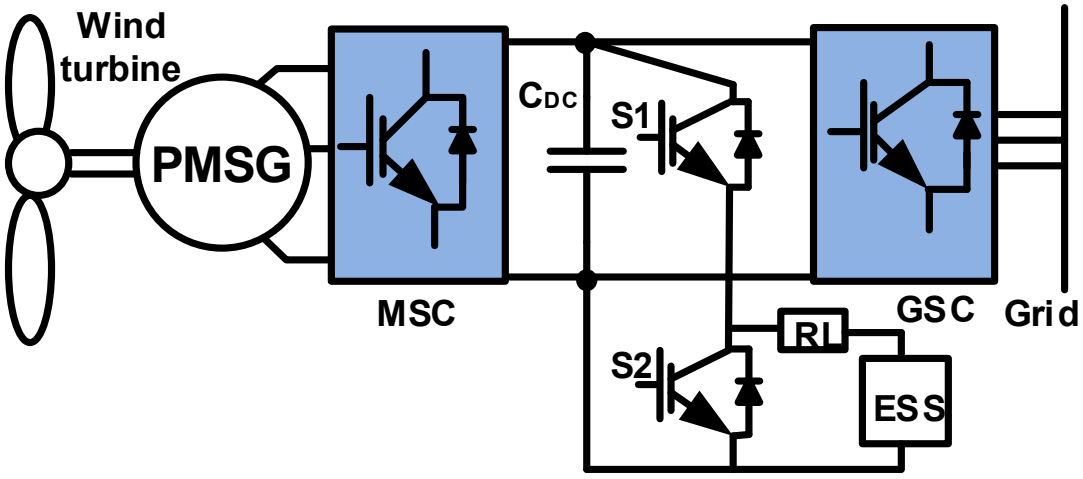

(a)

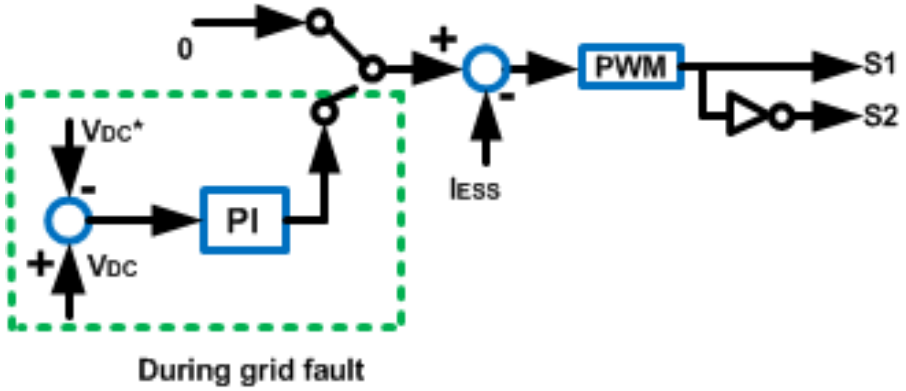

(b)

Fig. 4. 16. Wind turbine with ESS protection (a) Block diagram (b) Control diagram

4.5. Simulation Results and Analysis

PMSG based WECS with coordinated controller (pitch angle control and flux weakening control) is built in the MATLAB/SIMULINK environment and the time series simulation results are obtained for the symmetrical and asymmetrical grid faults. Then the results are compared with ESS results for verification. Simulation time is 5 seconds.

4.5.1. Performance Verification considering Single Wind Turbine

4.5.1.1. Single Symmetrical Fault

The variable wind speed is set to 8-18m/s as shown in Fig.4.17 (a). Rated wind speed is 12m/s and pitch angle remain zero until wind speed is equal or less than the rated speed.

As pitch angle controller's response is slow, it takes some time to operate. It increases the pitch to limit the output power and rotor speed according to wind speed variations. At t = 1s, a three line to ground fault is applied on the transmission line. The fault duration is 0.15s. As shown in Fig.4.17 (b), the grid voltage falls from 100% to 25 %. The transient behaviours of the grid real power and reactive power is shown in Fig.4.17 (d) and (e) respectively.

During this fault, the active power injection from the GSC to the grid is limited; however, the MSC injects power to the DC-link capacitor. So, the DC-link capacitor voltage increases to almost 1.5 times of its nominal value and is shown in Fig.4.17(f). The pitch angle is increased in the transient state. From Fig.4.17(f), it is found that the proposed coordinated control performs better compared to the conventional ESS control to regulate the DC-link voltage within the acceptable limit and the DC-link voltage fluctuations are reduced.

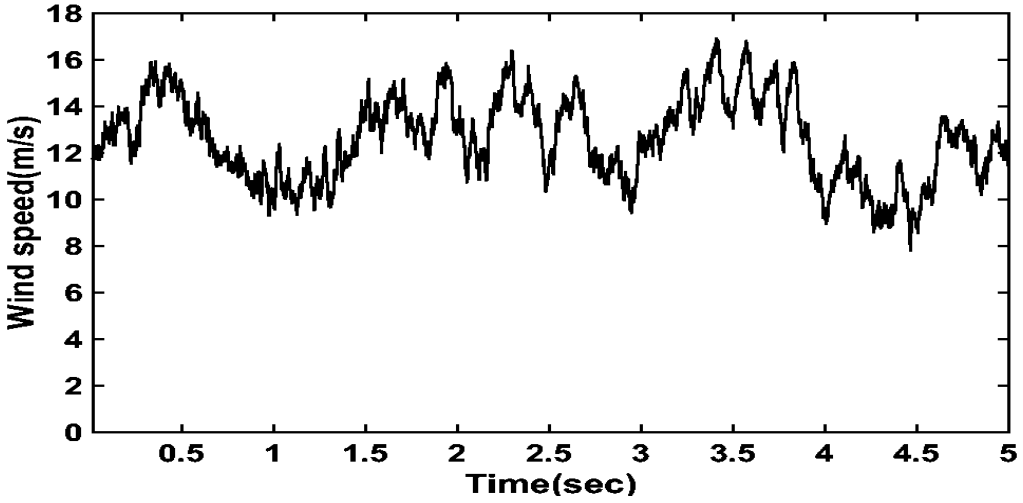

(a)

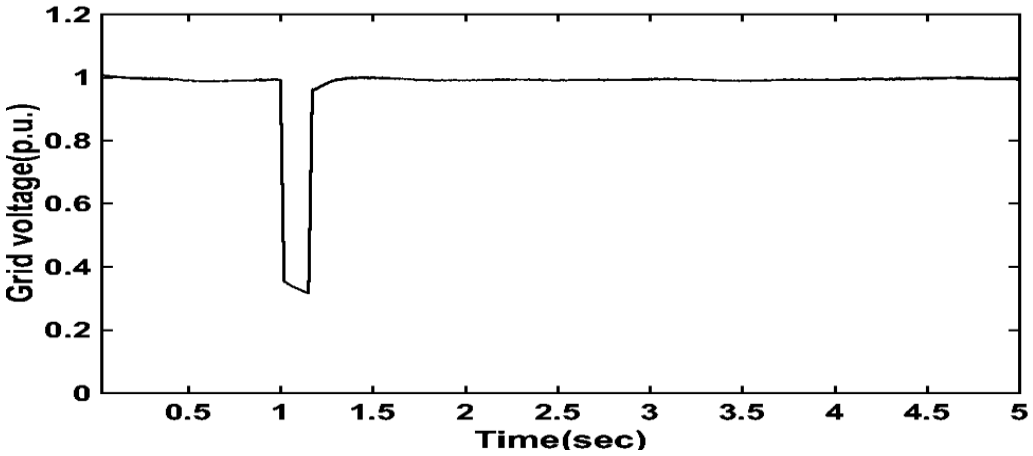
Grid voltage(p.u.)
Time(sec)

(b)

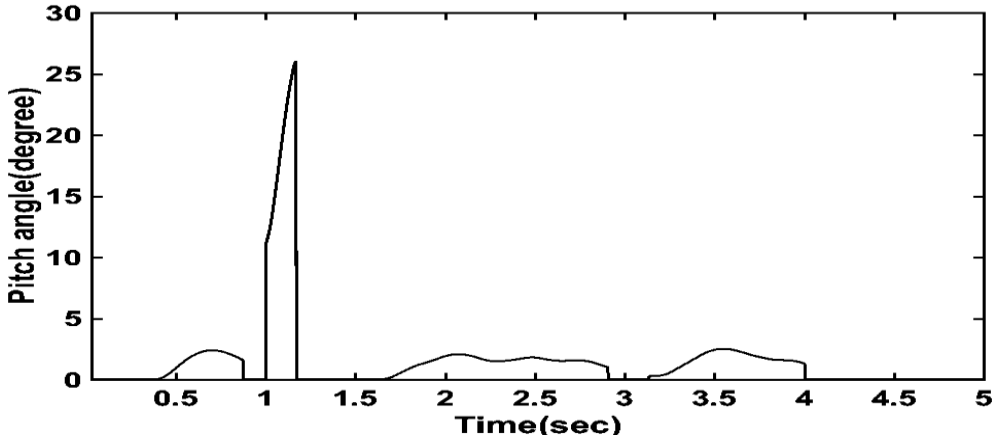
Pitch angle(degree)
Time(sec)

(c)

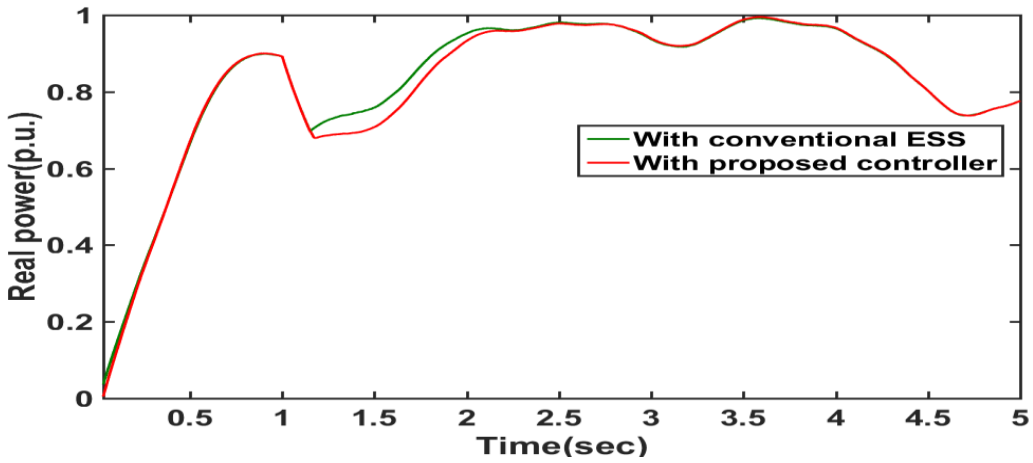
Real power(p.u.)
Time(sec)
With conventional ESS
With proposed controller

(d)

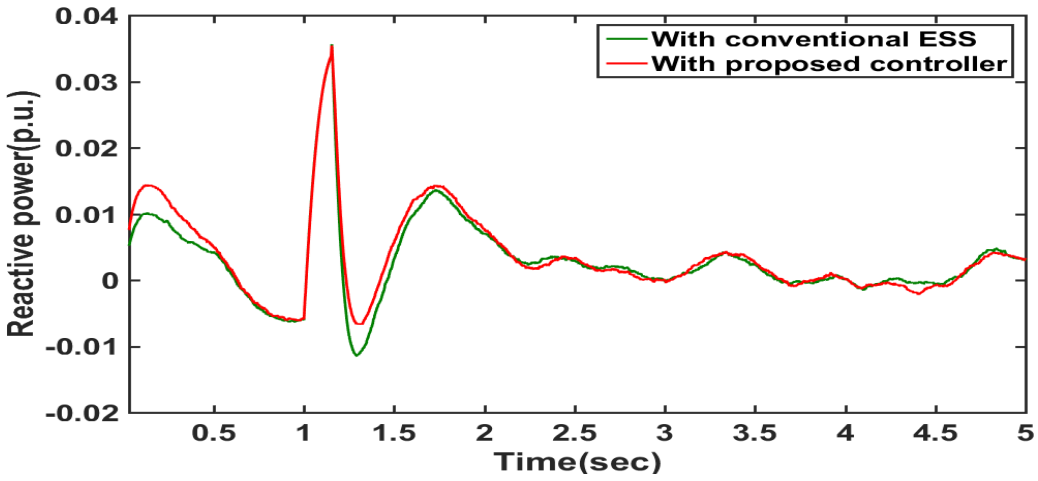

(e)

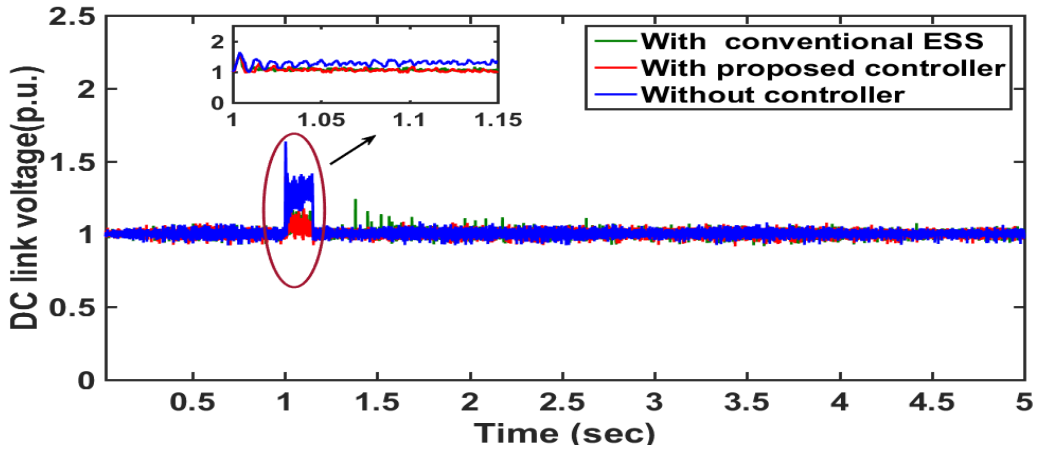

(f)

Fig.4.17. Simulation result for single symmetrical fault a) Variable wind speed b) Grid voltage c) Pitch angle d) Grid real power e) Grid reactive power f) DC link voltage

4.5.1.2. Repetitive Symmetrical Faults

This scenario describes the performance of proposed controller under the three grid faults. The first fault occurs at 1s for 0.15s duration. The second fault occurs at 1.2s for duration of 0.15s. Similarly, the third fault occurs at 1.4 s lasts for 1.55s. The grid voltage dip occurs and the voltage falls from 1p.u. to about 0.25 p.u as shown in Fig.4.18 (a). Rated wind speed is 12m/s and pitch angle remain zero until wind speed is equal or less than the rated speed. It increases to limit the output power and rotor speed according to wind speed variation. The pitch angle is increased in the transient state as shown in Fig.4.18

(b). The transient behaviours of the grid real power and reactive power is shown in Fig.4.18 (c) and (d) respectively. During this fault, the active power injection from the GSC to the grid is limited; however, the MSC injects power to the DC link capacitor. So, the DC-link capacitor voltage increases to almost 1.5 times of its nominal value and is shown in Fig. 4.18(e). From Fig.4.18 (e), it is found that the proposed coordinated control performs better compared to the conventional ESS control to regulate the DC-link voltage within the acceptable limit and the DC-link voltage fluctuations are reduced.

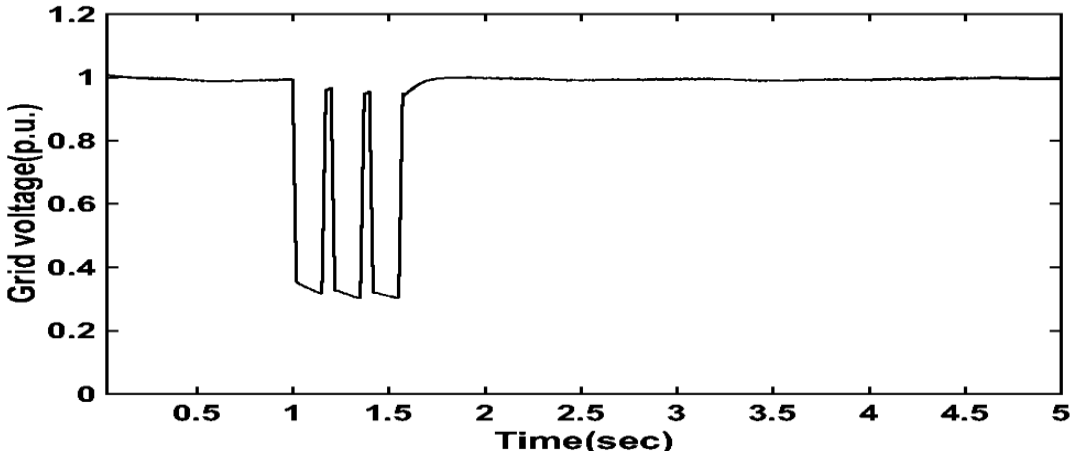

(a)

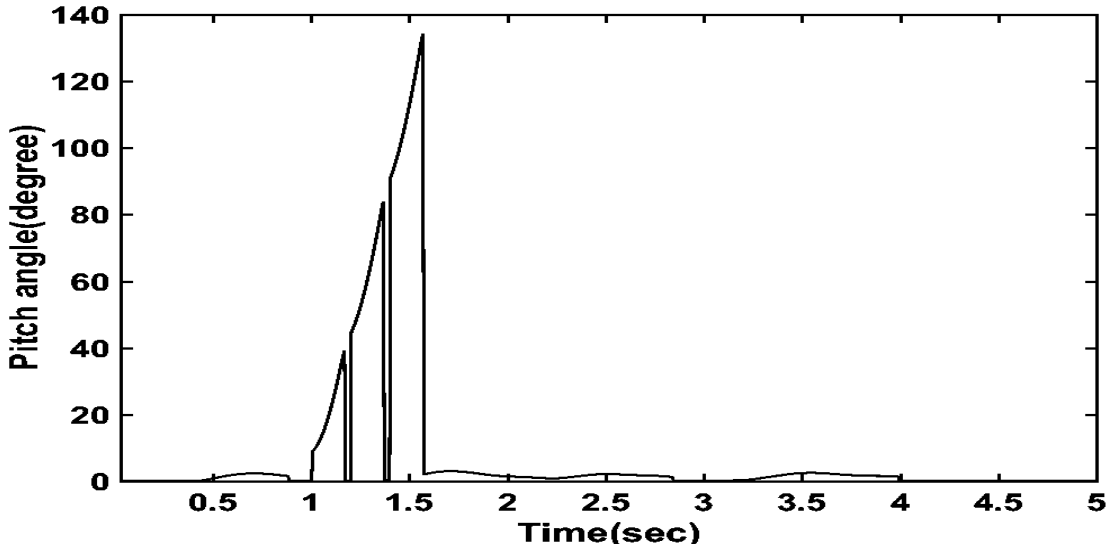

(b)

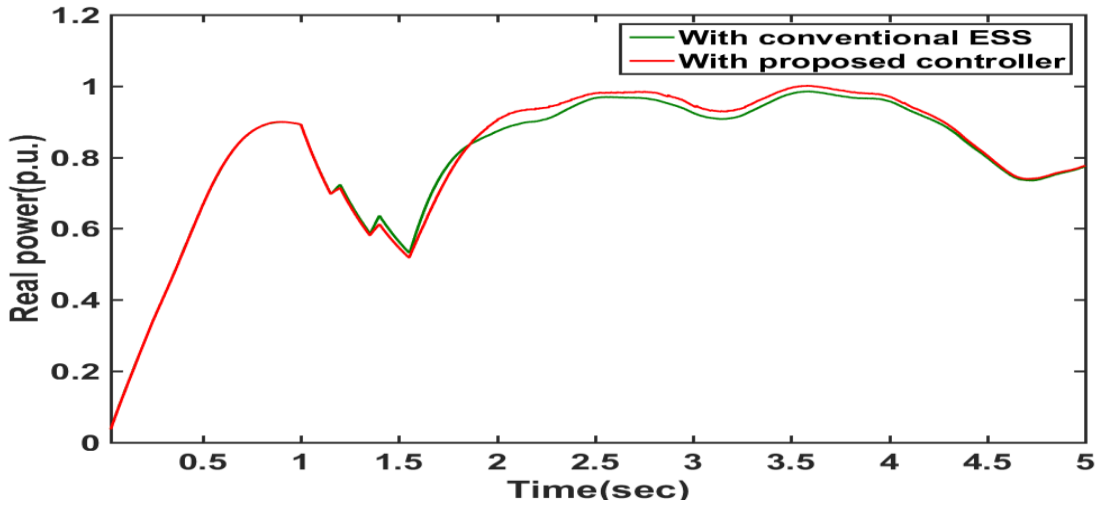

(c)

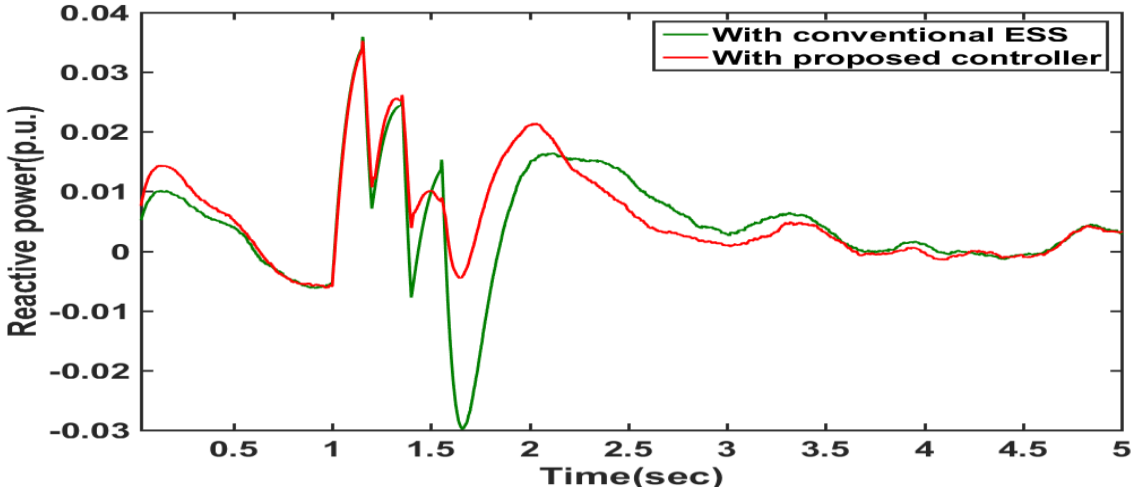

(d)

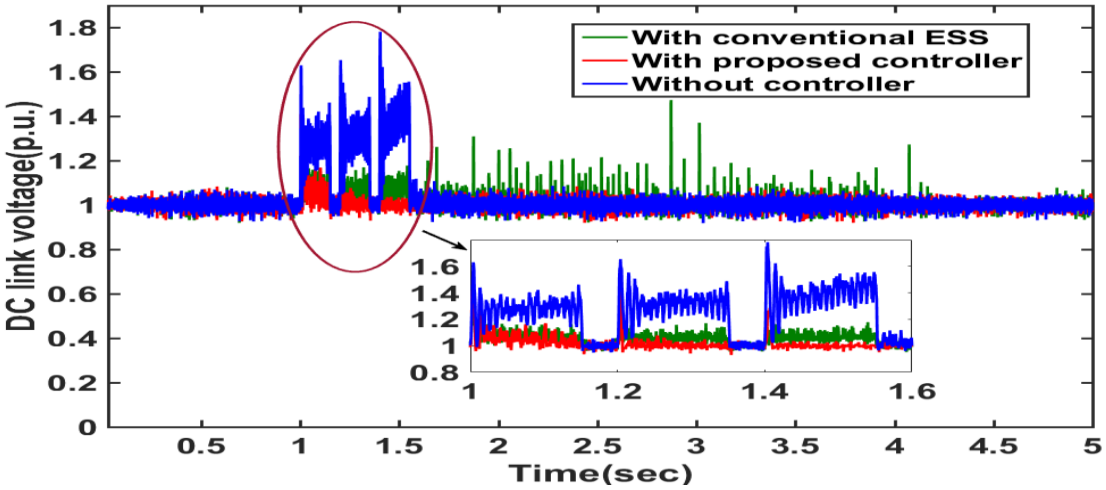

(e)

Fig.4.18. Simulation result for repetitive symmetrical fault a) Grid voltage b) Pitch angle c) Grid real power d) Grid reactive power e) DC link voltage

4.5.1.3. Single Asymmetrical Fault

At t = 1s, a double line to ground fault is applied on the transmission line. Similarly, the fault duration is 0.15s. The grid voltage is reduced to 0.55p.u. as shown in Fig. 4.19(a). The pitch angle is increased in the transient state to reduce incoming power as shown in Fig.4.19(b). The transient behaviours of the grid real power, reactive power is shown in Fig.4.19(c) and (d) respectively. With limited active power injection to the grid during this fault, the voltage of the DC-link capacitor increases to 1.6 times from its nominal value and is shown in Fig. 4.19(e). Using the coordinated controller, effects of the grid fault are mitigated. It is found that the proposed coordinated control performs better compared to the conventional ESS control in DC-link voltage regulation reducing fluctuations and transients and the performances are shown in Fig. 4.19(e).

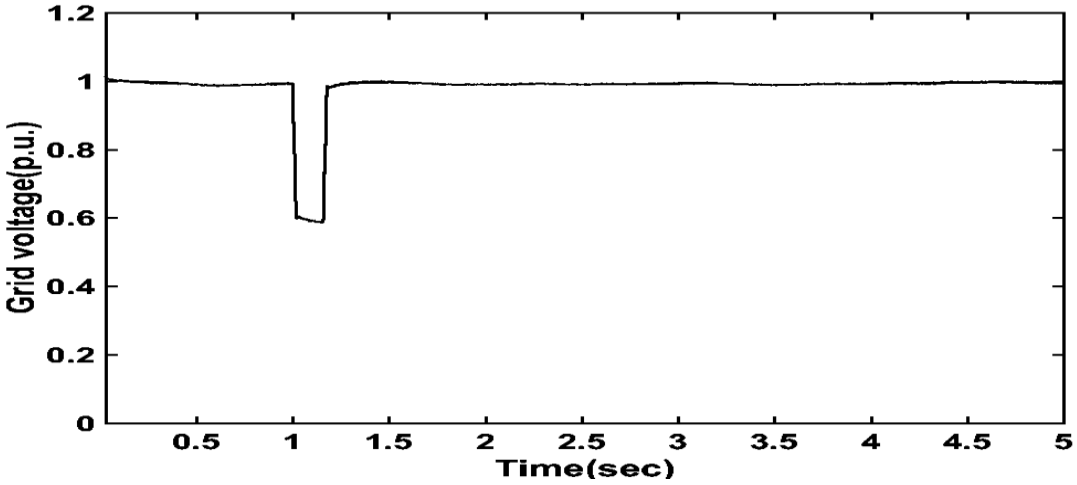

(a)

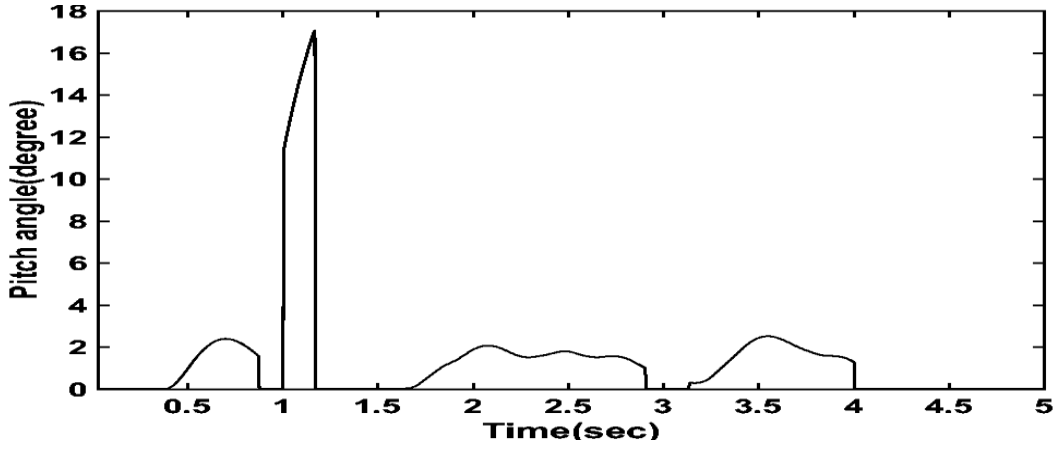

(b)

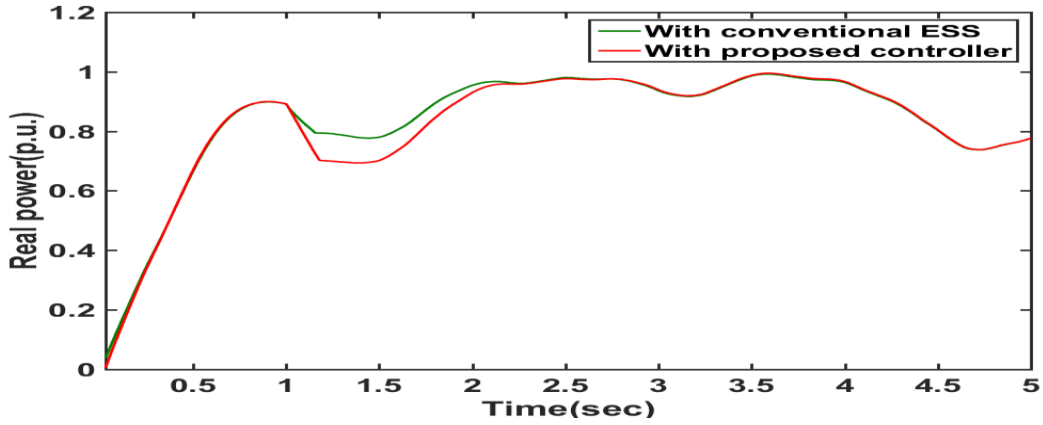

(c)

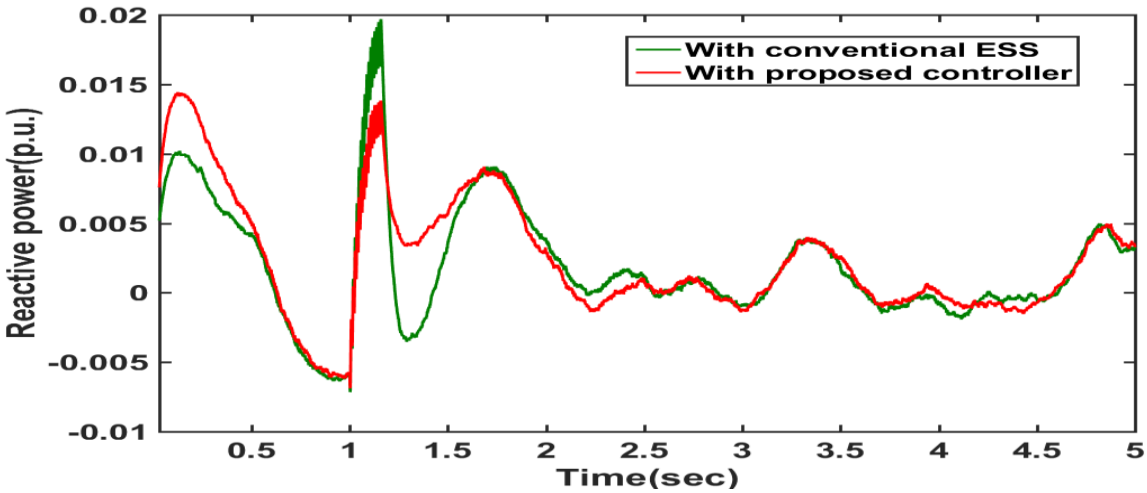

(d)

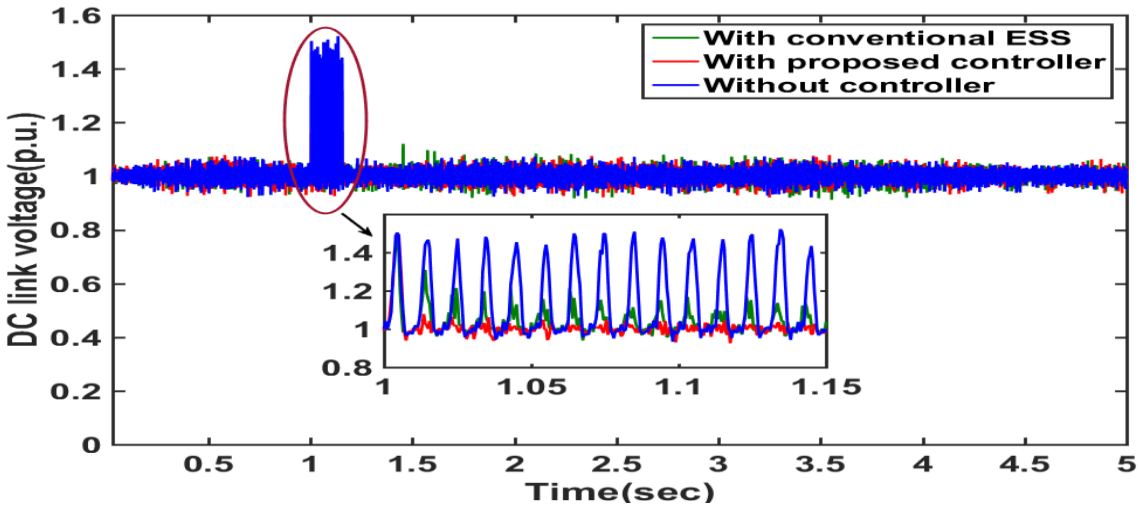

(e)

Fig.4.19. Simulation result for single asymmetrical fault a) Grid voltage b) Pitch angle c) Grid real power d) Grid reactive power e) DC link voltage

4.5.1.4. Repetitive Asymmetrical Faults

This scenario describes the performance of proposed controller under the three asymmetrical grid faults. The first fault occurs at 1s for 0.15s duration. The second fault occurs at 1.2s for duration of 0.15s. Similarly, the third fault occurs at 1.4 s lasts for 1.55s. The grid voltage dip occurs and the voltage falls from 1p.u. to about 0.55 p.u as shown in Fig.4.20(a). Rated wind speed is 12m/s and pitch angle remain zero until wind speed is equal or less than the rated speed. It increases to limit the output power and rotor speed according to wind speed variation. The pitch angle is increased in the transient state as shown in Fig.4.20 (b). The transient behaviors of the grid real power, reactive power and generator speed is shown in Fig.4.20(c) and (d) respectively. During this fault, the active power injection from the GSC to the grid is limited; however, the MSC injects power to the DC link capacitor. So, the DC-link capacitor voltage increases to almost 1.5 times of its nominal value and is shown in Fig.4.20 (e). From Fig.4.20 (e), it is found that the proposed coordinated control performs better compared to the conventional ESS control to regulate the DC-link voltage within the acceptable limit and the DC-link voltage fluctuations are reduced.

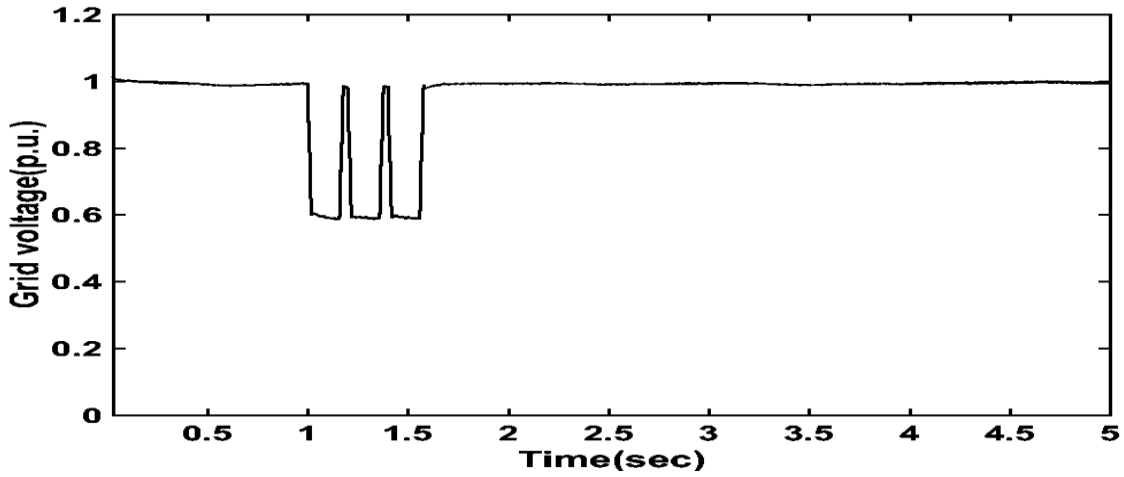

(a)

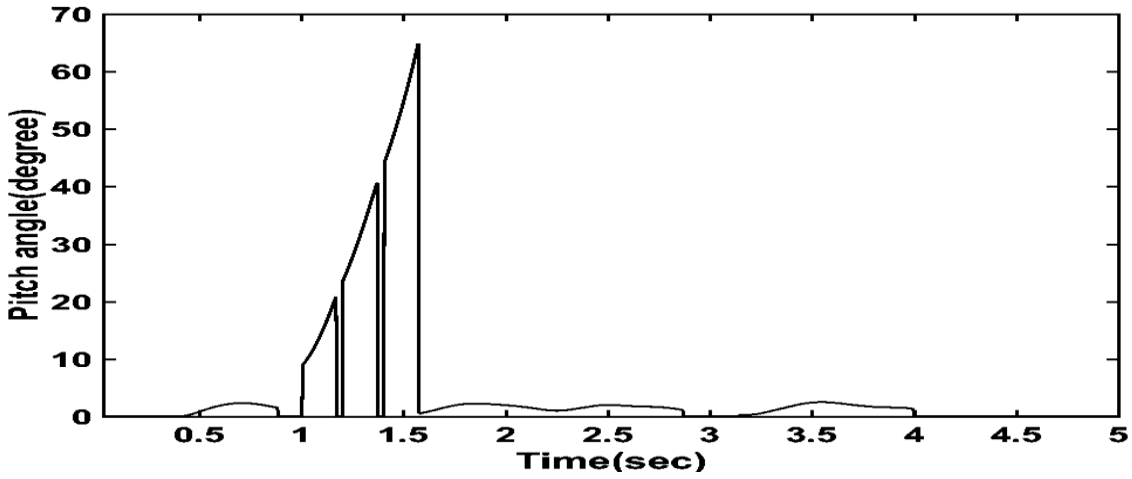
Pitch angle(degree)
Time(sec)

(b)

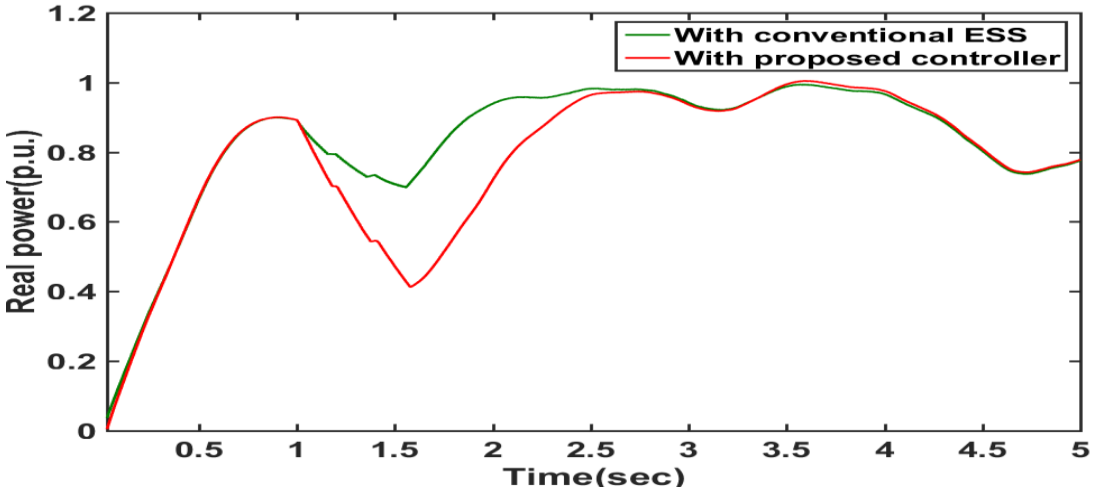
With conventional ESS
With proposed controller
Real power(p.u.)
Time(sec)

(c)

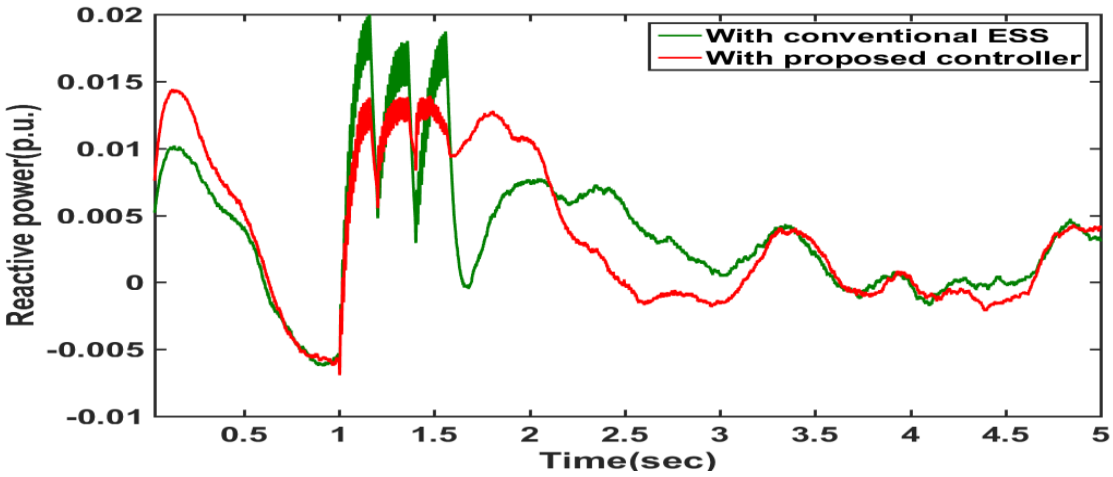
With conventional ESS
With proposed controller
Reactive power(p.u.)
Time(sec)

(d)

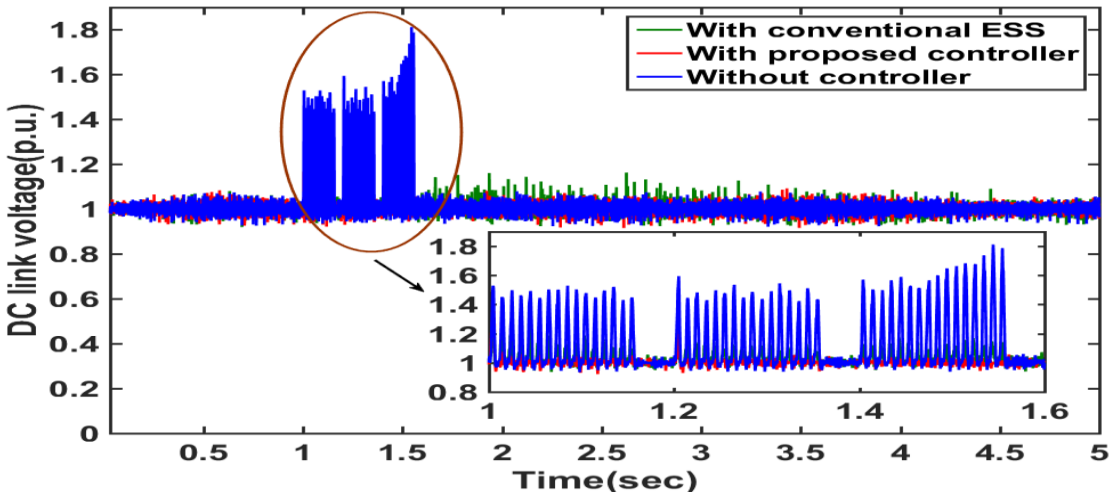

(e)

Fig.4.20. Simulation result for repetitive asymmetrical fault a) Grid voltage b) Pitch angle c) Grid real power d) Grid reactive power e) DC link voltage

4.5.2. Performance Verification considering a Wind Farm

In this section, the coordinated controller performance is verified under on an aggregated wind farm for severe symmetrical fault. The proposed controller and the conventional ESS are connected with each wind turbine. The grid system consists of four wind farms. Each of the wind farms consists of four wind turbines and the rated power is 1.5 MW. So, the total power of wind farm is 24 MW. The wind farms are connected to the grid via transformer and transmission line as shown in Fig.4.21.

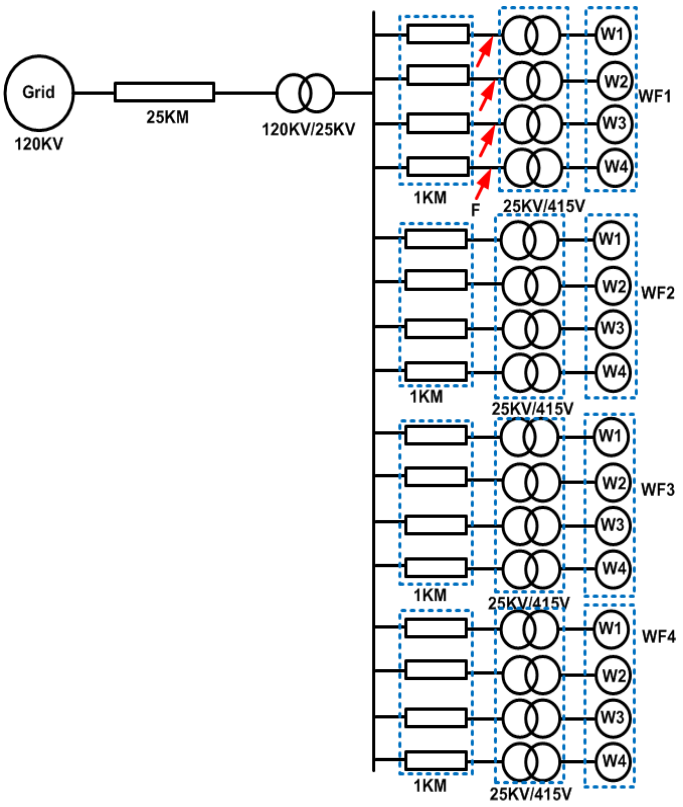

Fig.4.21. Grid connected wind farm

4.5.2.1. Single Symmetrical Fault

At t = 1s, a single three-line to ground fault is applied on the transmission line in wind farm 1. Similarly, the fault duration is 0.15s. The grid voltage is reduced to 0.2p.u. as shown in Fig.4.22(a). The transient response of grid real and reactive power is presented in Fig.4.22(c) and Fig.4.22(d) respectively. The conventional ESS based method and the proposed controller, both can inject some reactive power, but it is not very significant. The DC link voltage is increased to 1.3 p.u. for WF1 and 1.25 p.u. for WF2, WF3 and WF4 respectively without any LVRT control. By using the conventional and proposed control the DC link voltage is under permissible limit. They are illustrated in Fig.4.22(e) and Fig.4.22(f) respectively. From those figures, it is observed that the proposed controller provides better response than the conventional ESS.

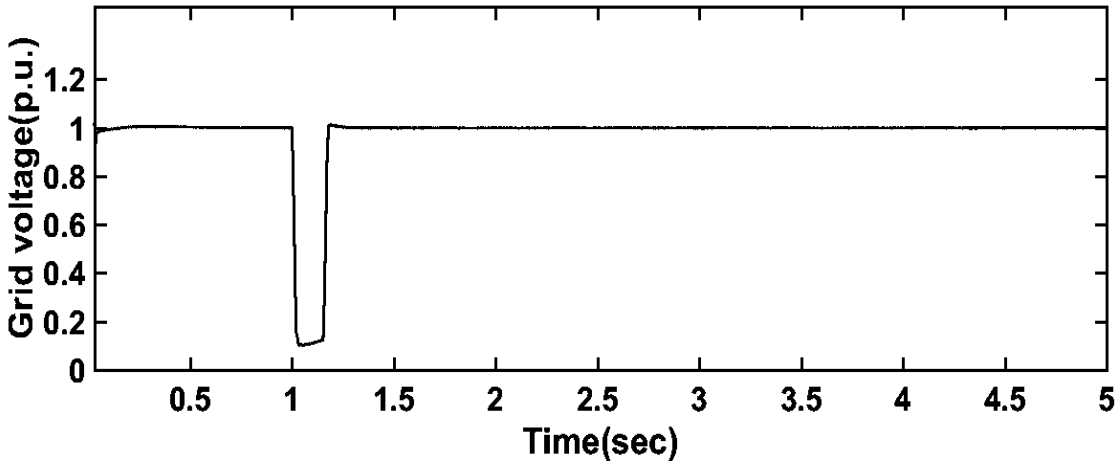
Grid voltage(p.u.)
1.2
1
0.8
0.6
0.4
0.2
0
0.5
1
1.5
2
2.5
3
3.5
4
4.5
5
Time(sec)

(a)

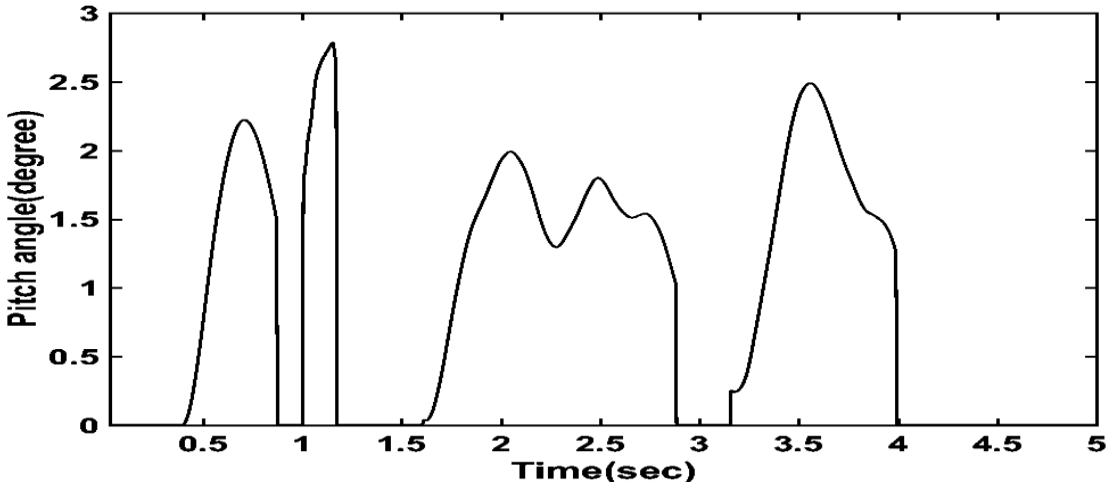
Pitch angle(degree)
3
2.5
2
1.5
1
0.5
0
0.5
1
1.5
2
2.5
3
3.5
4
4.5
5
Time(sec)

(b)

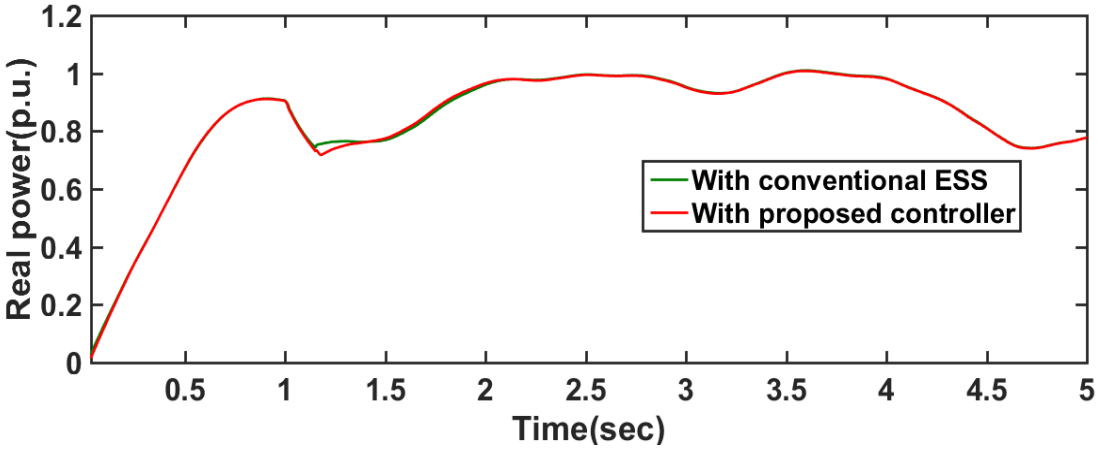
Real power(p.u.)
1.2
1
0.8
0.6
0.4
0.2
0
0.5
1
1.5
2
2.5
3
3.5
4
4.5
5
Time(sec)
With conventional ESS
With proposed controller

(c)

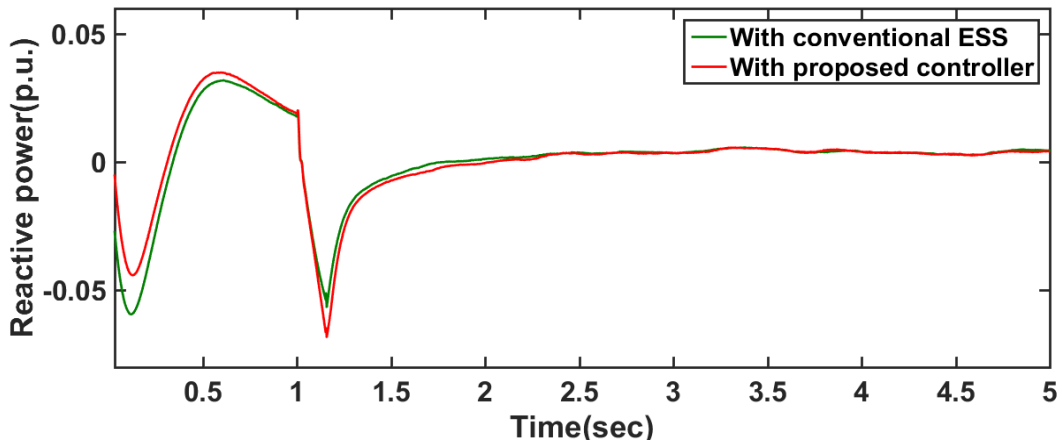

(d)

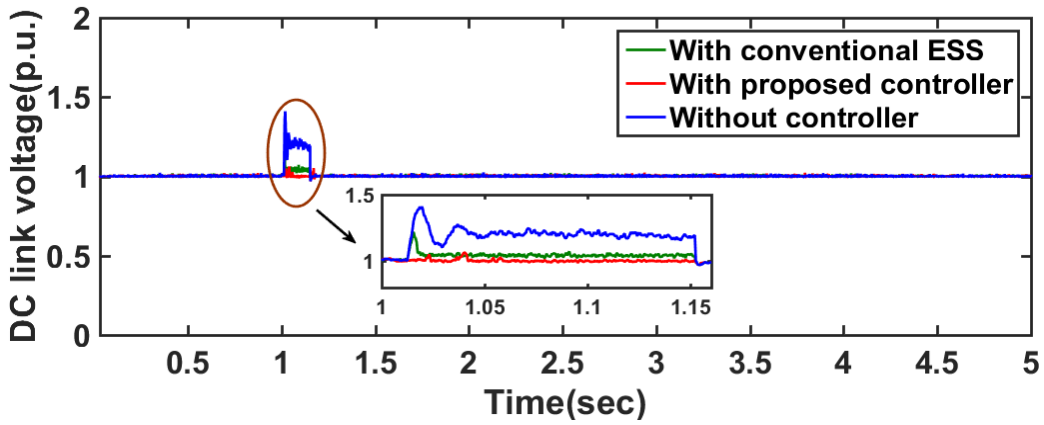

(e)

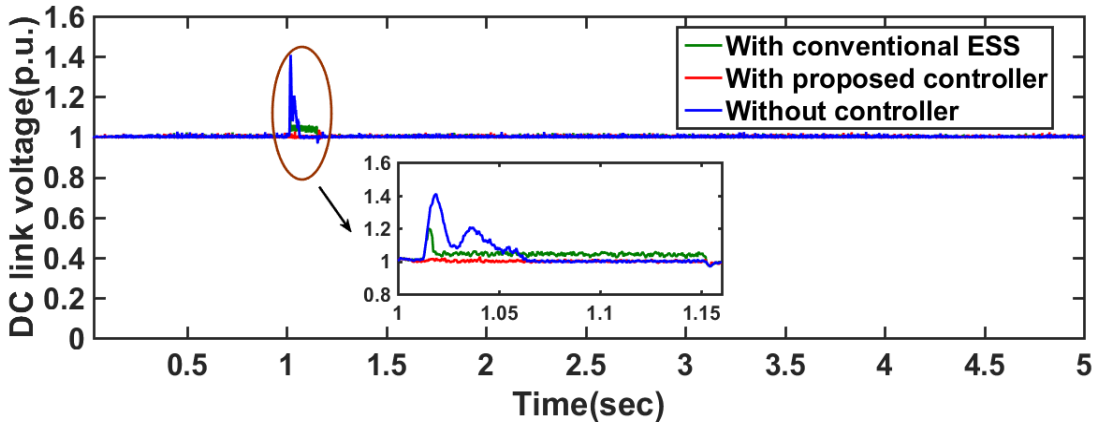

(f)

Fig.4.22. Simulation results for single symmetrical fault of grid connected wind farm a) Grid voltage b) Pitch angle c) Grid real power d) Grid reactive power e) DC link voltage for WF1 f) DC link voltage for WF2

4.5.2.2. Repetitive Symmetrical Faults

This scenario describes the performance of proposed controller under the three symmetrical grid faults. The first fault occurs at 1s for 0.15s duration. The second fault occurs at 1.2s for duration of 0.15s. Similarly, the third fault occurs at 1.4 s lasts for 1.55s. The grid voltage dip occurs and the voltage falls from 1p.u. to about 0.55 p.u as shown in Fig.4.23 (a). Rated wind speed is 12m/s and pitch angle remains zero until wind speed is equal or less than the rated speed. It increases to limit the output power and rotor speed according to wind speed variation. The pitch angle is increased in the transient state as shown in Fig.4.23 (b). The transient behaviours of the grid real power and reactive power is shown in Fig.4.23(c) and (d) respectively.

During this fault, the active power injection from the GSC to the grid is limited; however, the MSC injects power to the DC-link capacitor. So, the DC-link capacitor voltage increases to almost1.3 times of its nominal value and is shown in Fig.4.23 (e). From Fig. 4.23(e), it is found that the proposed coordinated control performs better compared to the conventional ESS control to regulate the DC-link voltage within the acceptable limit and the DC-link voltage fluctuations are reduced.

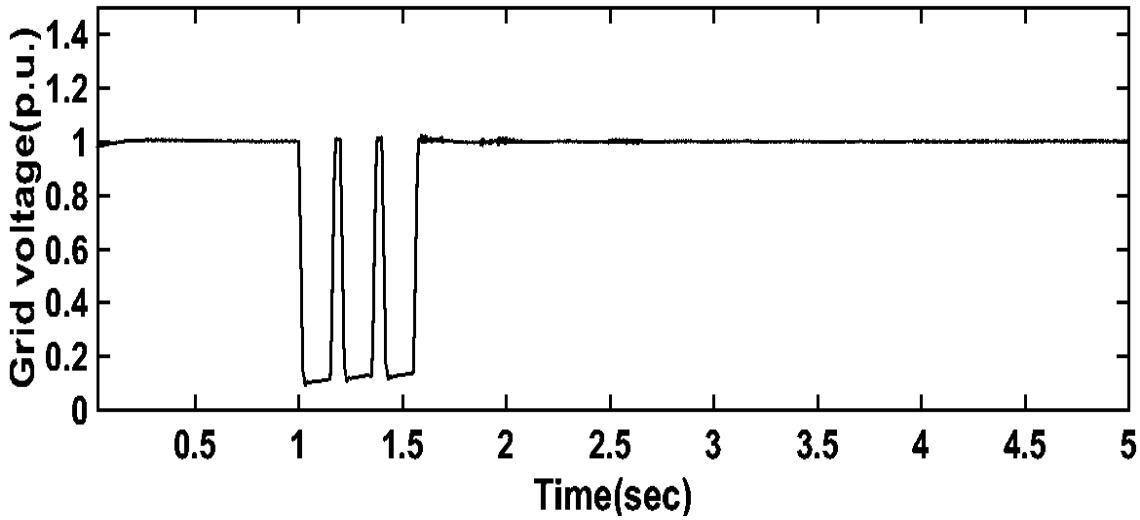

(a)

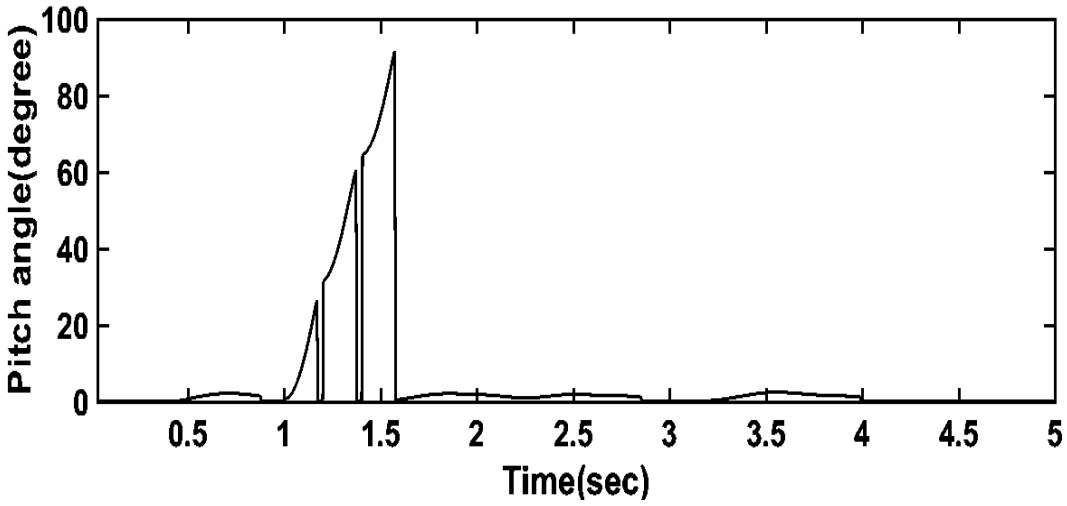
Pitch angle(degree)
100
80
60
40
20
0
0.5
1
1.5
2
2.5
3
3.5
4
4.5
5
Time(sec)

(b)

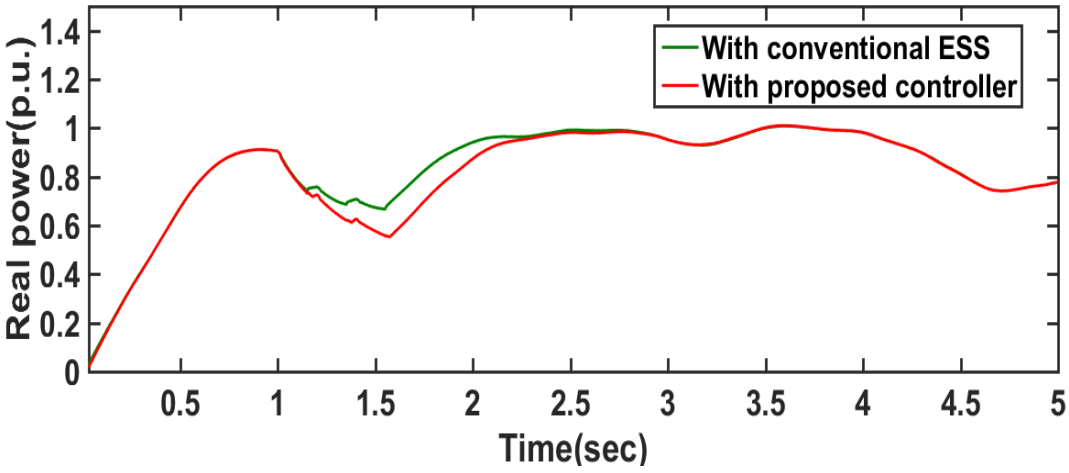
Real power(p.u.)
1.4
1.2
1
0.8
0.6
0.4
0.2
0
With conventional ESS
With proposed controller
0.5
1
1.5
2
2.5
3
3.5
4
4.5
5
Time(sec)

(c)

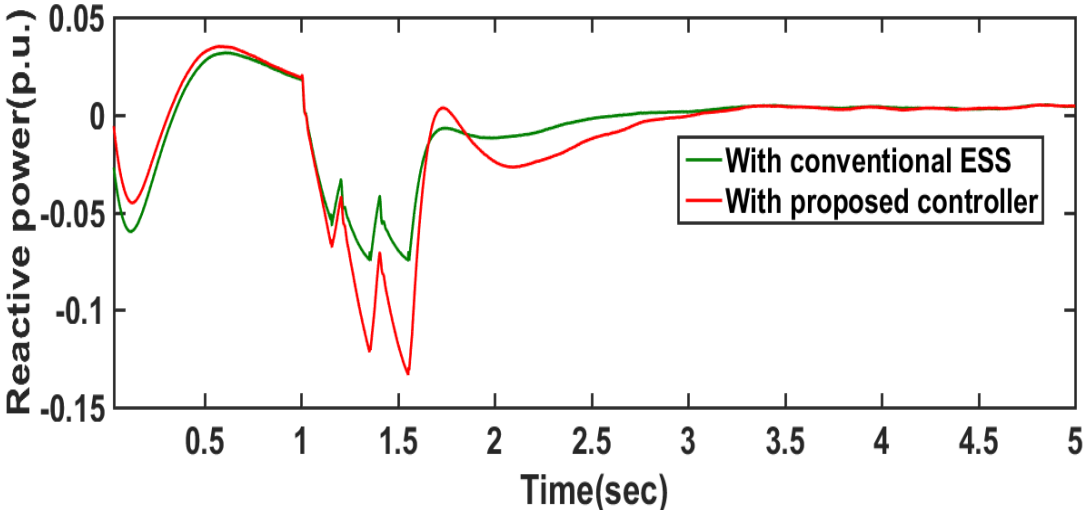
Reactive power(p.u.)
0.05
0
-0.05
-0.1
-0.15
With conventional ESS
With proposed controller
0.5
1
1.5
2
2.5
3
3.5
4
4.5
5
Time(sec)

(d)

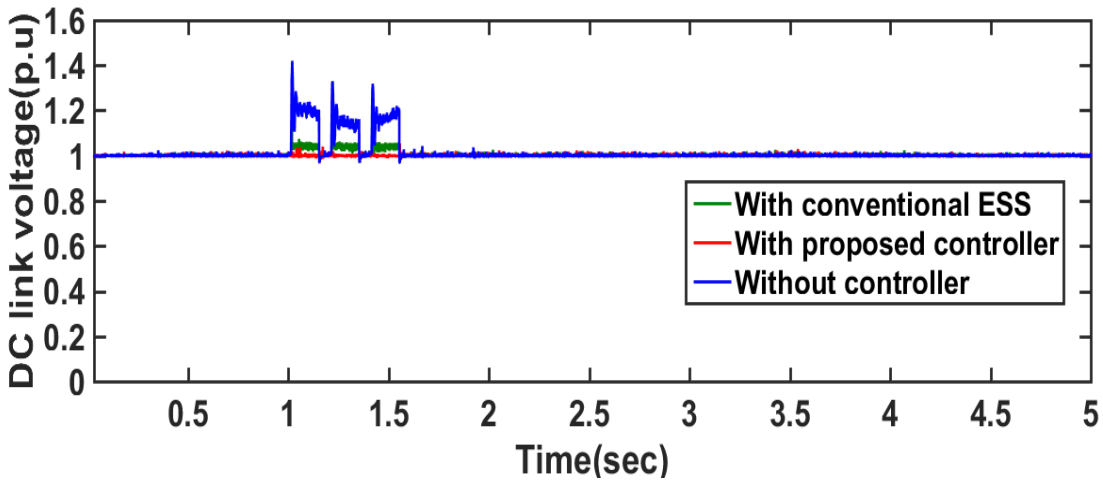

(e)

Fig.4.23. Simulation results for repetitive symmetrical fault of grid connected wind farm a) Grid voltage b) Pitch angle c) Grid real power d) Grid reactive power e) DC link voltage

4.5.3. Performance Verification considering interconnected power systems

The WECS is connected with the average model of IEEE-9 bus system to evaluate the realistic performance of the proposed coordinated controller as shown in Fig.4.24. IEEE-9 bus system consists of nine buses, three generators, three loads, six transmission lines and three transformers. Bus1 where generator 1 is connected is considered as the slack bus.

The WECS is connected at bus 8 via transformer. Parameter of IEEE 9 bus system is presented in Appendix B. MATLAB simulation is done for real wind speed and the significant results are obtained. Simulation is run for 5 seconds. The proposed coordinated control is verified under single and repetitive symmetrical grid faults.

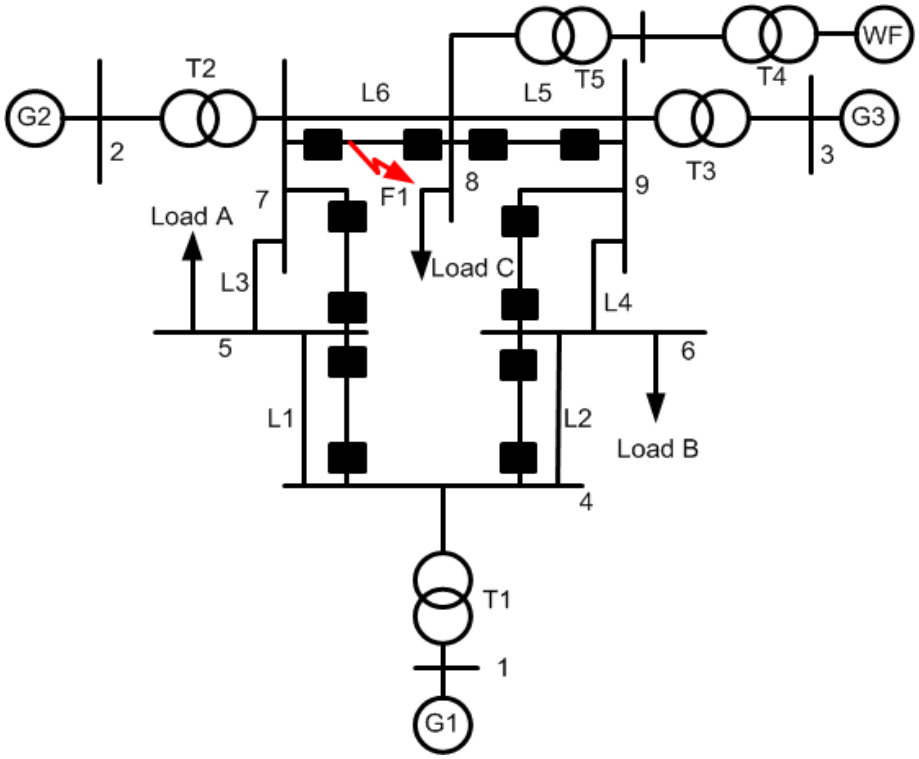

Fig.4.24. Connection of wind farm in IEEE-9 bus system

4.5.3.1. Single Symmetrical Fault

At t = 1s, a three line to ground fault is applied on the transmission line at fault point F1 as shown in Fig.4.25 (a). The fault duration is 0.15s. The pitch angle is increased in the transient state. The DC-link capacitor voltage increases to almost 1.28 times of its nominal value as shown in Fig.4.25(c). From Fig.4.25(c), it is found that the proposed coordinated control provides effective performance in DC-link voltage regulation by reducing fluctuations and transients.

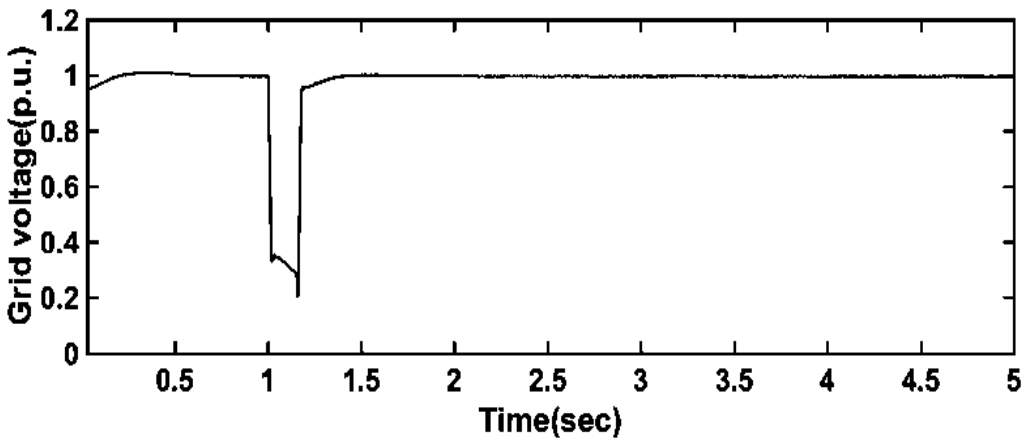

(a)

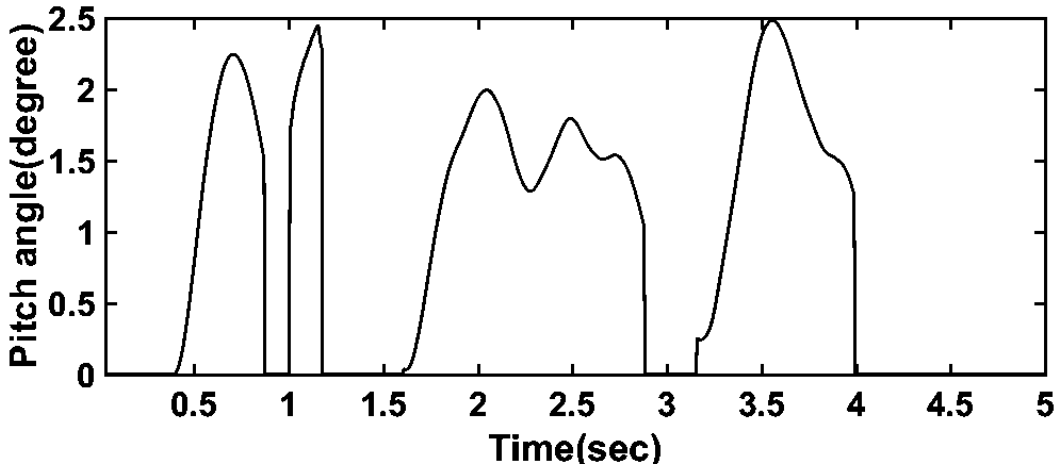
Pitch angle(degree)
2.5
2
1.5
1
0.5
0
0.5
1
1.5
2
2.5
3
3.5
4
4.5
5
Time(sec)

(b)

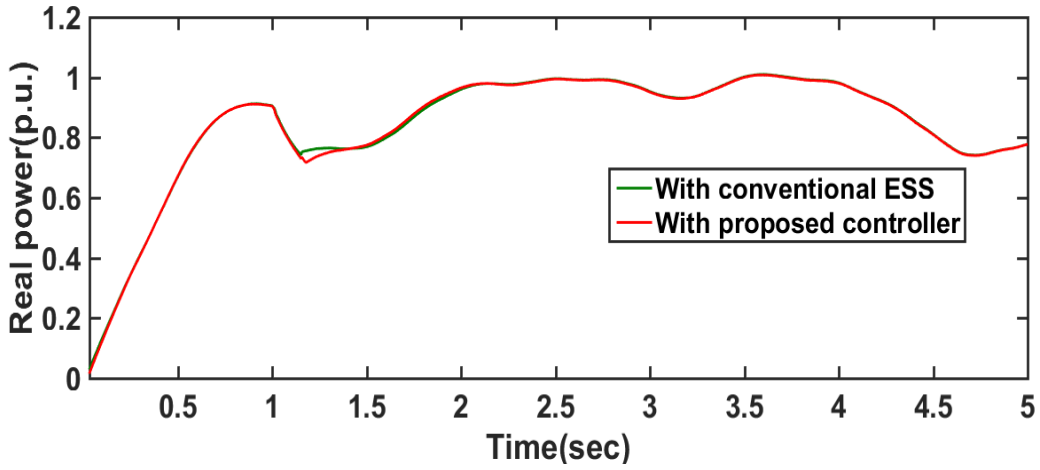
Real power(p.u.)
1.2
1
0.8
0.6
0.4
0.2
0
0.5
1
1.5
2
2.5
3
3.5
4
4.5
5
Time(sec)
With conventional ESS
With proposed controller

(c)

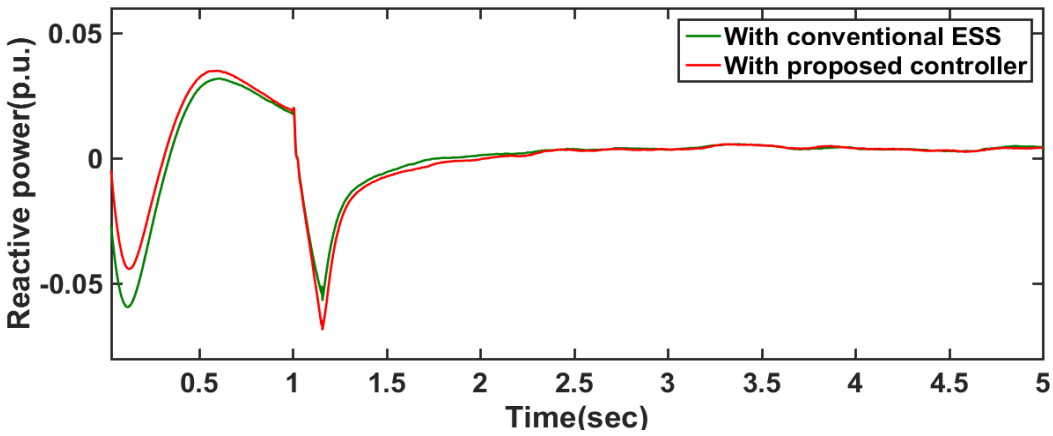
Reactive power(p.u.)
0.05
0
-0.05
0.5
1
1.5
2
2.5
3
3.5
4
4.5
5
Time(sec)
With conventional ESS
With proposed controller

(d)

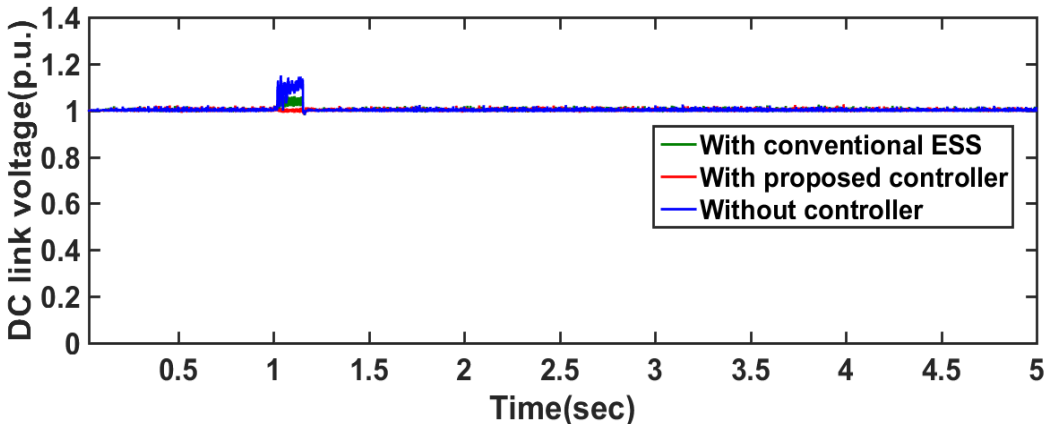

(e)

Fig.4.25. Simulation results for single symmetrical fault of IEEE 9 bus connected wind farm a) Grid voltage b) Pitch angle c) Grid real power d) Grid reactive power e) DC link voltage

4.5.3.2. Repetitive Symmetrical Faults

At t = 1s, a repetitive three line to ground fault is applied on the transmission line at fault point F1 as shown in Fig.4.26 (a). The fault duration is 0.15s. The pitch angle is increased in the transient state.

The DC-link capacitor voltage increases to almost 1.28 times of its nominal value for first fault, 1.34 times for second fault and 3 times for third fault respectively as shown in Fig.4.26(c). From Fig.4.26(c), it is found that the proposed coordinated control provides effective performance in DC-link voltage regulation by reducing fluctuations and transients.

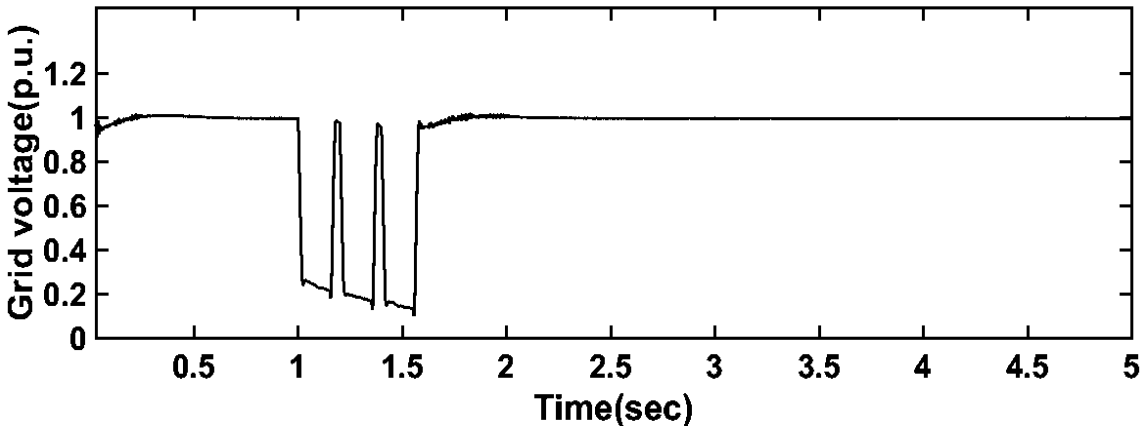

(a)

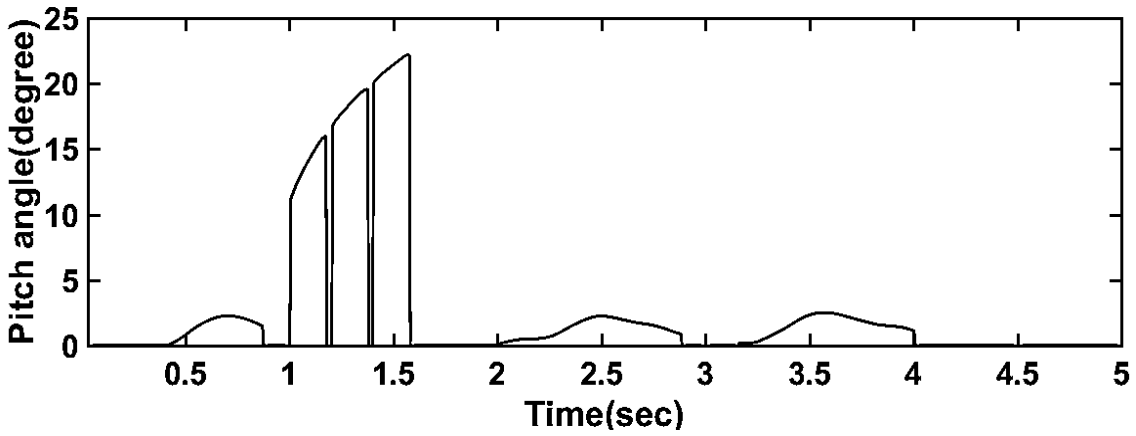
Pitch angle(degree)
25
20
15
10
5
0
0.5
1
1.5
2
2.5
3
3.5
4
4.5
5
Time(sec)

(b)

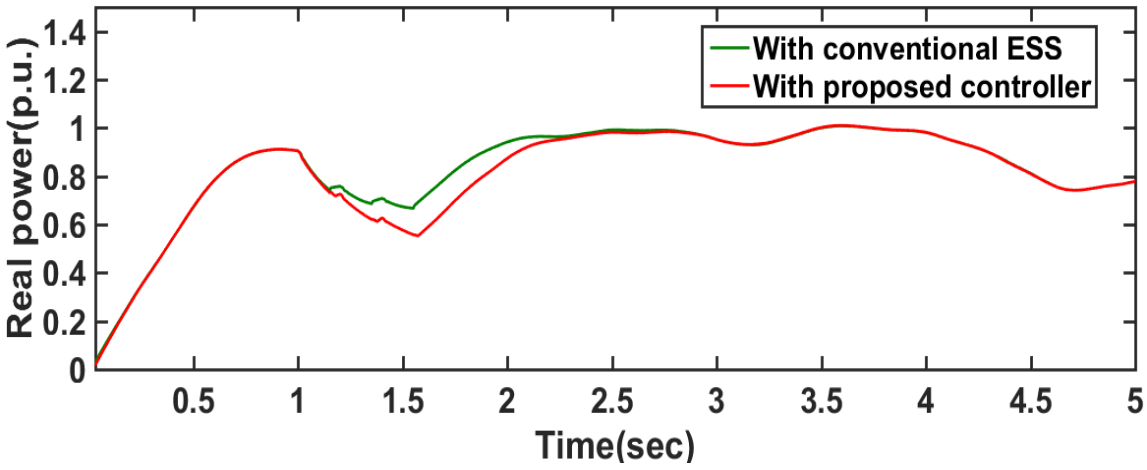
Real power(p.u.)
1.4
1.2
1
0.8
0.6
0.4
0.2
0
With conventional ESS
With proposed controller
0.5
1
1.5
2
2.5
3
3.5
4
4.5
5
Time(sec)

(c)

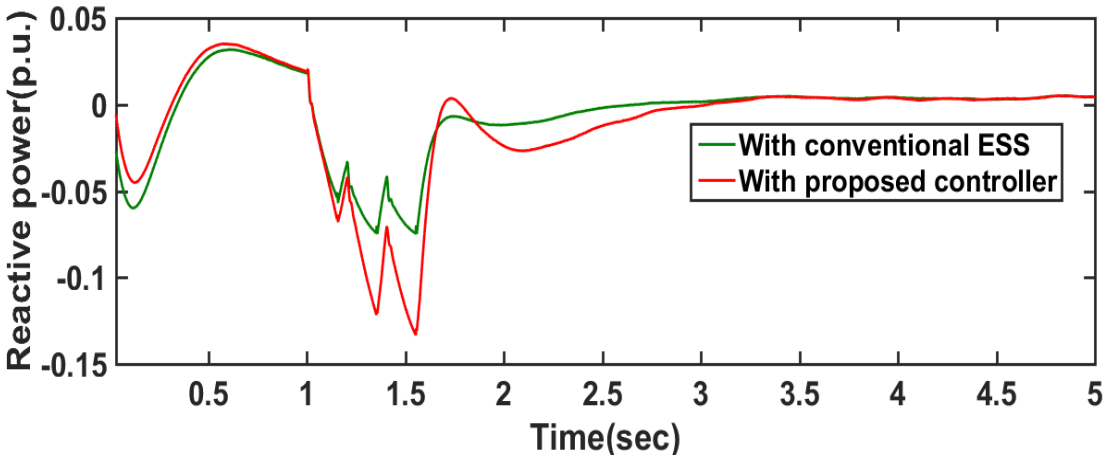
Reactive power(p.u.)
0.05
0
-0.05
-0.1
-0.15
With conventional ESS
With proposed controller
0.5
1
1.5
2
2.5
3
3.5
4
4.5
5
Time(sec)

(d)

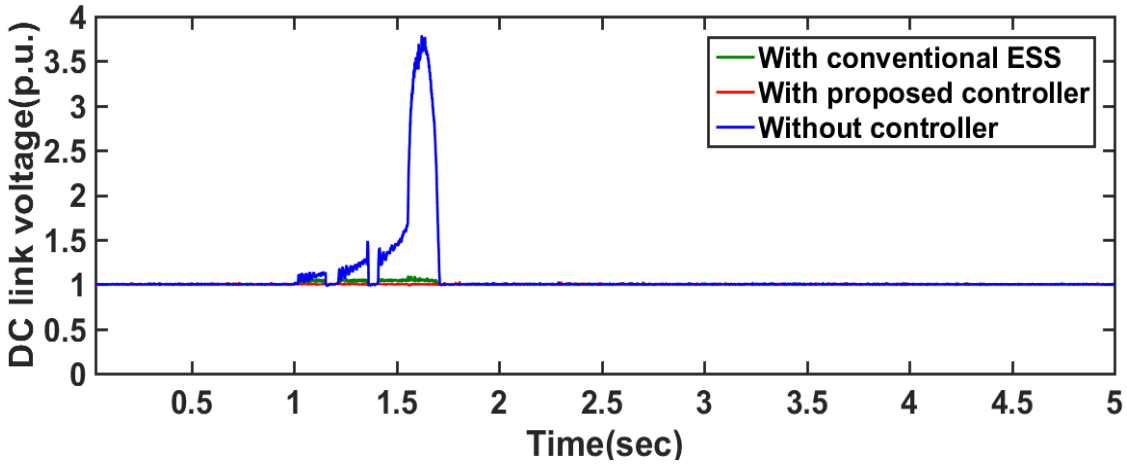

(e)

Fig.4.26. Simulation results for repetitive symmetrical fault of IEEE 9 bus connected wind farm a) Grid voltage b) Pitch angle c) Grid real power d) Grid reactive power e) DC link voltage

4.5.4. Performance Evaluation Considering Wake Effect

Wind speeds of the rear turbines are lower than the upstream wind speeds in a wind farm. Wind energy deficit is known as the wake of the turbine. The turbine wake causes a reduction of the output power at turbines downwind [14]. The wake wind speed can be computed on the basis of the principle of mass conservation [15], [16]. The wind wake model and the wind speed decay in ten turbines aligned in a row is shown in Fig. 4.27 and Fig.4.28. Detailed of these two figures are described in ref. [15] and [16].

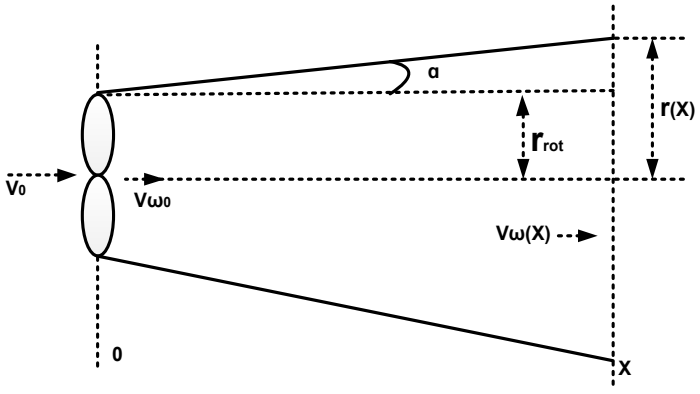

Where r(x) = radius of the shadow cone,
r_{rot} = radius of the shadowing (upstream) turbine,

x = the radial distance between the turbine and an arbitrary location,

α = the apex factor of the cone.

Fig.4.27. Wind wake model [15], [16]

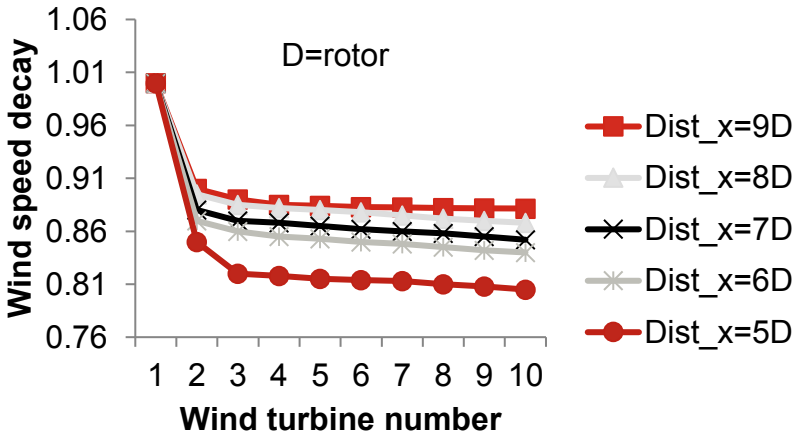

Fig.4.28. Wind speed decay ten turbines aligned in a row [15], [16]

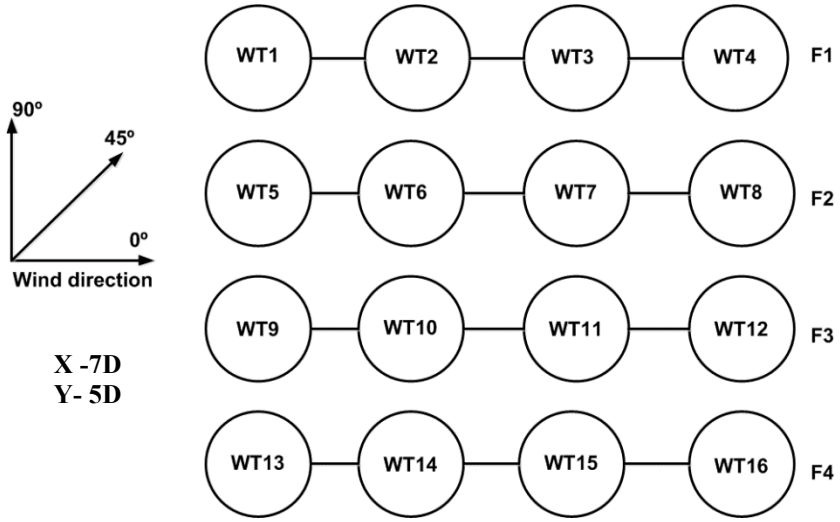

Fig.4.29. Wind farm model

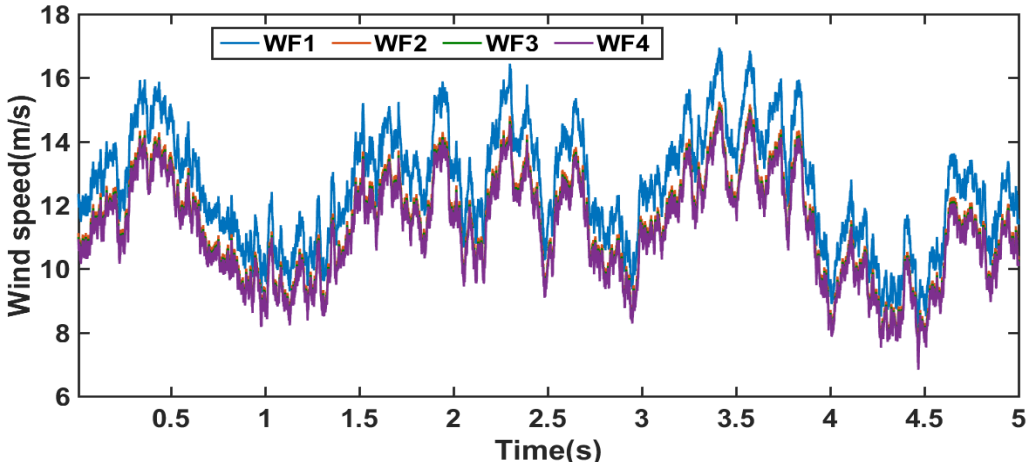

(a)

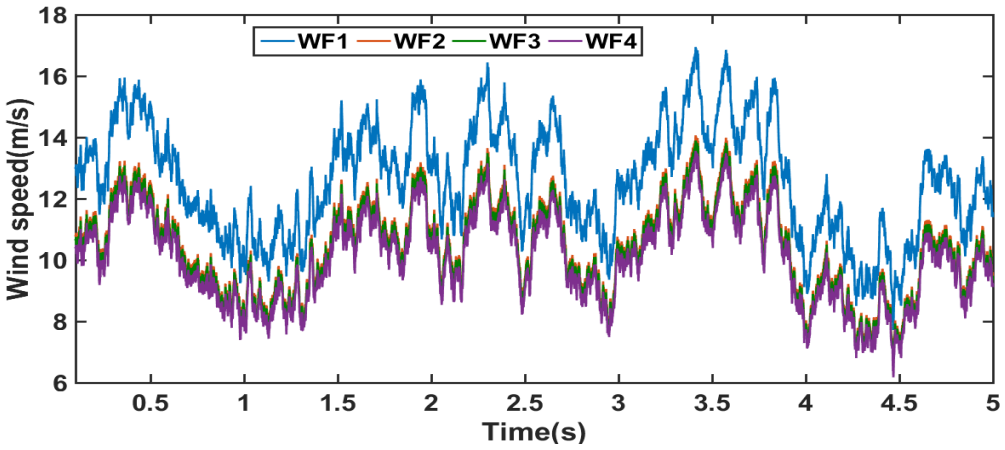

(b)

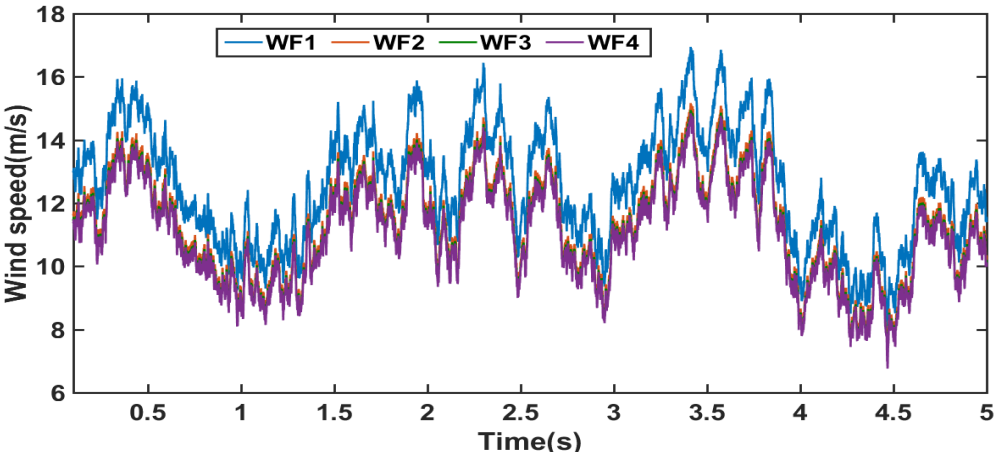

(c)

Fig.4.30. Wind speed direction a) 0º b) 90º c) 45º

The wind farm model and the wind speed in different direction as 0º, 90º and 45º is shown in Fig.4.29 and Fig.4.30. Here, for analysis the results for wind speed direction 90º is considered.

The symmetrical grid fault is applied in WF1. As the power imbalance occurs between MSC and GSC the DC link voltage goes up beyond its limit for WF1 without any control as shown in Fig.4.31 (a). The DC link voltage of other wind farms also goes up due to the power imbalance as shown in Fig.4.31(b), (c) and (d) respectively for WF2, WF3 and WF4. The DC link voltage of WF1 is affected too much and it shows the higher value of

DC link overvoltage. The effect of DC link overvoltage is less in other wind farm as they are far from the grid fault point.

By using the proposed controller, the DC link voltage is reduced from 3.1 p.u. to 1.01 p.u. for WF1, 1.3 p.u. to 1.01 p.u. for WF2, 1.1 p.u. to 1.02 p.u. for WF3 and 1.2 p.u. to 1.03 p.u. for WF4 as shown in Fig.4.31(a), (b), (c) and (d) respectively. The real power generation from different wind farm is also shown in Fig.4.31 (e).

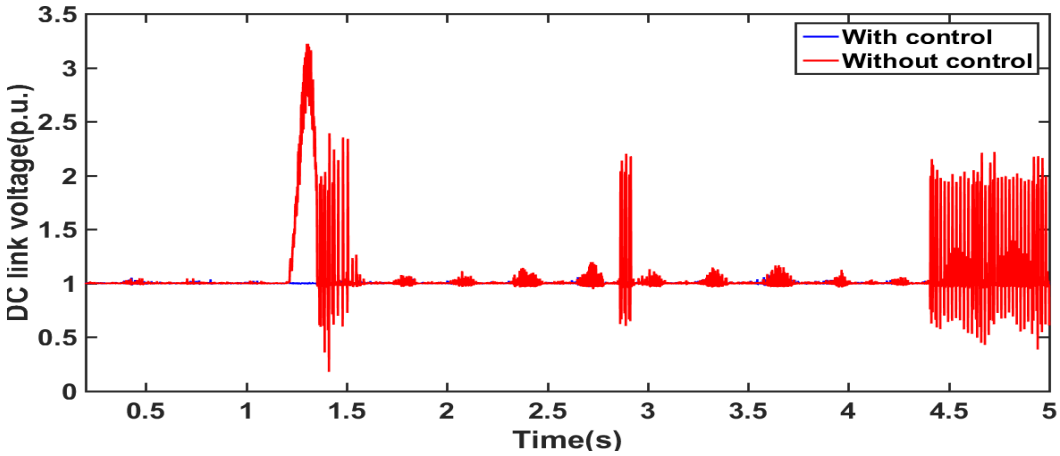

(a)

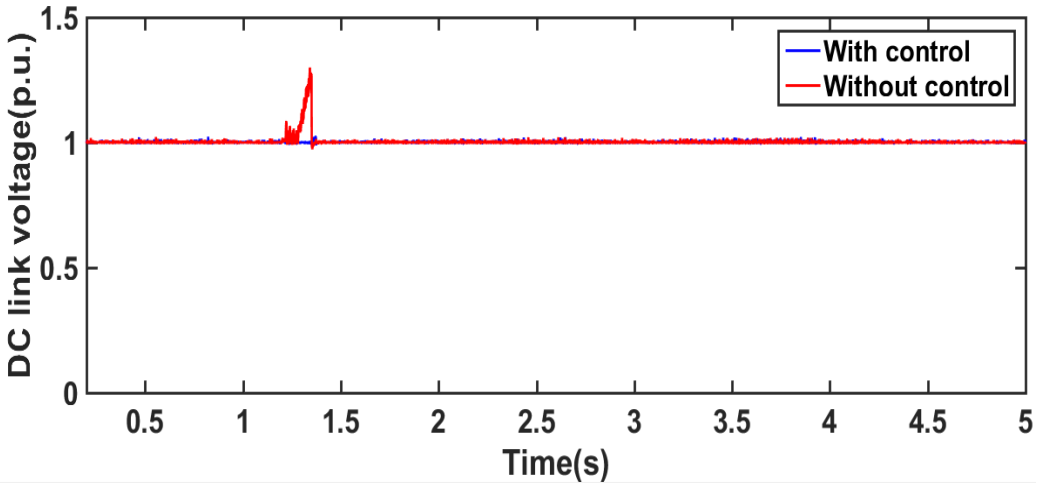

(b)

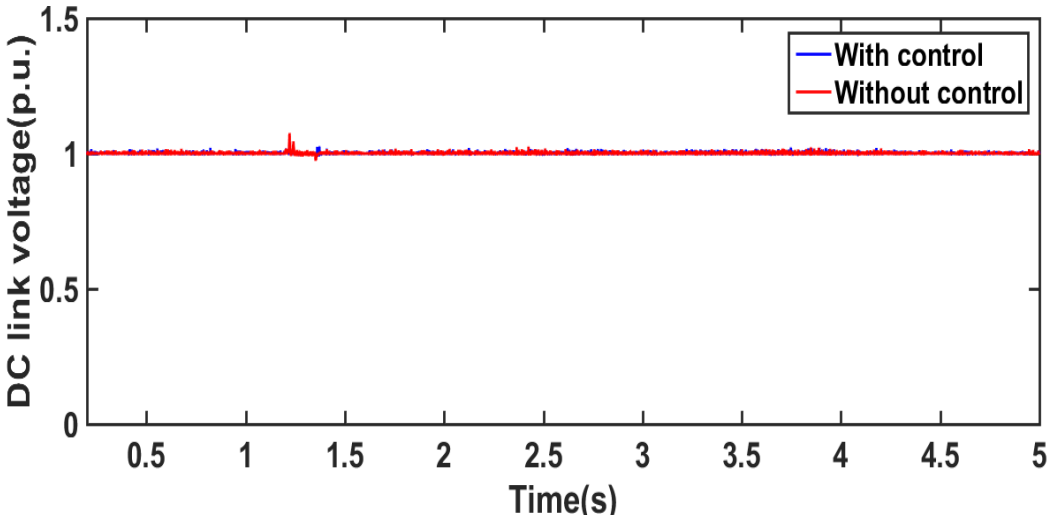

(c)

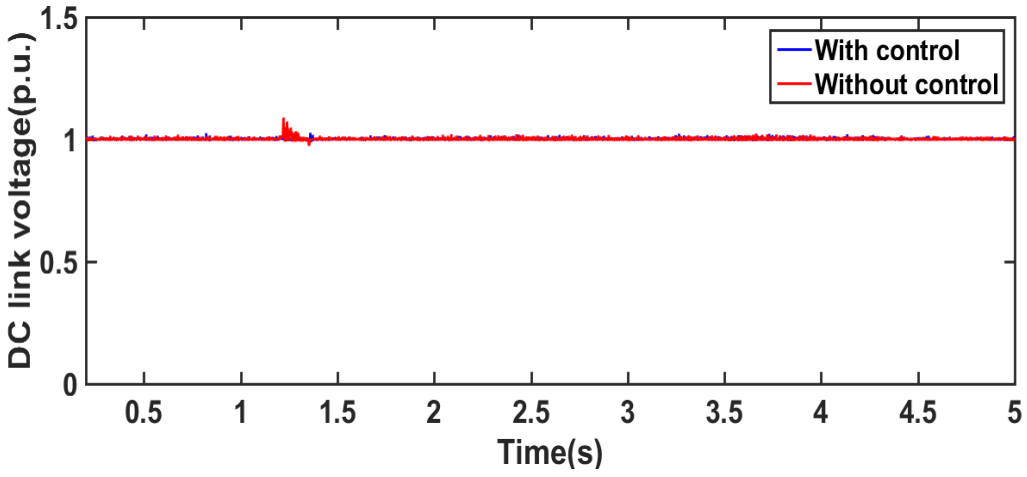

(d)

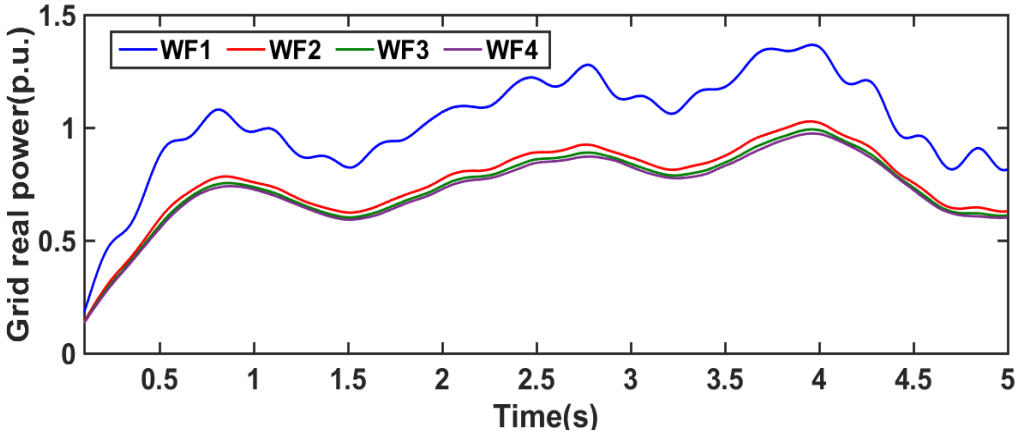

(e)

Fig.4.31. For wind speed direction 90º a) DC link voltage WF1 b) DC link voltage WF2 c) DC link voltage WF3 d) DC link voltage WF4 e) Real power in WF1, WF2, WF3, WF4

4.6. Summary

A coordinated control method is developed in this Chapter to improve the LVRT performance of a variable speed PMSG based grid connected WECS. Then the proposed approach is verified under different cases considering step and real wind speeds, single wind turbine, wind farms with the wake effect, single wind turbine and a wind farm connected to IEEE 9 bus test system during single and repetitive symmetrical and asymmetrical grid faults. From the simulation results, it has been demonstrated that the proposed method can limit the DC-link overvoltage under symmetrical and asymmetrical grid faults. Due to the simplicity and effectiveness of the proposed control, it can be a better choice compared to the conventional ESS based to provide LVRT.

REFERENCES

[1] A. K. Thet, H. Saitoh, "Pitch control for improving the low-voltage ride-through of wind farm", *Proc. Transmission Distribution Conf. Exposition: Asia and Pacific*, 2009, pp. 1-4.

[2] M. Q. Duong, F. Grimaccia, S. Leva, M. Mussetta, and E. Ogliari, " Pitch angle control using hybrid controller for all operating regions of SCIG wind turbine system," *Renewable Energy*, 2014

[3] A. Rezaeiha, I. Kalkman, and B. Blocken, "Effect of pitch angle on power performance and aerodynamics of a vertical axis wind turbine," *Applied Energy*, vol. 197, pp. 132-150, 2017.

[4] P. Dey, M. Datta, N. Fernando, and T. Senjyu, "A method to reduce DC-link overvoltage of PMSG based WECS during LVRT," in *IEEE Region 10 Conference (TENCON),* 2016, pp. 1894-1899.

[5] Mahadi, A., Tang, W.H., and Wu, Q.H., "Derivation of a complete transfer function for a wind turbine generator system by experiments". *In Proceedings of the 2011 IEEE Power Engineering and Automation Conference (PEAM),* Wuhan, China, 8–9 September 2011; pp. 35–38.

[6] T. Kalitjuka, "Control of Voltage Source Converters for Power System Applications", July 2011.

[7] C Bajracharya,"Control of VSC-HVDC for wind power," *Master of Science in Energy and Environment*, Department of Electrical Power Engineering, Norwegian University of Science and Technology, Trondheim, 2008.

[8] J.A. Suul, M. Molinas, L. Norum, T. Undeland, "Tuning of control loops for grid connected voltage source converters", *IEEE 2nd International Power and Energy Conference ,PECon 2008.*, pp. 797-802.

[9] O. Aydin, A. Akdag, P. Stefanutti, N. Hugo, “Optimum Controller Design for a Multilevel AC-DC Converter System”, *Proc. of Twentieth Annual IEEE Applied Power Electronics Conference and Exposition, APEC 2005*, Vol. 3, pp. 1660-1666

[10] A. C. Antoulas, D. C. Sorensen, S. Gugercin, "A survey of model reduction methods for large-scale systems", *Contemp. Math.*, vol. 280, pp. 193-219, 2000.

[11]. S. Ghosh, S. Kamalasadan, "An energy function-based optimal control strategy for output stabilization of integrated DFIG-Flywheel energy storage system", *IEEE Transaction on Smart Grid*, vol. PP, no. 99, pp. 1-10.

[12] T.H. Nauyen and D.C. Lee, “Ride-through technique for PMSG wind turbines using energy storage systems”, *Journal of Power Electronics*, 10 (2010), pp. 733-738

[13] C. Abbey, W. Li, L. Owatta, G. Jos, "Power electronic converter control techniques for improved low voltage ride through performance in WTGs", *Proc. 37th IEEE Power Electronics Specialists Conf.*, vol. 1, pp. 422-427, 2006

[14] J. Kim, J. Lee, Y. Suh, B. Lee, Y. Kang, "Fault response of a DFIG-based wind power plant taking into account the wake effect", *Journal of Electrical Engineering Technology*, vol. 9, no. 3, pp. 820-826, May 2014.

[15] A. M. Howlader, T. Senjyu, and A. Y. Saber, “An integrated power smoothing control for a grid-interactive wind farm considering wake effects”, *IEEE Systems Journal*, vol. 9, pp. 954-965, 2015.

[16] Koch F, Gresch and M, Shewarega F, “Consideration of wind farm wake effect in power system dynamic simulation”, *IEEE Conference; Power Tech*, Russia; 2005 Jun 27–30; St. Petersburg, Russia.

CHAPTER FIVE

COORDINATED CONTROLLER WITH THE GSC AND STATCOM FOR THE LVRT

5.1. Introduction

The coordinated control which is presented in the Chapter four is modified and extended in this chapter. This coordinated controller now combines the pitch angle control of Chapter 4, the flux weakening control of Chapter 3 and the reactive power controls from the GSC and STATCOM to enhance the LVRT capability of the PMSG based variable speed WECS. In this strategy, pitch angle controller is modified to adjust the pitch for power smoothing as well as the LVRT during variable wind speeds and grid faults respectively. The flux weakening controller is used to reduce the flux linkages of the PMSG by supplying the negative field regulating current to reduce the DC link overvoltage during grid voltage dips. And a reactive power controller is added to the GSC or STATCOM to enhance the overall LVRT. The GSC is used primarily to supply the reactive power. Additionally, static compensator (STATCOM) is used to provide more reactive power support during the grid faults. Extensive simulations of proposed method have been carried out under different fault cases in MATLAB/SIMULINK. The effectiveness of the proposed controller is verified and compared with the Braking Chopper (BC) based conventional method.

5.2. Extended Coordinated Control: Combining the Pitch Angle Control, the Flux Weakening Control and the Reactive Power Support

The proposed control strategy is demonstrated with combining the pitch angle control, flux weakening control and reactive power support. This control method is developed to

smooth wind turbine power output, limit the DC link over voltage and grid voltage support.

5.2.1. Reactive Power Support by the GSC

Figure 5.1(a) shows the GSC controller in the proposed scheme. For normal operation, MSC is controlled by MPPT and torque reference. But during grid voltage dip it is switched to fault ride through mode [1], [2]. The MPPT control is canceled and MSC regulates the DC voltage.

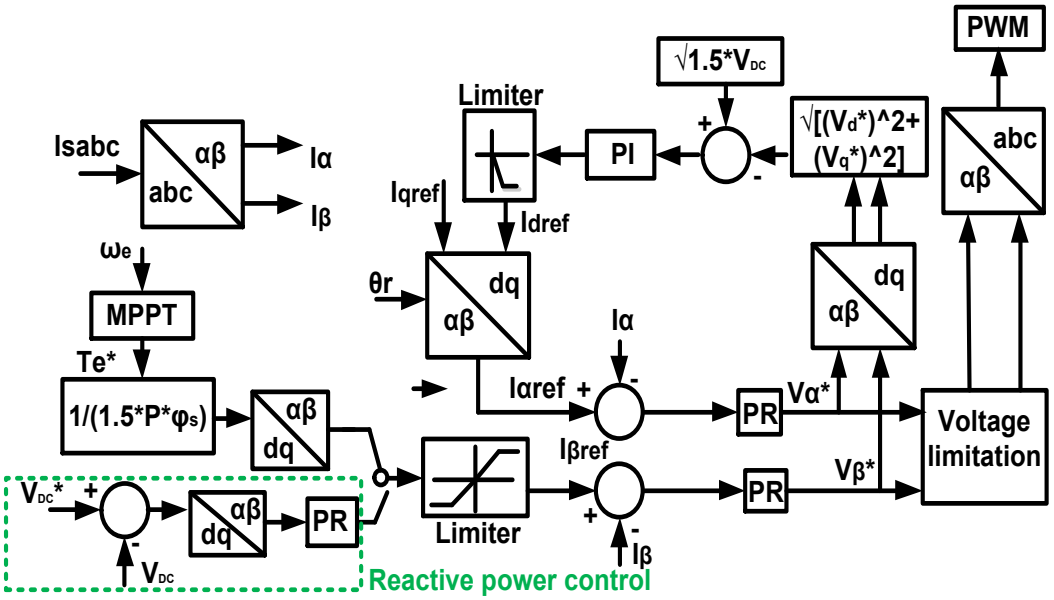

(a)

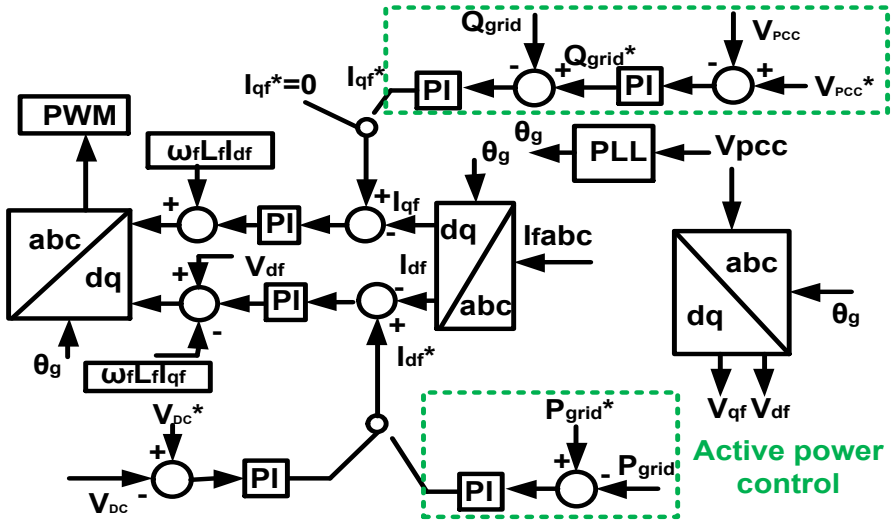

(b)

Fig.5.1. Reactive power control a) block diagram for MSC b) block diagram for GSC

On the other hand, the GSC controller changes the priorities of real and reactive currents during the terminal voltage drops below the predefined value 0.9 p.u. The direct-axis current regulation gets high priority if the grid voltage is equal to or larger than 0.9 p.u. Otherwise, high priority is given to the quadrature-axis current (reactive current) as presented in Fig.5.1 (b).

5.2.2. Reactive Power Support by the STATCOM

The STATCOM is consists of a MOSFET PWM inverter and DC link super capacitors. It is connected in parallel to PCC through three phase coupling filter [3]. It regulates the AC voltage at PCC through reactive power exchange and DC bus voltage through the real power exchange with the system. Block diagram of STATCOM control is shown in Fig.5.2 (a). The three phase grid currents at PCC are measured and are converted to the active component, I_d and the reactive component, I_q. They are passed through a Butterworth low pass filter to obtain the active fundamental current, I_d-DC and reactive fundamental current I_q-AC.

The PCC voltage of the grid connected WECS is measured and it is compared with the PCC reference voltage. The difference between the voltages at the n^{th} sampling instant goes through the PI controller which generates the peak reference current magnitude for I_q. Similarly, the DC-link capacitor voltage is maintained within the acceptable limit with the I_d reference current control obtained via the PI controller. The references for the modulator are generated with the filtered active and reactive currents in given in (4.38).

$$\begin{bmatrix} I_d AC \\ I_q AC \end{bmatrix} = \begin{bmatrix} I_d \\ I_q \end{bmatrix} - \begin{bmatrix} I_d DC \\ I_q DC \end{bmatrix} \qquad (5.1)$$

And the reference currents in the a-b-c frame are:

$$\begin{bmatrix} I_{ar} \\ I_{br} \\ I_{cr} \end{bmatrix} = \begin{bmatrix} \sin(\omega_s t) & \cos(\omega_s t) \\ \sin(\omega_s t - \frac{2\pi}{3}) & \cos(\omega_s t - \frac{2\pi}{3}) \\ \sin(\omega_s t + \frac{2\pi}{3}) & \cos(\omega_s t + \frac{2\pi}{3}) \end{bmatrix} \begin{bmatrix} I_d{}^{AC} \\ I_q{}^{DC} \end{bmatrix} \quad (5.2)$$

A hysteresis comparator shown in Fig. 5.2(b) is considered here to obtain the gate pulses of STATCOM [4], [5]. It is based on upper and lower limit of hysteresis band. The difference between reference current, $I_r(t)$ and the injected inverter current, $I_f(t)$ is passed through the hysteresis comparator. When the current difference exceeds the hysteresis band upper limit, upper switch is turned OFF and the lower switch is turned ON for one arm of an inverter. Similarly, if the current difference crosses the hysteresis band lower limit, the inverter arm lower switch is turned OFF and the upper switch is turned ON. The STATCOM operation logic is shown in Fig.5.2 (c). Parameter of STATCOM is shown in Appendix C.

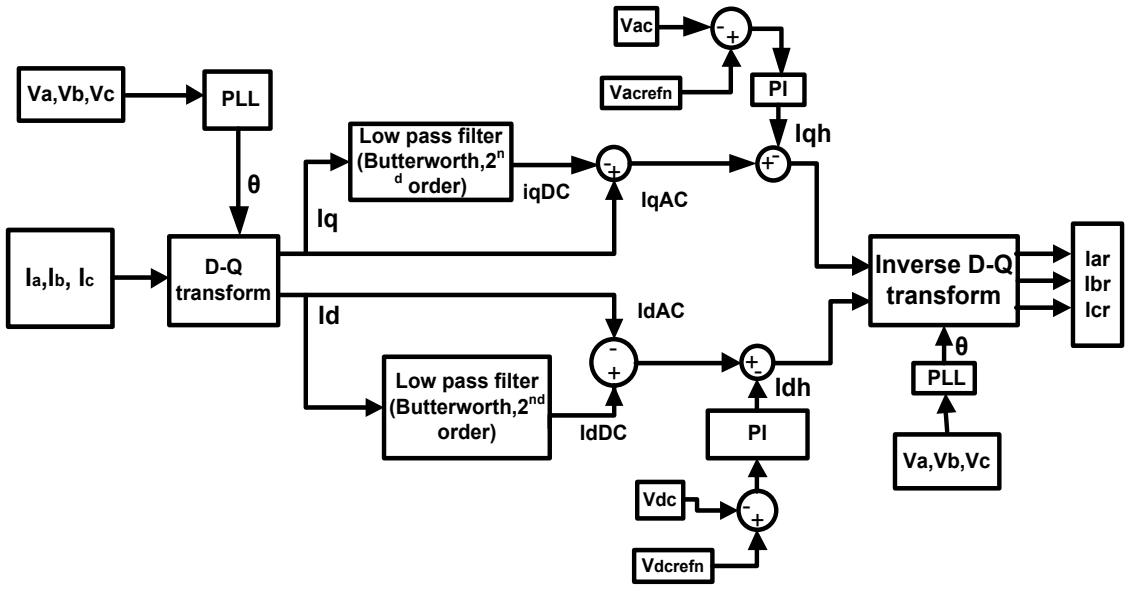

(a)

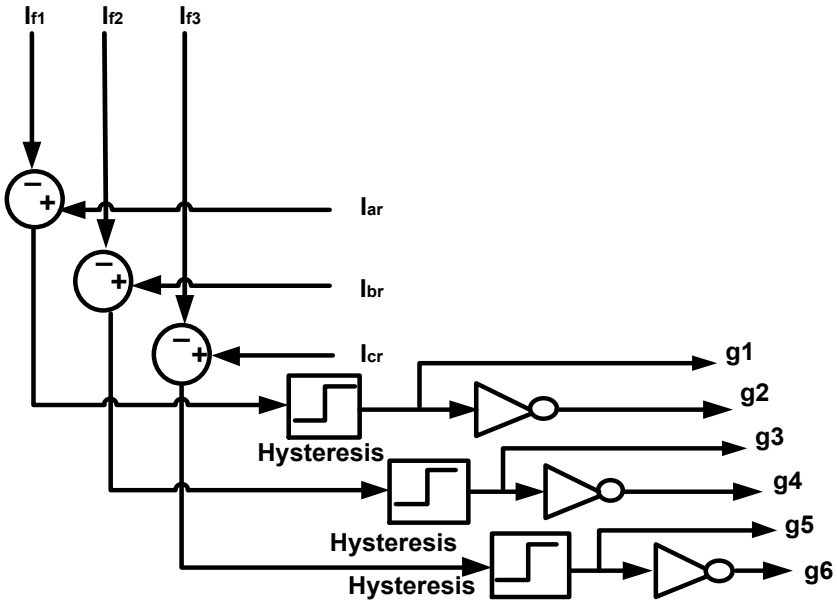

(b)

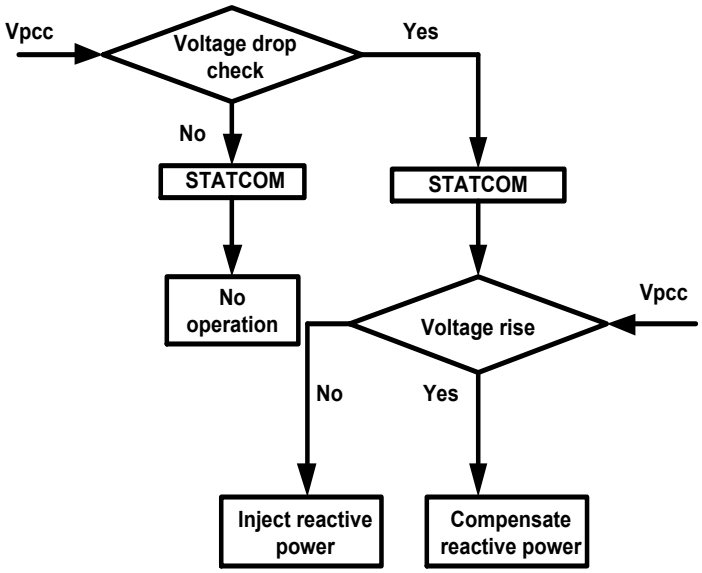

(c)

Fig.5.2. Control of STATCOM (a) Block diagram (b) Hysteresis controller (c) Flow chart

5.3. Simulation Results and Analysis

5.3.1. DC Link Voltage Control and Reactive Power Support from the GSC and their Coordinated Control

A coordinated control of pitch angle of a wind turbine, flux control PMSG and grid voltage support for LVRT enhancement is presented. Within this strategy, pitch angle controller is modified to adjust the pitch for power smoothing during variable wind speed as well as LVRT during repetitive grid fault. Flux controller is used to keep the DC link voltage within the permissible limit in grid voltage dips. And reactive power support from GSC is used here to provide grid voltage support during a grid fault.

5.2.3.1.1. Wind Turbine Connected to the IEEE 9 Bus Test System

The WECS is connected to the IEEE-9 bus system as shown in Fig.5.3 to evaluate the realistic performance of the proposed controller. The WECS is connected at bus 8 via a transformer. MATLAB simulation is done, and the significant results are obtained. Simulation is run for 5 seconds. The proposed coordinated control is verified under symmetrical and asymmetrical grid faults.

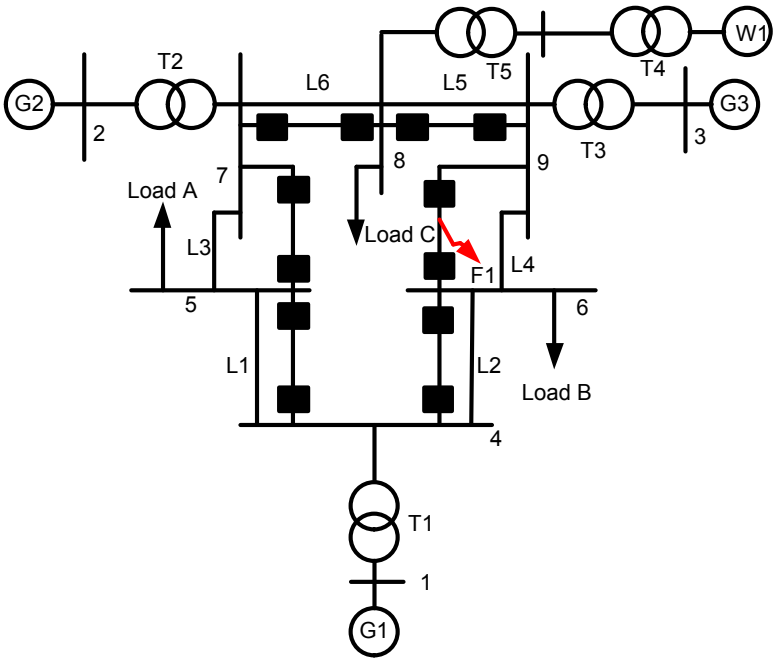

Fig.5.3. Connection of wind turbine in IEEE-9 bus system

5.2.3.1.1.1 For Symmetrical Faults

This scenario describes the performance of proposed controller under the three grid faults in line 6-9. The grid voltage dip occurs and the voltage falls from 1 p.u. to about 0.35 p.u as shown in Fig.5.4 (b). During this fault, the active power injection from the GSC to the grid is limited and reactive power is injected into the grid. It enables the grid supporting services during the fault. Grid voltage is improved from 35% to 50% as shown in Fig.5.4 (b). The pitch angle is increased in the transient state as shown in Fig.5.4(c). The transient behaviour of the grid real power and reactive power is observed better with the coordinated controller as shown in Fig.5.4 (d) and Fig.5.4 (e) respectively. The DC-link capacitor voltage increases to almost 1.5 times of its nominal value as shown in Fig.5.4 (f). From Fig. 5.4(f), it is found that the proposed coordinated control provides effective performance in DC-link voltage regulation by reducing fluctuations.

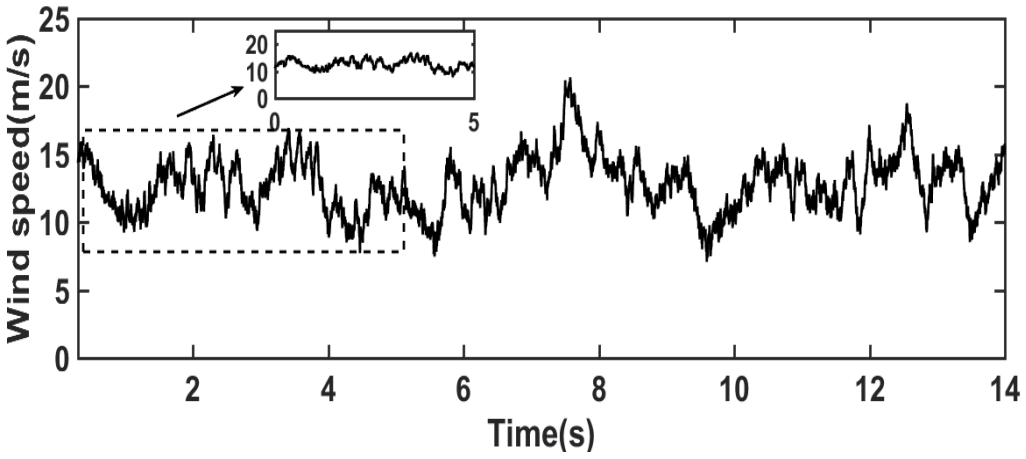

(a)

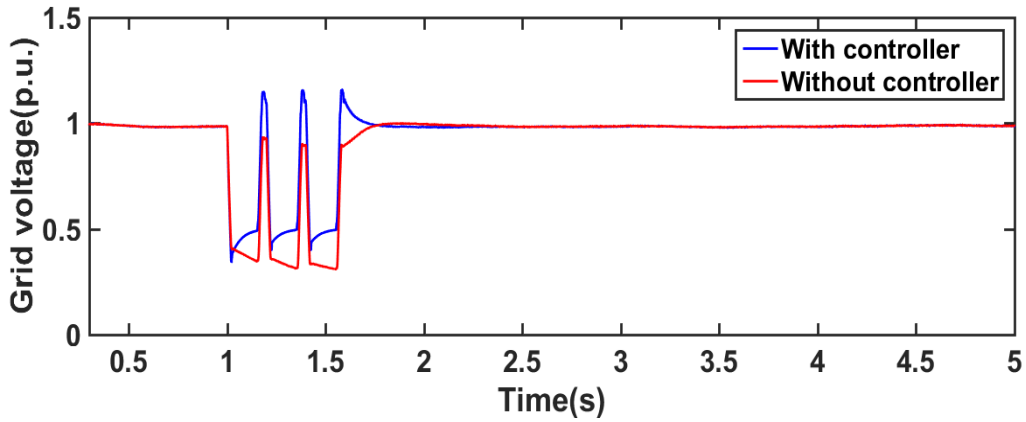

(b)

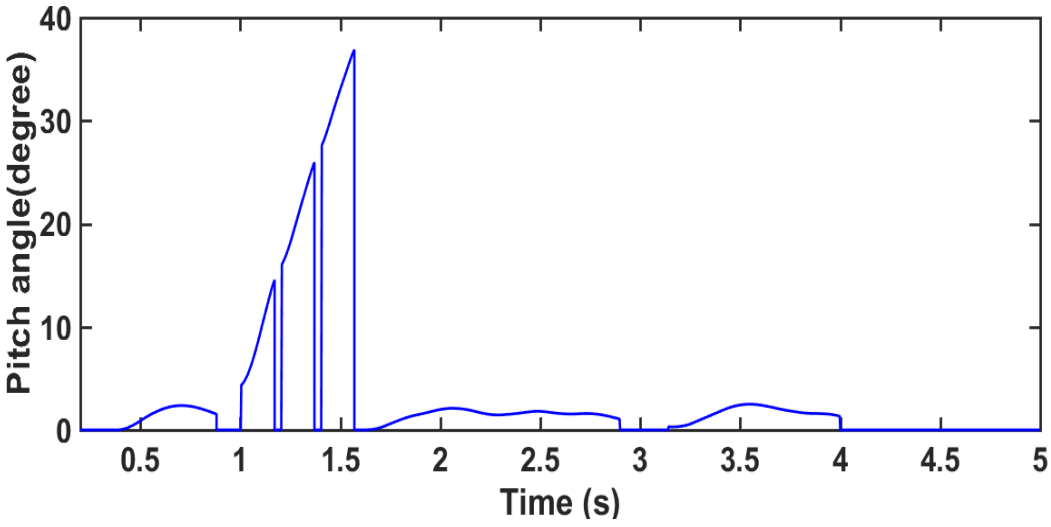
Pitch angle(degree)
Time (s)
0
10
20
30
40
0.5
1
1.5
2
2.5
3
3.5
4
4.5
5

(c)

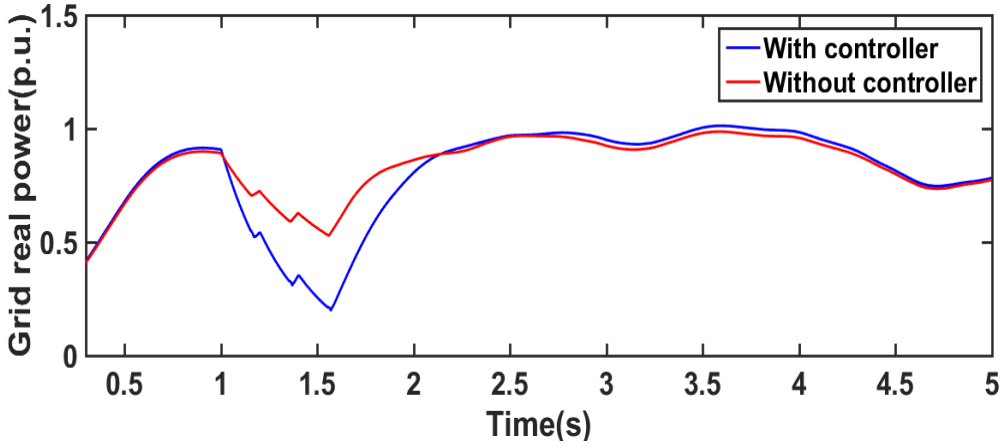
Grid real power(p.u.)
Time(s)
With controller
Without controller
0
0.5
1
1.5
0.5
1
1.5
2
2.5
3
3.5
4
4.5
5

(d)

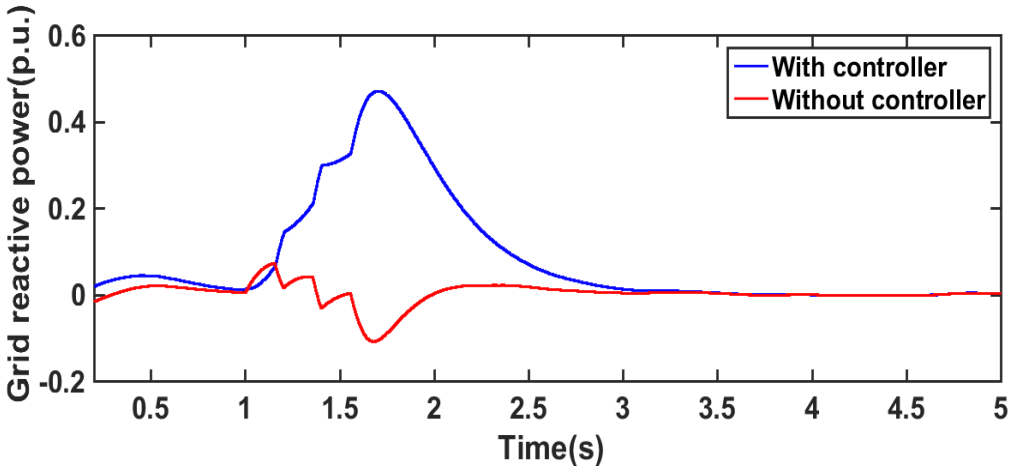
Grid reactive power(p.u.)
Time(s)
With controller
Without controller
-0.2
0
0.2
0.4
0.6
0.5
1
1.5
2
2.5
3
3.5
4
4.5
5

(e)

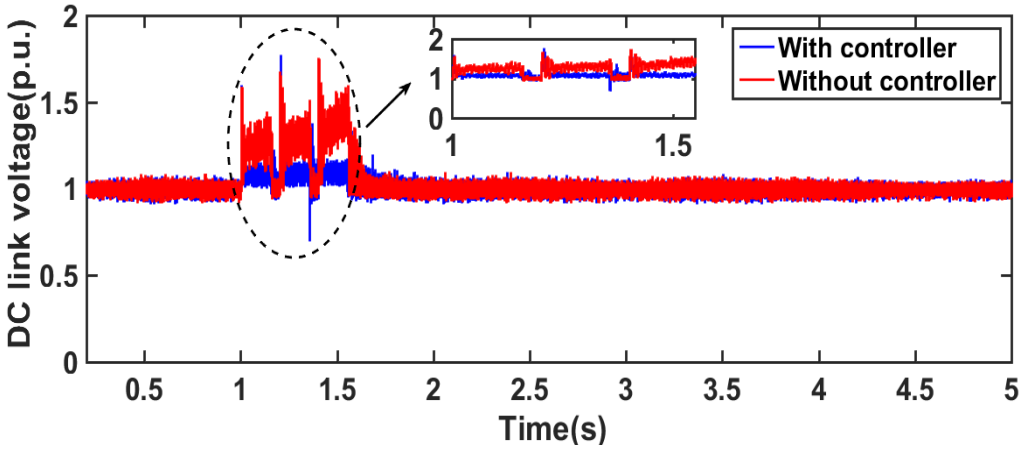

(f)

Fig.5.4. Simulation result for symmetrical fault a) Variable wind speed b) Grid voltage c) Pitch angle d) Grid real power e) Grid reactive power f) DC link voltage

5.3.1.1.2. For Asymmetrical Faults

This scenario describes the performance of proposed controller under the double line to ground faults in line 6-9. The grid voltage dip occurs, and the voltage falls from 1p.u. to about 0.6p.u. as shown in Fig.5.5(b). During this repetitive fault, the active power injection from the GSC to the grid is limited and reactive power is injected into the grid. It enables the grid supporting services during the fault. Grid voltage is improved from 60% to 74% as shown in Fig.5.5 (b). The pitch angle is increased in the transient state as shown in Fig.5.5(c). The transient behaviour of grid real power and reactive power is observed better with the coordinated controller as shown in Fig.5.5 (d) and Fig.5.5 (e) respectively. The DC-link capacitor voltage increases to almost 1.5 times of its nominal value as shown in Fig.5.5 (f). From Fig. 5.5(f), it is found that the proposed coordinated control provides effective performance in DC-link voltage regulation by reducing fluctuations.

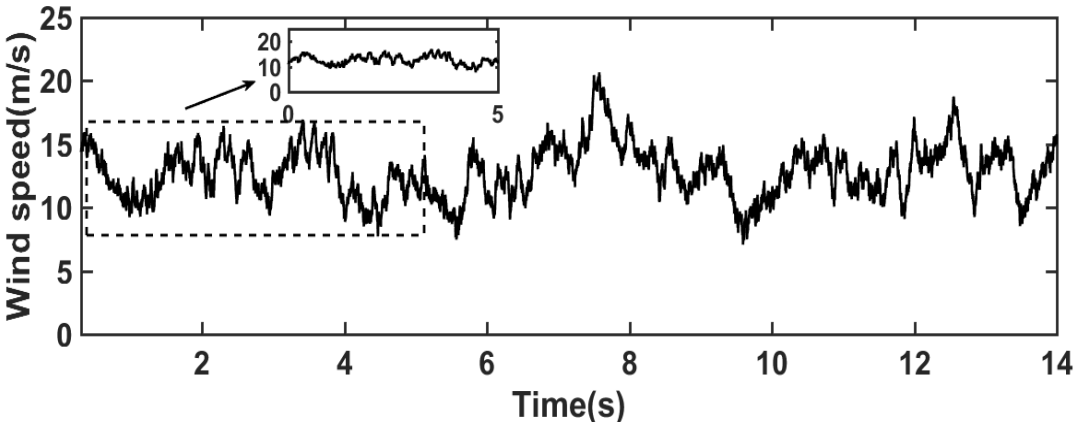
Wind speed(m/s)
Time(s)
25
20
15
10
5
0
2
4
6
8
10
12
14
20
10
0
0
5

(a)

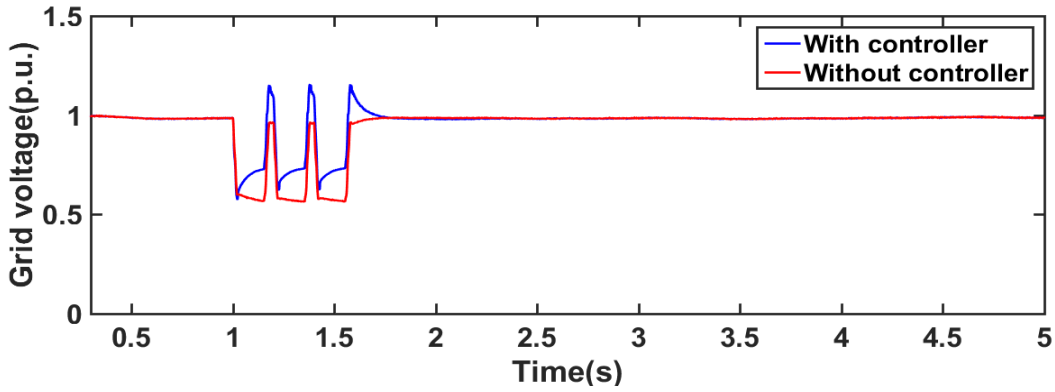
Grid voltage(p.u.)
Time(s)
With controller
Without controller
1.5
1
0.5
0
0.5
1
1.5
2
2.5
3
3.5
4
4.5
5

(b)

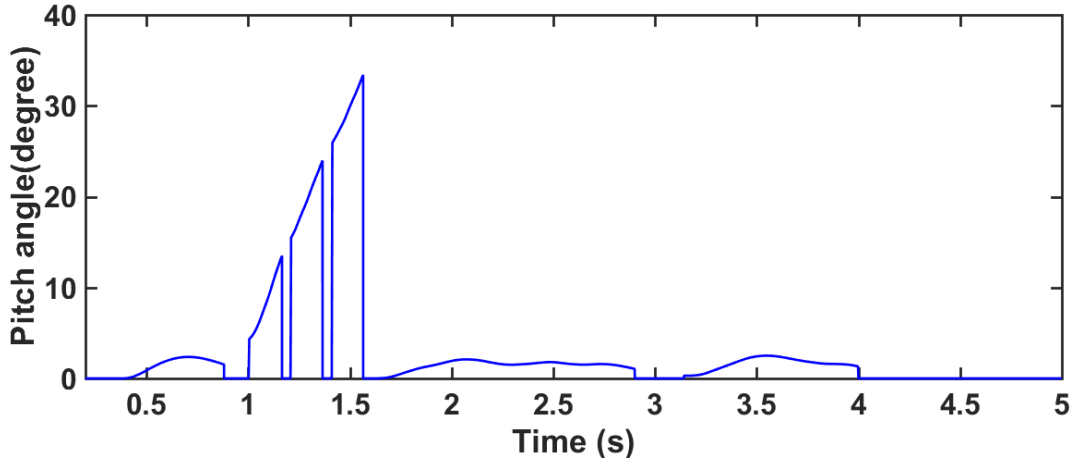
Pitch angle(degree)
Time (s)
40
30
20
10
0
0.5
1
1.5
2
2.5
3
3.5
4
4.5
5

(c)

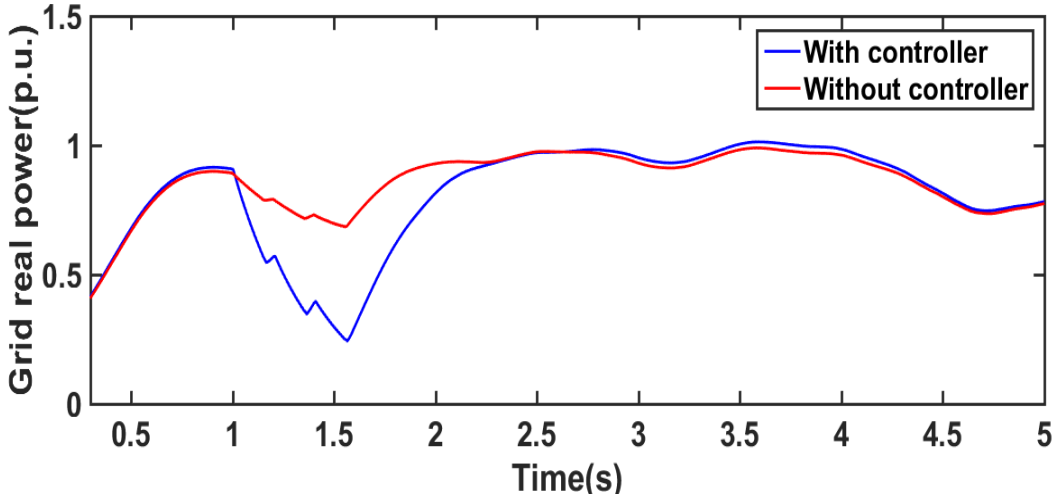

(d)

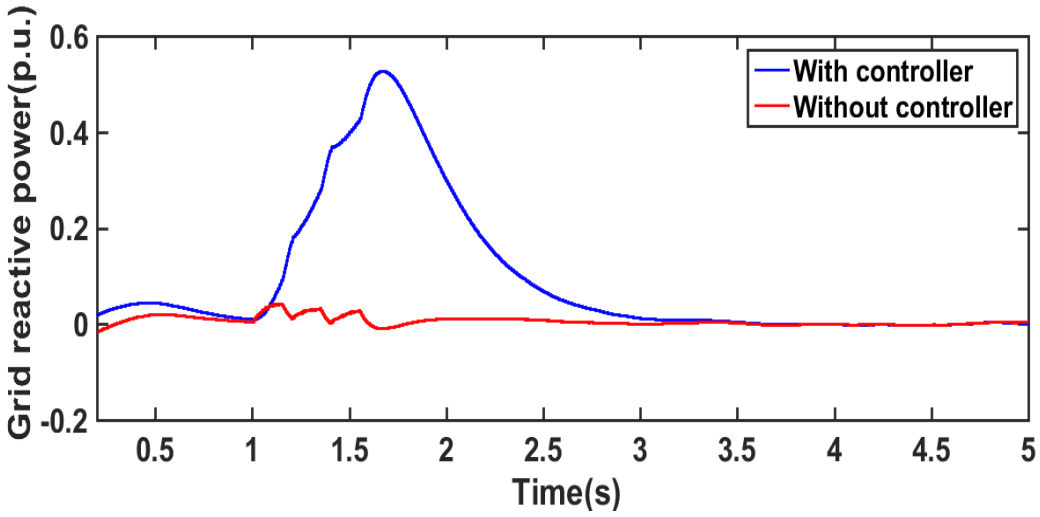

(e)

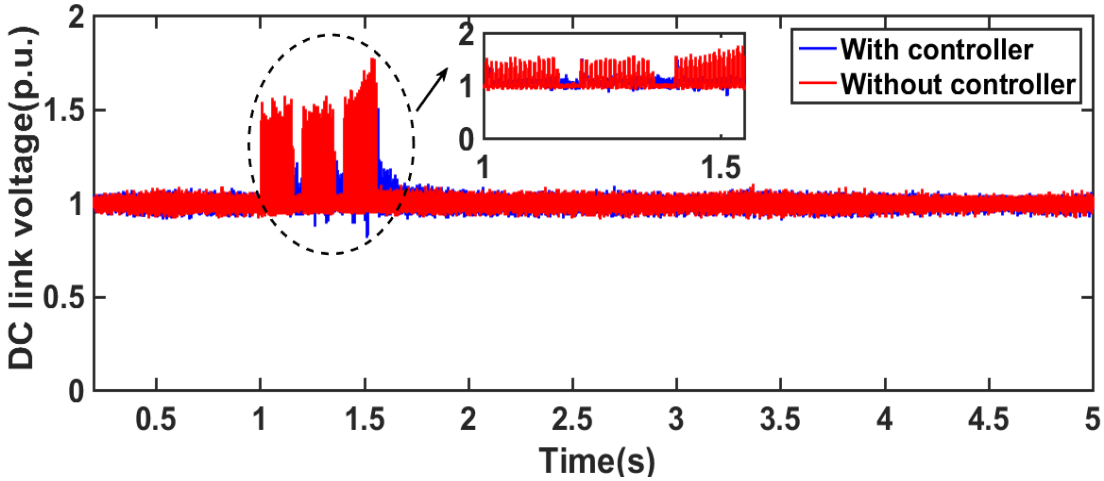

(f)

Fig.5.5. Simulation result for asymmetrical fault a) Variable wind speed b) Grid voltage c) Pitch angle d) Grid real power e) Grid reactive f) DC link voltage

5.3.2. DC Link Voltage Control and Reactive Power Support by the STATCOM and their Coordinated Control

Another approach is developed to improve the LVRT capability of PMSG based WECS. This coordinated control consists of a pitch angle control, a flux weakening control and a STATCOM [6]. Block diagram of grid connected WECS with STATCOM is shown in Fig.5.6. The STATCOM operates based on value of the grid voltage drop [7], [8]. It will inject the reactive power to improve the grid voltage is around 0.9 p.u. If the STATCOM is not able to inject enough reactive power for grid voltage support the wind turbine will disconnect from grid and it will operate as a stand-alone system [9].

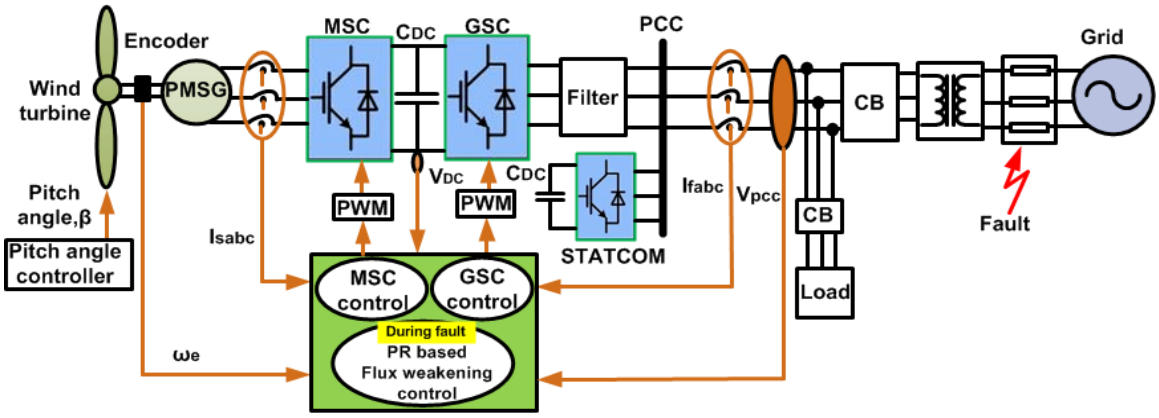

Fig.5.6. Grid connected PMSG with coordinated controller

5.3.2.1. Operation Under Symmetrical Faults for Step Change in the Wind Speeds

The variable wind speed is set to 8-18m/s as shown in Fig.5.7 (a). Rated wind speed is 12m/s and pitch angle remains zero until wind speed is equal or less than the rated speed. It increases to limit the output power and rotor speed according to wind speed variation. At t = 1s, a three line to ground fault is applied on the transmission line as shown in Fig. 5.7(b). The fault duration is 0.5s. As shown in Fig.5.7 (b), the grid voltage falls from 100% to 25 % for both control strategies. During this fault, the active power injection from the GSC to the grid is limited; however, the MSC injects power to the DC-link capacitor.

So, the DC-link capacitor voltage increases to almost 1.5 times of its nominal value and is shown in Fig.5.7(c). The pitch angle is increased in the transient state. From Fig. 5.7(c), it is found that the proposed coordinated control performs better compared to the conventional BC control to regulate the DC-link voltage within the acceptable limit and the DC-link voltage fluctuations are reduced. The transient behaviors of the grid real power are observed better than with the conventional braking chopper protection as shown in Fig.5.7 (d). Fig.5.7 (e) shows the response of pitch angle during the fault period. The STATCOM inject reactive power to enable the grid supporting services during the fault. Grid voltage is improved from 25% to 80% as shown in Fig.5.7 (f).

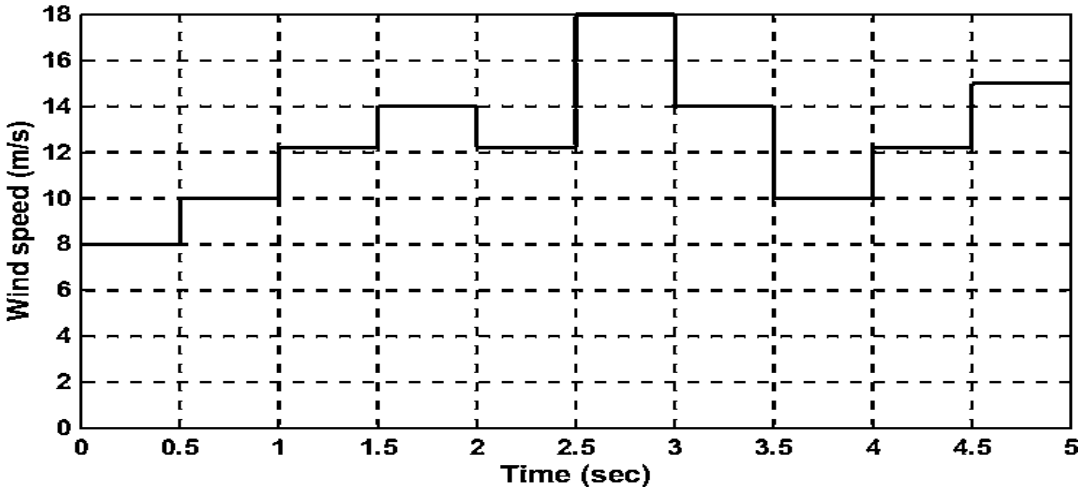

(a)

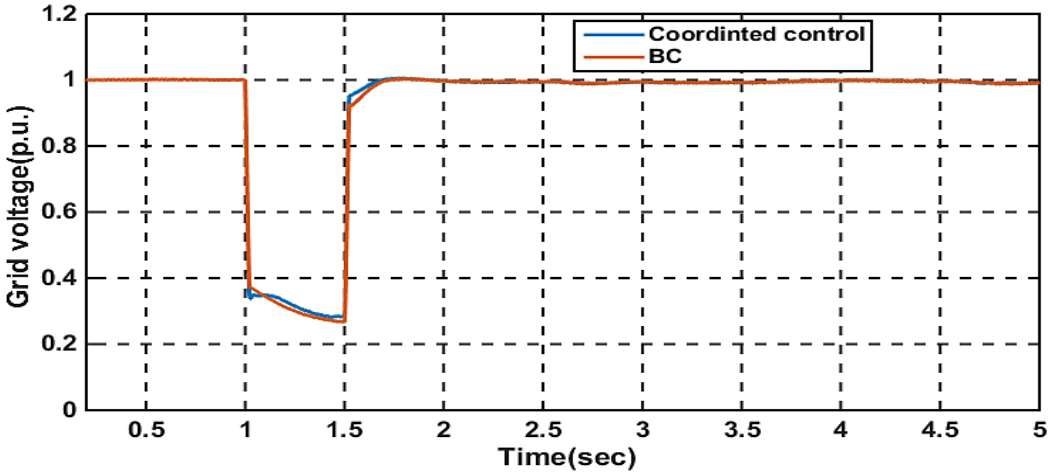

(b)

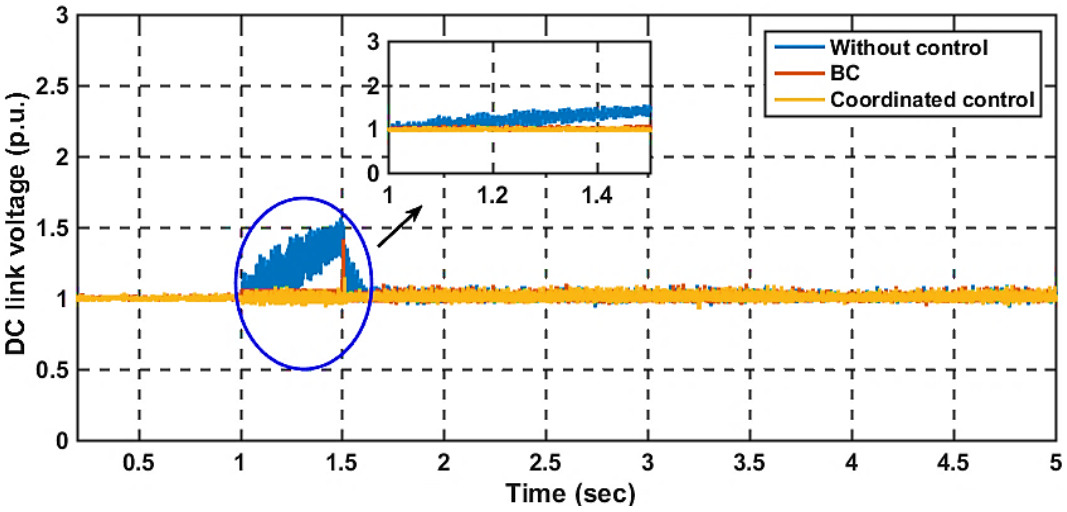
DC link voltage (p.u.)
Time (sec)
Without control
BC
Coordinated control

(c)

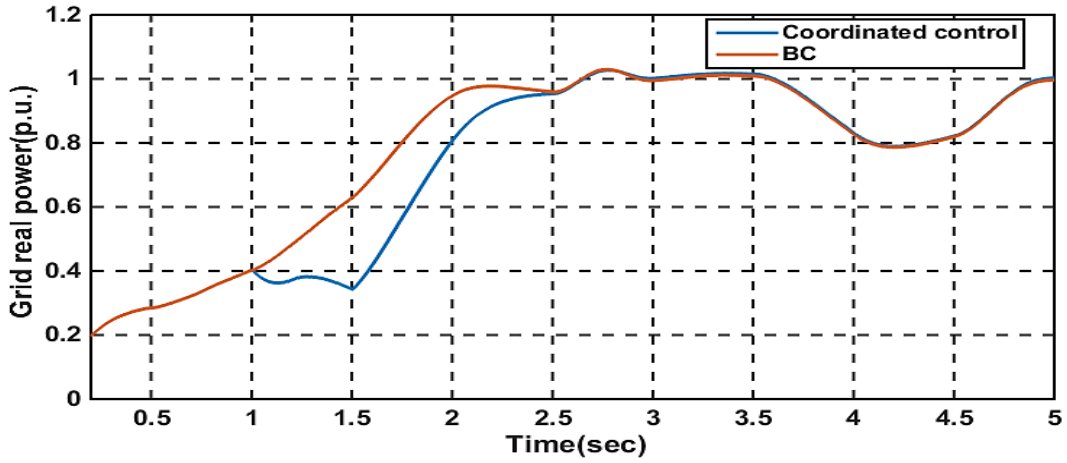
Grid real power(p.u.)
Time(sec)
Coordinated control
BC

(d)

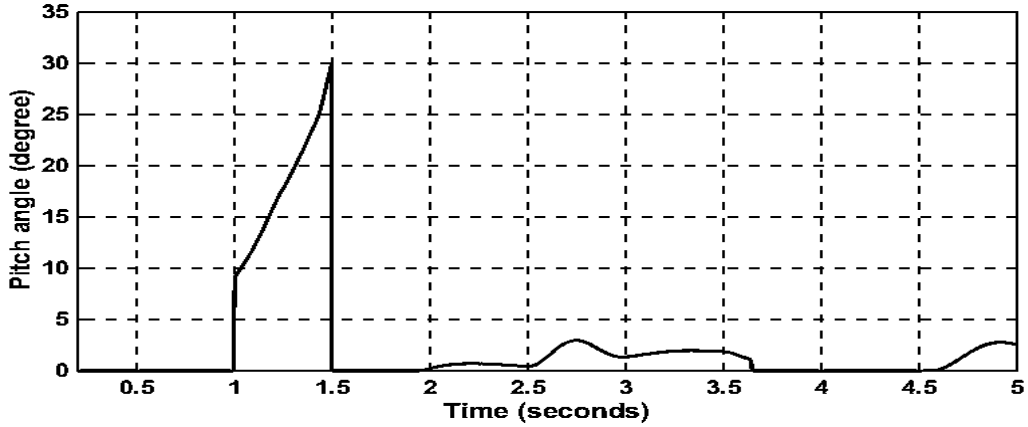
Pitch angle (degree)
Time (seconds)

(e)

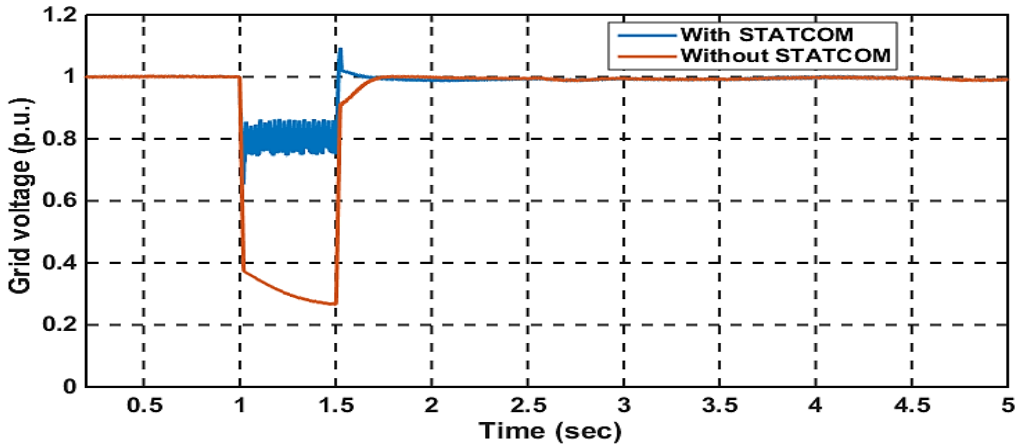

(f)

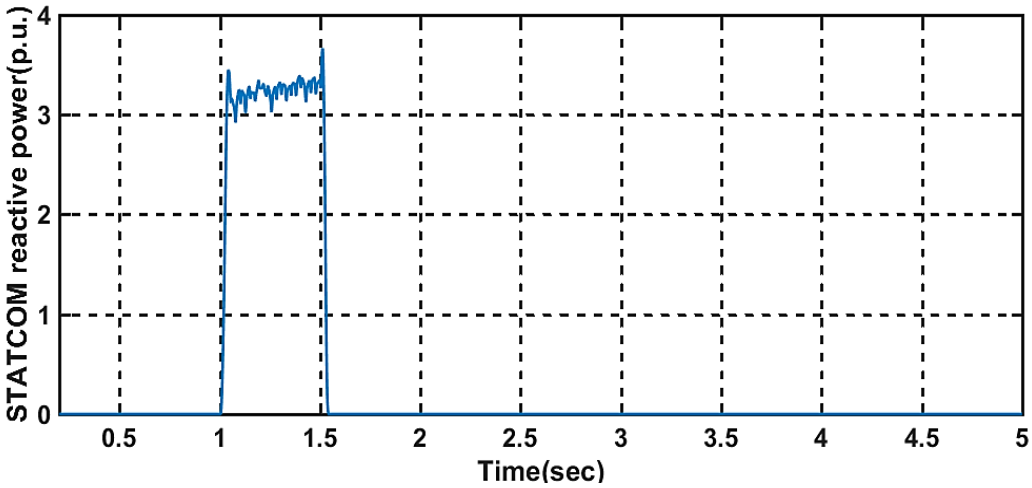

(g)

Fig.5.7. Simulation result for symmetrical fault (a) Variable wind speed (b) Grid voltage (c) DC link voltage (d) Grid real power (e) Pitch angle for LVRT (f) Grid voltage with STATCOM (g) STATCOM reactive power

5.3.2.2. Operation Under Asymmetrical Faults for Step Change in the Wind Speeds

At t = 1s, a double line to ground fault is applied on the transmission line. Similarly, the fault duration is 0.5s. The grid voltage is reduced to 0.55p.u. as shown in Fig. 5.8 (b). With limited active power injection to the grid during this fault, the voltage of the DC-link capacitor increases to 1.7 times from its nominal value and is shown in Fig. 5.8(c). Using the coordinated controller, effects of the grid fault are mitigated. The pitch angle

is increased in the transient state to reduce incoming power. It is found that the proposed coordinated control performs better compared to the conventional BC control in DC-link voltage regulation reducing fluctuations and transients and the performances are shown in Fig. 5.8(c). The transient behaviours of the grid real power, generator speed, generator current, grid current and torque are observed better than with the conventional braking chopper protection as shown in Fig. 5.8(d). Fig.5.8 (e) shows the response of pitch angle during the fault period. The STATCOM inject reactive power to enable the grid supporting services during the fault. Grid voltage is improved from 60% to 83% as shown in Fig.5.8 (f).

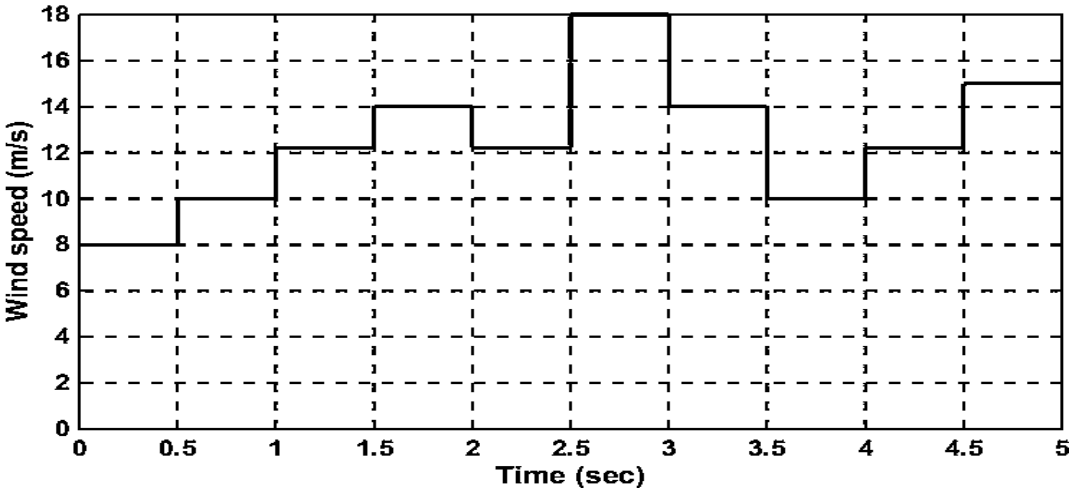

(a)

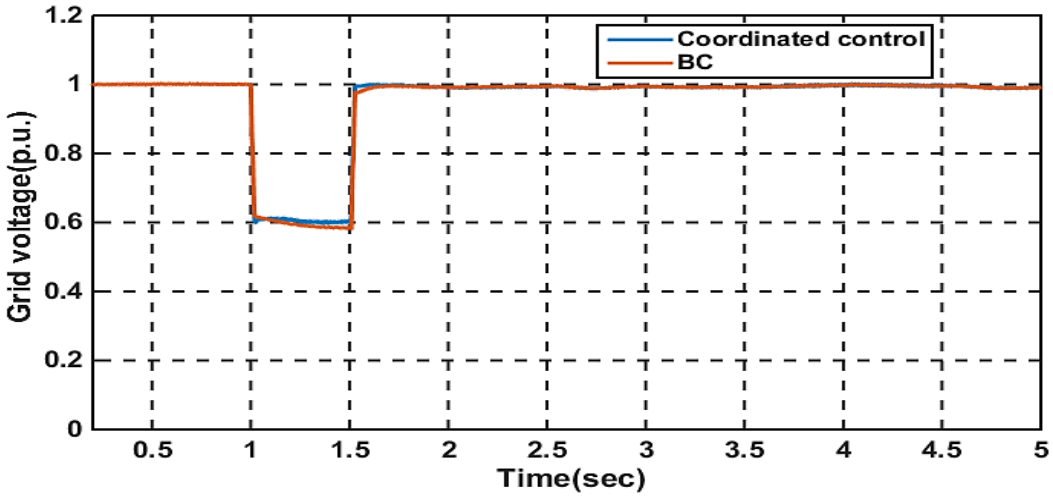

(b)

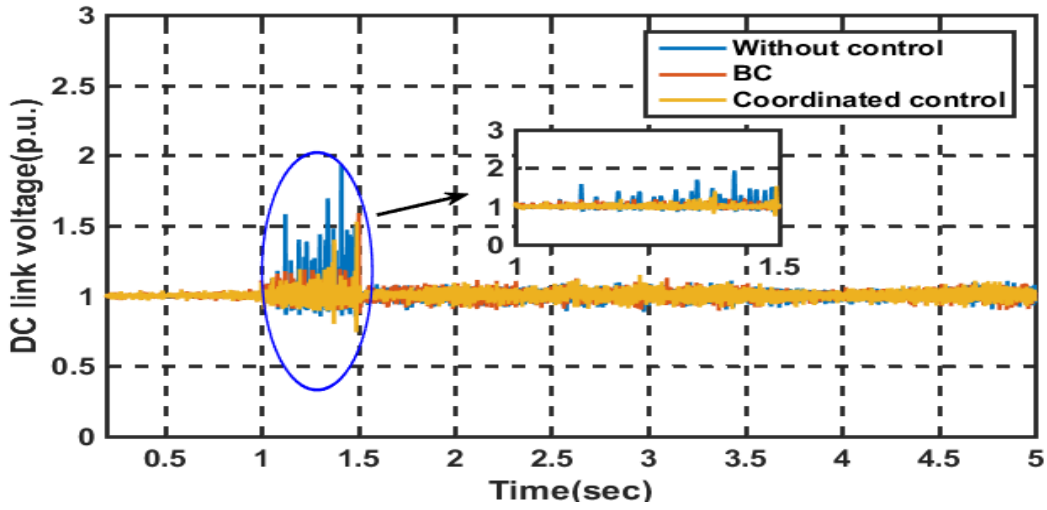
Without control
BC
Coordinated control
DC link voltage(p.u.)
Time(sec)

(c)

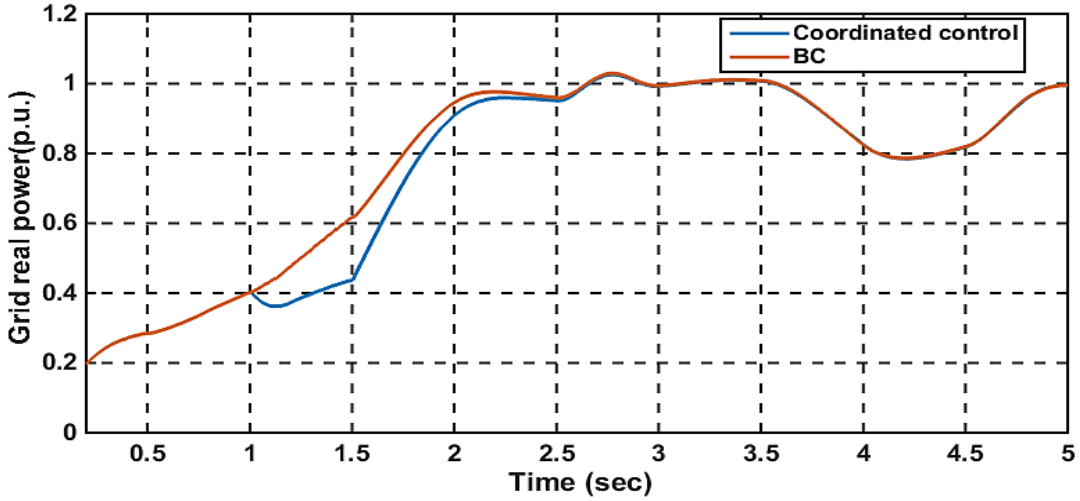
Coordinated control
BC
Grid real power(p.u.)
Time (sec)

(d)

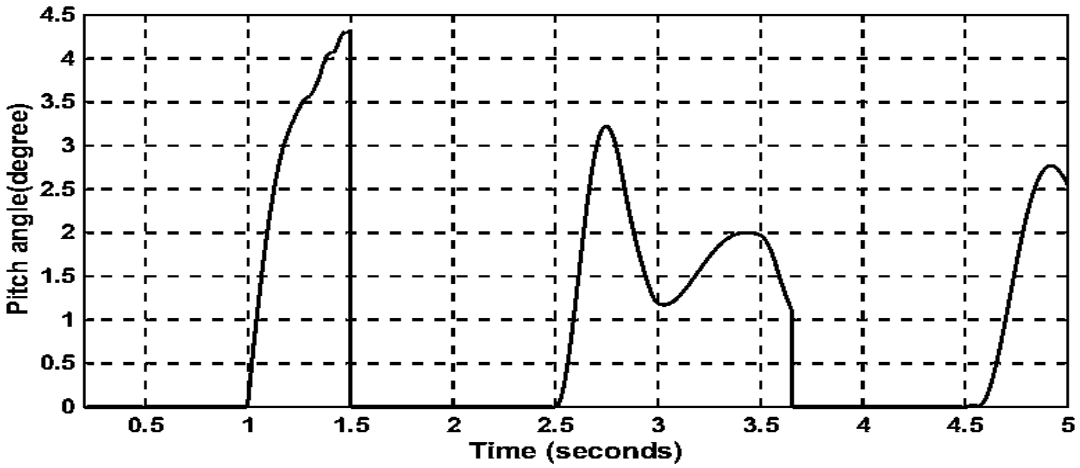
Pitch angle(degree)
Time (seconds)

(e)

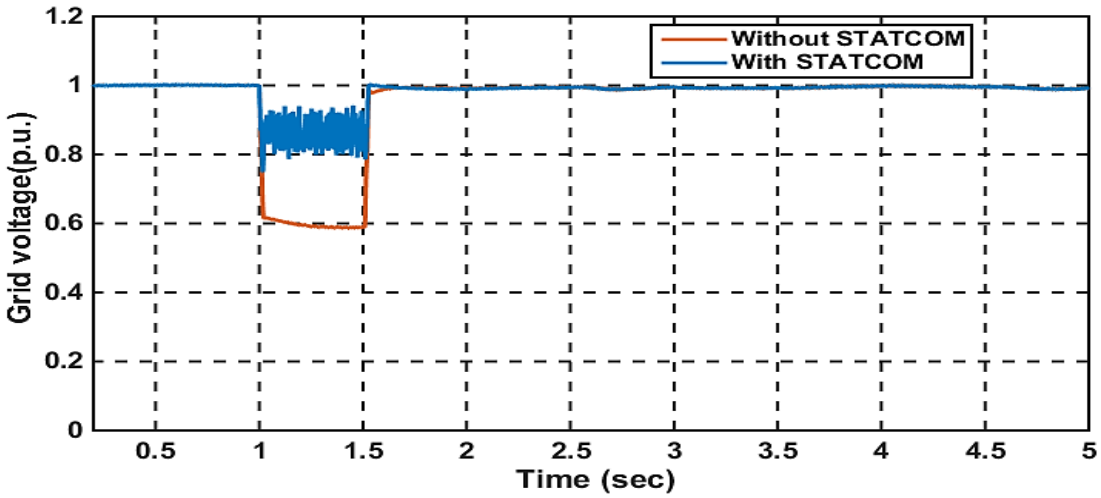

(f)

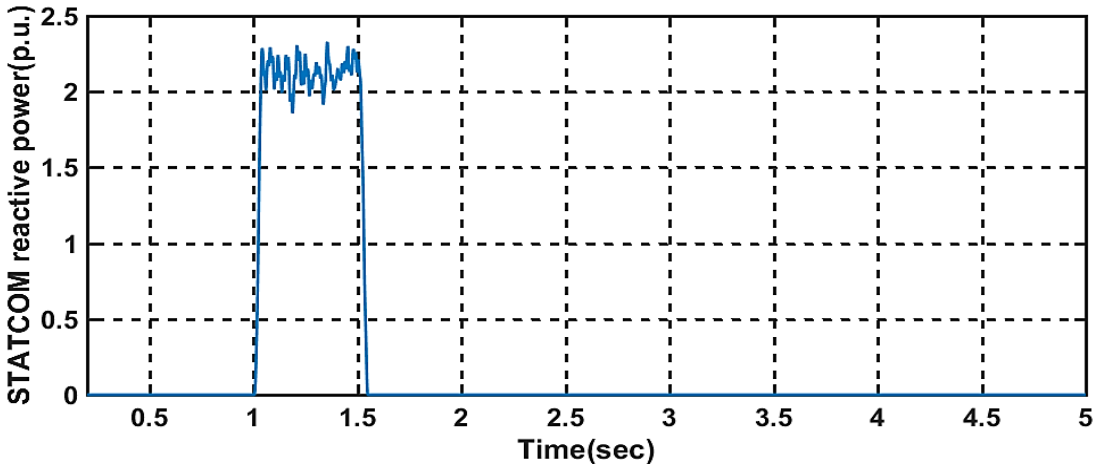

(g)

Fig.5.8. Simulation result for asymmetrical fault (a) Variable wind speed (b) Grid voltage (c) DC link voltage (d) Grid real power (e) Pitch angle for LVRT (f) Grid voltage with STATCOM g) STATCOM reactive power

5.3.2.3. Operation Under Symmetrical and Asymmetrical Faults for Actual Changes in the Wind Profile

Similarly, the controller effectiveness is tested under real wind speed profile. The wind speed varies from 8m/s to 16m/s as shown in Fig.5.9 (a). The pitch angle control works accordingly to the variable wind speed as shown in Fig. 5.9(b) and thus the wind turbine output power is limited. Without any controller the DC link voltage is increased to 1.5 p.u. and 1.7 p.u. as shown in Fig.5.9(c) and (d) for symmetrical and asymmetrical fault

respectively. It is beyond the permissible limit. The DC link voltage is kept within limit under symmetrical and asymmetrical fault by using the proposed coordinated control. From Fig.5.9(c) and (d) it is observed that the proposed controller provides better performance than the conventional controller.

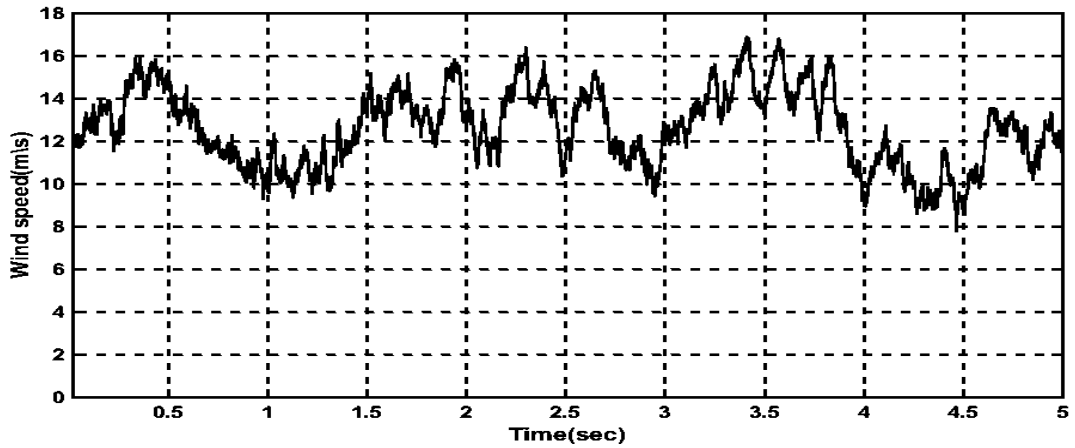

(a)

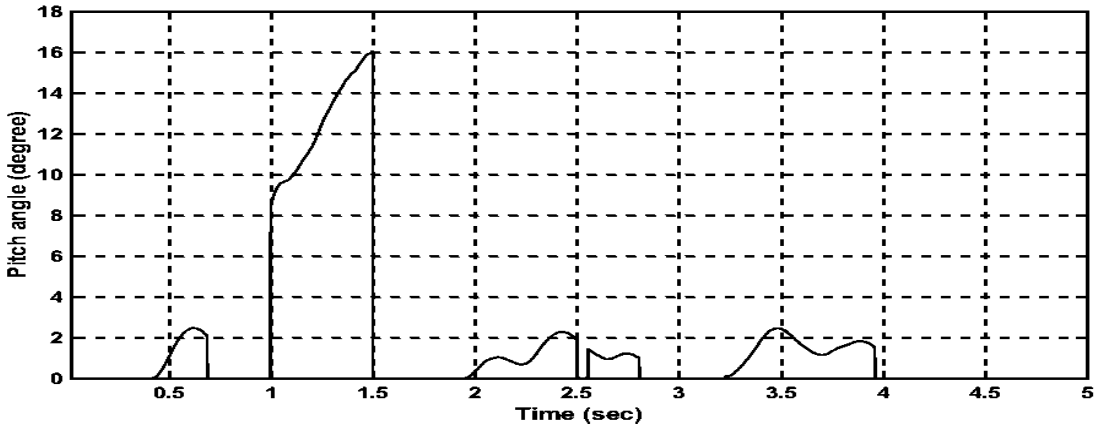

(b)

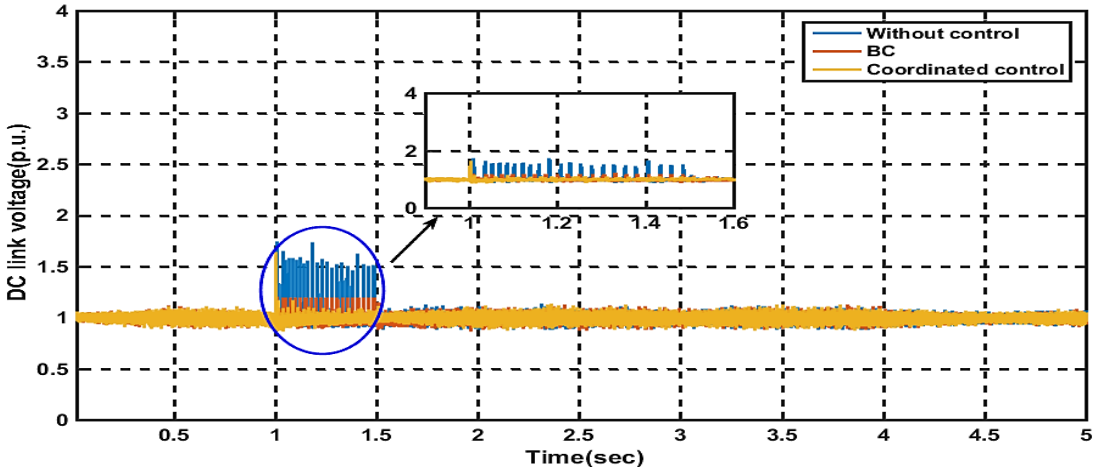

(c)

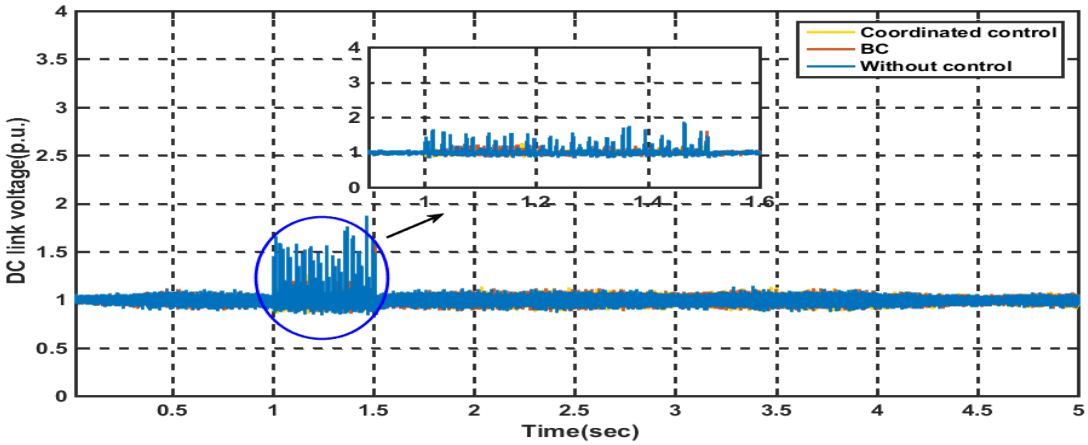

(d)

Fig.5.9. Simulation result for (a) Variable wind speed (b) Pitch angle (c) DC link voltage for symmetrical fault (d) DC link voltage for asymmetrical fault

5.3.2.4. Robustness of the proposed controller

The proposed controller performance is verified under different scenarios for step wind speed profile. Fig.5.10 compares voltage of the DC link with the braking chopper if the fault detection delays for 100 ms. Fig. 5.11 gives the simulated DC link voltage during the starting time of the fault is shifted to one quarter or half of a cycle moment after the original one happened. The voltage profiles remain same. It shows that the proposed method is insensitive to the fault timing. Concerning the variation of PMSG stator resistance and inductance (+20%), the simulation results are shown in Fig.5.12, where it is found that the system response with coordination controller remains remarkably insensible to the variation of the stator inductance.

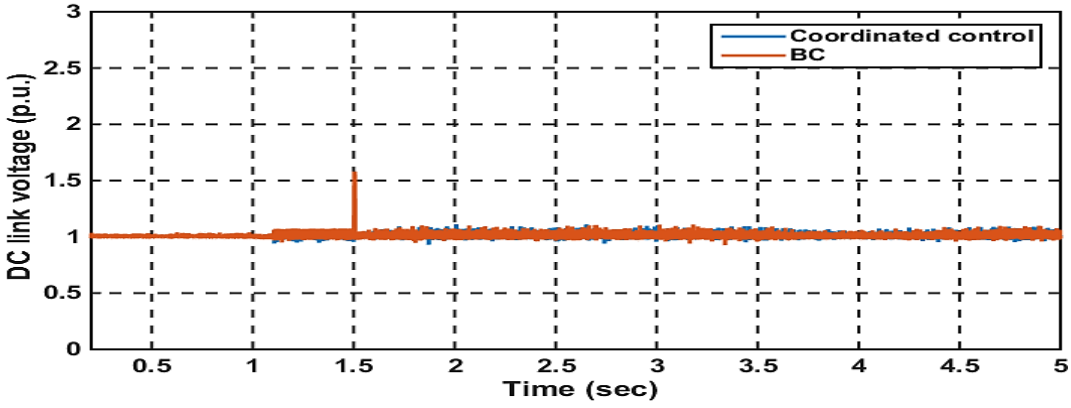

Fig.5.10. DC link voltage for fault detection delay for 0.1s

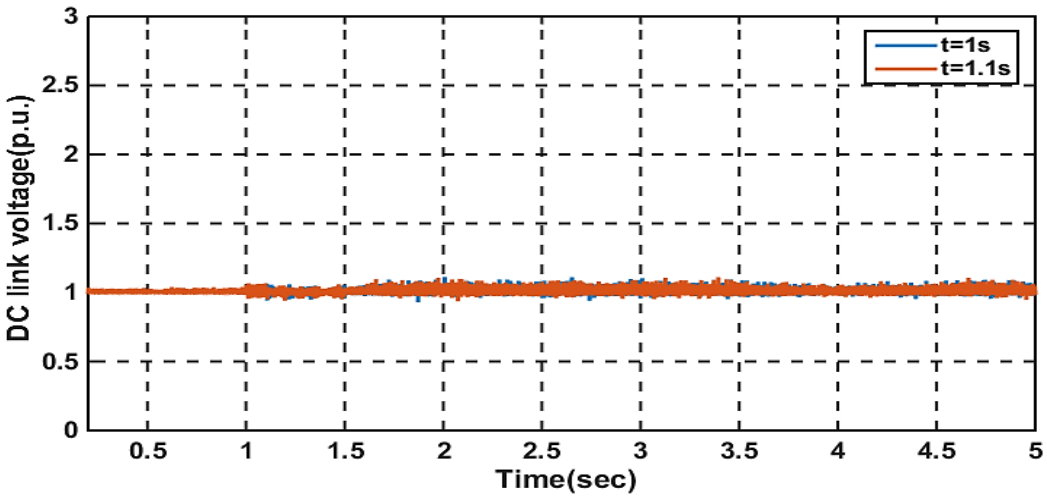

Fig.5.11. DC link voltage for different starting time of fault

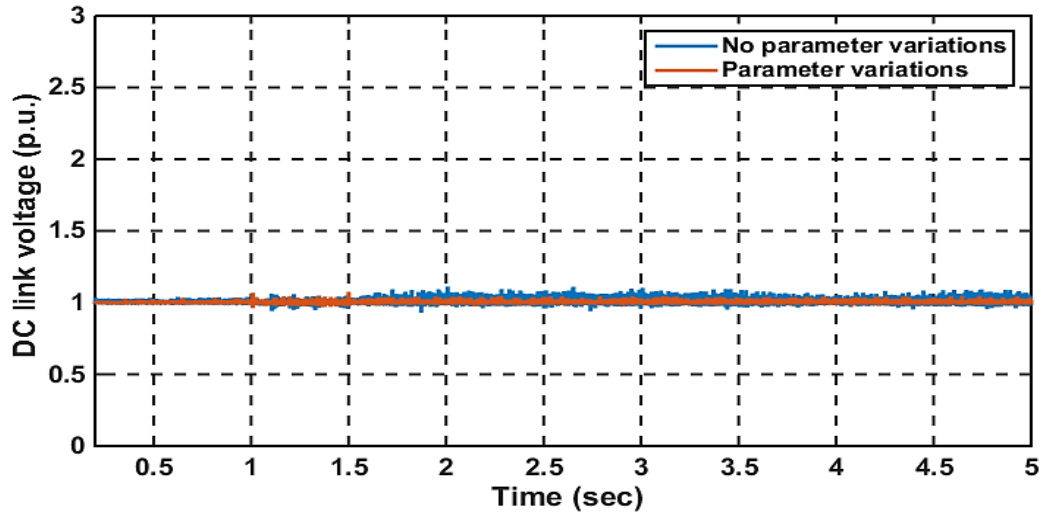

Fig.5.12. DC link voltage for different values of stator resistance and inductance

5.3.3. DC Link Voltage Control and Reactive Power Support with Coordinated Control

For better improvement, another approach has been taken to enhance the fault ride through performance. The approach is combined on flux weakening controller, pitch angle controller, reactive power support from GSC and STATCOM. Controller performance is verified for real wind speed profile under symmetrical and asymmetrical grid fault.

5.3.3.1. Under Symmetrical Faults

At t = 1s, a three line to ground fault is applied on the transmission line as shown in Fig. 5.13(a). The fault duration is 0.15s. As shown in Fig.5.13 (a), the grid voltage falls from 100% to 35%. The DC-link capacitor voltage increases to almost 1.5 times of its nominal value and is shown in Fig.5.13 (b). It is beyond the permissible limit. The DC link voltage is kept within limit under symmetrical and asymmetrical fault by using the proposed coordinated control. The controller can inject reactive power to enable the grid supporting services during the fault. Grid voltage is improved from 35% to 90% as shown in Fig.5.13 (a). The transient behaviours of the grid real power and generator speed are shown in Fig.5.13(c) and (d).

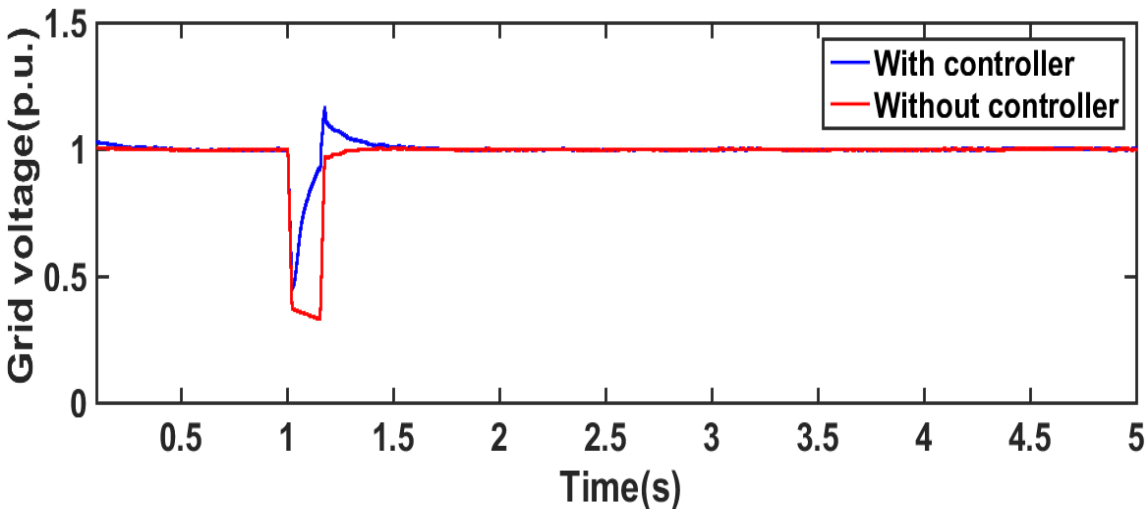

(a)

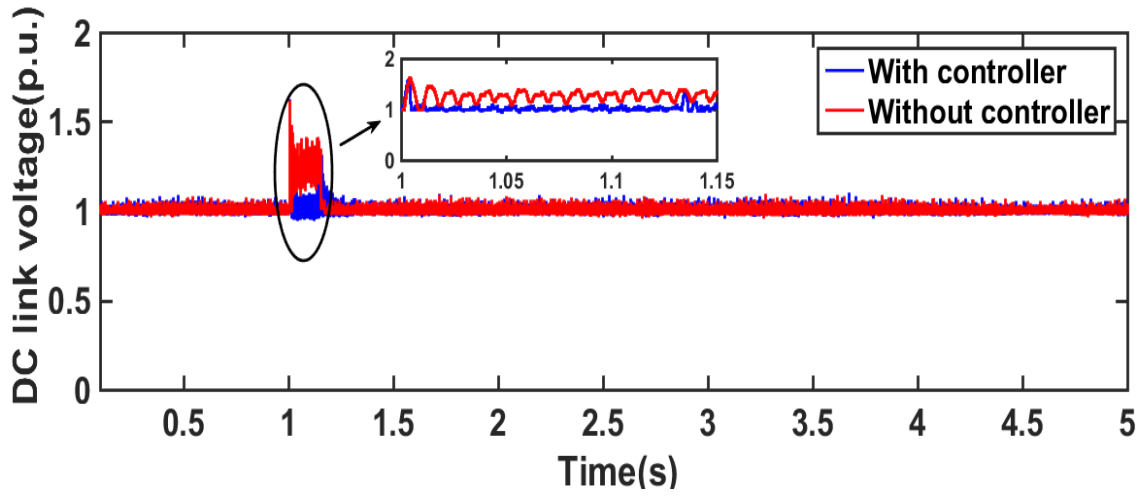

(b)

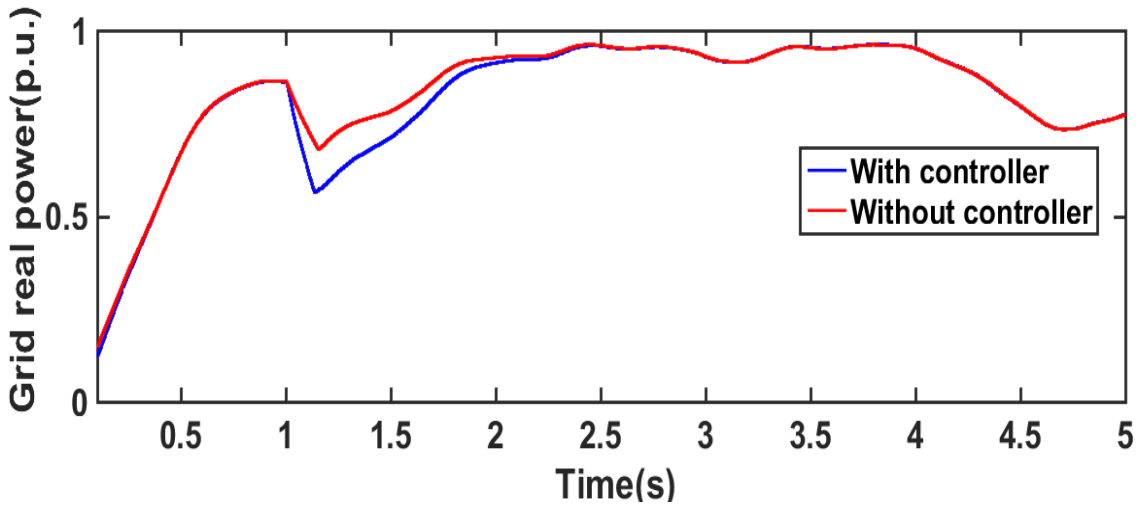

(c)

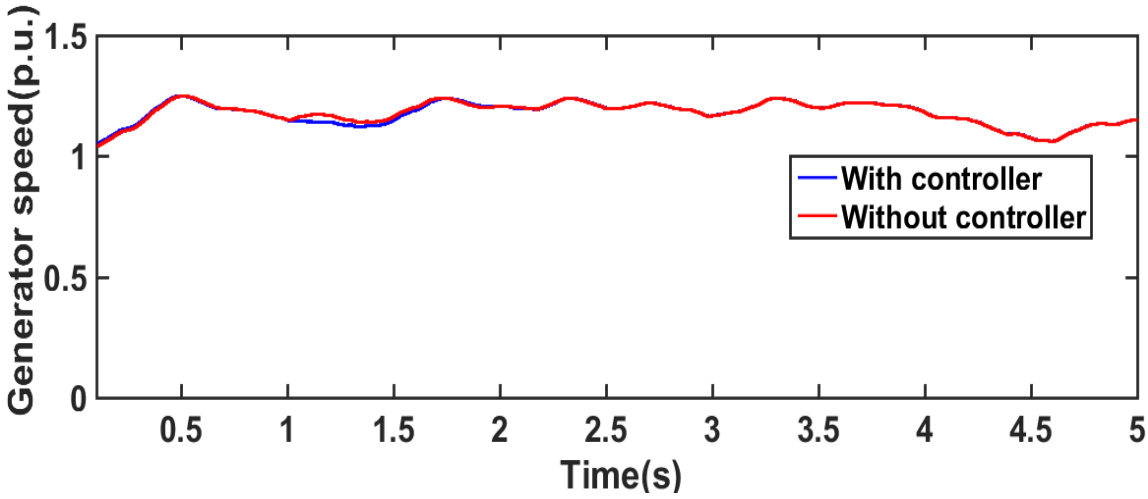

(d)

Fig.5.13. Simulation result for symmetrical fault (a) Grid voltage (b) Grid real power (c) DC link voltage (d) Generator speed

5.3.3.2. Under Asymmetrical Faults

At t = 1s, a three line to ground fault is applied on the transmission line as shown in Fig. 4.45(a). The fault duration is 0.15s. As shown in Fig.5.14(a), the grid voltage falls from 100% to 55 %. The DC-link capacitor voltage increases to almost 1.53 times of its nominal value and is shown in Fig.5.14(b). It is beyond the permissible limit. The DC link voltage is kept within limit under symmetrical and asymmetrical fault by using the proposed coordinated control. The controller can inject reactive power to enable the grid

supporting services during the fault. Grid voltage is improved from 35% to 90% as shown in Fig.5.14 (a). The transient behaviours of the grid real power and generator speed are shown in Fig.5.14(c) and (d).

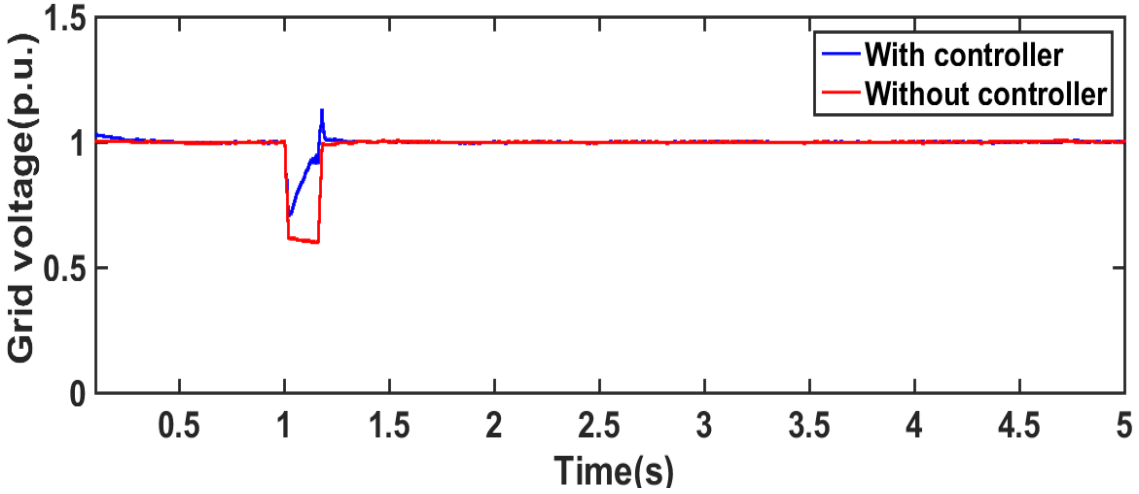

(a)

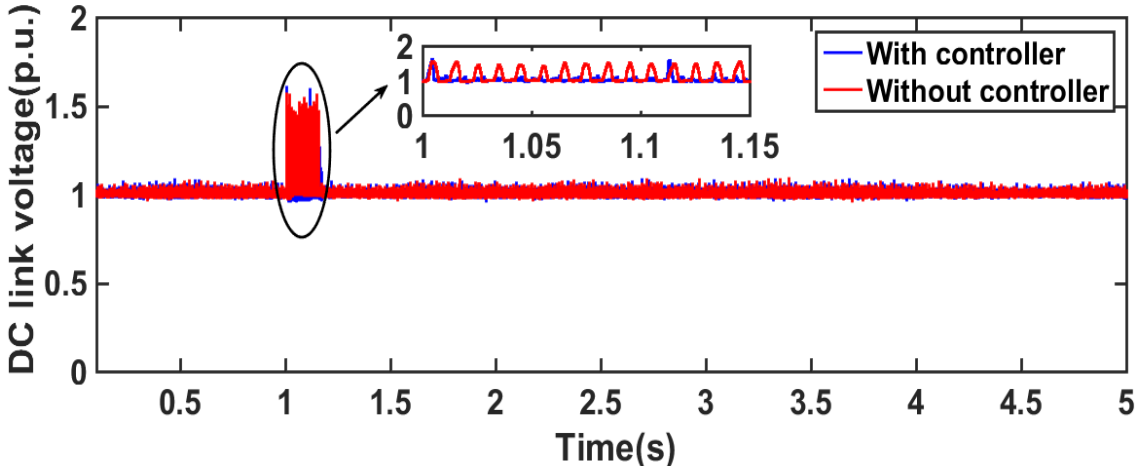

(b)

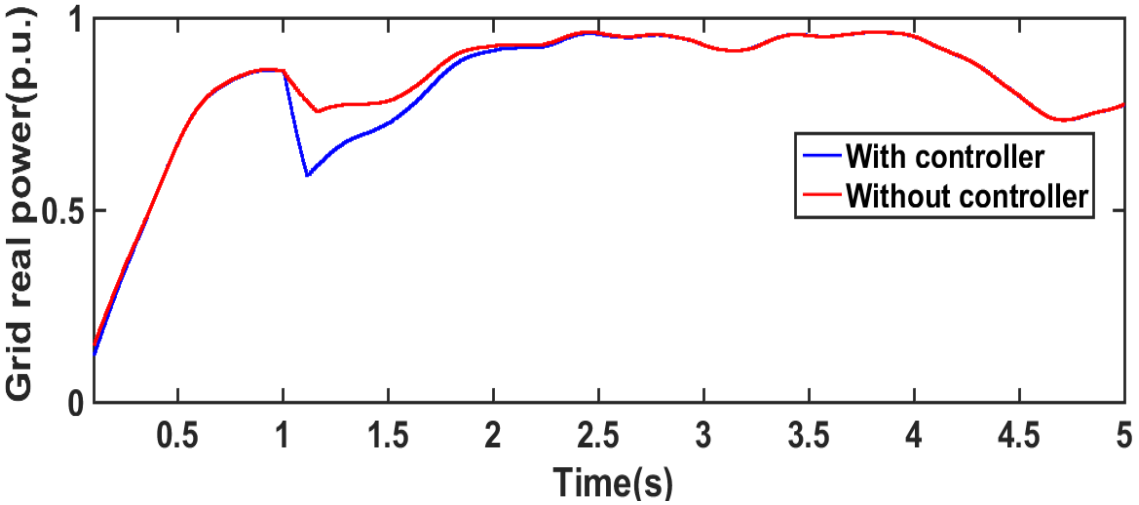

(c)

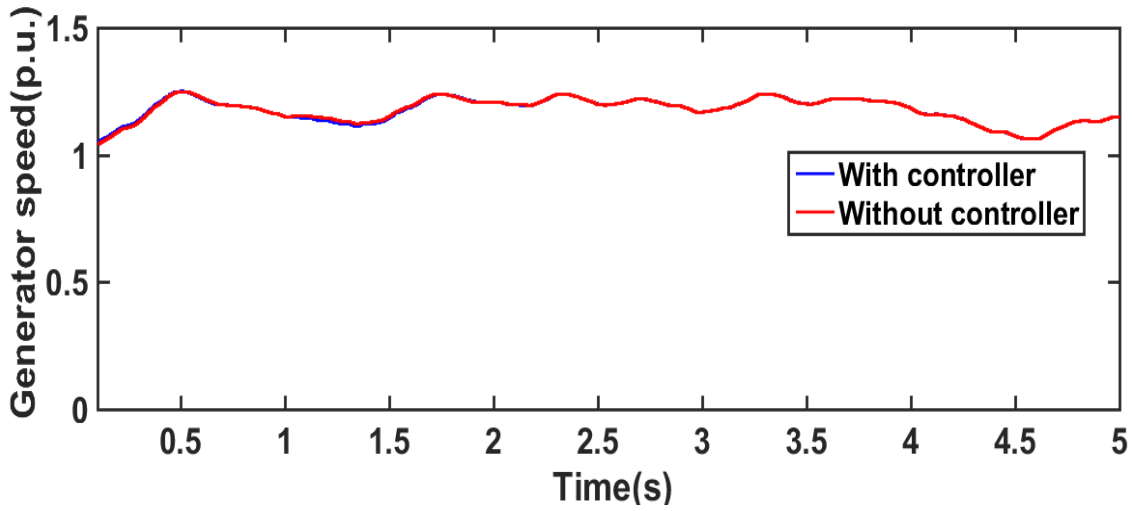

(d)

Fig.5.14. Simulation result for asymmetrical fault (a) Grid voltage (b) Grid real power (c) DC link voltage (d) Generator speed

5.4. LVRT with Fuzzy Logic based Coordination Control

Different from previous PI controller based coordinated controller, a Fuzzy Logic (FL) based coordinated controller [10]- [12] is developed for LVRT enhancement of PMSG based WECS during symmetrical and asymmetrical grid fault. This coordinated control consists of a pitch angle control, a flux weakening control and a reactive power injection by GSC. For the pitch angle controller and flux weakening controller, the PI controller block discussed in previous section is replaced with FL. And for the reactive power support, the FL controller is developed in GSC side to improve grid voltage profile during grid disturbances.

5.4.1. Pitch Angle Control

The control diagram of pitch angle with switching logic is shown in Fig.5.15. The switching logic is operated between normal mode and FRT mode [13]. In normal mode, the operation is based on rotor speed. The normal mode is activated when the wind speed is greater than the rated wind speed. And in FRT mode the pitch angle is operated based on grid voltage. If the grid voltage drops the reference is changed and it is regulated by

grid voltage variation, V_{PCC} instead of the rotor speed variation. The measured DC link capacitor voltage is compared with the reference DC voltage value to get the V_{DC_error}. This error signal and the rate of change of error ($V_{DC\_error\_rate}$) are given as the inputs of a FL block. Three Fuzzy sets are chosen here to adapt these numerical variables into linguistic variables: big, medium and small.

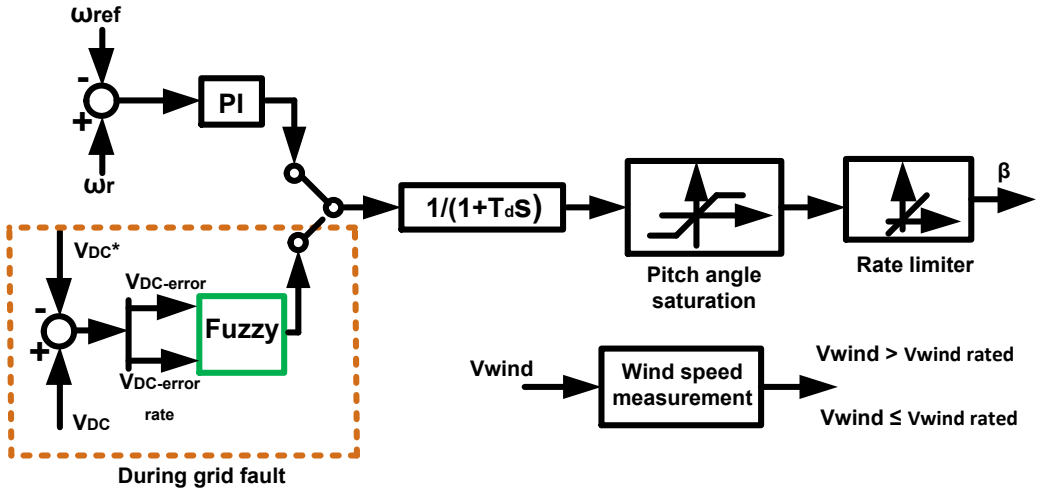

(a)

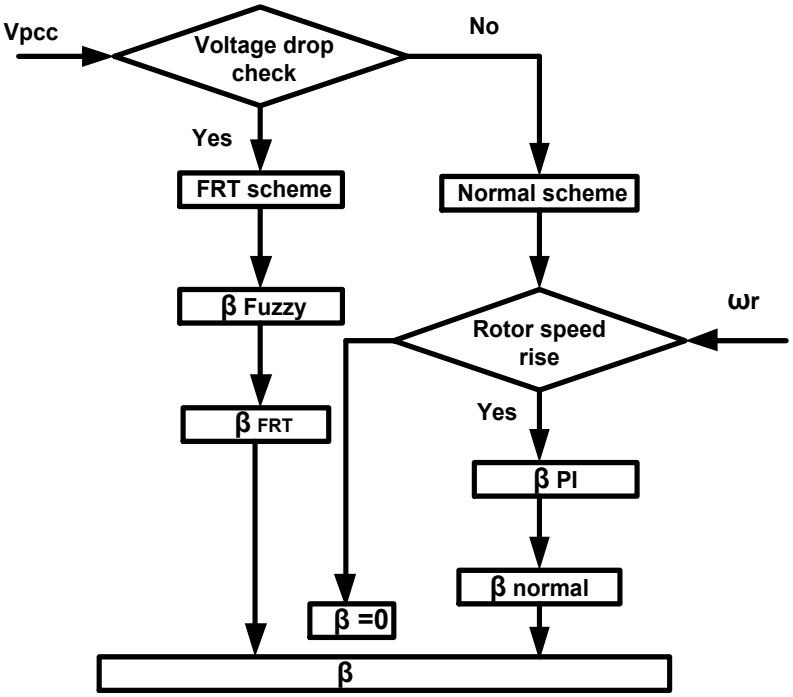

(b)

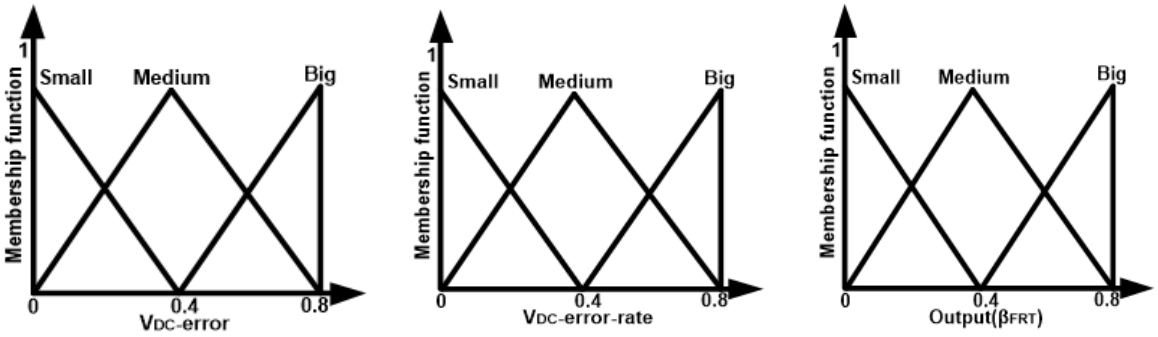

(c)

Fig.5.15. Pitch angle control system a) Block diagram b) Flow chart c) Normalized membership functions

5.4.2. Flux Weakening Control Using Fuzzy Logic Controller

Flux weakening controller [14] is applied in the machine side to generate the negative α axis current. The DC link voltage limits the converter output voltage. So, this method is enabling to utilize DC link voltage by using the capability of current control. The control method is illustrated in Fig.5.16. The difference of converter output voltage and the current controller output is used to produce the $V_{d\ \text{error}}$. The error signal and the rate of change of error are passed through the FL controller. Three fuzzy sets are chosen, and their ranges are from -0.5 to -200. The voltage difference of $\sqrt{1.5}\,V_{DC}$ and the magnitude of voltage references in *dq* coordinate V_d* and V_q* is given to the FL input. The output of FL is I_{dref}. The *q*-axis reference current is obtained based on I_{dref}. Where I_q* is the *q* axis reference saturation current, the I_{dref} is the output of the flux-weakening controller. The current output of the controller is limited between - I_{dqmax} and 0. Then both *d-q* components of stator current are transferred into *a-β* coordinate to generate required current for PR controller.

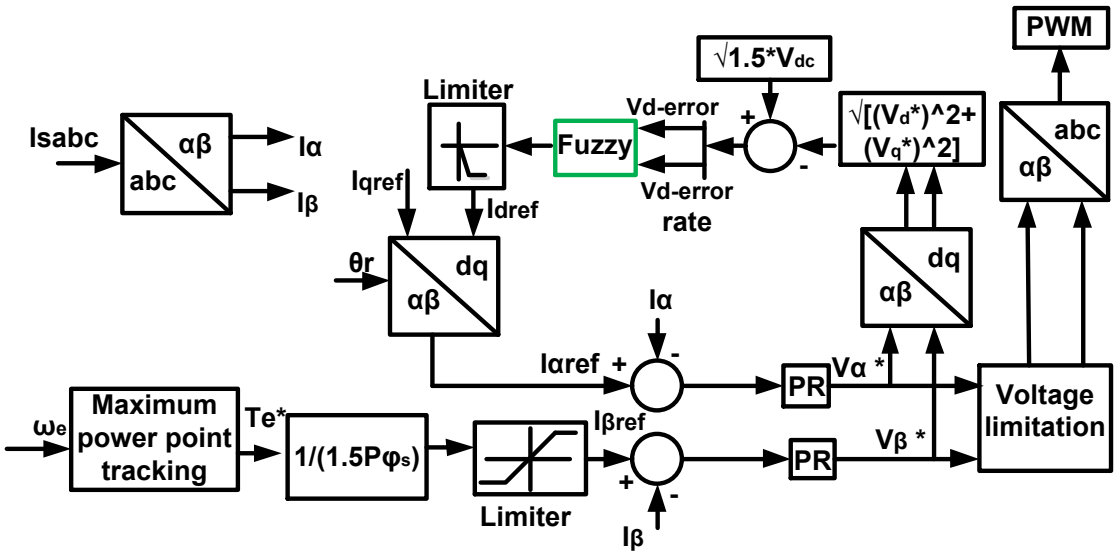

(a)

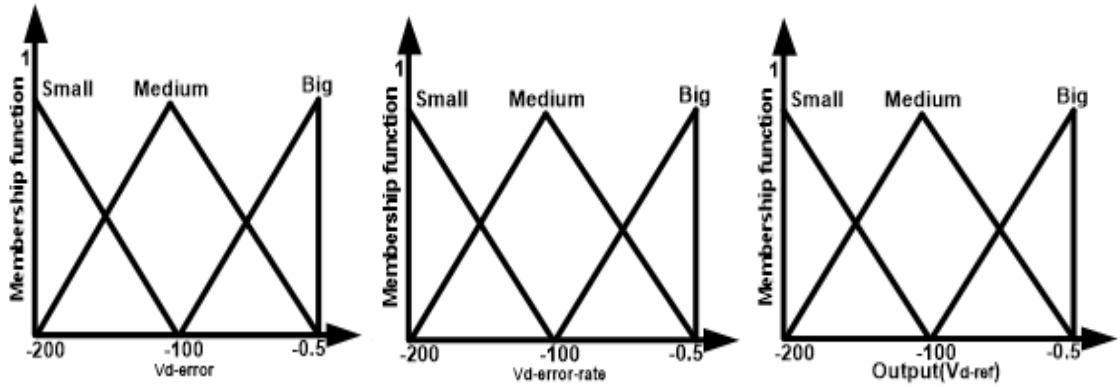

(b)

Fig.5.16. Flux weakening control a) Block diagram b) Normalized membership functions

5.4.3. Reactive Power Control

This controller is developed in the grid side converter. For normal operation, I_{qref}=0. But during grid fault it can inject the reactive power to improve the grid voltage profile. The controller block diagram is shown in Fig.5.17. The common coupling voltage is measured, V_{PCC}. Then it is subtracted from reference value, V_{PCC}* to get the error signal, V_{PCC}_error.

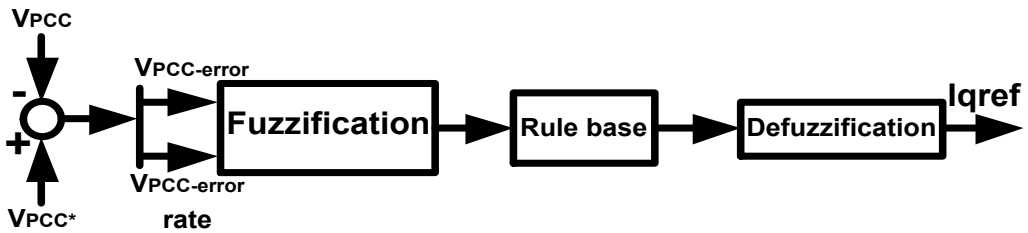

(a)

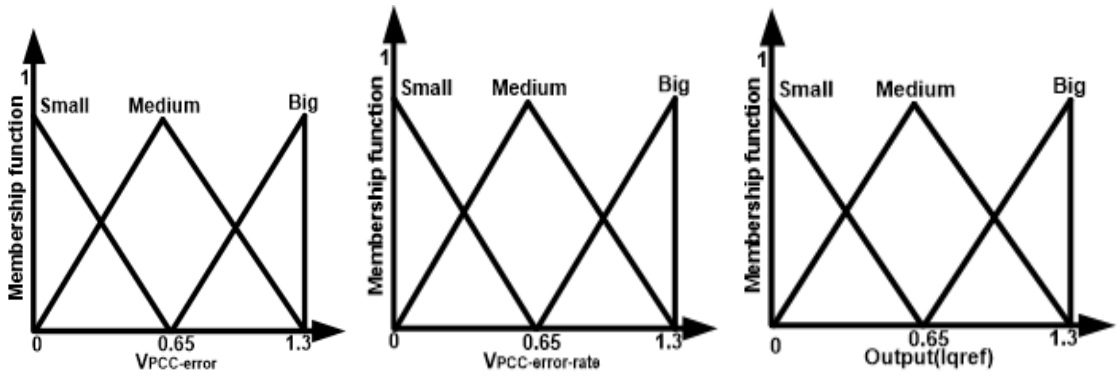

(b)

Fig.5.17. Flux weakening control a) Block diagram b) Normalized membership functions

The rate of change of error and the error signal are passed to the inputs of a FL block which is presented in Fig. 5.17. Fuzzification, rule base and de-fuzzification are three steps to get the required reference signal. Three Fuzzy sets are chosen here to adapt these numerical variables into linguistic variables: big, medium and small and their ranges are from 0 to 1.3.

5.4.4. Simulation Results with the Fuzzy Logic Based Coordination Control

Simulation is done in MATLAB/SIMULINK environment for 1.5 MW PMSG based wind turbine. The simulation is run for 5 second. Time series simulation results are obtained for symmetrical and asymmetrical grid faults.

5.4.4.1. Under Symmetrical Faults

The profile of variable wind speed is presented in Fig.5.18(a). Rated wind speed is 12m/s and pitch angle remains zero until wind speed is equal or less than 12.1m/s. It increases to limit the output power and rotor speed according to wind speed variation. A three line to ground fault is occurred at 1s. The fault duration is 0.2s. During the fault period, the grid voltage is decreased from 1 p.u. to 0.35 p.u. As the power imbalance occurs voltage of the DC link capacitor is increased. Without any LVRT control, the voltage is beyond its limit. It is observed from Fig.5.18(c) that the DC link over voltage is minimized.

Moreover, the voltage transients as well as fluctuations are also less for the proposed LVRT control.

Generator speed and grid real power in this period are shown in Fig.5.18(d)-Fig. 5.18(e). According to Fig. 5.18(f) without LVRT controller the reactive power injection was 0.05 p.u. As soon as the proposed FL based coordinated control applied the reactive power injection is increased to 0.16 p.u. As per Fig. 5.18(g) the grid voltage profile before LVRT control was 0.32 p.u. during fault period. While it has increased to 0.49 p.u. after fuzzy coordinated control applied to the system.

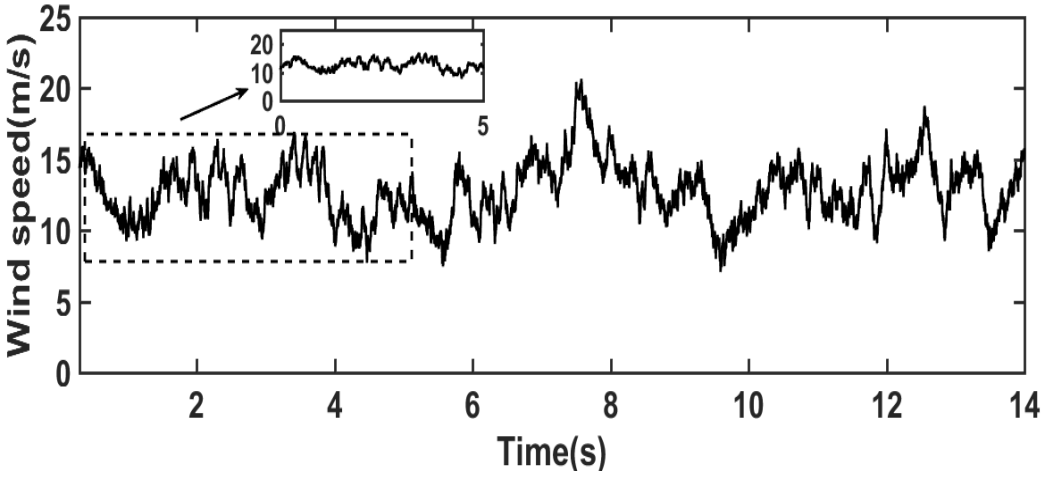

(a)

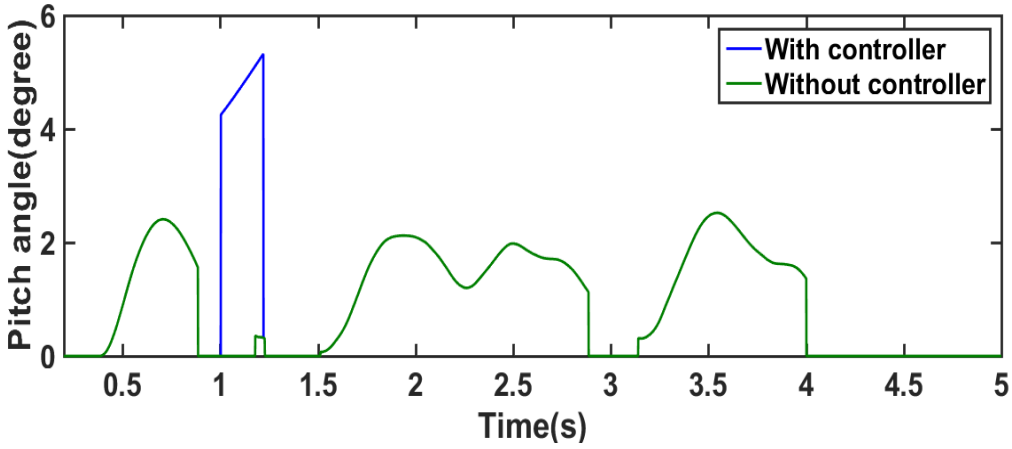

(b)

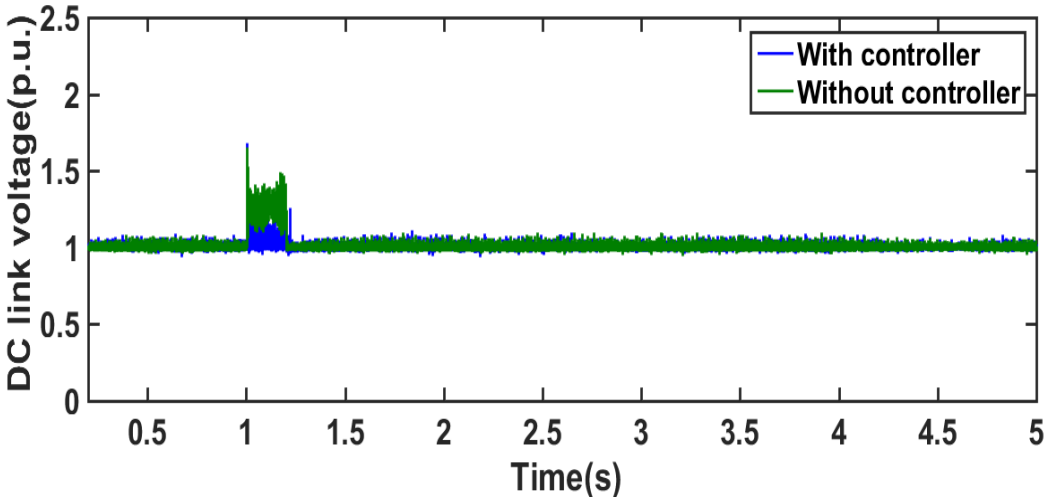
DC link voltage(p.u.)
Time(s)
With controller
Without controller

(c)

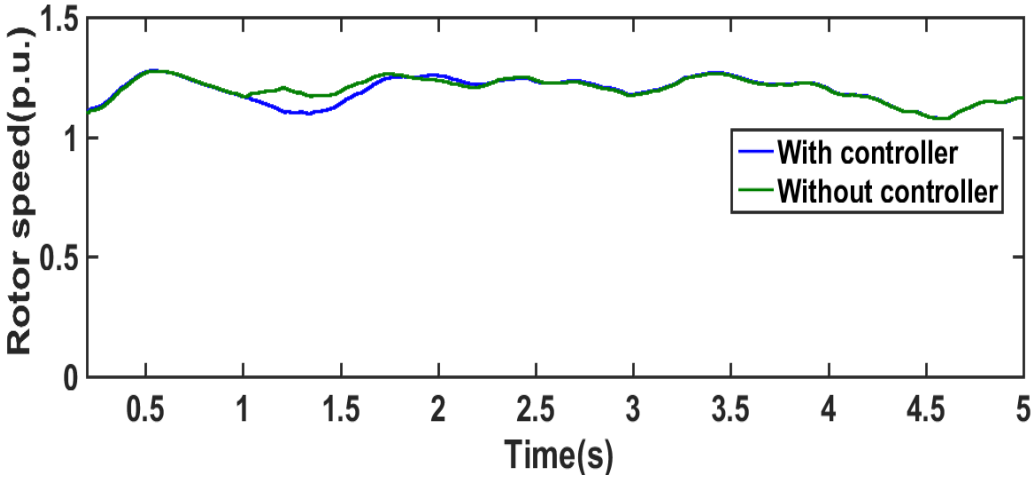
Rotor speed(p.u.)
Time(s)
With controller
Without controller

(d)

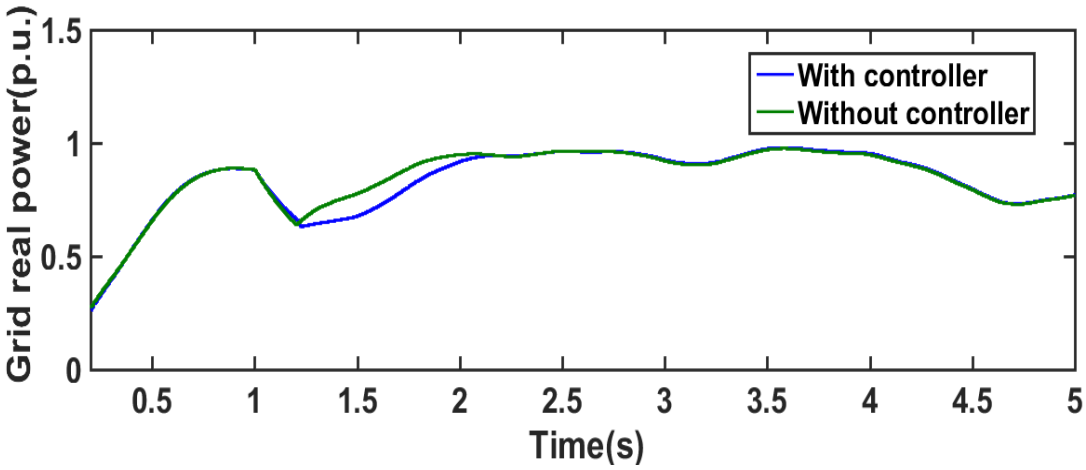
Grid real power(p.u.)
Time(s)
With controller
Without controller

(e)

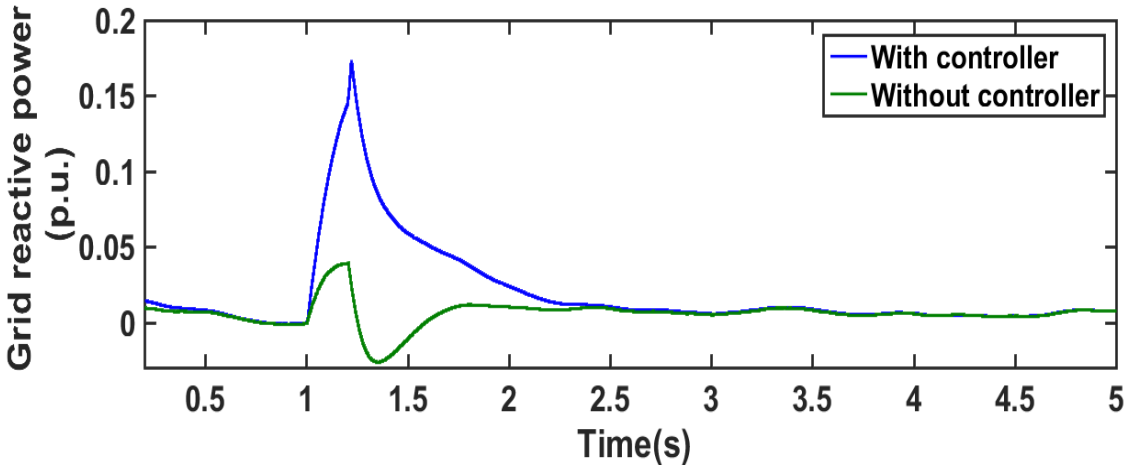

(f)

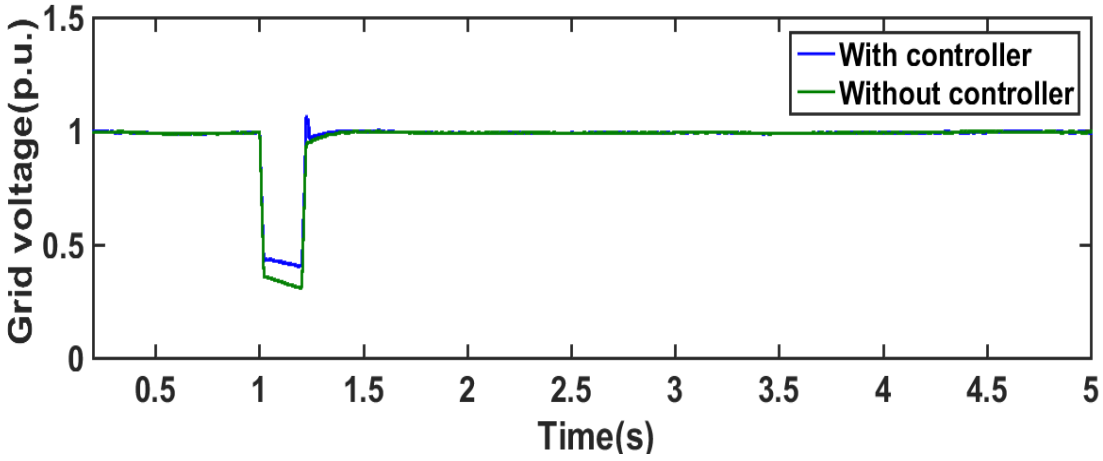

(g)

Fig.5.18. Simulation result for symmetrical fault a) Variable wind speed b) Pitch angle c) DC link voltage d) Generator speed e) Grid real power f) Grid reactive power g) Grid voltage

5.4.4.2. Under Asymmetrical Faults

A double line to ground fault is occurred at line at 1s. The fault is cleared at 1.2s. A medium dip is occurred. So, the grid voltage is decreased from 1 p.u. to 0.6 p.u. DC link voltage of capacitor is increased from 1p.u. to 1.6 p.u. without LVRT control as shown in Fig.5.19(c). It is beyond the acceptable limit. From Fig.5.19(b) It is found that the pitch angle becomes zero during fault period without LVRT control but it is increased to 5.7 degree to limit DC link voltage with proposed control. Referring to Fig.5.19(c) the

fluctuation of DC link voltage is minimized as well as it is well regulated with the proposed fuzzy coordinated control. Fig.5.19(d)-Fig.5.19(e) illustrated the scenario of generator speed and grid real power in the fault period without LVRT control and with proposed control. As per Fig. 5.19(f) without LVRT controller the reactive power injection was 0.045 p.u. The reactive power injection is enhanced to 0.22 p.u as soon as the proposed fuzzy coordinated control is applied. According to Fig. 5.19(g) the grid voltage profile before LVRT control was 0.53 p.u. during fault period. While it has increased to 0.69 p.u. after the proposed coordinated control is applied to the grid connected WECS.

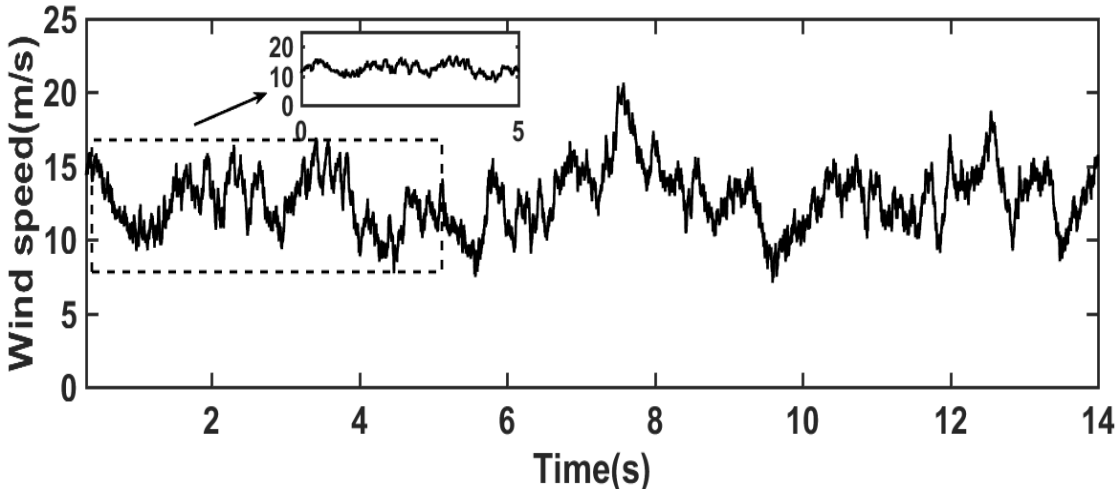

(a)

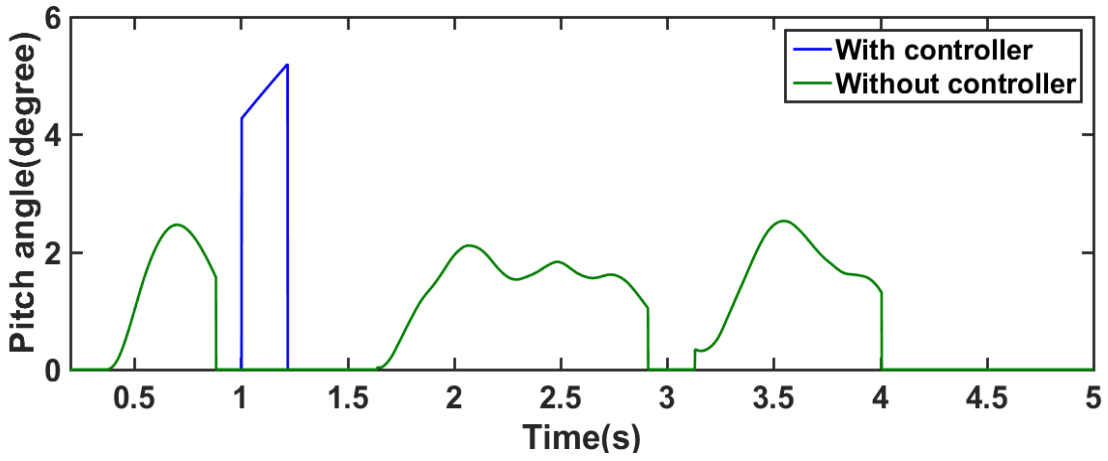

(b)

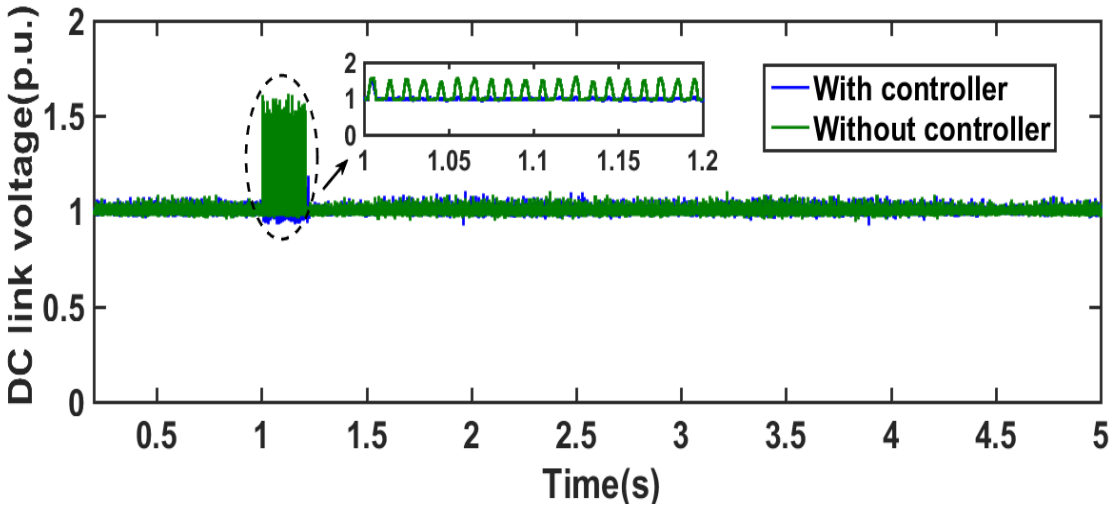
DC link voltage(p.u.)
Time(s)
With controller
Without controller

(c)

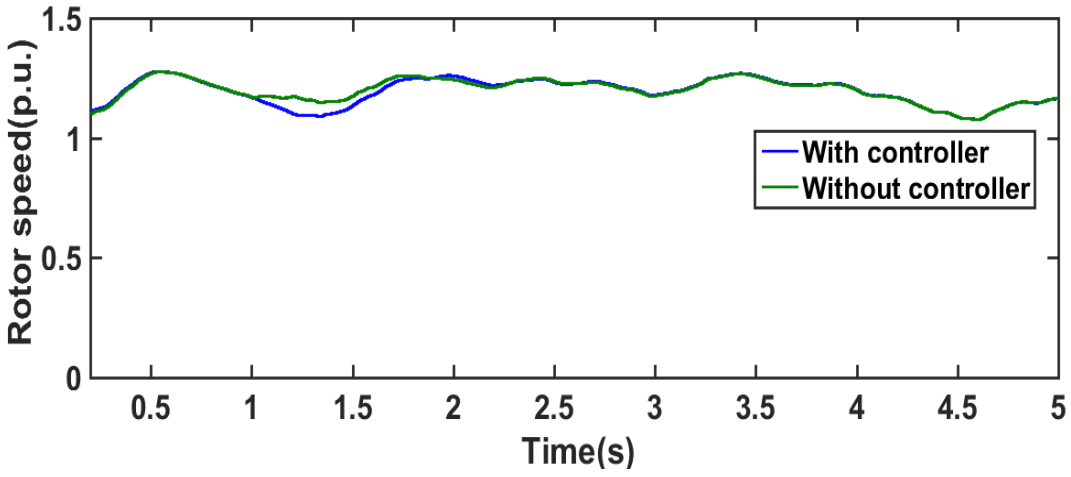
Rotor speed(p.u.)
Time(s)
With controller
Without controller

(d)

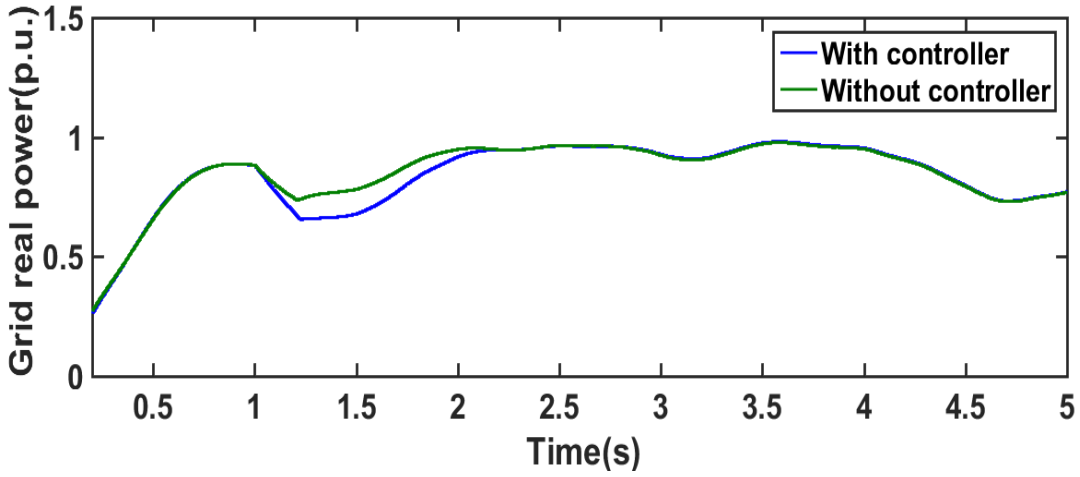
Grid real power(p.u.)
Time(s)
With controller
Without controller

(e)

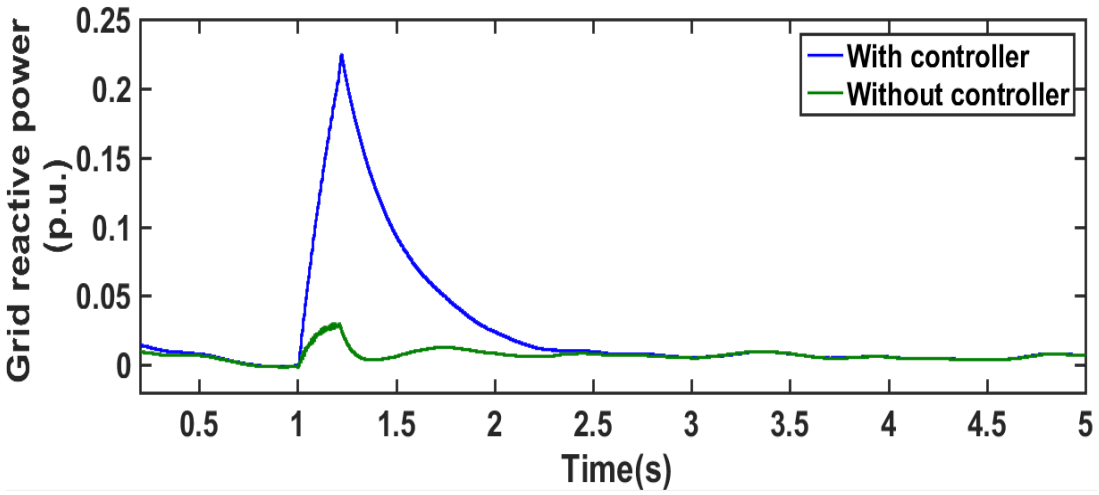

(f)

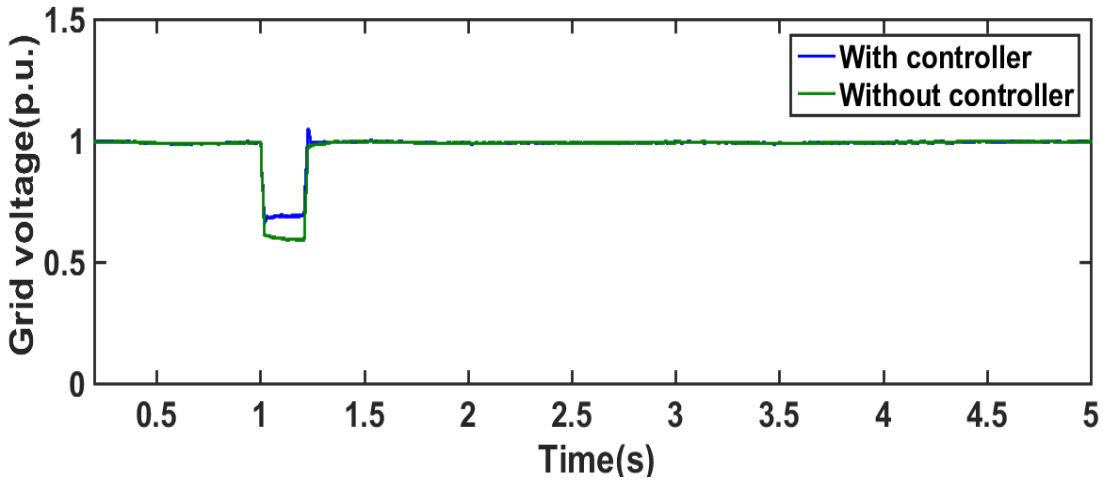

(g)

Fig.5.19. Simulation result for asymmetrical fault a) Variable wind speed b) Pitch angle c) DC link voltage d) Generator speed e) Grid real power f) Grid reactive power g) Grid voltage

5.5. Summary

A PI based coordinated control method is proposed in this chapter to improve the LVRT performance of a variable speed PMSG based grid connected WECS. Then the proposed approach is verified under different scenarios during the symmetrical and asymmetrical grid faults. From the simulation results, it has been demonstrated that the proposed method can enhance the LVRT performance by injecting enough reactive power to

support the grid voltage during the grid faults with the help of the GSC and the STATCOM. Due to the simplicity and effectiveness of the proposed control, it can be a better choice compared to the conventional control with the BC during the LVRT.

Next, a Fuzzy Logic based coordinated control method is also proposed to improve the LVRT performance of a grid connected WECS. The proposed method is tested for a 1.5 MW wind turbine for symmetrical and asymmetrical grid faults. From the simulation results, it is found that the proposed coordinated control method can limit the DC-link overvoltage as well as can inject the reactive power for supporting the grid voltage under grid faults.

REFERENCES

[1] H. M. Yassin, H. H. Hanafy, and M. M. Hallouda, "Enhancement of low-voltage ride through capability of permanent magnet synchronous generator-based wind turbines using interval type-2 fuzzy control," *IET Renewable Power Generation*, vol. 10, pp. 339-348, 2016.

[2] Khagendra Thapa, Jinho Kim and Yong Cheol Kang, "Coordinated control for low voltage ride-through of a PMSG-based wind power plant", *Journal of International Council on Electrical Engineering*, 6:1, 242-251,2016

[3] V. F. Corasaniti, M. B. Barbieri, P. L. Arnera, and M. I. Valla, "Hybrid power filter to enhance power quality in a medium-voltage distribution network," *IEEE Transactions on Industrial Electronics*, vol. 56, pp. 2885-2893, 2009.

[4] M. Kesler and E. Ozdemir, "Synchronous-reference-frame-based control method for UPQC under unbalanced and distorted load conditions," *IEEE Transactions on Industrial Electronics*, vol. 58, pp. 3967-3975,2011.

[5] Sushree Sangita Patnaik and Anup Kumar Panda,"Real-time performance analysis and comparison of various control schemes for particle swarm optimization-based shunt active power filters'', *International journal of Electrical Power and Energy Systems*, 52 (2013), pp. 185–197

[6] P. Dey, M. Datta, N. Fernando, "A coordinated control of grid connected PMSG based wind energy conversion system under grid faults", *3rd IEEE International Future Energy Electronics Conference and ECCE Asia (IFEEC 2017-ECCE Asia)*, pp. 597-602, 3−7 June 2017.

[7] H. Gaztanaga, I. Etxeberria-Otadui, D. Ocnasu, and S. Bacha, "Real-time analysis of the transient response improvement of fixed-speed wind farms by using a reduced-scale STATCOM prototype," *IEEE Transactions on Power Syst*em, vol. 22, no. 2, pp. 658–666, May 2007.

[8] Wang Li, Chia-Tien Hsiung, "Dynamic stability improvement of an integrated grid-connected offshore wind farm and marine-current farm using a STATCOM", *IEEE Transactions on Power Systems*, vol. 26, no. 2, pp. 690-698, 2011.

[9] B. Singh, "Introduction to FACTS controllers in wind power farms: a technological review," *International Journal of Renewable Energy Research*., vol. 2, no. 2, pp. 166-212, 2012

[10] S. Ahmad, F. M. Albatsh, S. Mekhilef, and H. Mokhlis, "Fuzzy based controller for dynamic Unified Power Flow Controller to enhance power transfer capability," *Energy Conversion and Management*, vol. 79, pp. 652-665, 2014.

[11] L. Jerbi, L. Krichen, and A. Ouali, "A fuzzy logic supervisor for active and reactive power control of a variable speed wind energy conversion system associated to a flywheel storage system," *Electric Power Systems Research*, vol. 79, no. 6, pp. 919–925, 2009

[12] G. Mokryani, P. Siano, A. Piccolo, and V. Calderaro, "A fuzzy logic controller to increase fault ride-through capability of variable speed wind turbines," *Applied Computational Intelligence and Soft Computing*, vol. 2012, p. 7, 2012.

[13] M. Q. Duong, F. Grimaccia, S. Leva, M. Mussetta, K. H. Le, "Improving transient stability in a grid-connected squirrel-cage induction generator wind turbine system using a fuzzy logic controller", *Energies*, vol. 8, no. 7, pp. 6328-6349, 2015.

[14] H. Wu, S. Wang, C. Gu, "Simplified fuzzy logic based flux weakening speed control of IPMSM drive", *2011 International Conference on Electrical Machines and Systems*, pp. 1-4, 2011.

CHAPTER SIX

FREQUENCY REGULATION BY THE GRID CONNECTED WECS UNDER NORMAL AND FAULT RECOVERY CONDITIONS

6.1. Introduction

Frequency regulation by using the grid connected WECS during usual load frequency deviations and the frequency deviations after a grid fault recovery is described in this chapter. The following two approaches such as the physical inertia-based control and the flux linkage control with a Superconducting Magnetic Energy Storage (SMES) system are proposed. Performance of the proposed controllers is validated by dynamic simulations under different scenarios.

6.2. Physical Inertia based Frequency Control

The primary frequency control strategy can be demonstrated combining the inertia support from wind turbine and the DC link capacitor as shown in Fig.5.1. The inertia of the system plays a vital role as it defines the sensitivity of frequency under unbalancing of power; when variations of load or generation appear in the system if the system inertia is low, the rate of frequency change is high. So, storing or releasing kinetic energy can be considered as a part of primary control [1], [2].

6.2.1. Physical Inertia Support from the Wind Turbine-Generator Shaft

The inertial control scheme is used to generate incremental of active power of wind turbine during frequency decline occurs. The electromagnetic torque of wind turbine is given by:

$$T_{ref} = \frac{3}{2}\frac{P}{2}\varphi I_{\beta s} \qquad (6.1)$$

Where φ, P, $I_{\beta s}$ and T_{ref} are the magnetic flux ,the pole number, stator current in β coordinate and reference torque respectively.

Usually, the T_{ref} is obtained with MPPT. It corresponds with the output power based on power tracking curve [3], [4]. Consequently, during frequency disturbances the overall reference torque injected into the converter T_{ref} will be decreased by the maximum power point, which is working to bring back the system to the optimum curve of MPPT. When frequency deviation occurs, T_{ref} increases and rotor speed ω_r decreases. Moreover, based on the rate of change of frequency, deceleration occurs in the synchronous generator and the stored kinetic energy is released to the grid. As the generator rotational speed is directly related with the frequency, f_{sys}, so the decelerating torque is also proportional to the system frequency rate of change, df_{sys}/dt.

Based on this, for PMSGs inertial response, an additional torque term from equation (6.2) is used to generate the reference torque

$$\Delta T_H = K_H \frac{df_{sys}}{dt} \qquad (6.2)$$

Where K_H is a weighting constant.

By using equation (6.3) the electromagnetic torque reference (T_{ref}) is given as

$$T_{ref} = T(\omega_r) - \Delta T_H \qquad (6.3)$$

The frequency control block diagram for MSC is shown in Fig.6.1(a). The system frequency is measured by phase lock loop and it is passed through a derivative function block. A low pass filter is added to reduce the unwanted ripple. An inertial gain, K_H is tuned properly to get the desired response from the controller.

6.2.2. Synthetic Inertia Support From the DC Link Capacitor

During normal operation, significant amount of energy is stored by the DC-link capacitor. For aiding the inertial response at the time of frequency events some of the stored energy can be extracted [5]- [7].

The DC-link capacitor voltage is given by:

$$CV_{DC}\frac{dV_{DC}}{dt} = P_{Gen} - P_{Grid} \qquad (6.4)$$

Where V_{DC}, C, $P_{Gen,}$ and P_{Grid} are the DC voltage, DC capacitance, DC-link incoming power, and the outgoing power respectively.

For normal operation, DC link capacitor voltage is well regulated with the PI controller. But during frequency event, an auxiliary DC voltage controller is utilized in GSC to achieve the frequency control. The extra DC voltage reference is resolved by the frequency deviation, which is passed to a proportional controller as shown in Fig.6.1(b). The difference between measured frequency and nominal frequency is passed to a proportional gain which generates the If component. The proportional gain, G is tuned properly to obtain the better frequency response. The proposed frequency controller operation logic is shown in Fig.6.1(c). The auxiliary controller of DC voltage and inertia controller of wind turbine are initiated when the system frequency is beyond 49.8-50.2 Hz.

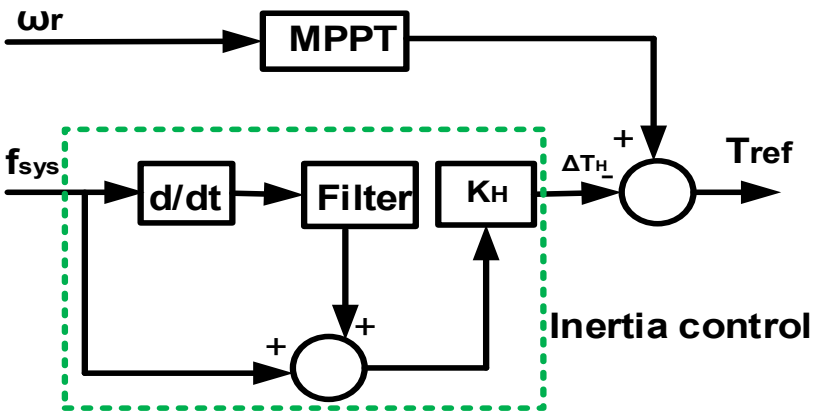

(a)

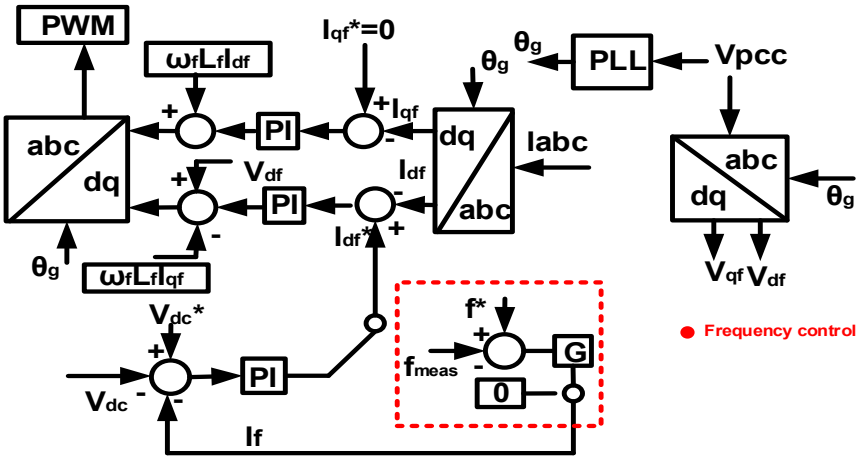

(b)

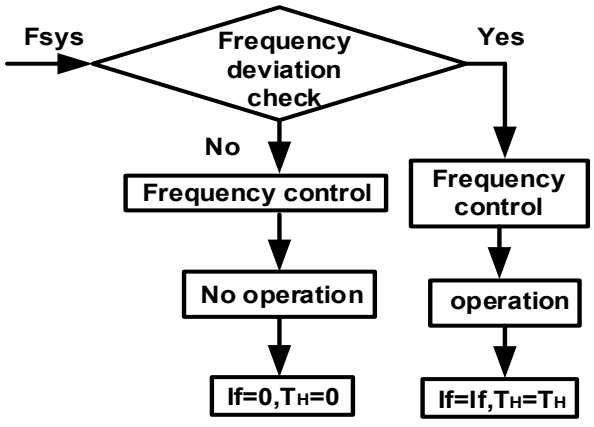

(c)

Fig.6.1. Frequency control a) Block diagram for MSC b) Block diagram for GSC c) Flow chart

6.3. Frequency Regulation via a Flux Linkage Control

The frequency deviation or frequency fluctuation can be improved by strengthening or weakening of PMSG flux during the disturbances. For normal operation reference of flux component is zero. But during disturbances the flux reference component can be either positive or negative during the frequency deviation or frequency fluctuation respectively [8]-[10]. The block diagram of proposed control method is shown in Fig.5.2.

The three phase stator currents are measured and converted into orthogonal α-β currents using the Clarke transformation. The difference between the real machine voltage and the controller output voltages (V_α^*, V_β^*) passes through a PI controller. The output of PI controller is limited by 0 to I_{dmax}. It generates the I_d reference current. Based on the I_d reference current, the I_q reference current is defined. The difference between maximum converter current, $I_{\max}$ and I_d reference current generates the I_q reference current. The generated I_d and I_q reference currents are transformed to α-β coordinate quantities to obtain the required positive or negative I_α reference current.

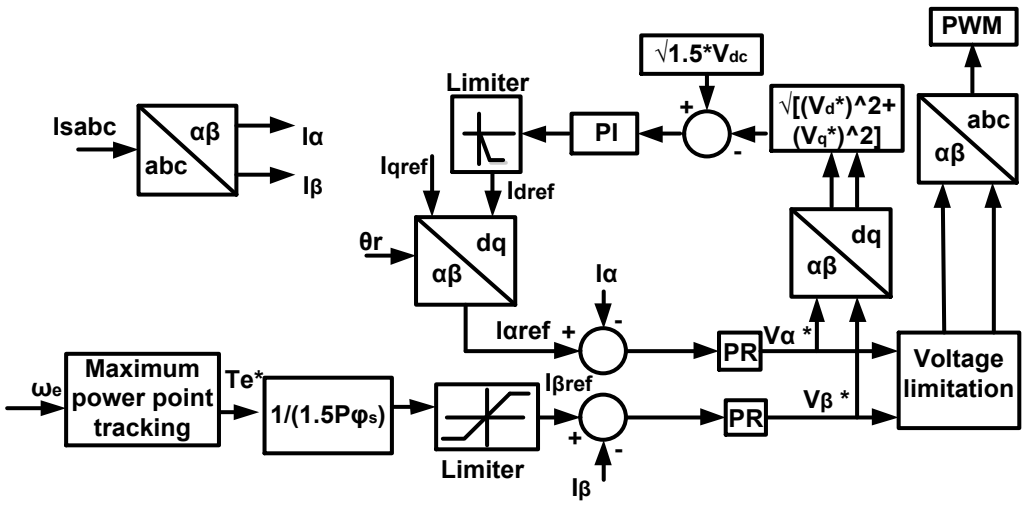

Fig.6.2. Flux strengthening control for MSC

6.4. Modelling and Control of Superconducting Magnetic Energy Storage (SMES) for Frequency Regulation

The SMES unit consists of a VSC and a DC-DC chopper. They are connected by a DC link capacitor [11]. Hysteresis current controller is used for generating the gate pulse for VSC and the DC-DC chopper is operated by the switching logic based on duty cycle [12], [13].

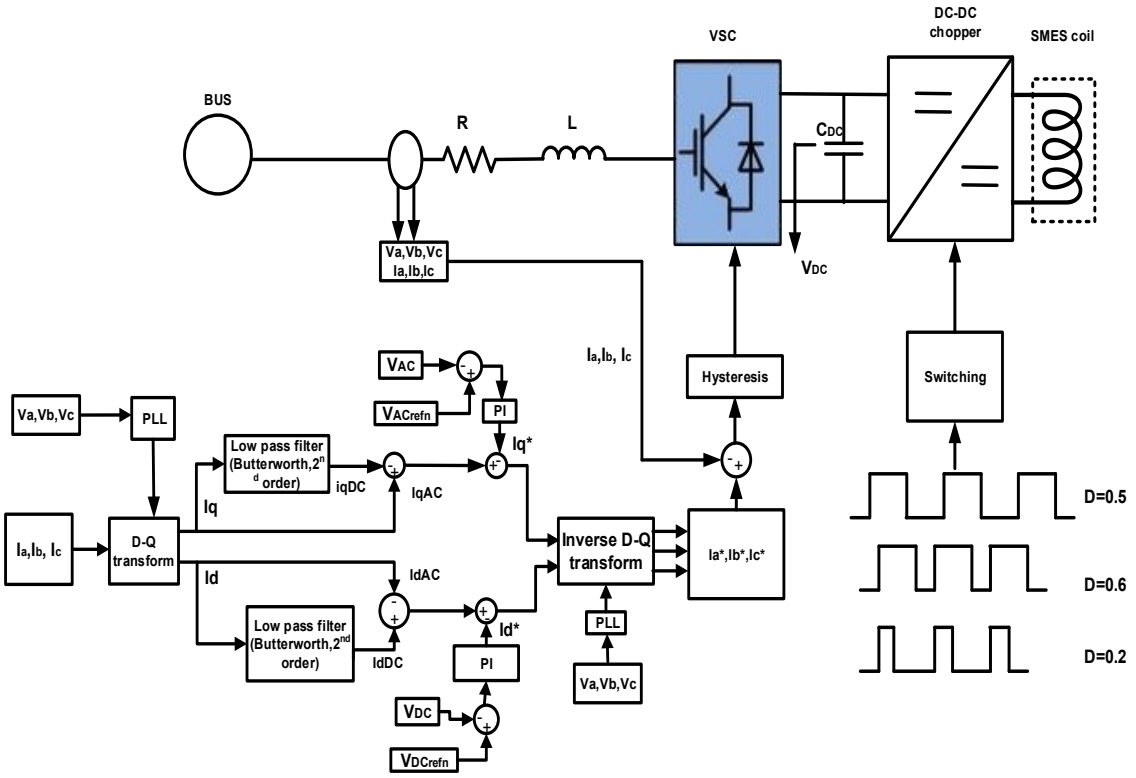

Fig.6.3. SMES unit configuration and the control scheme

Two voltage control loops are used to generate the reference current for VSC. One is the AC voltage control loop which generates the I_q reference current via PI controller and another one is DC voltage control loop which generates the I_d reference current via PI controller. Then the I_d and I_q currents are transformed into *abc* coordinates and generate the reference currents (I_{abc}*). The difference between measured three phase currents (I_{abc}) and the reference currents (I_{abc}*) are passed through a hysteresis band. The hysteresis band is then used for generating the gate pulses for voltage source converter. SMES coil operation depends on the value of the duty cycle [14]. When the value of duty cycle, *D* is

equal to 0.5, under normal operating condition the coil does not take any action. The value of duty cycle will be reduced within the range 0 to 0.5 when the grid power is reduced. The SMES coil stored energy will then transferred to the grid during the discharging period. Now the SMES coil will become energised when the duty cycle value is operated within the range 0.5 to 1.0. A diagram of the full control concept of SMES is provided in Fig.6.3.

6.5. Simulation Result and Analysis

Simulation studies are carried out for 1.5 MW direct drive PMSG wind turbine. The simulation time is for 5 second. Conventional pitch controllers are considered for smooth the PMSG output power. The proposed control algorithm is tested for wind turbine connected with single and multi-machine system. The SMES parameters and synchronous generator (SG) parameters are shown in Appendix C.

6.5.1. Performance evaluation when the WTG is connected to Single Machine System

Fig.6.4 represents the outline of single machine system. The configuration consists of a SG, a PMSG based WT and two local loads L1, L2 respectively. L1consists of fixed load as 1.2 MW and L2 as 1 MW which is considered as a dump load. The dump load is connected to the system via a circuit breaker.

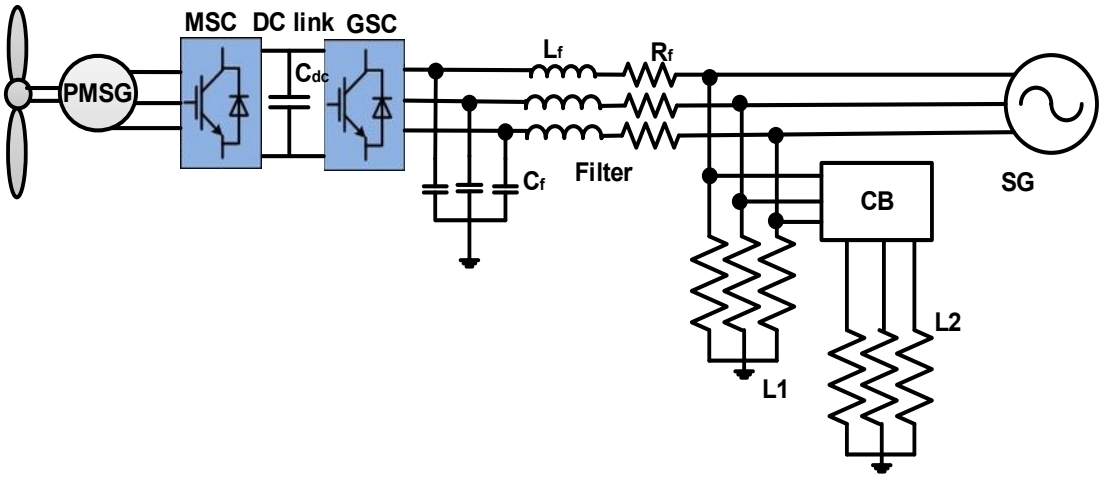

Fig.6.4. Outline of single machine system

6.5.1.1. Operation Under Constant Wind Speed

The constant wind speed profile is shown in Fig.6.5(a). The sudden load is increased in single machine power system where the dump load is switched on at t=3s. As the power imbalance occurs so the system frequency drops down from its nominal frequency. Four different types of simulations are done and compared with each other as shown in Fig.6.5 (b). The simulation is based on without any control, WT inertia control only, DC voltage control only and simultaneous WT inertia and DC control. From Fig.6.5 (b) it is observed that the three control strategies improved the frequency nadir. With DC inertia control the frequency is improved from 49.51Hz to 49.55 Hz and 49.51 Hz to 49.82 Hz with the WT inertia control. On the other hand, by using simultaneous control the frequency nadir is improved from 49.5 Hz to 49.85 Hz. It is also shown in Fig.6.5(c). The same pattern as system frequency is observed in DC link voltage as it provides inertia support to the system. The DC link voltage is presented in Fig.6.5 (d). More real power is transmitted to the load from PMSG as shown in Fig.6.5 (e).

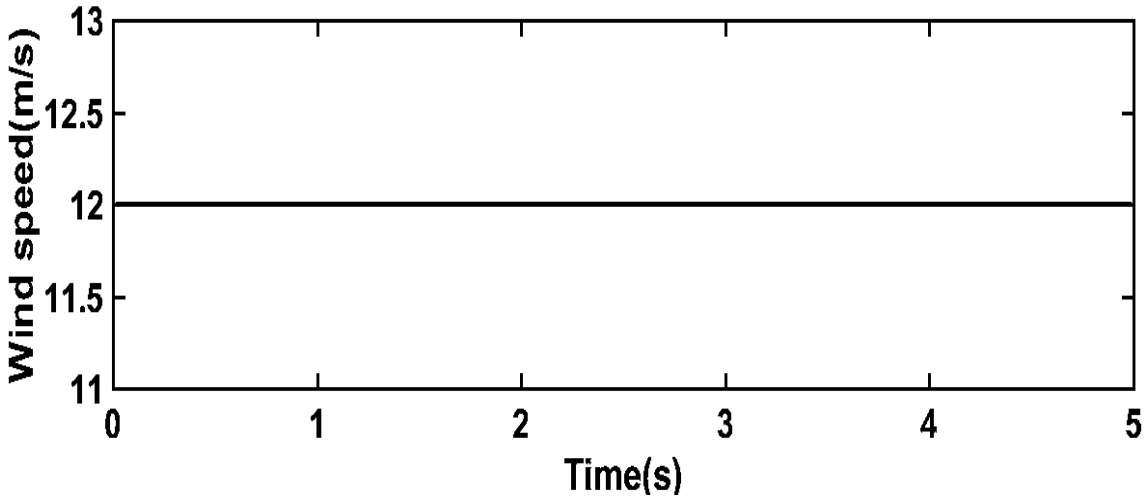

(a)

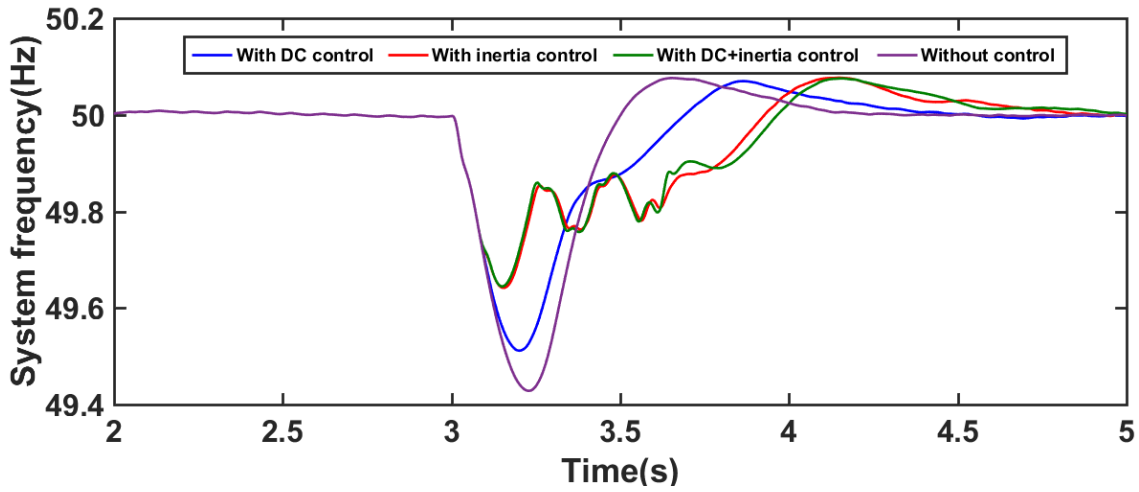
With DC control
With inertia control
With DC+inertia control
Without control
System frequency(Hz)
50.2
50
49.8
49.6
49.4
2
2.5
3
3.5
4
4.5
5
Time(s)

(b)

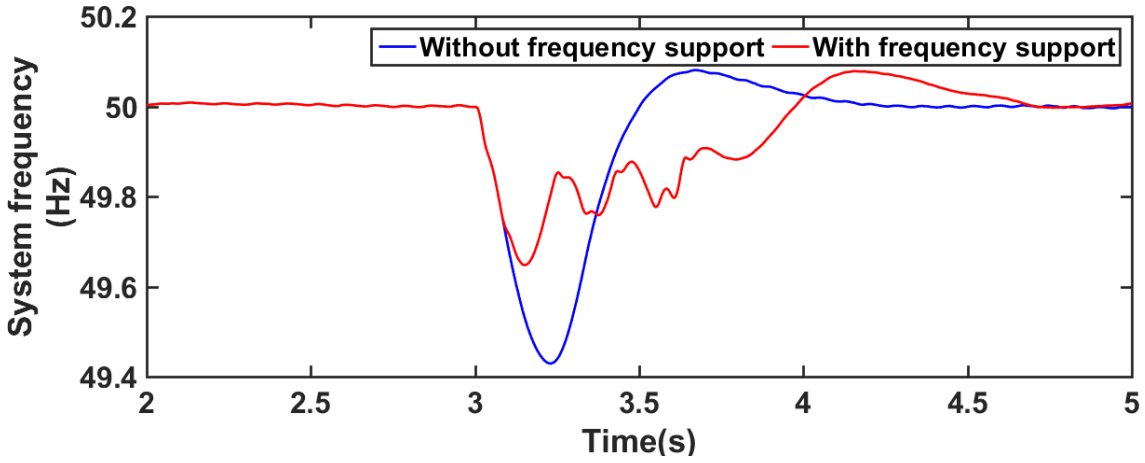
Without frequency support
With frequency support
System frequency (Hz)
50.2
50
49.8
49.6
49.4
2
2.5
3
3.5
4
4.5
5
Time(s)

(c)

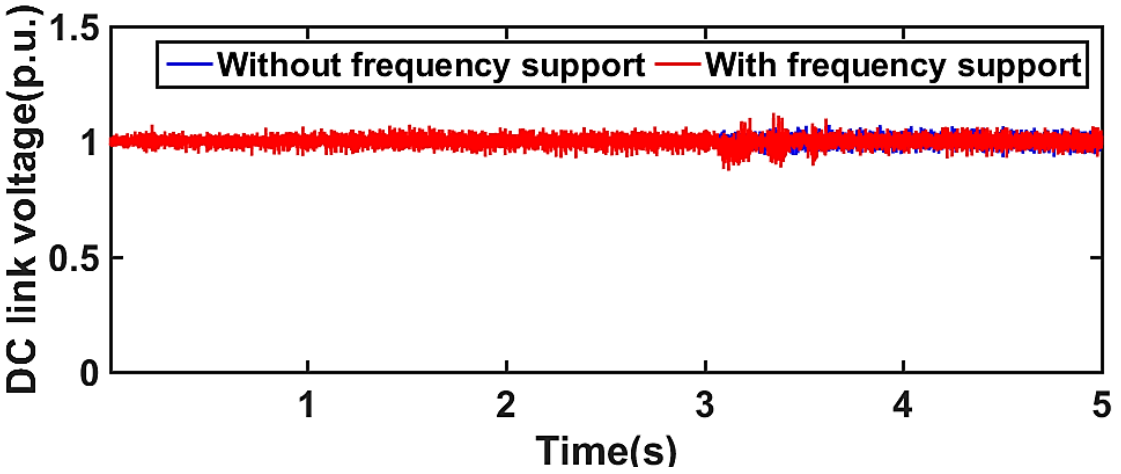
Without frequency support
With frequency support
DC link voltage(p.u.)
1.5
1
0.5
0
1
2
3
4
5
Time(s)

(d)

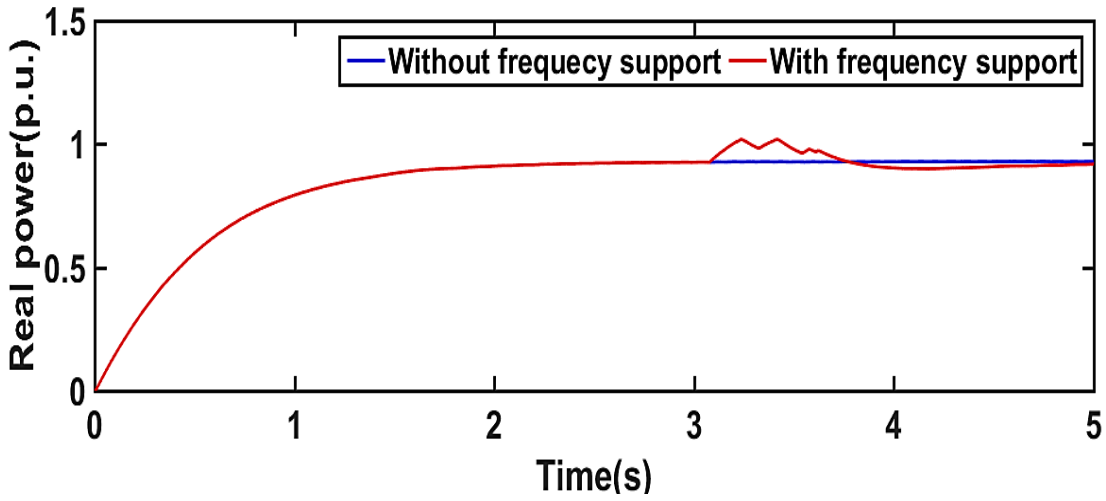

(e)

Fig.6.5. Results for constant wind speed a) Wind speed b) System frequency for different controller c) System frequency d) DC link voltage e) Real power

6.5.1.2. Operation Under Step Change in Wind Speed

For second simulation scenario, the step wind speed profile is shown in Fig.6.6(a). The sudden load is increased in single machine power system where the dump load is switched on at t=3s.As the power imbalance occurs so the system frequency drops down from its nominal frequency. Four different types of simulations are done and compared with each other as shown in Fig.6.6 (b). The simulation is based on without any control, WT inertia control only, DC voltage control only and simultaneous WT inertia and DC control. From Fig.6.6 (b) it is observed that the three control strategies improved the frequency nadir. With DC inertia control the frequency is improved from 49.49Hz to 49.54 Hz and 49.49 Hz to 49.83 Hz with the WT inertia control. On the other hand, by using simultaneous control the frequency nadir is improved from 49.49 Hz to 49.84Hz. It is also shown in Fig.6.6(c). The same pattern as system frequency is observed in DC link voltage as it provides inertia support to the system. The DC link voltage is presented in Fig.6.6 (d). More real power is transmitted to the load from PMSG as shown in Fig.6.6 (e).

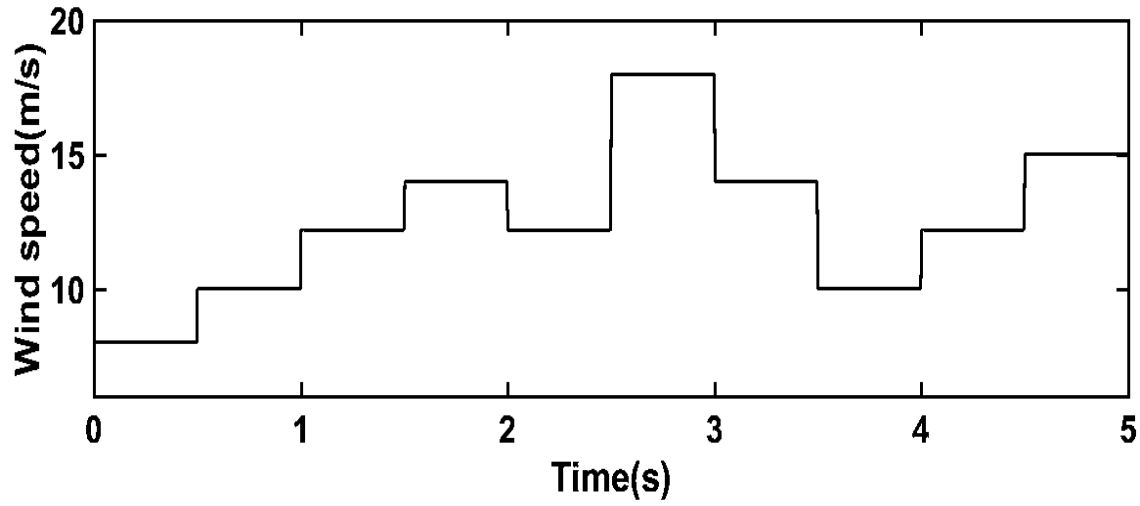
Wind speed(m/s)
20
15
10
0
1
2
3
4
5
Time(s)

(a)

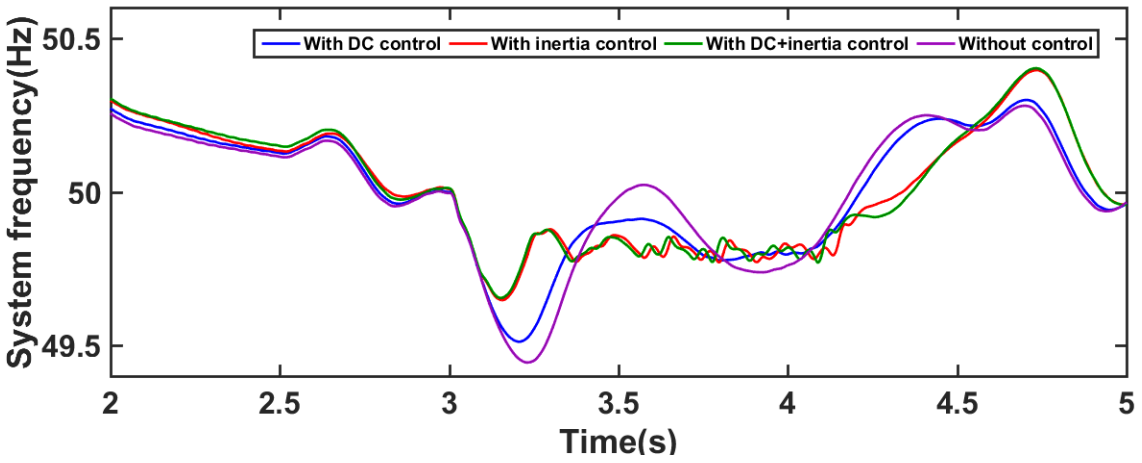
With DC control
With inertia control
With DC+inertia control
Without control
System frequency(Hz)
50.5
50
49.5
2
2.5
3
3.5
4
4.5
5
Time(s)

(b)

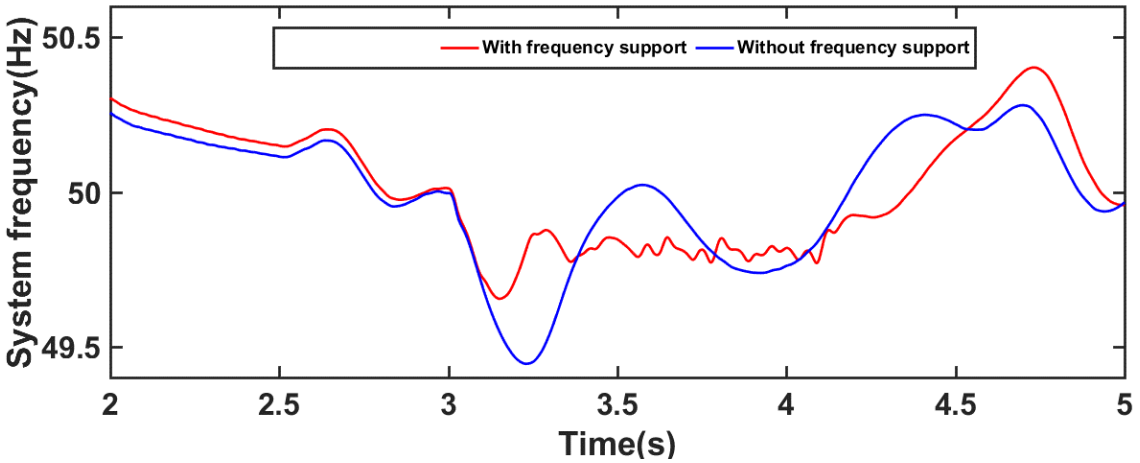
With frequency support
Without frequency support
System frequency(Hz)
50.5
50
49.5
2
2.5
3
3.5
4
4.5
5
Time(s)

(c)

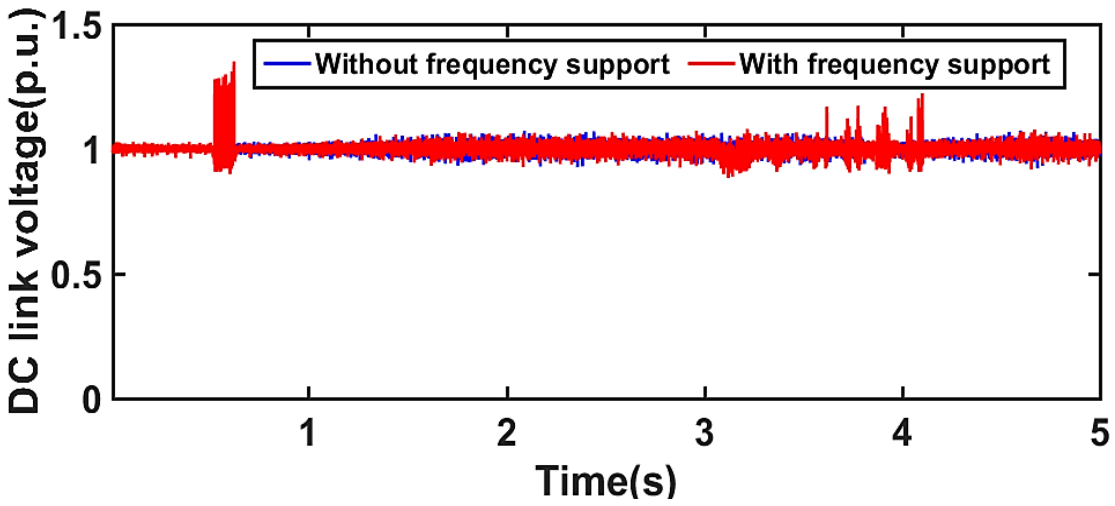

(d)

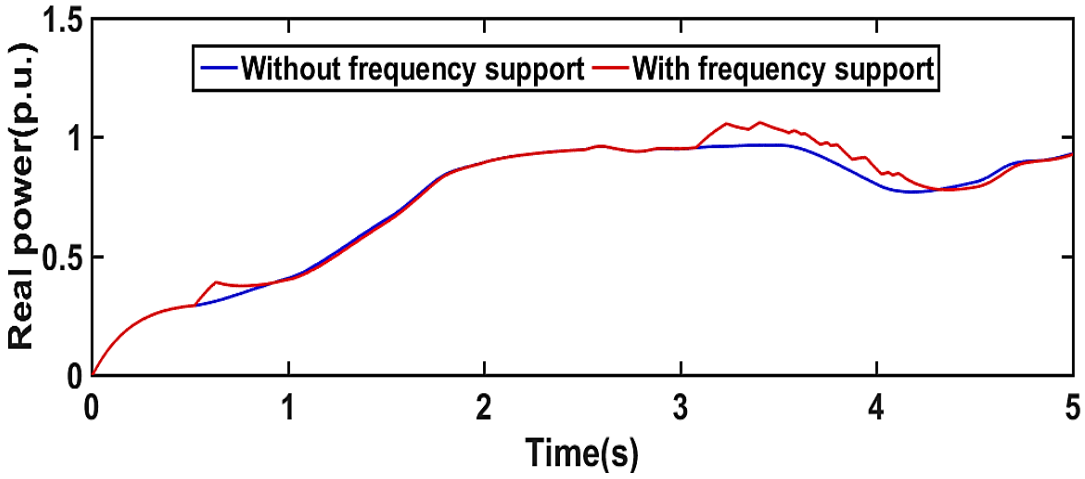

(e)

Fig.6.6. Results for step wind speed a) Wind speed b) System frequency for different controller c) System frequency d) DC link voltage e) Real power

6.5.1.3. Operation Under Real Wind Speeds

For another simulation scenario, the real wind speed is considered as shown in Fig.6.7 (a). The sudden load is increased in single machine power system where the dump load is switched on at t=3s.As the power imbalance occurs so the system frequency drops down from its nominal frequency. Four different types of simulations are done and compared with each other as shown in Fig. 6.7(b). The simulation is based on without any control, WT inertia control only, DC voltage control only and simultaneous WT inertia and DC control. From Fig. 6.7(b) it is observed that the three control strategies

improved the frequency nadir. With DC inertia control the frequency is improved from 49.47Hz to 49.55 Hz and 49.47 Hz to 49.84 Hz with the WT inertia control. On the other hand, by using simultaneous control the frequency nadir is improved from 49.47 Hz to 49.89Hz. It is also shown in Fig.6.7(c). The same pattern as system frequency is observed in DC link voltage as it provides inertia support to the system. The DC link voltage is presented in Fig. 6.7(d). More real power is transmitted to the load from PMSG as shown in Fig. 6.7(e).

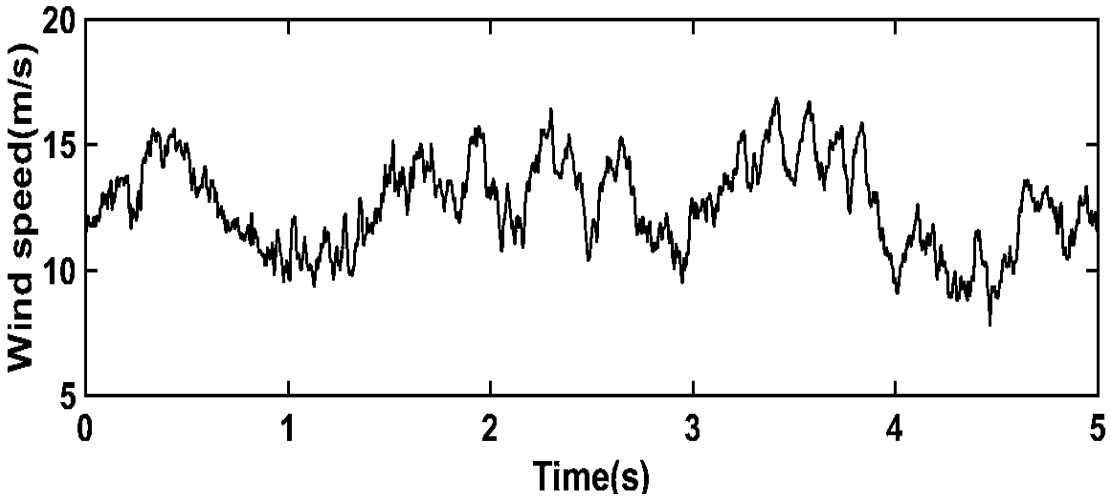

(a)

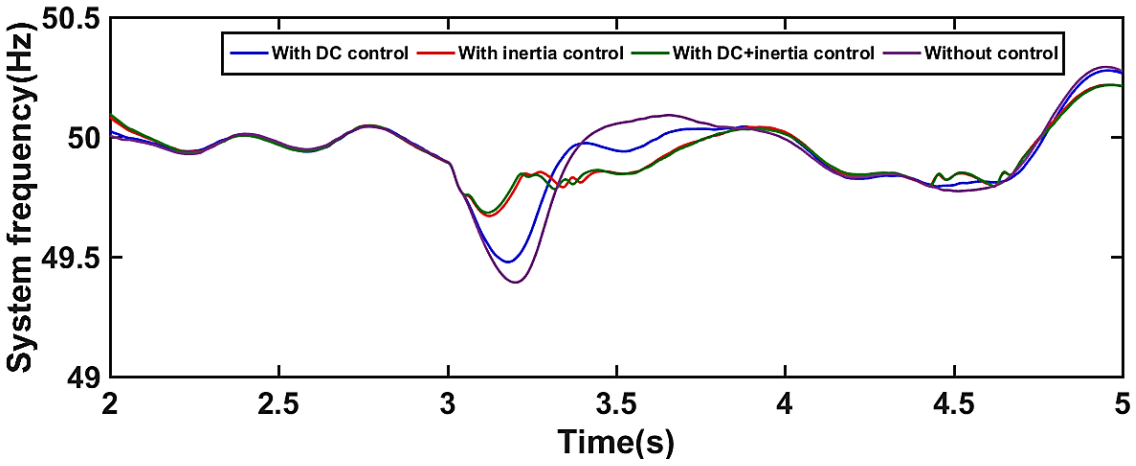

(b)

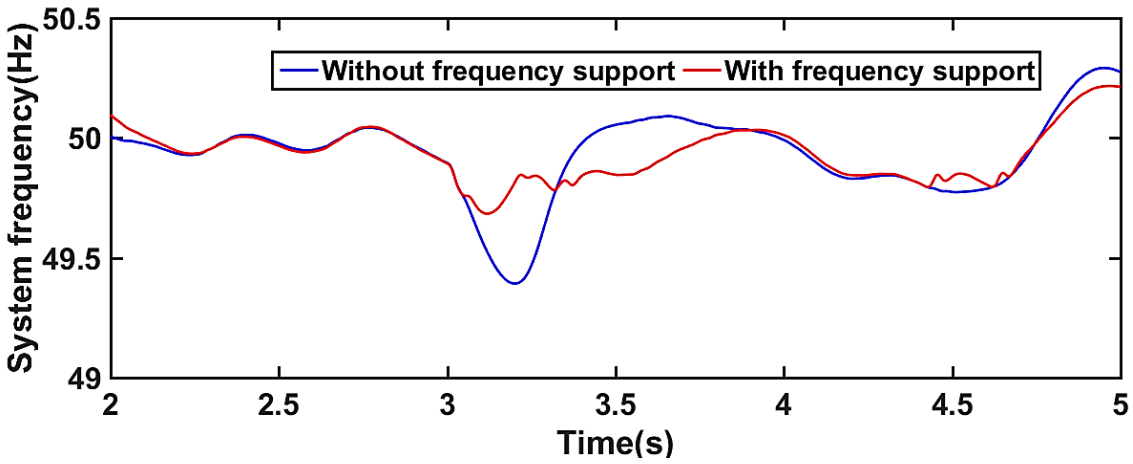

(c)

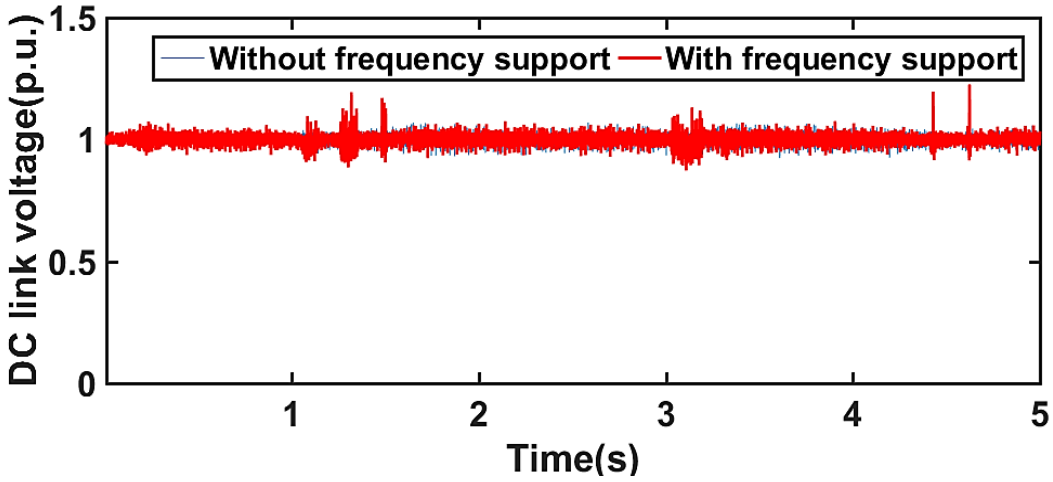

(d)

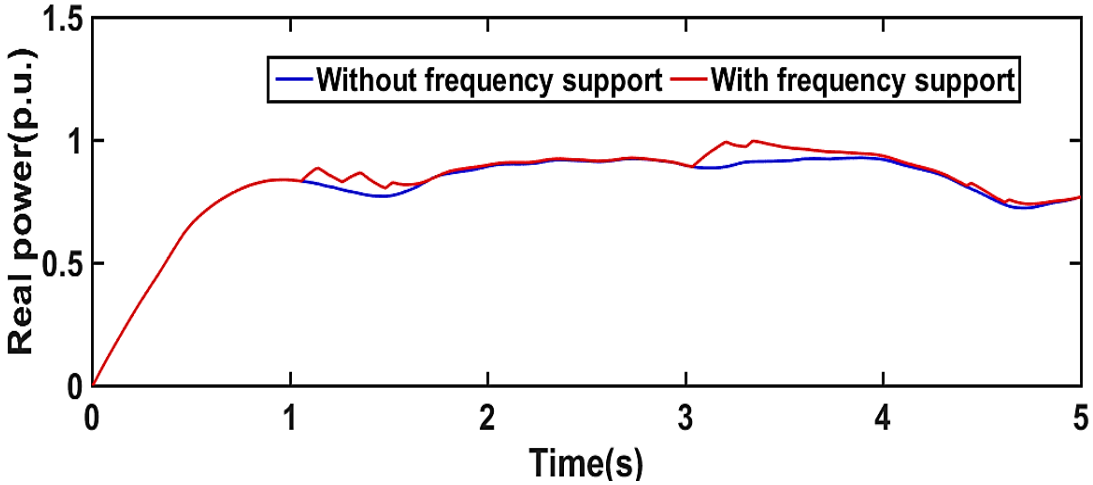

(e)

Fig.6.7. Results for real wind speed a) Wind speed b) System frequency for different controller c) System frequency d) DC link voltage e) Real power

6.6. Performance Evaluations when the WTG is connected to Multimachine Systems

A small scale multi-machine power system is depicted in Fig.6.8. It consists of a PMSG based WECS, four synchronous generators, three fixed loads and one dump load. L1, L2, L3 are consists of fixed load and L4 is consists of dump load. The WECS, SG and loads are connected to PCC via 415V/11 KV transformer and the circuit breaker. And F is the grid fault point.

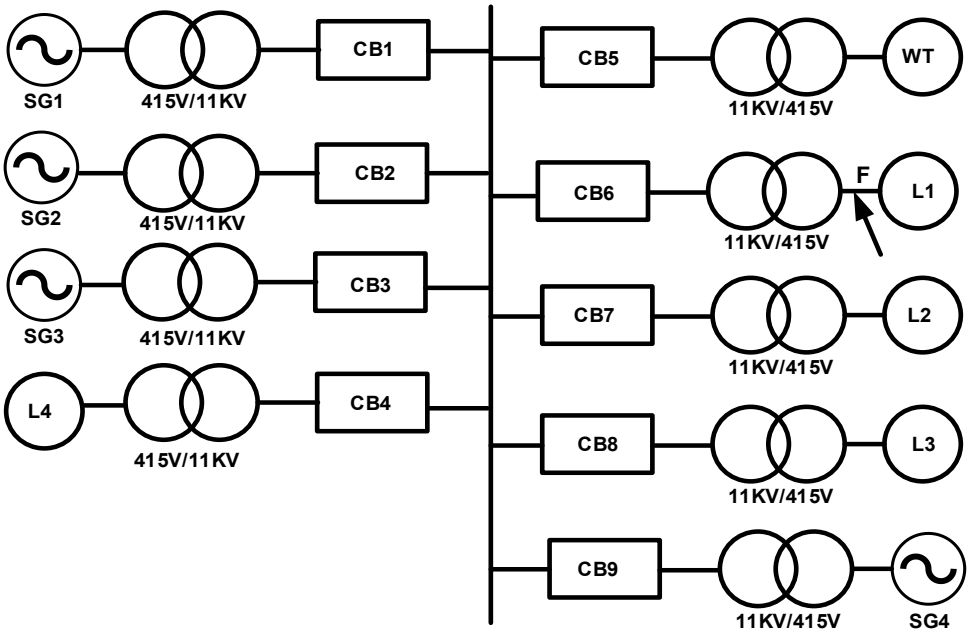

Fig.6. 8. Configuration of a small-scale multi-machine power system

6.6.1. Considering Sudden Trip of a Synchronous Generator

The sudden trip of SG4 is occurred at 2s. As the power imbalance occurs so the system frequency is declined rapidly from its nominal frequency, 50 Hz. It is found from Fig.6.9 that the frequency is decreased from 50 Hz to 49.61 Hz, 50 Hz to 49.62Hz and 50 Hz to 49.625Hz respectively for constant wind speed, step wind speed and real wind speed without any frequency controller. The frequency nadir is improved from 49.61 Hz to 49.72Hz, 49.62Hz to 49.68Hz and 49.625 Hz to 49.69 Hz by using the proposed controller.

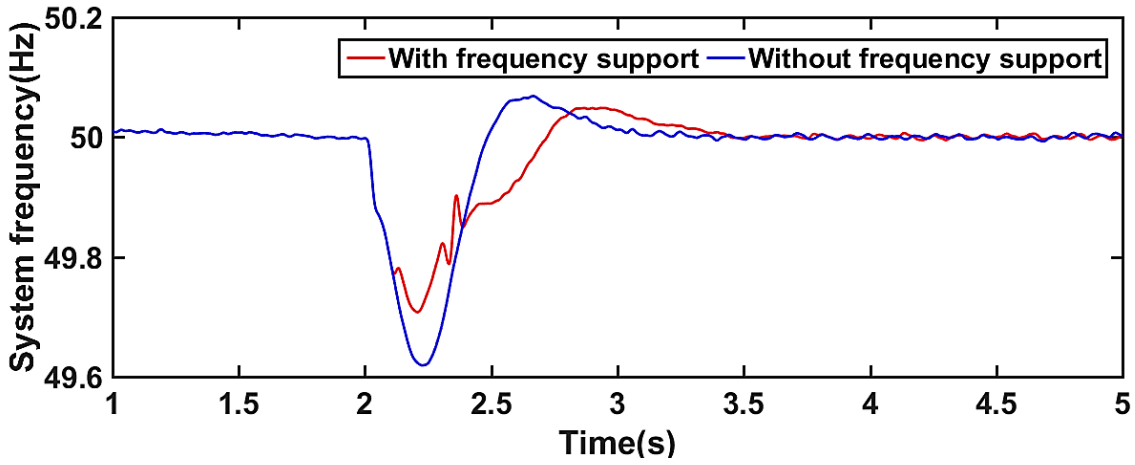

(a)

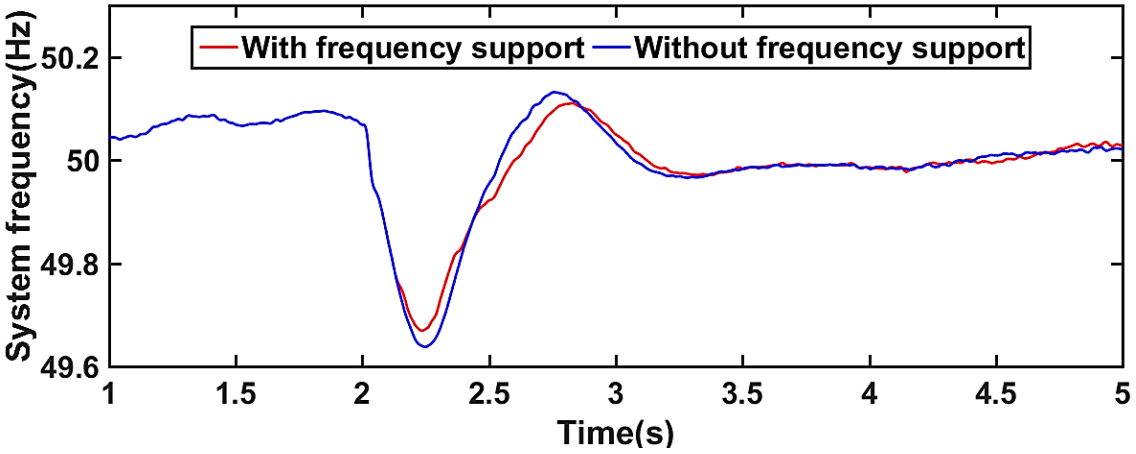

(b)

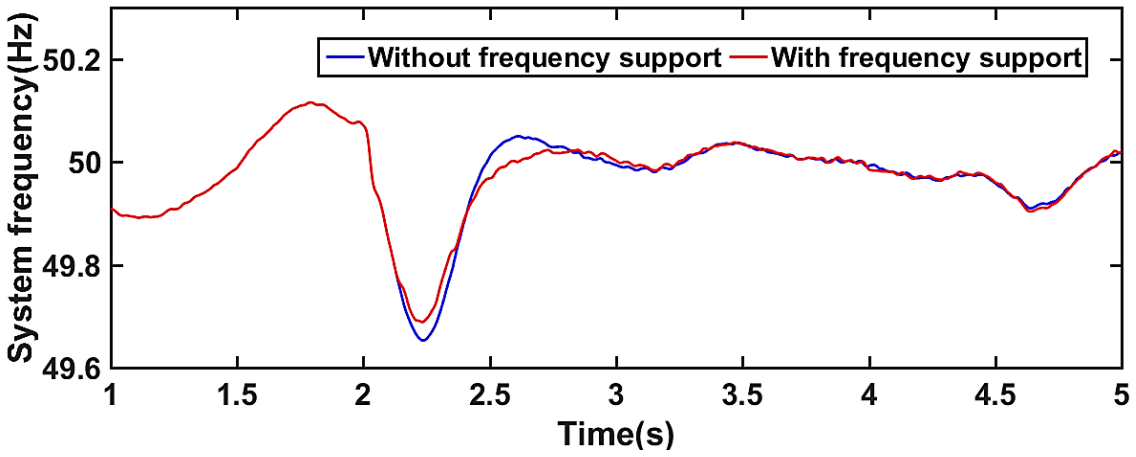

(c)

Fig.6.9. System frequency for a) Constant wind speed b) Step wind speed c) Real wind speed

6.6.2. Considering Sudden Increase of the Load Demand

For another scenario, the sudden load is increased in single machine power system where the dump load is switched on at t=2s. As the power imbalance occurs so the system frequency drops down from its nominal frequency. It is found from Fig.6.10 that the frequency is decreased from 50 Hz to 49.4 Hz, 50 Hz to 49.41Hz and 50 Hz to 49.42Hz respectively for constant wind speed, step wind speed and real wind speed without any frequency controller. The frequency nadir is improved from 49.4 Hz to 49.58 Hz, 49.41Hz to 49.49 Hz and 49.42 Hz to 49.47 Hz by using the proposed controller.

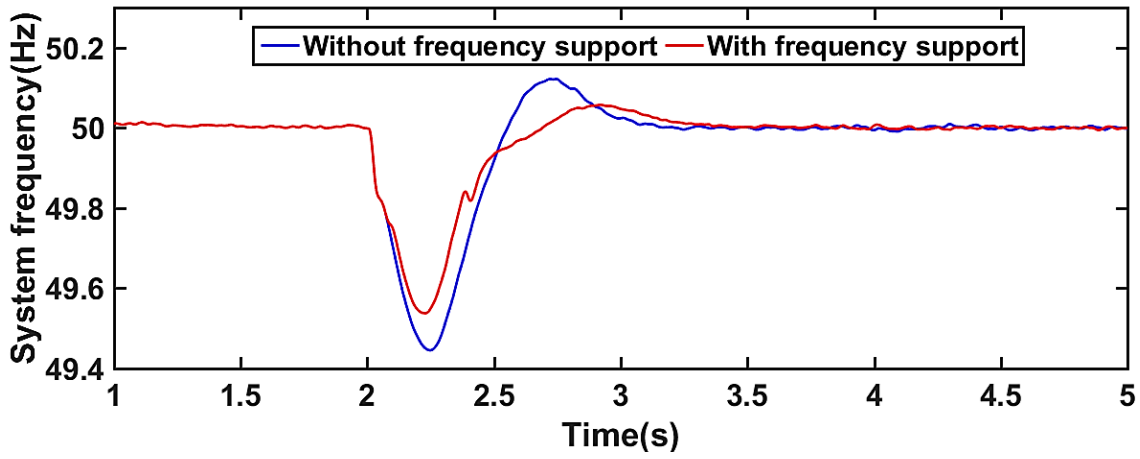

(a)

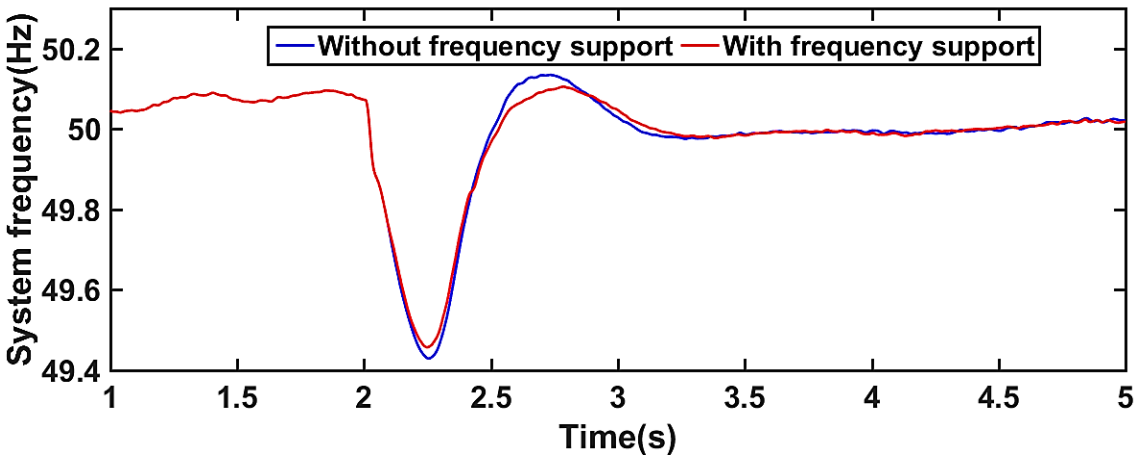

(b)

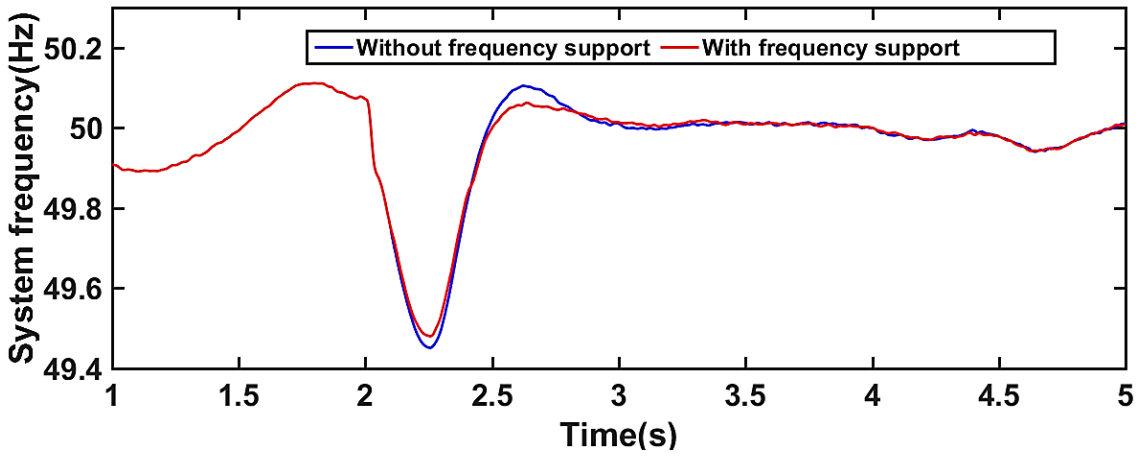

(c)

Fig.6.10. System frequency for a) Constant wind speed b) Step wind speed c) Real wind speed

6.6.3. Under Grid Faults

The results of proposed coordinated controller under three-phase to ground fault is shown in Fig.6.11. The start-up transient is shown. The fault is applied at 1s and cleared at 1.15s. The AC grid voltage profile is shown in Fig.6.11 (a). During grid fault initially, the frequency is increased as load is decreased due to voltage reduction and the frequency is decreased for generator tripping [15]- [17]. From this figure it is observed that the frequency deviation during grid fault is improved by using the proposed frequency controller. The DC link capacitor released some energy during this fault period by using the proposed controller.

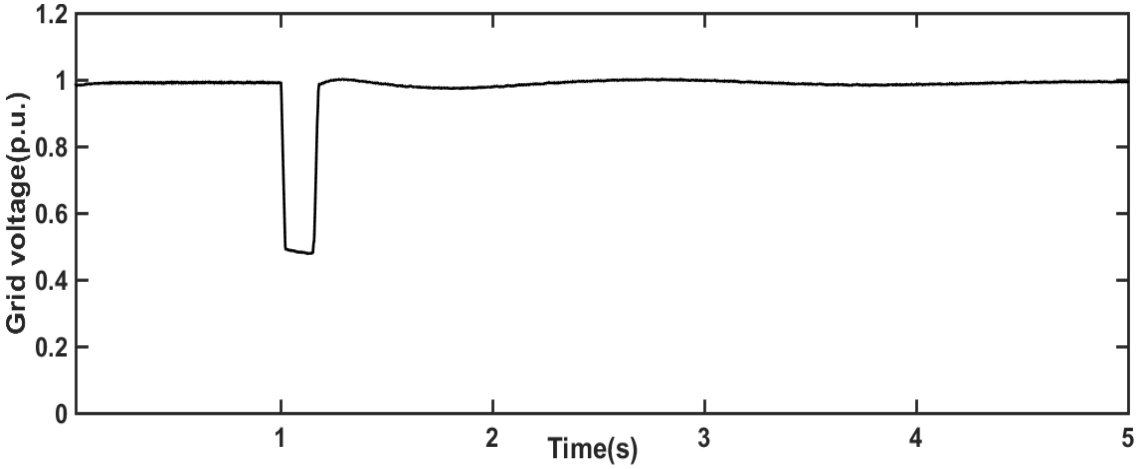

(a)

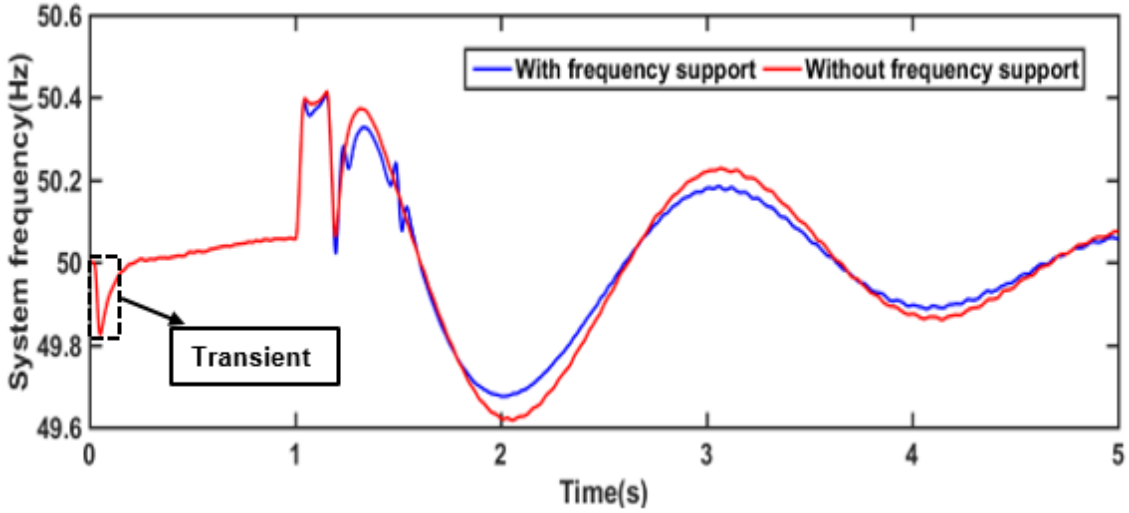
With frequency support
Without frequency support
System frequency(Hz)
Transient
Time(s)

(b)

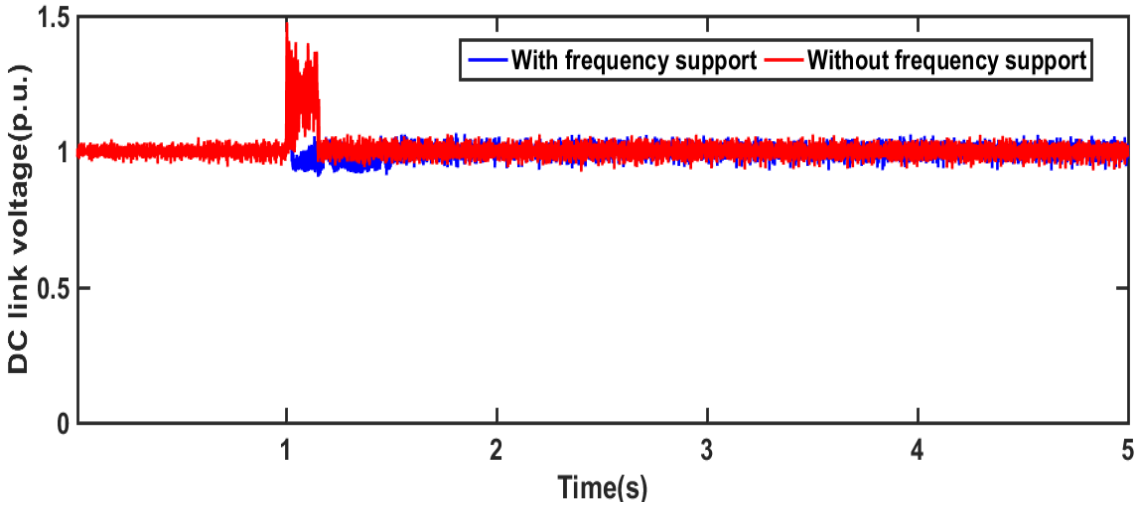
With frequency support
Without frequency support
DC link voltage(p.u.)
Time(s)

(c)

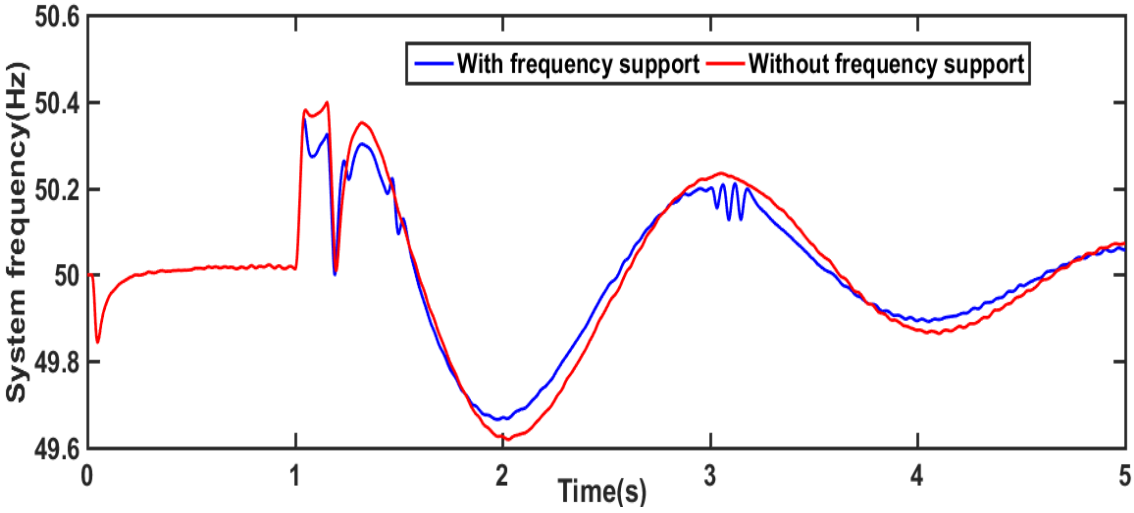
With frequency support
Without frequency support
System frequency(Hz)
Time(s)

(d)

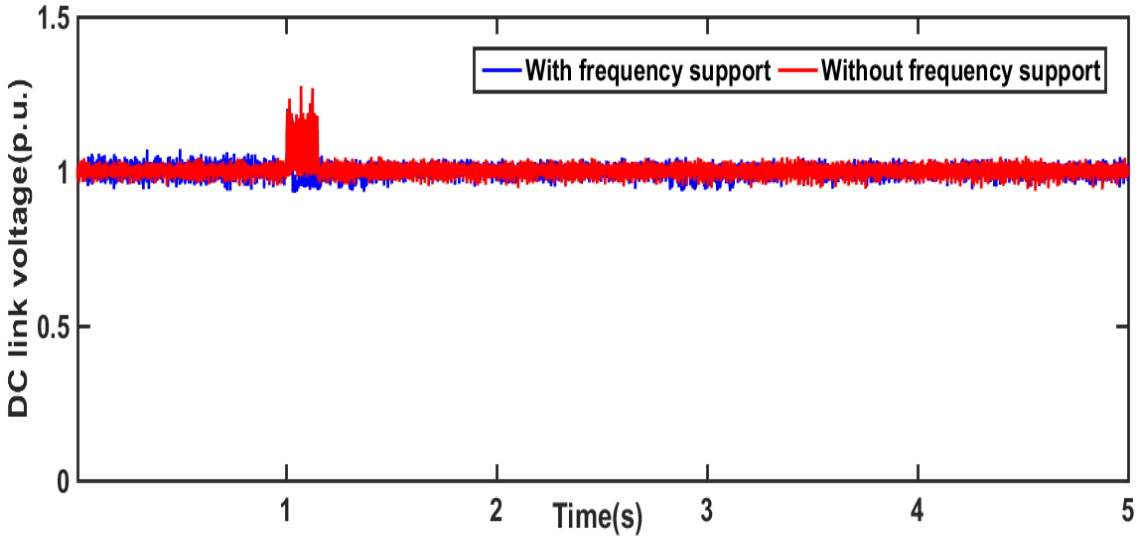
With frequency support
Without frequency support
DC link voltage(p.u.)
Time(s)
1.5
1
0.5
0
1
2
3
4
5

(e)

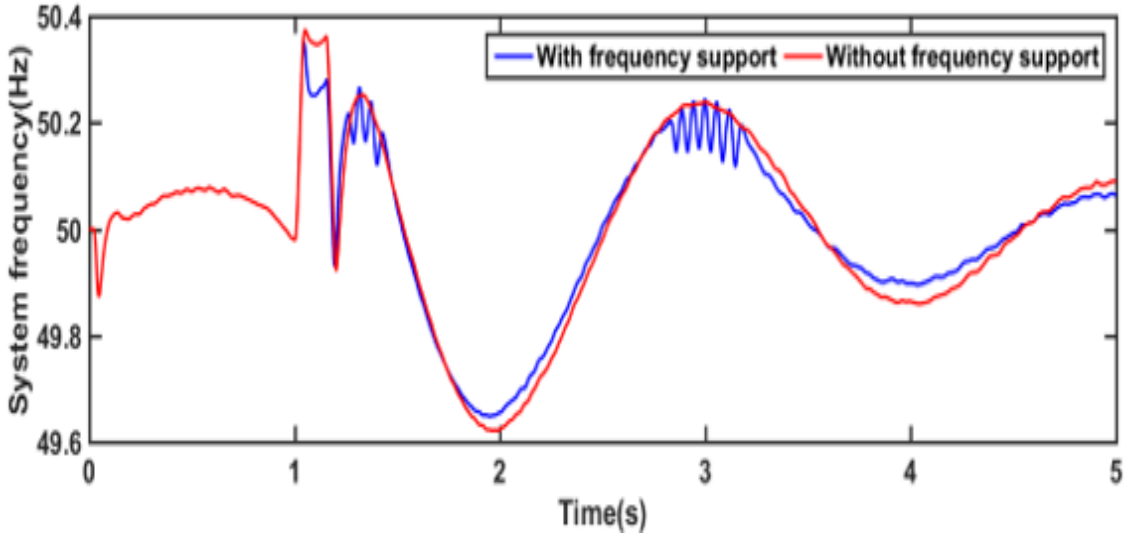
With frequency support
Without frequency support
System frequency(Hz)
Time(s)
50.4
50.2
50
49.8
49.6
0
1
2
3
4
5

(f)

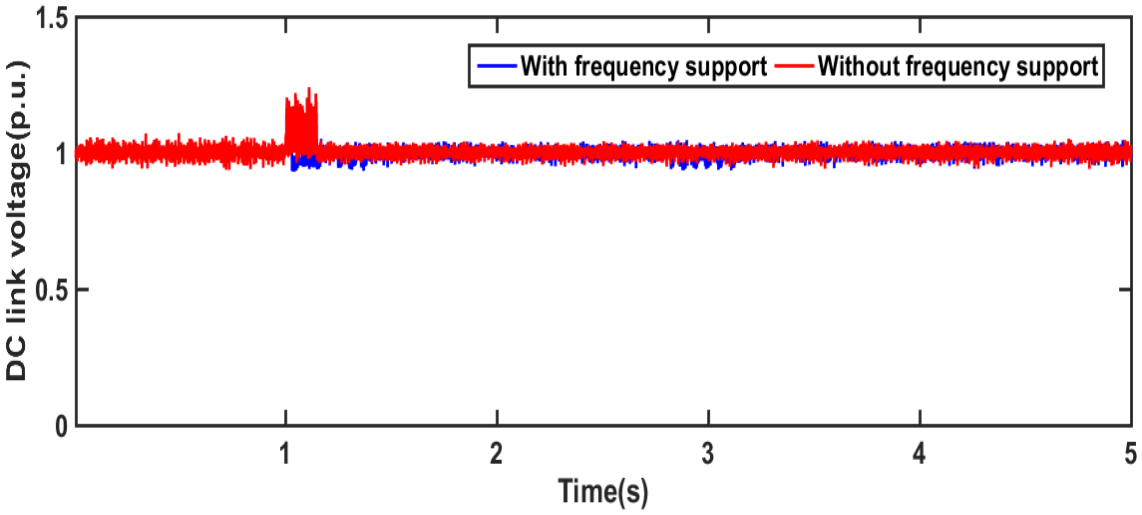
With frequency support
Without frequency support
DC link voltage(p.u.)
Time(s)
1.5
1
0.5
0
1
2
3
4
5

(g)

Fig.6.11. a) AC voltage b) System frequency for constant wind speed c) DC link voltage for constant wind speed d) System frequency for step wind speed e) DC link voltage for step wind speed f) System frequency for real wind speed g) DC link voltage for real wind speed

A comparison of frequency response with the proposed controller for different scenarios is illustrated in Table 6.1. From this table, it is found that the proposed controller is not only improved frequency nadir but also reduce the frequency deviation of steady state.

Table 6.1: System Frequency

Methods \ Parameters		Frequency nadir (Hz)	Post disturbance stable freq.(Hz)	Overshoot during stable freq.(Hz)
Single machine without controller	Constant	49.51	50.11	50.15
	Step	49.52	50.1	50.13
	Real	49.48	50.12	50.14
Single machine with controller	Constant	49.85	49.97	50.1
	Step	49.87	49.99	50.11
	Real	49.89	49.96	50.07
Multimachine without controller (Case I)	Constant	49.61	50.07	50.09
	Step	49.62	50.06	50.08
	Real	49.625	50.08	50.09
Multimachine with controller (Case I)	Constant	49.72	50.03	50.01
	Step	49.68	50.04	50.05
	Real	49.69	50.04	50.045
Multimachine without controller (Case II)	Constant	49.4	50.07	50.12
	Step	49.41	50.1	50.11
	Real	49.42	50.08	50.09
Multimachine with controller (Case II)	Constant	49.58	50.01	50.02
	Step	49.49	50.07	50.08
	Real	49.47	50.04	50.06
Multimachine without controller (Case III)	Constant	49.59	50.21	50.22
	Step	49.61	50.22	50.23
	Real	49.62	50.19	50.21
Multimachine with controller (Case III)	Constant	49.68	50.20	50.19
	Step	49.67	50.19	50.18
	Real	49.69	50.185	50.192

6.7. Impact of Flux Linkage Control with SMES on the Primary Frequency Regulation

6.7.1. When connected to the Single Machine System

For another scenario, the sudden load is increased in single machine power system where the dump load is switched on at t=3s. As the power imbalance occurs so the system frequency drops down from its nominal frequency. It is found from Fig.6.12 that the frequency is decreased from 50 Hz to 48.56 Hz, 50 Hz to 48.58Hz and 50 Hz to 48.55Hz respectively for constant wind speed, step wind speed and real wind speed without any frequency controller. The frequency nadir is improved from 48.56 Hz to 49.92 Hz, 48.58Hz to 49.9 Hz and 48.55 Hz to 49.92 Hz by using the proposed controller.

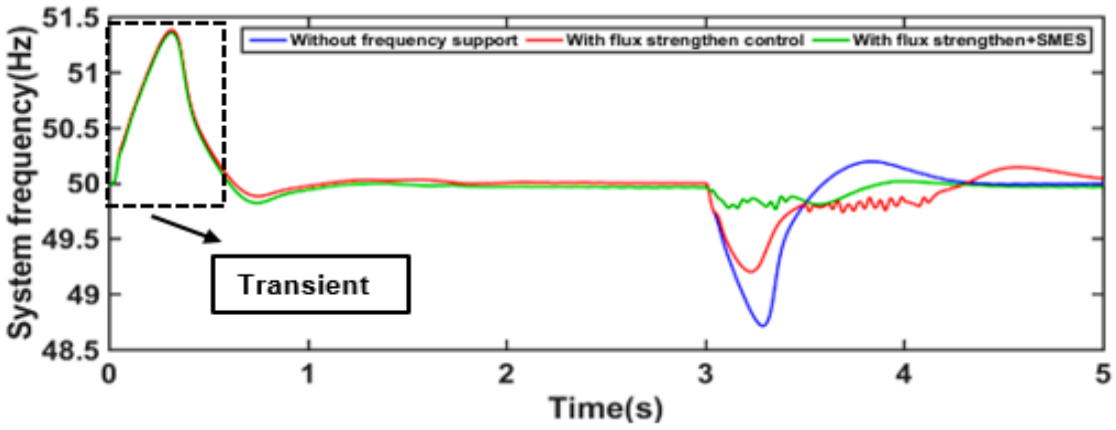

(a)

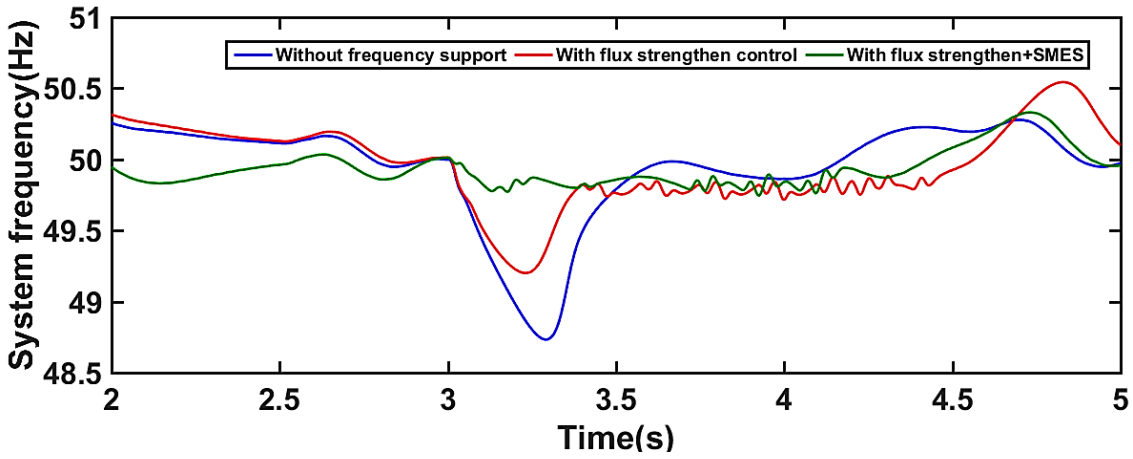

(b)

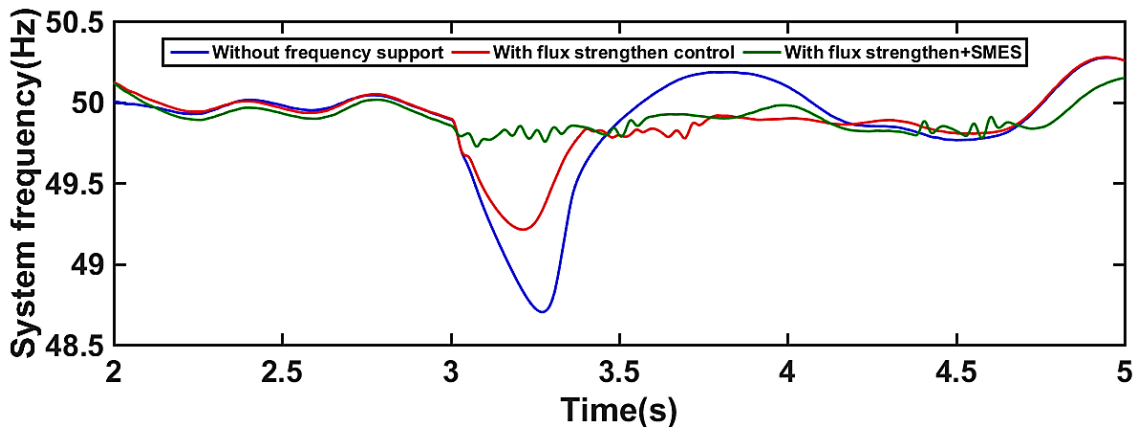

(c)

Fig.6.12. System frequency for a) Constant wind speed b) Step wind speed c) Real wind speed

6.7.2. When connected to the Multi Machine Systems

The sudden trip of SG4 is occurred at 3s. As the power imbalance occurs so the system frequency is declined rapidly from its nominal frequency, 50 Hz. It is found from Fig.6.13 that the frequency is decreased from 50 Hz to 49.62 Hz, 50 Hz to 49.611Hz and 50 Hz to 49.615Hz respectively for constant wind speed, step wind speed and real wind speed without any frequency controller. The frequency nadir is improved from 49.61 Hz to 49.92Hz, 49.62Hz to 49.93Hz and 49.625 Hz to 49.94 Hz by using the proposed controller

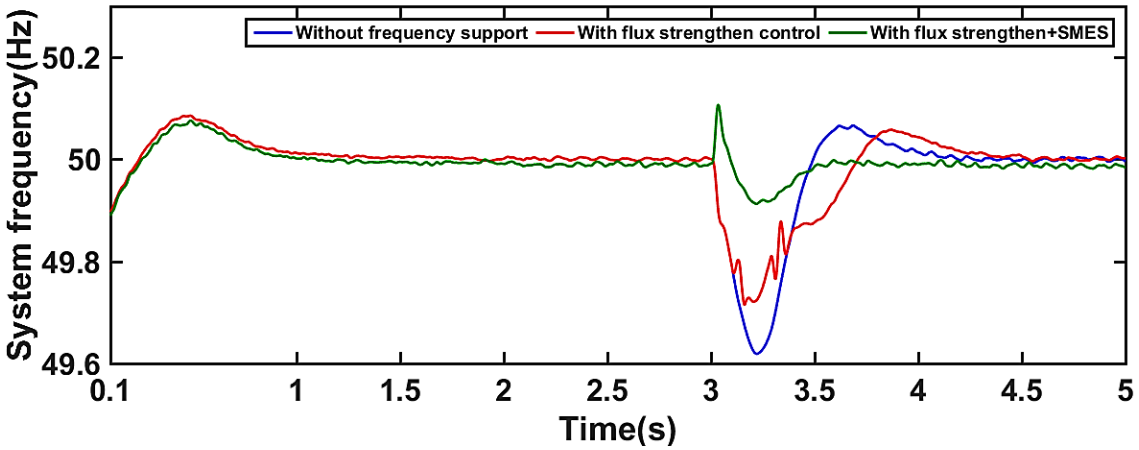

(a)

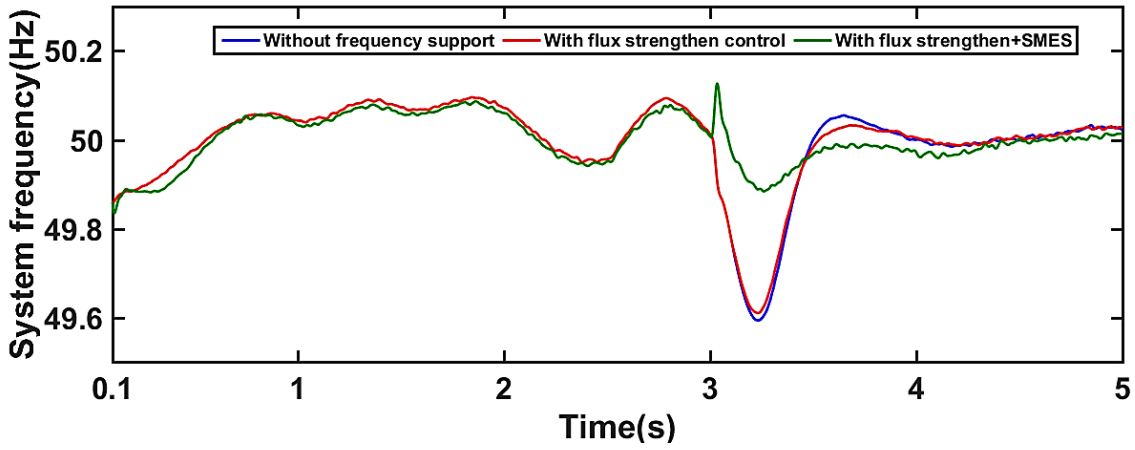

(b)

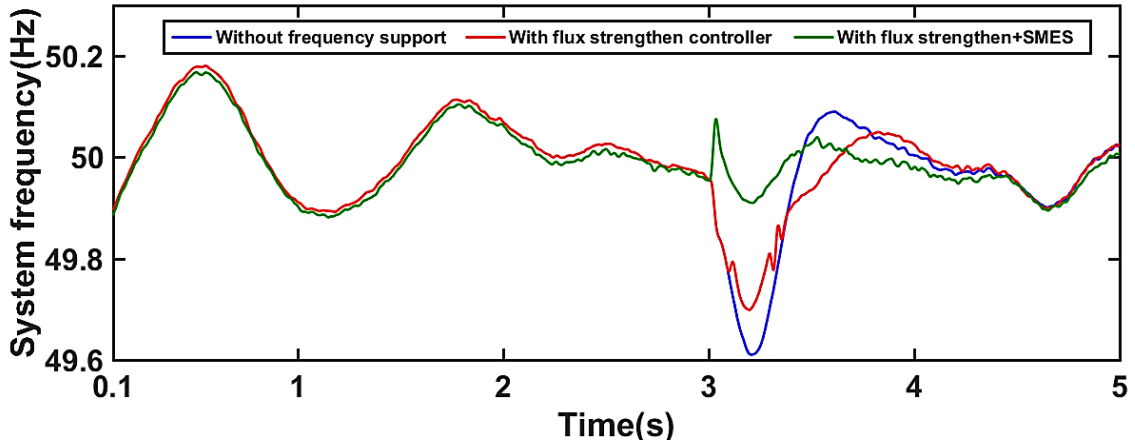

(c)

Fig.6.13. System frequency for a) Constant wind speed b) Step wind speed c) Real wind speed

The results of proposed coordinated controller under three-phase to ground fault is shown in Fig.6.14. The fault is applied at 1s and cleared at 1.15s. The AC grid voltage profile is shown in Fig.6.14 (a). From this figure it is observed that the frequency deviation during grid fault is improved by using the proposed frequency controller.

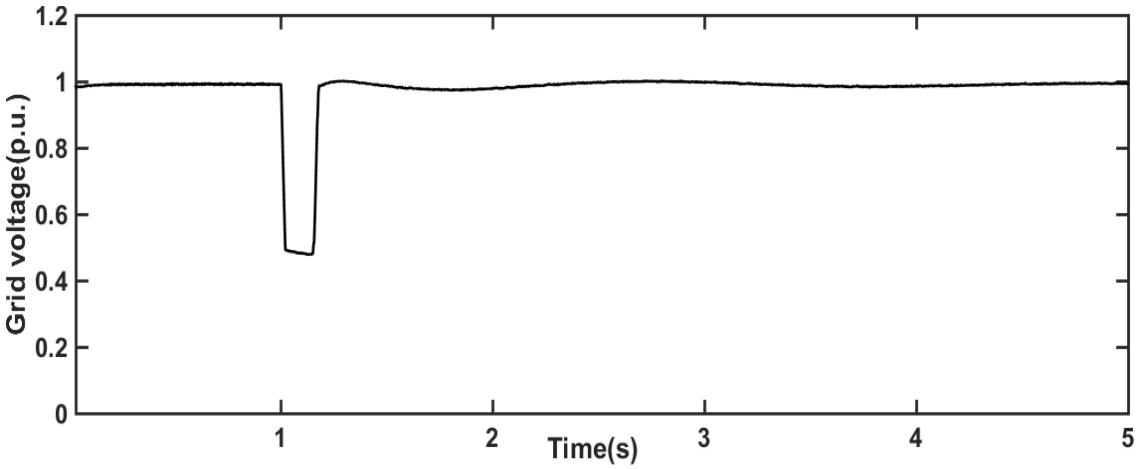
Grid voltage(p.u.)
Time(s)

(a)

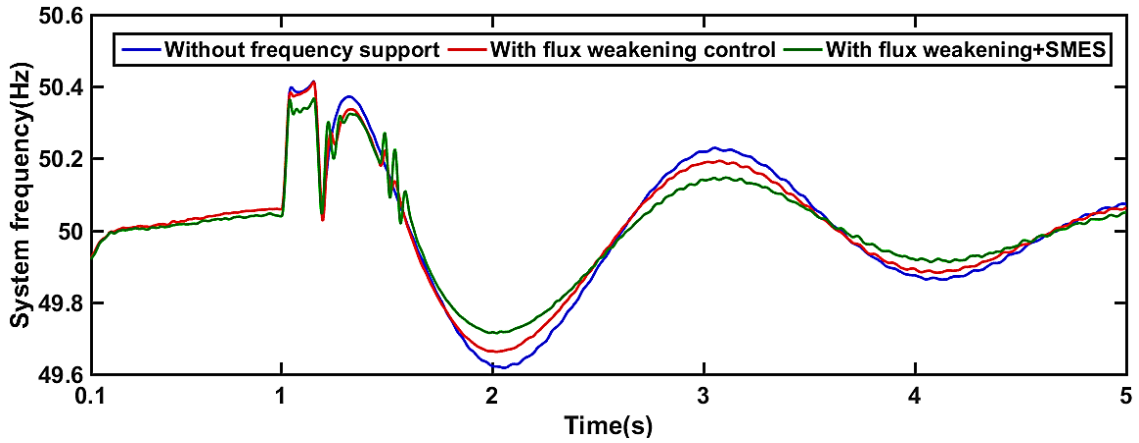
Without frequency support
With flux weakening control
With flux weakening+SMES
System frequency(Hz)
Time(s)

(b)

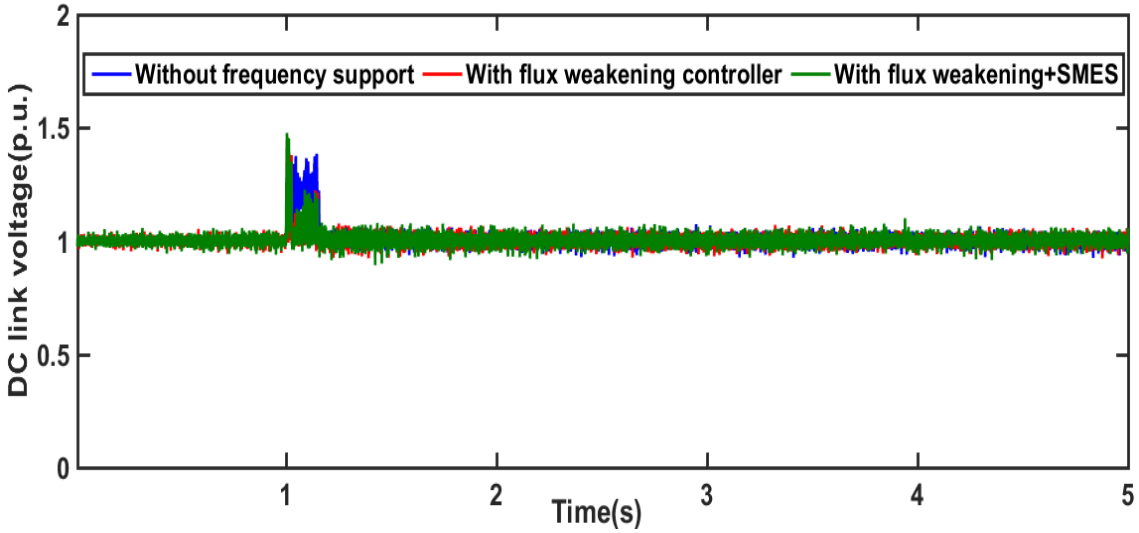
Without frequency support
With flux weakening controller
With flux weakening+SMES
DC link voltage(p.u.)
Time(s)

(c)

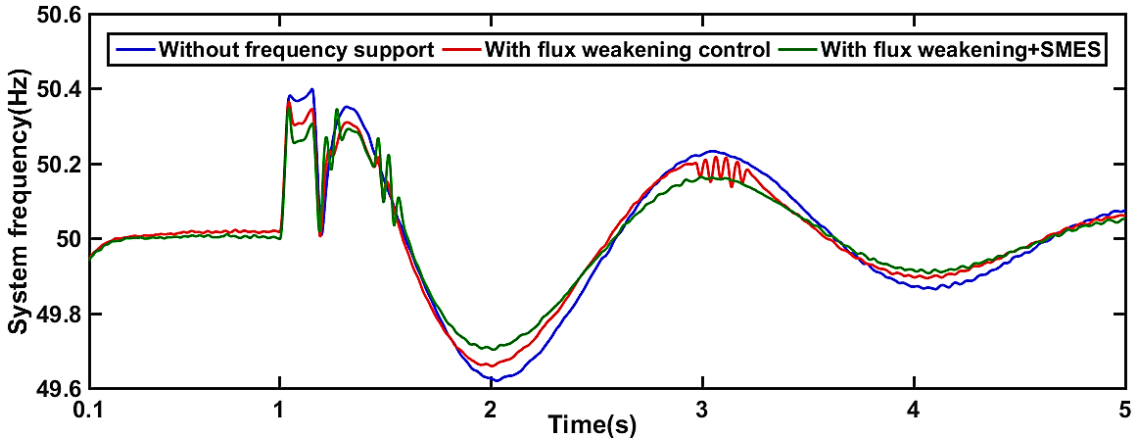
Without frequency support
With flux weakening control
With flux weakening+SMES
System frequency(Hz)
50.6
50.4
50.2
50
49.8
49.6
0.1
1
2
3
4
5
Time(s)

(d)

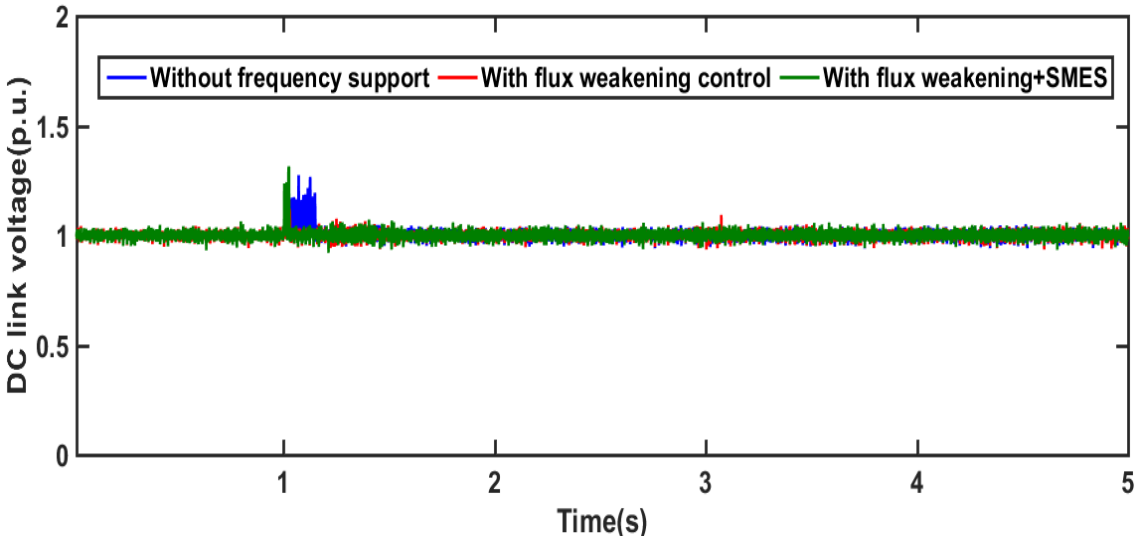
Without frequency support
With flux weakening control
With flux weakening+SMES
DC link voltage(p.u.)
2
1.5
1
0.5
0
1
2
3
4
5
Time(s)

(e)

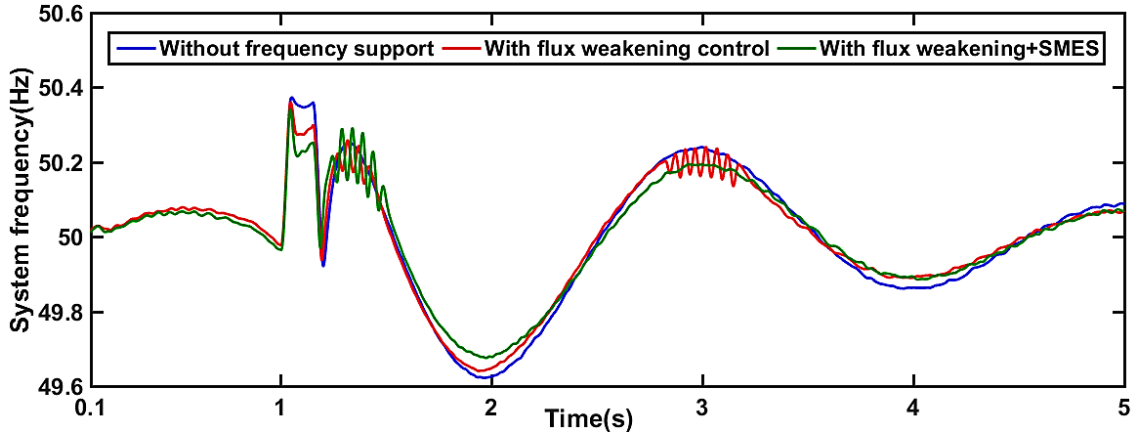
Without frequency support
With flux weakening control
With flux weakening+SMES
System frequency(Hz)
50.6
50.4
50.2
50
49.8
49.6
0.1
1
2
3
4
5
Time(s)

(f)

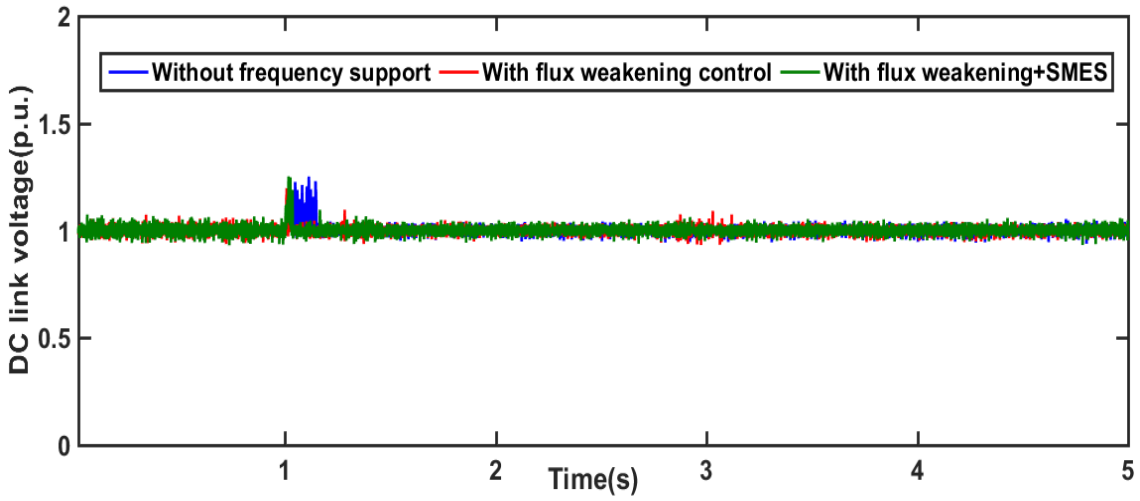

(g)

Fig.6.14. a) AC voltage b) System frequency for constant wind speed c) DC link voltage for constant wind speed d) System frequency for step wind speed e) DC link voltage for step wind speed f) System frequency for real wind speed g) DC link voltage for real wind speed

Table 6.2: System Frequency

Parameters / Methods		Frequency nadir (Hz)	Post disturbance stable freq.(Hz)	Overshoot during stable freq.(Hz)
Single machine without controller	Constant	49.51	50.11	50.15
	Step	49.52	50.1	50.13
	Real	49.48	50.12	50.14
Single machine with controller	Constant	49.98	50.03	50.01
	Step	49.97	50.04	50.01
	Real	49.99	50.03	50.02
Multi-machine without controller (Case I)	Constant	49.61	50.07	50.09
	Step	49.62	50.06	50.08
	Real	49.625	50.08	50.09
Multi-machine with controller (Case I)	Constant	49.92	50.02	50.05
	Step	49.93	50.02	50.025
	Real	49.94	50.01	50.035
Multi-machine without controller (Case II)	Constant	49.59	50.21	50.22
	Step	49.61	50.22	50.23
	Real	49.62	50.19	50.21
Multi-machine with controller (Case II)	Constant	49.78	50.10	50.11
	Step	49.79	50.11	50.13
	Real	49.76	50.12	50.11

Another comparison of frequency response with the proposed controller for different scenarios is illustrated in Table 6.2.

From this table, it is also found that the proposed controller can improve frequency nadir as well as reduce the frequency deviation of steady state.

6.8. Summary

This chapter has presented two approaches of primary frequency regulations to minimise the frequency deviations by using the PMSG based WECS. The first method proposed is developed based on the inertia support from the WTG and the DC link capacitor. As it uses physical inertia of the turbine-generator shaft as well as the synthetic inertia from the DC-link capacitor, it can be called hybrid inertia-based frequency control from the grid-connected WECS. The second approach is developed based on the flux linkage control with the SMES.

Both approaches are verified for a 1.5 MW PMSG base WECS connected to the single machine and multi-machine power systems. From the simulation results, it has been demonstrated that the proposed methods can limit the frequency deviations under different wind profiles and after grid fault recovery.

Between these methods, the combination of flux linkage controller and SMES provide better response than the inertia control. However, it is expensive. So, it can only be chosen based on the application and the requirements of the power system.

REFERENCES

[1] H. Bevrani, A. Ghosh, G. Ledwich, "Renewable energy sources and frequency regulation: Survey and new perspectives", *IET Renewable Power Generation.*, vol. 4, no. 5, pp. 438-457, Sep. 2010.

[2] O. Anaya-Lara, F. M. Hughes, N. Jenkins, G. Strbac, "Contribution of DFIG-based wind farms to power system short-term frequency regulation", *Proc. Inst. Elect. Eng. Gen. Transm. Distrib.*, vol. 153, no. 2, pp. 164-170, 2006.

[3] Y. Tan, L. Meegahapola, and K. M. Muttaqi, "A suboptimal power-point-tracking-based primary frequency response strategy for DFIGs in hybrid remote area power supply systems", *IEEE Transactions on Energy Conversion*, vol. 31, no. 1, pp. 93-105, Mar. 2016.

[4] J. M. Mauricio, A. Marano, A. Gomez-Exposito, J. L. Martinez Ramos, "Frequency regulation contribution through variable-speed wind energy conversion systems", *IEEE Transactions on Power System*, vol. 24, no. 1, pp. 173-180, Feb. 2009.

[5] Y. Li, Z. Xu, and K. P. Wong, "Advanced control strategies of PMSG-based wind turbines for system inertia support", *IEEE Transactions on Power System.*, vol. 32, no. 4, pp. 3027-3037, Jul. 2017

[6] Y. Li, Z. Xu, J. Østergaard, D.J. Hill, "Coordinated Control Strategies for Offshore Wind Farm Integration via VSC-HVDC for System Frequency Support", *IEEE Transactions on Energy Conversion*, vol. 32, no. 3, pp. 843-856, Sept. 2017.

[7] M. F. M. Arani, E. F. El-Saadany, "Implementing virtual inertia in DFIG-based wind power generation", *IEEE Transactions on Power System*, vol. 28, no. 2, pp. 1373-1384, May 2013.

[8] P. Dey, M. Datta, N. Fernando, "A coordinated control of grid connected PMSG based wind energy conversion system under grid faults", *3rd IEEE International Future Energy Electronics Conference and ECCE Asia (IFEEC 2017-ECCE Asia)*, pp. 597-602, 3−7 June 2017.

[9] P. Dey, M. Datta, N. Fernando, and T. Senjyu, "A method to reduce DC-link overvoltage of PMSG based WECS during LVRT," in *IEEE Region 10 Conference (TENCON), 2016*, pp. 1894-1899.

[10] S. K. Gupta and R. K. Srivastava, "LVRT capability evaluation of variable-flux PMSG based WECS," *2017 IEEE Transportation Electrification Conference (ITEC-India)*, Pune, India, 2017, pp. 1-5.

[11] M. H. Ali, W. Bin, and R. A. Dougal, “An Overview of SMES Applications in Power and Energy Systems", *IEEE Transactions on Sustainable Energy*, vol. 1, pp. 38-47. 2010

[12] Lei Chen, Hongkun Chen, Yanhong Li, Guocheng Li, Jun Yang, Xin Liu, Ying Xu, Li Ren, Yuejin Tang, "SMES-Battery Energy Storage System for the Stabilization of a Photovoltaic-Based Microgrid", *IEEE Transactions on Applied Superconductivity* vol. 28, pp. 1-7, 2018, ISSN 1051-8223.

[13] A. Abu-Siada and S. Islam, "Application of SMES Unit in Improving the Performance of an AC/DC Power System", *IEEE Transactions on Sustainable Energy*, vol. 2, pp. 109-121. 2011

[14] A. S. Yunus, M. A. Masoum, and A. Abu-Siada, "Application of SMES to enhance the dynamic performance of DFIG during voltage sag and swell," *IEEE Transactions on Applied Superconductivity,* vol. 22, pp. 5702009-5702009, 2012.

[15] L. Meegahapola and D. Flynn, "Frequency dynamics during high CCGT and wind penetrations," in *Power Engineering Conference (AUPEC), 2011 21st Australasian Universities*, 2011, pp. 1-6.

[16] N. Mukherjee, D. De and N. Nandagaoli, "Effect of sudden variation of grid voltage in primary frequency control application using converter based energy storage systems for weak grid systems," *2017 19th European Conference on Power Electronics and Applications (EPE'17 ECCE Europe)*, Warsaw, 2017, pp. P.1-P.10.

[17] Yingcheng, X.; Nengling, T., " Review of contribution to frequency control through variable speed wind turbine", *Renewable Energy* 2011, vol.36, pp.1671–1677.

CHAPTER SEVEN

CONCLUSIONS AND FUTURE WORKS

7.1. Concluding Remarks

Due to the grid faults and their associated transient instabilities, namely the voltage deviations and frequency fluctuations, LVRT of the PMSG based WECS is considered an important and interesting research area in recent years. DC link overvoltage minimisation, grid voltage support, and frequency regulation are considered as main challenges in the grid connected WECS as these are required by the grid codes.

This PhD research presented a new application of the flux weakening controller which can minimise the DC link overvoltage during symmetrical and asymmetrical grid faults. The flux weakening control method has been developed based on the synchronous and stationary reference frames. It has been found that the PR based flux weakening control provides better response and performances in comparison with the conventional Braking Chopper based method under the constant wind speed condition. Thus, the PR based flux weakening controller is used to develop the proposed coordinated controller.

The coordinated control is then developed combining a pitch angle control and the PR flux weakening technique to limit the DC link overvoltage under variable wind speeds. This controller performance is investigated for different cases and compared with the conventional Energy Storage System based method. It is found that the performance of the proposed coordinated controller is better in DC link overvoltage regulation and in smoothing the wind power fluctuations.

Then this arrangement is again coordinated with the GSC and the STATCOM to improve the grid voltage profile by providing better reactive power support. The controller performance is again tested under different cases. It is concluded that the GSC

alone cannot provide enough reactive power support for an improved FRT however; with the help of a STATCOM, the GSC and WECS can support the grid voltage profile to ride through the faults.

Then, this coordinated controller is replaced by a Fuzzy Logic based coordinated controller and is tested for the 1.5 MW WECS. It is found that this fuzzy based control configuration can also enhance the LVRT performance by providing reactive power support as well as by limiting the DC link overvoltage under symmetrical and asymmetrical grid faults.

Finally, for frequency regulation, based on the inertia support, flux linkage control and SMES, two approaches are demonstrated. Both strategies are verified for different wind speeds in single and multi-machine power systems.

7.2. List of Contributions

The main contributions of this PhD research work are as follows:

- A new application of the flux weakening controller for the LVRT is presented. The controller is developed in different reference frames based on the synchronous frame PI current controller, stationary frame PI current controller and stationary frame PR current controller. The controller performance is verified under symmetrical and asymmetrical grid faults. A comparison with the conventional method has been made to prove the effectiveness of the proposed controller.
- A PI controller based coordinated control algorithm is developed for the improvement of transient responses from the PMSG based WECS. This is based on the flux weakening control, STATCOM control, pitch angle control, MSC control and GSC control. Stability analysis for the PMSG based WECS is shown in the frequency and time domains. The controller performance is verified for a single WTG and a wind farm considering symmetrical single and repetitive grid faults,

asymmetrical single and repetitive grid faults, and wind wake effects with different wind direction of0º, 45º and 90º where the WTG is connected to the the IEEE-9 bus test system. A comparison between the proposed and conventional controllers has been provided to show the effectiveness of the proposed coordinated controller. Moreover, another coordinated controller is developed based on the Fuzzy Logic to improve the fault ride through performance of the grid connected WECS.

- Two frequency controllers for the PMSG based WECS are developed based on the inertia support, flux linkage control and energy storage device. The controller performances are verified to regulate frequency deviations and frequency fluctuations considering single and multi-machine power systems for constant, step and real wind speeds.

7.3. Suggestions for Future Work

In this PhD research work, several control strategies are developed to improve the transient stability of the PMSG based grid connected WECS during and after the grid faults. Following are the future works which can significantly put new directions of research as well as validate the research experimentally.

- The proposed coordinated controller is developed based on the classical PI and PR controllers in the machine side and grid side. Application of the improved control strategies like model predictive control (MPC) and artificial intelligence-based control may further improve the performance with a better coordination of the MSC and GSC controls.
- The size of the STATCOM used in this research for reactive power injection is decided based on the grid voltage drops during the grid faults. By using different real time optimization techniques optimal size of the STATCOM size can be found.

- For the STATCOM control, instead of the conventional hysteresis controller, fuzzy based adaptive hysteresis current controller can be used, and this could be more effective for avoiding spikes of the generated gate pulse for the STATCOM.
- The proposed controller is verified for the IEEE 9 bus test system. It can also be verified for a large complex power system like the IEEE 57 bus test system or the IEEE 118 bus test system.
- For the frequency control by using the wind turbine and the DC link capacitor energy, constant inertial gain is used. Variable gain can be used too and could be more effective to improve the frequency stability. Optimum capacity of the SMES can also be found by using different optimization techniques.
- All the simulation results can be verified by developing a small WECS prototype in a laboratory.

APPENDIX A

Table A.1: Parameters of PMSG, wind turbine and grid

Parameter of PMSG	Rated power	1.5MW
	Number of poles	48
	Stator resistance	0.006 Ω
	Stator inductance	0.000835 H
	Flux linkage	1.14 Wb
Parameter of wind turbine	Wind speed	12 m/s
	Blade radius	33 m
	Air density	1.225kg/m^3
	Optimal TSR	8.1
Grid Parameter	Resistance	0.03Ω
	Inductance	0.3H
	Transformer	415V/25KV
	Frequency	50 Hz
	DC link voltage	750 V
	DC link capacitor	4000e-6F
	Transmission line	1 KM
	Rated Voltage	415V

Table A.2: Parameters of BC

Braking resistor	0.35Ω
Threshold voltage	789 V

APPENDIX B

Table B.1: Transfer function parameters during normal condition

Variable	Value	Variable	Value
K_1	5.854e05	D_8	1.367e07
K_2	1.681e08	D_9	3.458e09
K_3	5.777e10	D_{10}	8.936e11
K_4	1.659e13	D_{11}	1.665e13
D_1	7.042e-17	D_{12}	1.659e13
D_2	5.859e-13	A	1
D_3	3.217e-09	B	20.01
D_4	1.114e-05	C	20.01
D_5	0.03108	X	-6.542e-05
D_6	47.89	Y	0.007885
D_7	3.637e04	Z	20.01

Table B.2: Transfer function parameters during fault condition

Variable	Value	Variable	Value
L_1	2.798e08	M_8	1.556e13
L_2	8.459e10	M_9	4.208e15
L_3	2.779e13	M_{10}	1.668e16
L_4	8.349e15	M_{11}	2.494e16
L_5	1.659e16	M_{12}	1.659e16
M_1	1.123e-12	M	7.811e-06
M_2	4.258e-06	N	0.000721
M_3	0.03466	O	2
M_4	136.4	P	1
M_5	2.269e05	Q	2
M_6	1.694e08	R	2
M_7	6.469e10		

Table B.3: Parameters of ESS

Rated voltage	750 V
Rated capacitance	40 F
Equivalent DC series resistance	8.9e-3 Ω
Number of series capacitors	18
Number of parallel capacitors	10
Initial voltage	0 V
Operating temperature (Celsius)	25

Table B.4: Parameters of IEEE 9 bus system

IEEE 9 bus system	Generator1	N/A, infinite
	Generator2	163MW
	Generator3	85MW
	Load A	125MW,50MVAR
	Load B	90MW,30MVAR
	Load C	100MW,35MVAR
	Transformer1	16.5/230KV
	Transformer2	18/230KV
	Transformer3	13.8/230KV
	Transformer4	415V/25KV
	Transformer5	25/230KV
	Transmission line1	R=0.0100+j0.0850, b/2=0.088p.u.
	Transmission line2	R=0.0170+j0.0920, b/2= 0.079p.u.
	Transmission line3	R=0.0320+j0.1610, b/2= 0.1530p.u.
	Transmission line4	R=0.0390+j0.1700, b/2= 0.1790p.u.
	Transmission line5	R=0.0085+j0.0720, b/2= 0.0745p.u.
	Transmission line6	R=0.0119+j0.1008, b/2= 0.1045

APPENDIX C

Table C.1: Parameters of STATCOM

Rated voltage	1000 V
Rated capacitance	40 F
Equivalent DC series resistance (Ohms)	8.9e-3
Number of series capacitors	42
Number of parallel capacitors	1
Operating temperature (Celsius)	25

APPENDIX D

Table D.1: Parameters of synchronous generator

Nominal power	2 MW
Nominal voltage	415 V
Nominal frequency	50 Hz
Inertia	0.6 s(normal condition),5s(fault condition)
Internal impedance	R=0.0036 p.u., X=0.16 p.u.
Pole pairs	2
Generator type	swing

Table D.2: Parameters of SMES unit

L_{SMES}	10 H
DC link voltage	1200 V
DC link capacitor	4000e-6 F

APPENDIX E

Schematic diagram of PMSG based wind turbine with controller

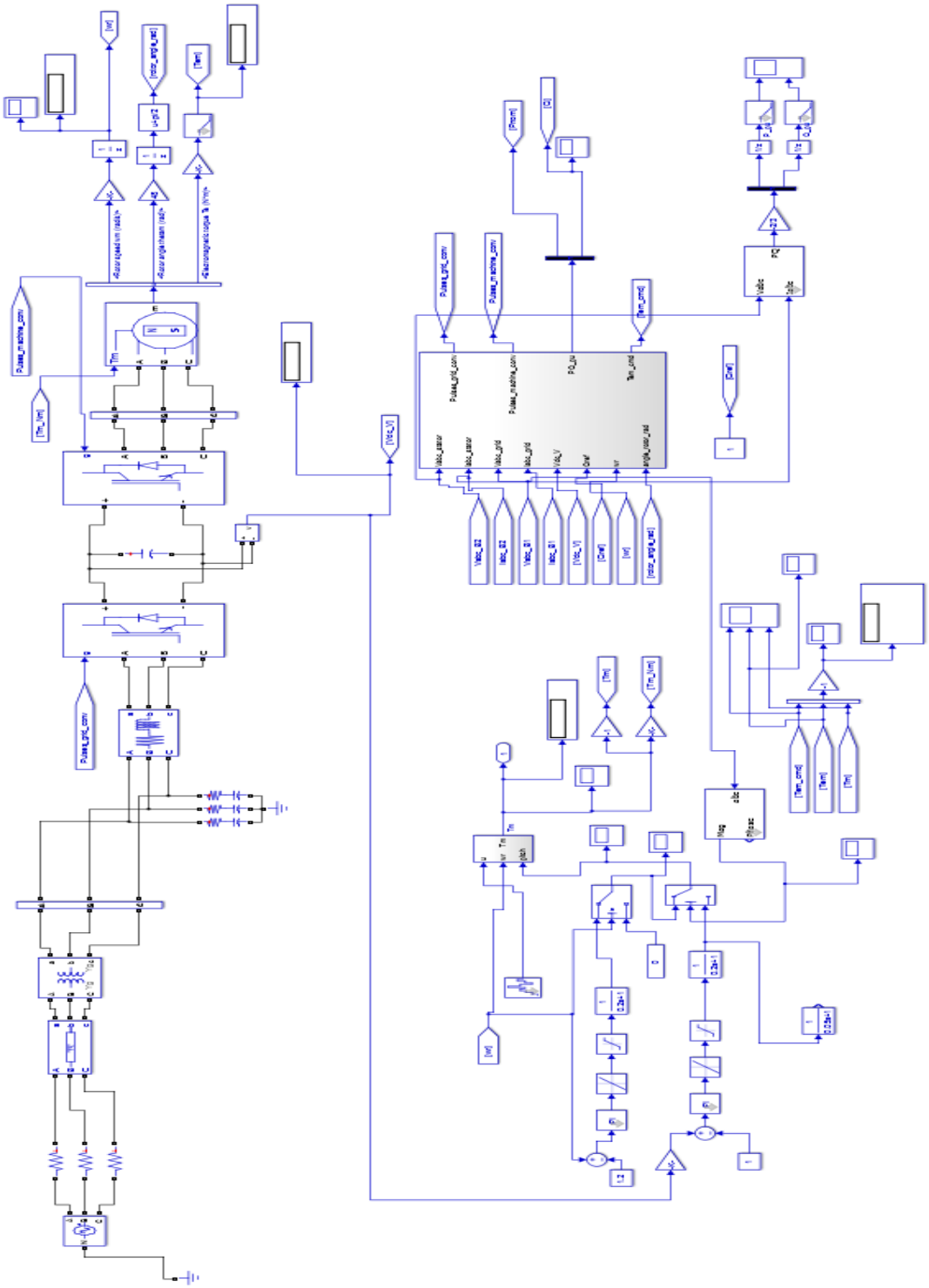

APPENDIX F

Schematic diagram of BC

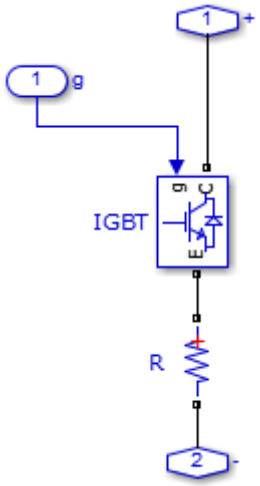

APPENDIX G

Schematic diagram of ESS

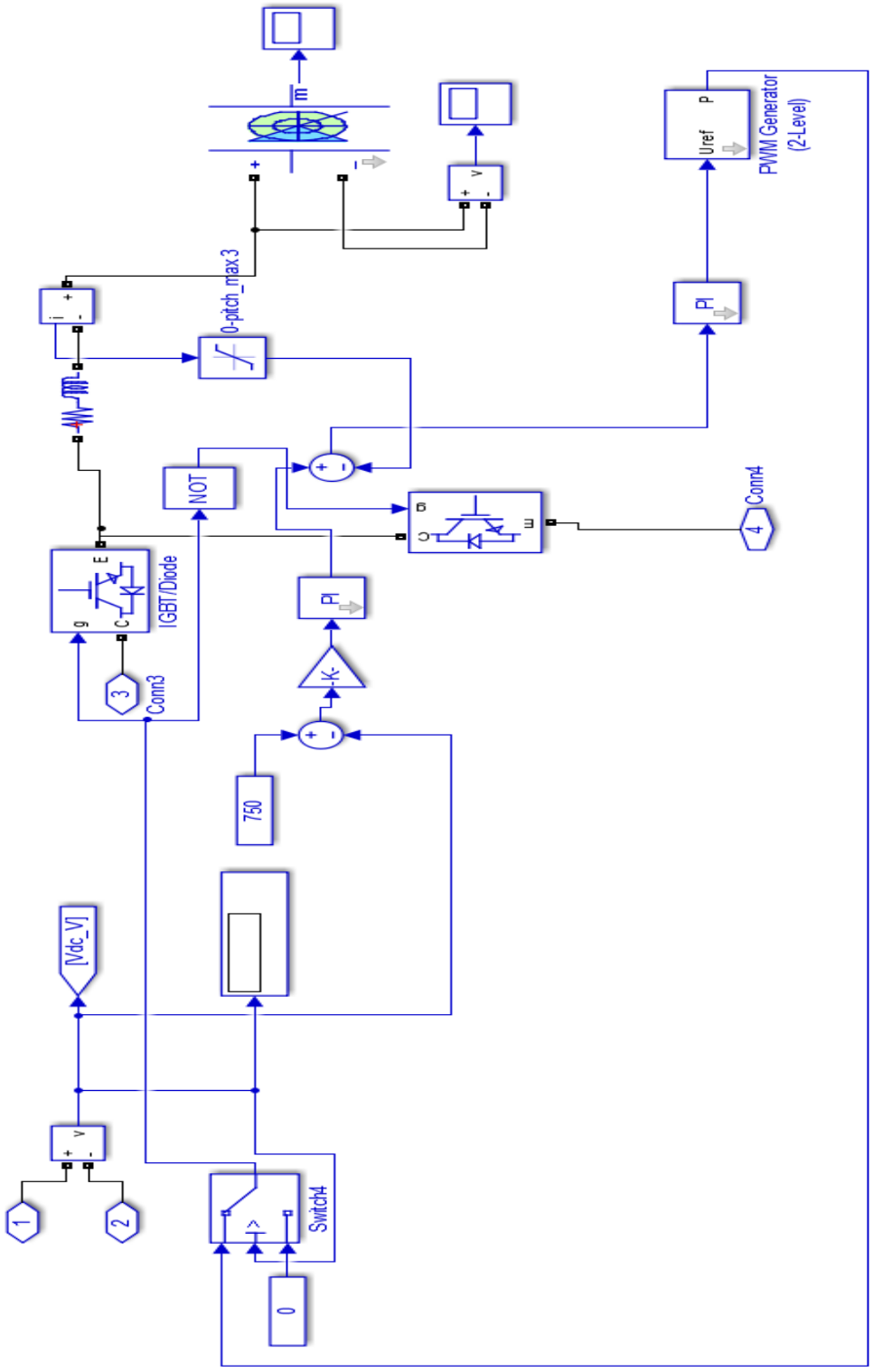

APPENDIX H

Schematic diagram of STATCOM

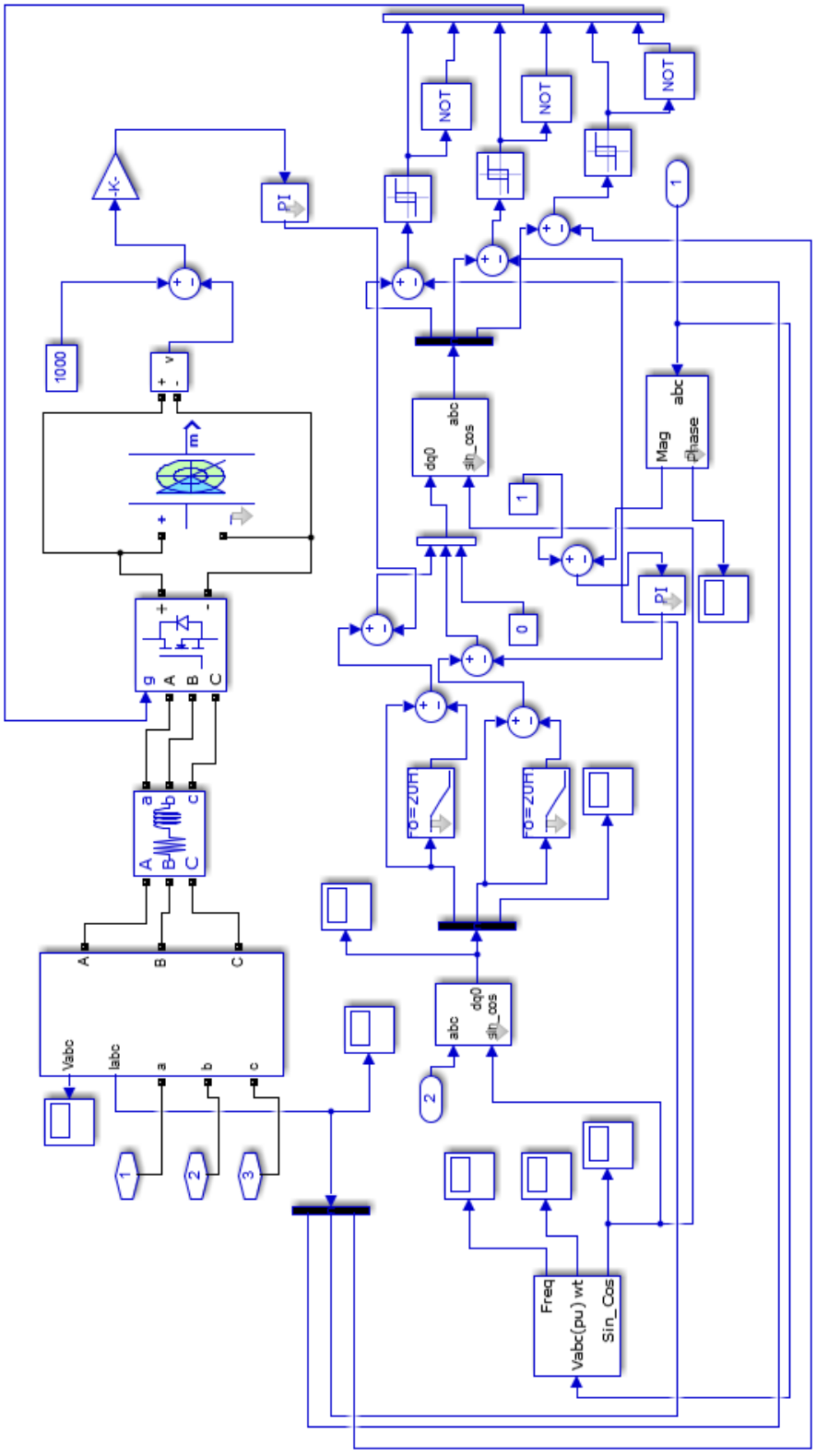

APPENDIX I

Schematic diagram of wind farm

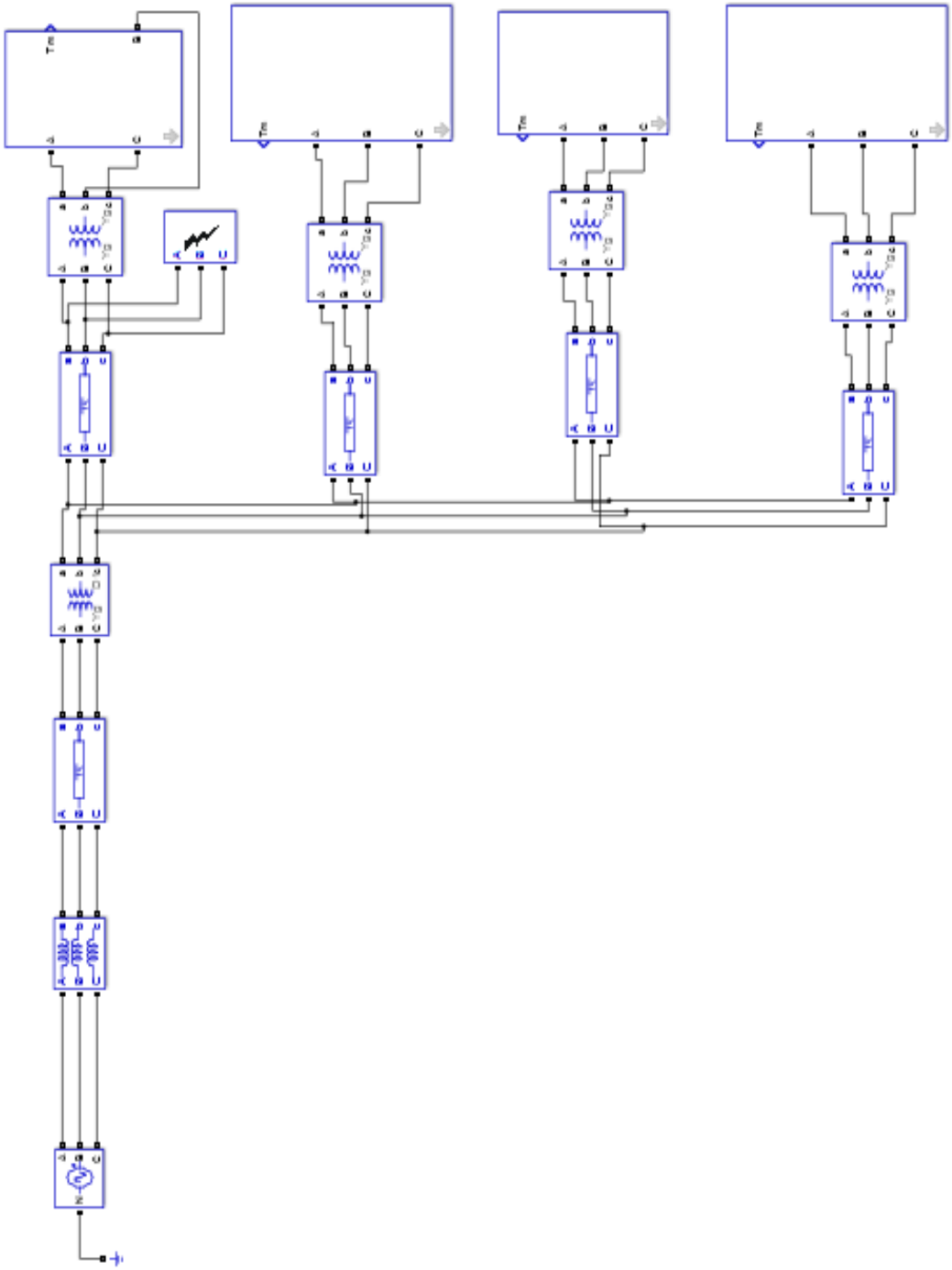

APPENDIX J

Schematic diagram of wind turbine connected with IEEE 9 bus system

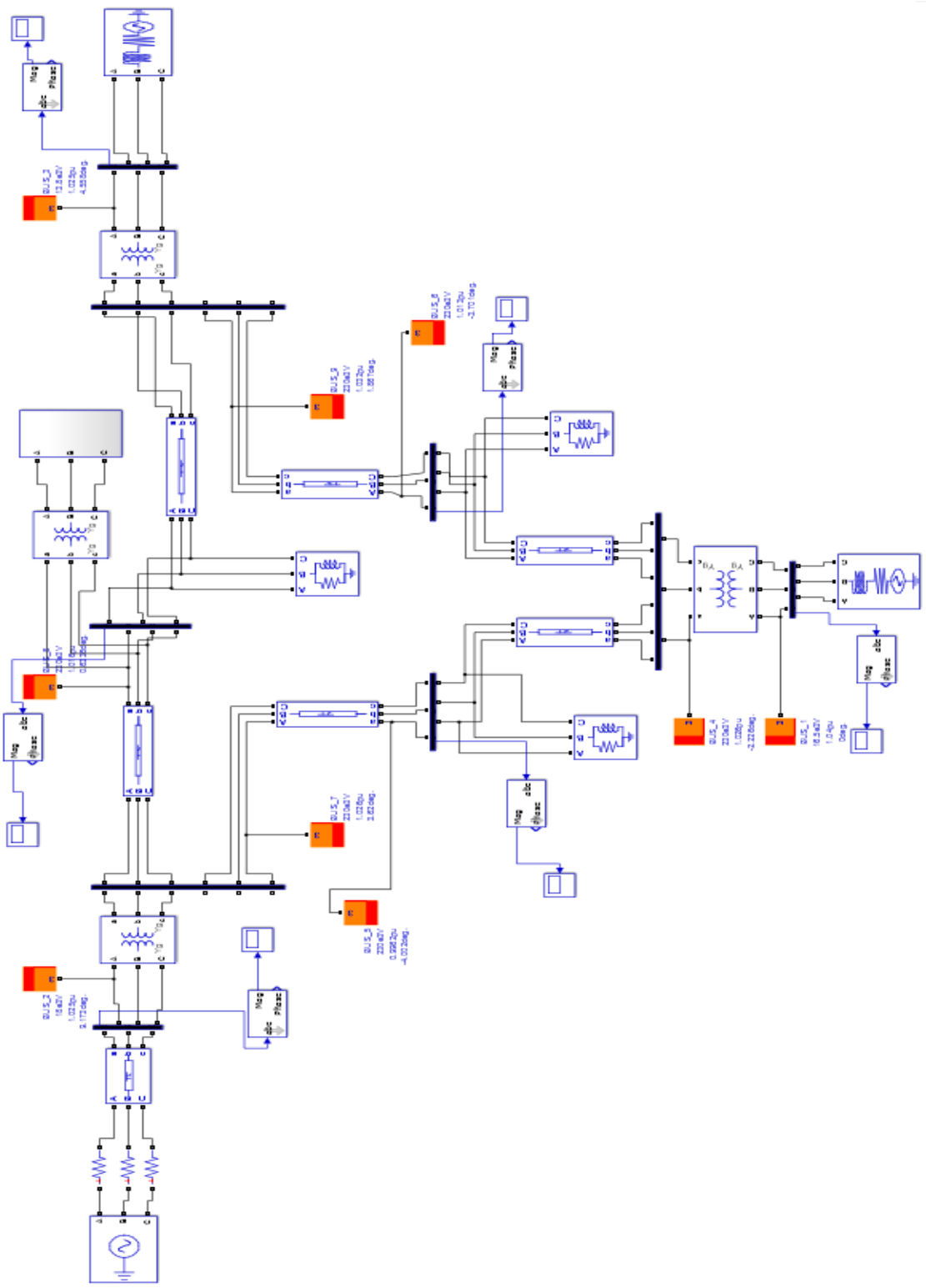

APPENDIX K

Schematic diagram of Fuzzy Logic controller with membership function and surface viewer

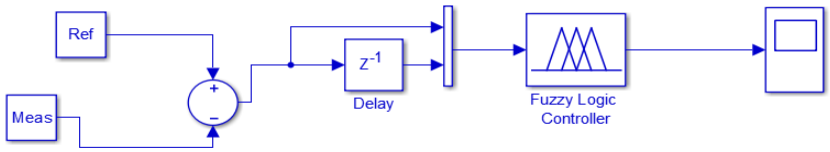

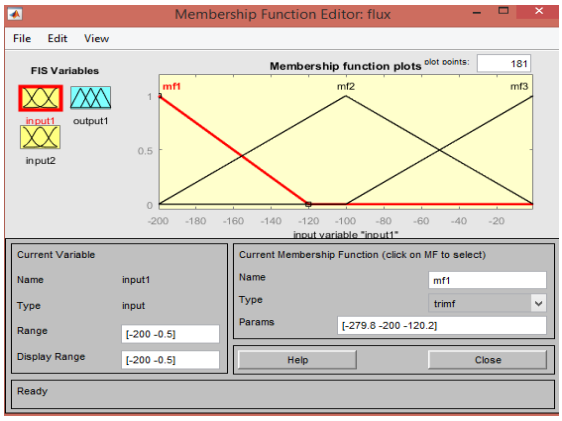

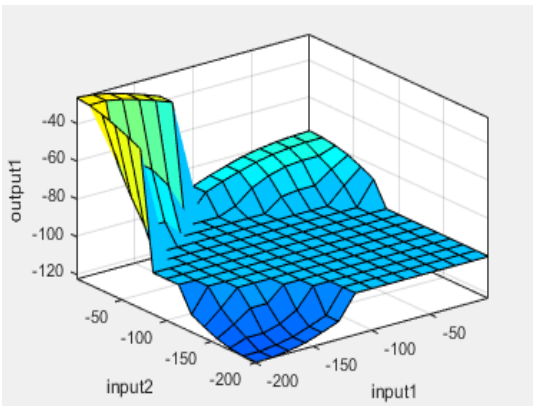

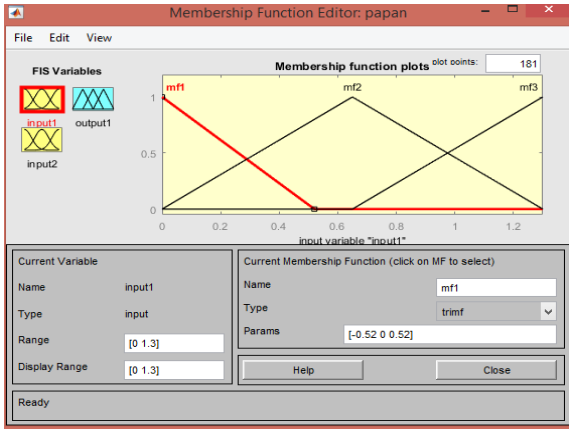

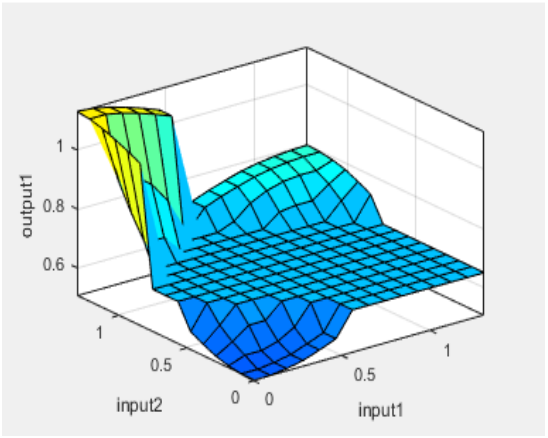

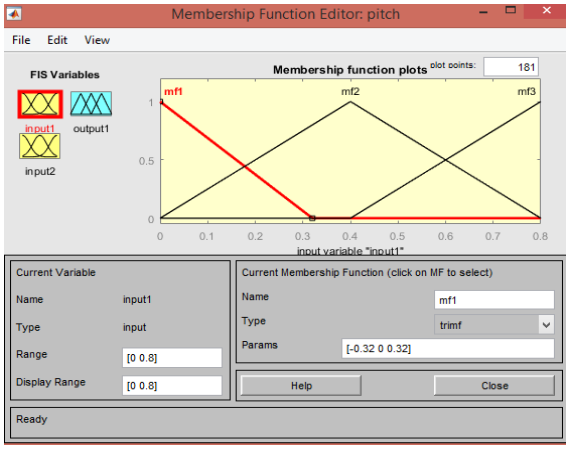

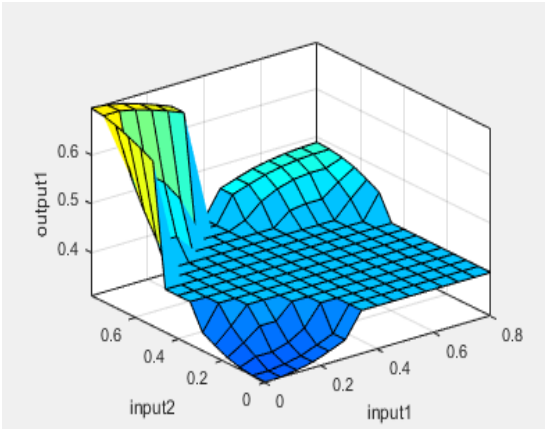

APPENDIX L

Schematic diagram of SMES unit

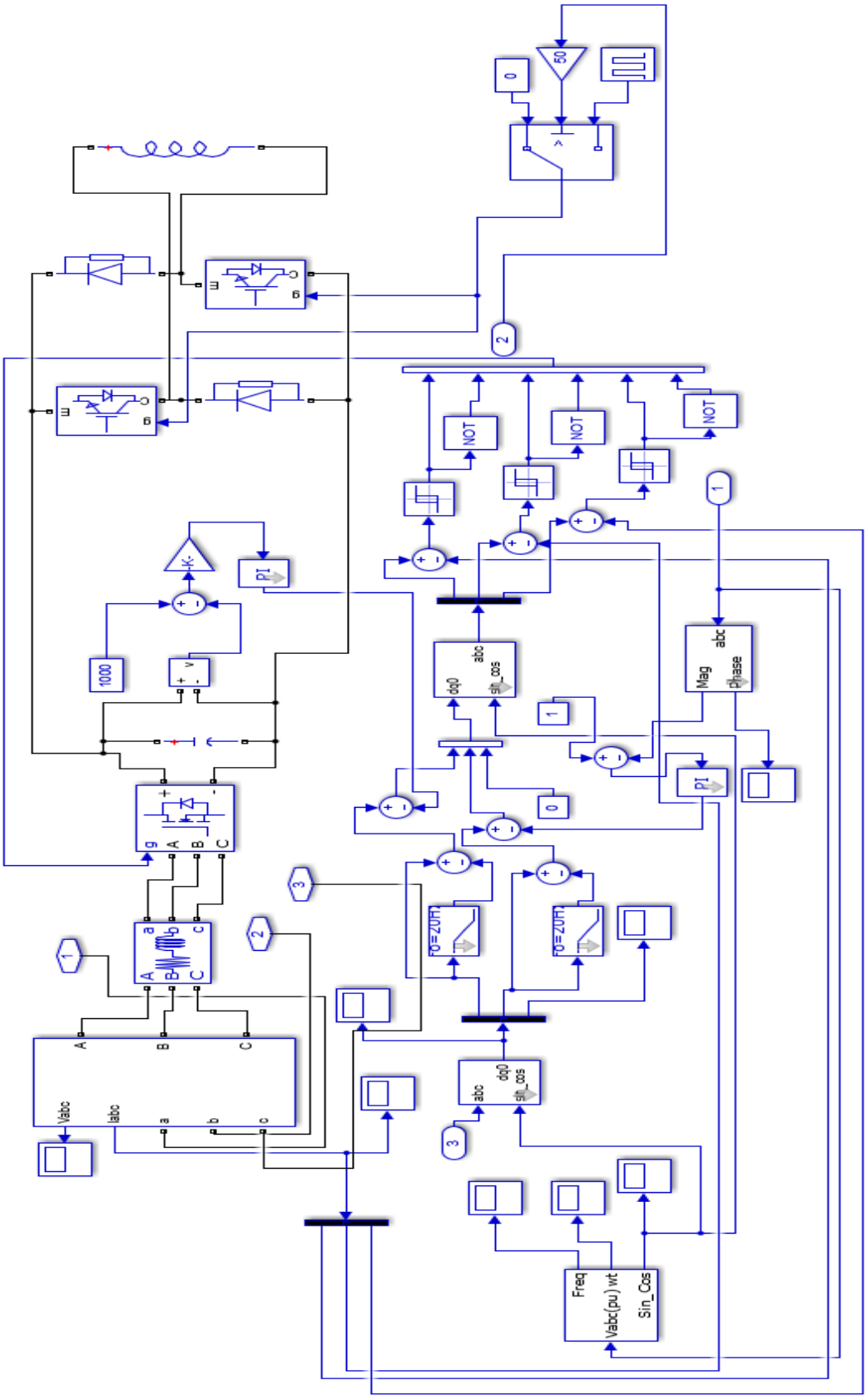

APPENDIX M

Schematic diagram of single machine system

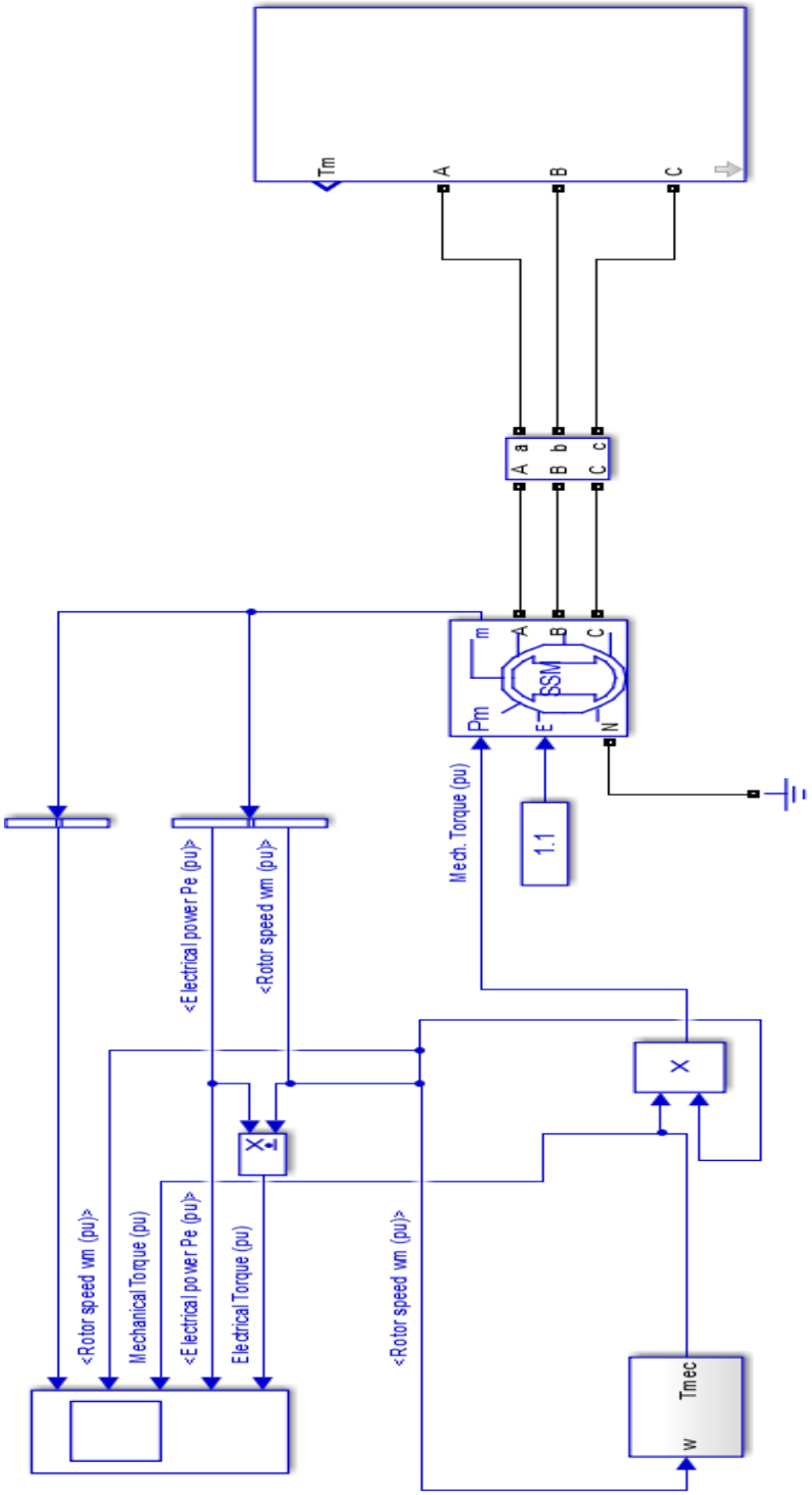

APPENDIX N

Schematic diagram of multi machine system